

“Hidden” Mechanisms in Photoredox Catalysis: Strategies to Promote Challenging Redox Events

By

Oliver Purdy Williams

A dissertation submitted in partial fulfillment of
the requirements for the degree of

Doctor of Philosophy

(Chemistry)

at the

UNIVERSITY OF WISCONSIN-MADISON

2023

Date of final oral examination: 2/7/2023

The Dissertation is approved by the following members of the Final Oral Committee:

Zachary K. Wickens, Assistant Professor, Organic Chemistry, Inorganic Chemistry

Shannon S. Stahl, Professor, Organic Chemistry, Inorganic Chemistry

Samuel H. Gellman, Professor, Organic Chemistry, Chemical Biology, Materials Chemistry, Physical Chemistry

Tehshik P. Yoon, Professor, Organic Chemistry, Inorganic Chemistry

Acknowledgments

I would like to begin by expressing my gratitude to all of my teachers who have inspired and encouraged me throughout my academic journey. Their teaching stoked my curiosity and provided me with the knowledge and tools to explore and answer questions.

I am especially thankful to Zach for being an impactful teacher and mentor. He not only taught me the technical aspects of doing great science but also how to be a great scientist and leader. He instilled in me the importance of building strong teams, treating people with respect, and navigating social interactions with kindness. I am grateful for the many hours we spent discussing chemistry and other topics, and for the opportunity to be a part of his group. His guidance and support were invaluable to my growth as a researcher, and I am proud of the group we built together. I am truly amazed by what we were able to accomplish, and it was an honor to be a part of such a dynamic and successful team.

I am grateful to my lab mates for creating a welcoming and stimulating environment that made me excited to come to lab every day. Their challenges pushed me to grow as a researcher, and their support enabled me to achieve that growth. Thank you for making my time in the lab full of success and fun.

I would also like to thank my family for their unwavering support. Their perspectives and encouragement were invaluable during times when it was easy to become overly focused on one aspect of life. My grandfather, in particular, passed on the value of being a lifelong learner, which has been an essential part of my personal and academic growth.

To my friends, thank you for providing a support network and enriching my life with your companionship.

Finally, I want to acknowledge the various institutions that support scientific research.

Table of Contents

ABSTRACT.....	III
CHAPTER 1: "HIDDEN" MECHANISMS IN PHOTOREDOX CATALYSIS.....	1
1. 1. <i>Introduction</i>	2
1. 2. <i>In situ catalyst modification</i>	6
1. 3. <i>Catalytic systems that sum the energy of two photons</i>	10
1. 4. <i>Electrochemical generation of potent photoredox catalysts</i>	17
1. 5. <i>Terminal redox reagent byproducts that promote reactions</i>	24
1. 6. <i>References</i>	30
CHAPTER 2: NON-INNOCENT RADICAL ION INTERMEDIATES IN PHOTOREDOX CATALYSIS: PARALLEL REDUCTION MODES ENABLE COUPLING OF DIVERSE ARYL CHLORIDES.....	34
2. 1. <i>Abstract</i>	35
2. 2. <i>Introduction</i>	35
2. 3. <i>Results and Discussion</i>	38
2. 4. <i>Conclusions</i>	46
2. 5. <i>Experimental</i>	46
2. 6. <i>References</i>	100
CHAPTER 3: UNVEILING POTENT PHOTOOXIDATION BEHAVIOR OF CATALYTIC PHOTOREDUCTANTS	106
3. 1. <i>Abstract</i>	107
3. 2. <i>Introduction</i>	107
3. 3. <i>Results and Discussion</i>	110
3. 4. <i>Conclusions</i>	120
3. 5. <i>Experimental</i>	120
3. 6. <i>References</i>	167
CHAPTER 4: PRACTICAL AND GENERAL ALCOHOL DEOXYGENATION PROTOCOL	174
4. 1. <i>Abstract</i>	175
4. 2. <i>Introduction</i>	175
4. 3. <i>Results and Discussion</i>	178
4. 4. <i>Conclusions</i>	188
4. 5. <i>Experimental</i>	189
4. 6. <i>References</i>	296
APPENDIX A: NMR SPECTRA NEW COMPOUNDS IN CHAPTER 2	303
APPENDIX A: NMR SPECTRA NEW COMPOUNDS IN CHAPTER 3	304
APPENDIX A: NMR SPECTRA NEW COMPOUNDS IN CHAPTER 4	305

Abstract

“Hidden” Mechanisms in Photoredox Catalysis: Strategies to Promote Challenging Redox Events

Oliver Purdy Williams

Under the supervision of Professor Zachary K. Wickens

At the University of Wisconsin-Madison

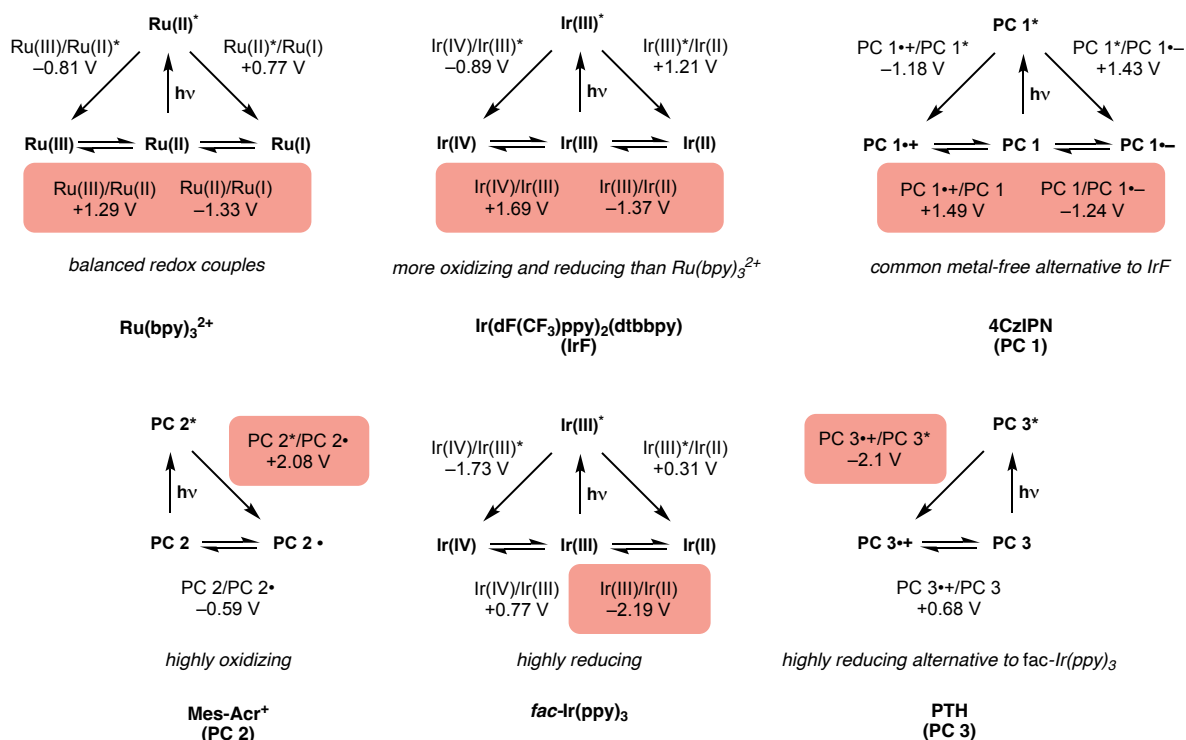
Photoredox catalysis offers an attractive way to synthesize molecules by using the energy of light. Under visible light irradiation, photocatalysts can selectively convert photonic energy into chemical potential without destructive excitation of substrates. However, operation of these catalysts under classic paradigms limits the range of substrates that can be engaged. This thesis discusses alternative mechanistic design principles that can be used to expand the redox limit of visible light absorbing catalysts. I describe how multiple energetic inputs can be summed to enable challenging redox events and, building from that concept, how I developed systems in which carefully chosen terminal redox reagents and additives promote multiple-photon processes for both challenging oxidations and reductions.

Chapter 1: “Hidden” mechanisms in photoredox catalysis

1. 1. Introduction

An important area of organic chemistry focuses on the use of light to provide the energy required to promote chemical reactions.^{1–6} This photochemical approach provides an appealing complement to thermally promoted approaches and to the deployment of energetic reagents in chemical synthesis. Contemporary research in photochemical synthesis largely focuses on photoredox, or the use of light to promote electron transfer. Furthermore, the focus has largely been on the use of visible light to avoid deleterious substrate excitation and promote selective catalyst excitation. Typically, when developing such reactions selection parameters based on tabulated properties of photocatalysts are consulted to determine suitable candidates. For example, Ru(bpy)₃ was a commonly employed catalyst during the recent ascension of photoredox catalysis. However, by contemporary standards it is neither a particularly oxidizing nor reducing catalyst, for example compared to IrF and 4CzIPN (Figure 1.1 A) Some catalysts are more biased toward highly oxidizing (Mes-Acr⁺) or highly reducing potentials (Ir(ppy)₃ and PTH). Analyzing the properties of currently available photocatalysts reveals an energetic bound of approximately –2 to +2 V vs. SCE (Figure 1.1 B). These bounds can be partially traced back to the finite energy found in visible light photons. Despite the abundant energy in visible light photons (400 nm = 71 kcal/mol = 3.1 eV), much is lost due to various photophysical processes, i.e., internal conversion and intersystem crossing.⁷ Unfortunately, these bounds exclude a wide range of substrates from being engaged in photochemically promoted electron transfer. Therefore, innovations in photochemical methods that enable electron transfer beyond these bounds are expected to positively impact synthetic organic chemistry. Design principles continue to be uncovered for making catalysts that more effectively convert photonic energy into electrochemical potential, although they have yet to significantly pass the approximate –2 to +2 V vs. SCE energetic bounds.^{8–11}

A Selection parameters of common photocatalysts



B Approximate energetic limitations of conventional photoredox catalysts

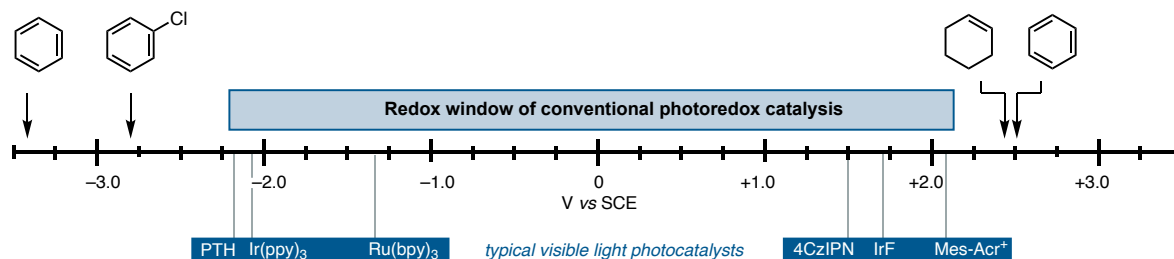


Figure 1.1 Overview of photocatalyst selection parameters and energetic limitations. bpy = 2,2'-bipyridine. dF(CF₃)ppy = 2-(2,4-difluorophenyl)-5-(trifluoromethyl)pyridine. dtbbpy = 4,4'-di-*tert*-butyl-2,2'-bipyridine. 4CzIPN = 2,4,5,6-tetra(9H-carbazol-9-yl)isophthalonitrile. Mes-Acr⁺ = 3,6-di-*tert*-butyl-9-mesityl-10-phenylacridin-10-ium. *fac* = facial. ppy = 2-phenylpyridine. PTH = 10-phenyl-10H-phenothiazine. SCE = standard calomel electrode.

There are however exceptions to these boundaries of photoredox catalysis. When removing the condition of visible light, more energetic ultraviolet (UV) light can be used to promote more challenging redox events. For example, ketyl radical intermediates can be generated via

ketone reduction, (approximately -2.2 V vs. SCE) using a UV light absorbing catalyst (Figure 1.2 A).¹² This approach comes with significant synthetic drawbacks as organic molecules besides the photocatalyst can absorb UV light and undergo deleterious reactions, such as Norrish type fragmentations of ketones. Interestingly, recent reports have demonstrated that even blue light can promote undesired reactivity, motivating the use of less energetic red light.¹³ An alternative strategy to surpass the energetic bounds is to start with already reactive catalysts and further energized them with visible light.¹⁴ For example, irradiation of quinones has been demonstrated to promote the single electron oxidation of benzene (Figure 1.2 B).^{15,16} Again, this approach has significant drawbacks, namely the ground state reactive catalysts tend to react unproductively and decompose. The final unusual exception traces back to the fundamental Nernst equation that describes electron transfer thermodynamics. Temperature is an integral component of the equation and therefore needs to be considered when assessing feasibility of electron transfer. Furthermore, the Nernst equation describes an equilibrium between oxidized and reduced species. Therefore, kinetically fast processes that consume low concentration species can drive forward electron transfer reactions that are thermodynamically unfavorable. One notable example describes a photochemical reaction that is intentionally heated (Figure 1.2 C).¹⁷ The influence of temperature on photochemical reactions in general is complicated and likely more commonplace than typically thought. Higher temperatures can facilitate irreversible non-redox steps, thus driving unfavorable redox equilibria. Due to current lack of photochemical reactors that can control internal reaction temperatures (i.e., more rigorously than fan cooling, ability to hold elevated and lowered temperatures) and significant amount of heat released by nonradiative decay, many photochemical reactions are probably being run at significantly higher temperatures than expected.^{5,7}

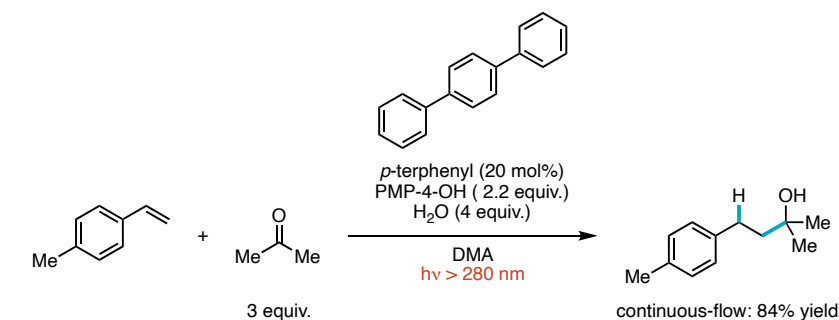
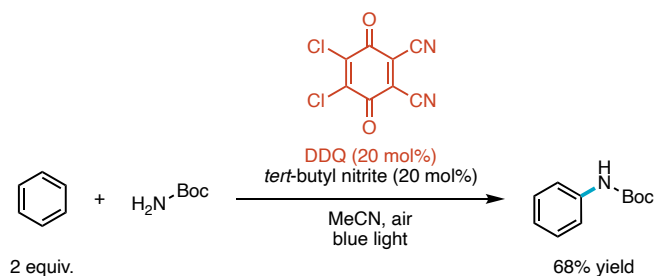
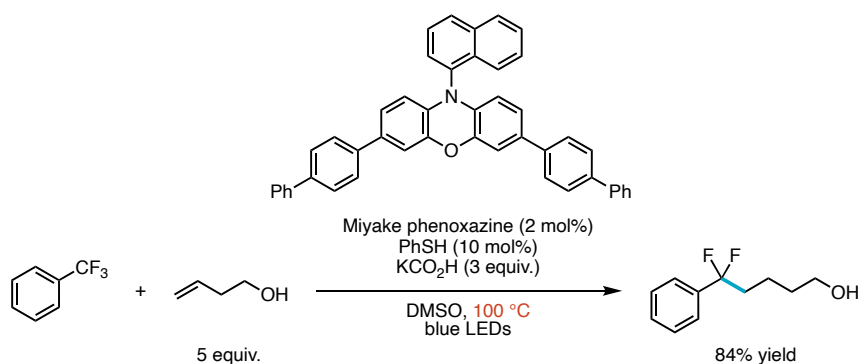
A Ultraviolet light absorbing photocatalyst**B** Reactive ground state species used as a photocatalyst**C** Reaction performed at elevated temperature

Figure 1.2 Strategies to surpass the energetic limitations of conventional photoredox catalysis with significant drawbacks. PMP-4-OH = 1,2,2,6,6-pentamethyl-4-piperidinol.

Given this understanding of the energetic limits of photoredox catalysis, sometimes unexpected reactivity is observed with respect to catalyst selection parameters, suggesting that these reactions are not functioning as simply as imagined. This chapter strives to explore and explain these hidden mechanisms in photoredox catalysis, providing context for the ensuing research thesis. Four categories of hidden photochemical mechanisms are presented in which

the classic photoredox paradigm is broken, and several representative reactions are discussed within each category. This collection of modern methodologies reveals the complexity of photochemical reactions and how new insights are being leveraged to promote otherwise challenging chemical transformations.

1. 2. In situ catalyst modification

The first case to consider when an unexpected redox event is observed is that the catalyst that is promoting the reaction is no longer the catalyst that was charged into the reaction mixture. Photocatalysts excel at the generation of reactive intermediates, and it is well documented that these reactive intermediates can react with the catalysts that generate them. For example, alkyl radicals have been demonstrated to add to the pyridyl backbones of ruthenium photocatalyst as well as displace the nitrile functional groups of cyanoarene donor-acceptor catalysts.^{18–20} In some cases, this results in catalyst death and in others a more active catalyst is formed (Figure 1.3 A and B). In a particularly interesting case of in situ catalyst modification the organic backbone of a classic iridium polypyridyl photocatalyst can be hydrogenated resulting in a significantly more reducing conventional photocatalyst (Figure 1.3 C).²¹ The classic selection parameters of the iridium catalyst employed (most reducing redox couple = -1.47 V vs. SCE) preclude its competency for the aryl bromide reduction that they observe (-2.72 V vs. SCE for 4-bromoanisole). These examples demonstrate that conventional catalyst selection parameters should not be used as a tool to exclude reactivity simply because the catalysts that are put in reaction mixtures are often not the catalysts that function during reactions.

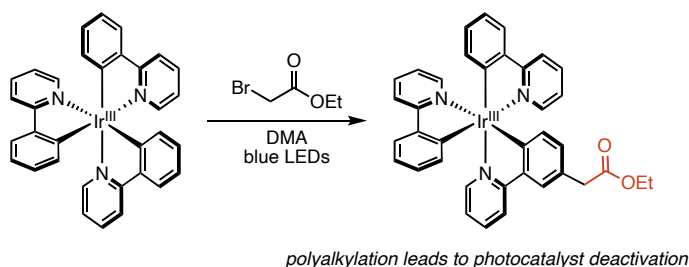
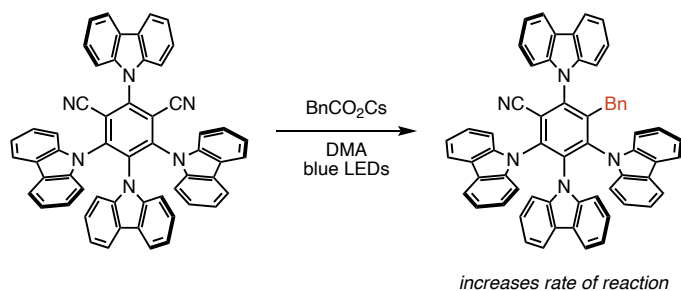
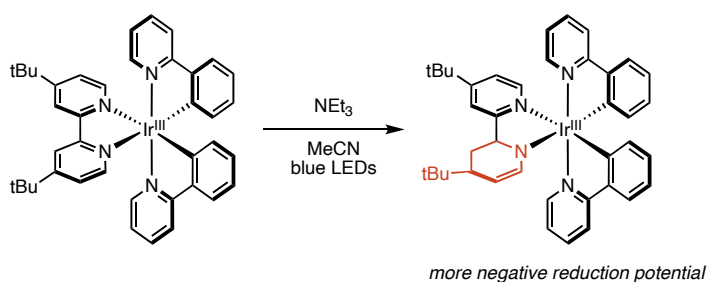
A Photocatalyst deactivation**B Generation of a more active photocatalyst****C Formation of a more reducing photocatalyst**

Figure 1.3 Examples of in situ covalent modifications to initially administered photocatalysts.

Related to in situ catalyst modification, there are several examples of in situ complexation to generate light absorbing complexes that can promote challenging redox events. These chromophore assemblies often consist of an electron donor-acceptor (EDA) or, synonymously, charge transfer complex. Two notable examples employ thiolates as electron donors and aryl halides as acceptors (Figure 1.4).^{22,23} Visible light excitation of these complexes results in electron transfer from the anionic thiolate to the aryl halide (-2.97 V vs. SCE for fluorobenzene). This

approach is broadly related to the concept discussed in the introduction of using destabilized ground state catalysts, e.g., anions, as photocatalysts. A major limitation of this EDA complex approach is the mechanistic constraint of identifying catalyst-substrate pairs that form such complexes. Furthermore, electron transfer and group transfer happen from the same intermediate, thus limiting what groups can be transferred.

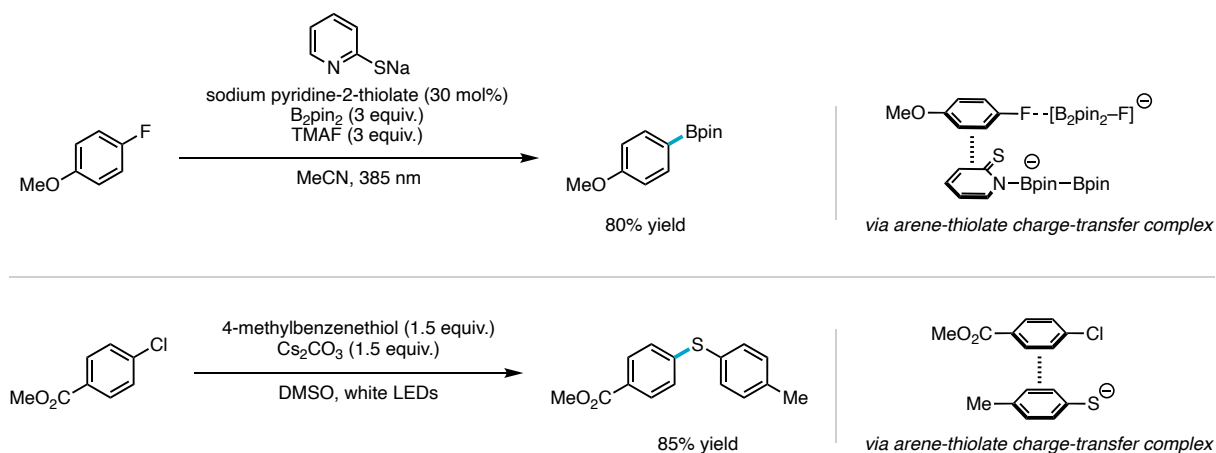


Figure 1.4 Examples of in situ formation of light-absorbing charge-transfer complexes. TMAF = tetramethylammonium fluoride

Another example related to in situ catalyst modification and distinct from EDA complex formation involves a proposed proton-coupled electron transfer event.²⁴ Hydrogen bonding between the N–H of a phenothiazine photocatalyst and a carbonate base facilitates photoinduced electron transfer (PET) to electron rich aryl phosphates (–2.97 V vs. SCE for *p*-tolyl diethyl phosphate), (Figure. 1.5) This is distinct from using a destabilized ground state catalyst as deprotonation was ruled out, i.e., the phenothiazine anion does not act as the photoreductant. Furthermore, phenothiazine is not a competent photocatalyst by itself and presence of a base was required for reactivity. Notably, this strategy has yet to be expanded beyond borylation which

may be due to the highly reducing intermediates that can be generated from diboron reagents (vide infra).

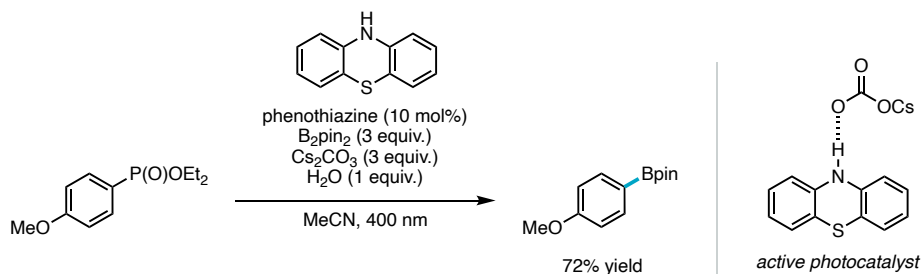


Figure 1.5 Photoinduced electron transfer enabled by proton-coupling.

The final example of in situ chromophore assembly involves the use of a pyridine base catalyst along with an alkoxide base to form a mixture of light-absorbing “super electron donors” with diboron reagents (excited state estimation–3.49 V vs. SCE) (Figure. 1.6).²⁵ Again, this example shares a similar theme with the use of destabilized ground state catalysts, where now boryl anion species are being leveraged as potent photoreductants capable of reducing electron-rich aryl chlorides (–2.9 V vs. SCE for 4-chloroanisole). This reaction does not proceed with strict use of a photocatalyst, instead the non-photoactive pyridine base catalyst is necessary to form a light absorbing species in situ. Although this strategy may not be trivial to apply beyond borylation, it has important implications for photocatalytic borylation reactions in general, which may be operating by this type of mechanism.

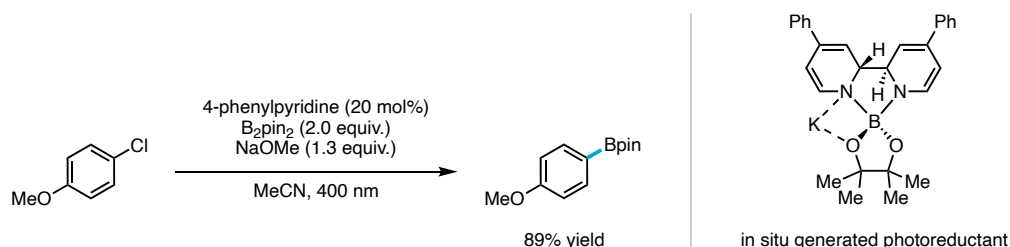
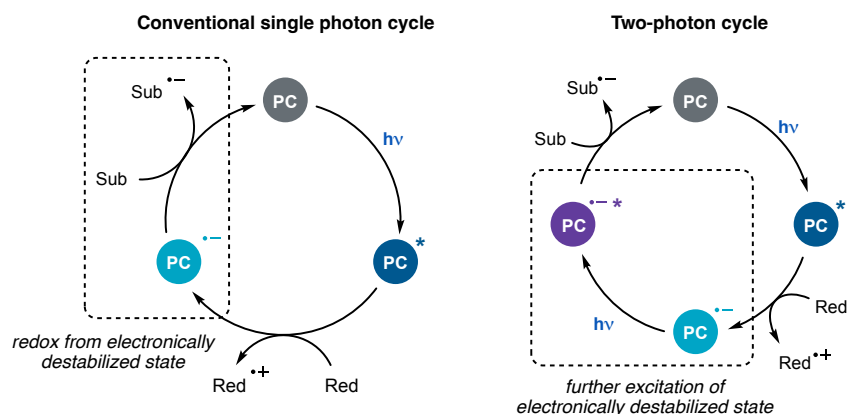
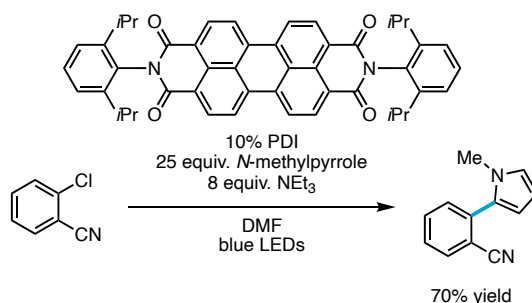


Figure 1.6. Electron-rich aryl halide radical borylation enabled by in situ formation of boryl anion photoreductant.

Taken together, these examples highlight the mechanistic complexity that arises when we consider catalyst modification or in situ chromophore generation as explanations for unexpected redox events. In all these examples, the reductive cleavage of strong bonds proceeds via electron transfer from unintuitive intermediates.

1. 3. Catalytic systems that sum the energy of two photons

Related the previous section in which catalysts are modified in situ, often covalently, catalysts can also be electronically modified prior to excitation. König first described this process in the context of organic synthesis, in which a poorly reducing PDI catalyst (-0.43 V vs. SCE for $\text{PDI}/\text{PDI}^{\bullet-}$) was demonstrated to be capable of reducing aryl bromides (-1.9 V vs. SCE for 2-chlorobenzonitrile) far outside of what was expected based on classic selection parameters.²⁶ In their system, a neutral photocatalyst is proposed to undergo classic PET with a trialkyl amine terminal reductant to generate its radical anion congener. As opposed to this destabilized form of the catalyst undergoing electron transfer with the substrate, as often occurs in a conventional photoredox cycle, instead the radical anion is further energized by a second photon absorption (Figure 1.7). The excited state of the radical anion then behaves as a potent reductant. They term this process consecutive photoinduced electron transfer, which will be referred to herein as a two-photon process.

A Conventional photoredox catalytic cycle compared to a two-photon cycle**B** Photochemical aryl radical heteroarylation via a two-photon process**Figure 1.7** Overview and example of a two-photon process.

The Nicewicz group built from this concept and disclosed that a conventional photoredox catalyst can demonstrate this two-photon behavior.²⁷ By providing highly oxidizing acridinium photocatalysts with an amine terminal reductant as opposed to the typical O_2 terminal oxidant, the catalyst instead displayed unexpected highly reducing behavior. In their system the excited state of the acridinium cation engages in PET with a terminal reductant to generate the acridine radical. This contrasts with its classic behavior of reductive quenching with substrates, thus effecting substrate oxidation, followed by oxidative turnover. The reduced acridine is then capable of further excitation and potent photoreductant behavior. With an estimated value of -3.36 V vs. SCE, the excited acridine radical promotes *N*-detosylation (-2.46 V vs. SCE for *N*-tosylpyrrolidine) (Figure 1.8)

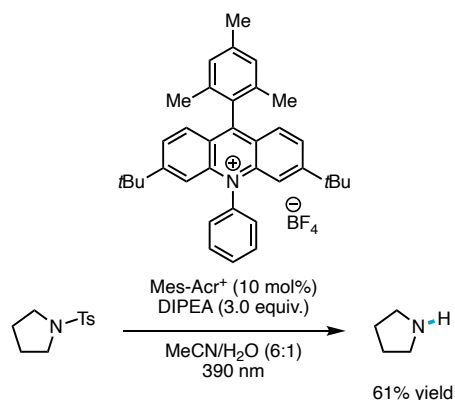


Figure 1.8 Use of a classic photooxidant for reductive amine detosylation via a two-photon process.

In electrochemical studies, *vide infra*, Wickens discovered that many structures with stable reduced congeners can act as potent photoreductants.²⁸ 4DPAIPN was found to be most effective for the challenging reduction of C(sp²)-O and C(sp²)-N bonds. Building from this discovery, Wickens further demonstrated how this catalyst can be adapted to a purely photochemical two-photon process, described in further detail in Chapter 2.²⁹ Via judicious terminal reductant selection, this catalytic system was able to surpass defunctionalization reactivity and promote coupling reactions of electron rich aryl chlorides (−2.9 V vs. SCE for 4-chloroanisole), despite selection parameters suggesting 4DPAIPN to be insufficiently reducing (most reducing couple −1.5 V vs. SCE) (Figure 1.9 A). Contemporaneously, Wu disclosed a new IPN catalyst capable of promoting challenging radical couplings of aryl chlorides in a two-photon cycle (Figure 1.9 B).³⁰ The catalyst design was inspired by the detection of carbazole in crude reaction mixtures. Replacement of one of the carbazole groups of 4CzIPN with other amines was observed to slow decomposition in this family of catalysts.

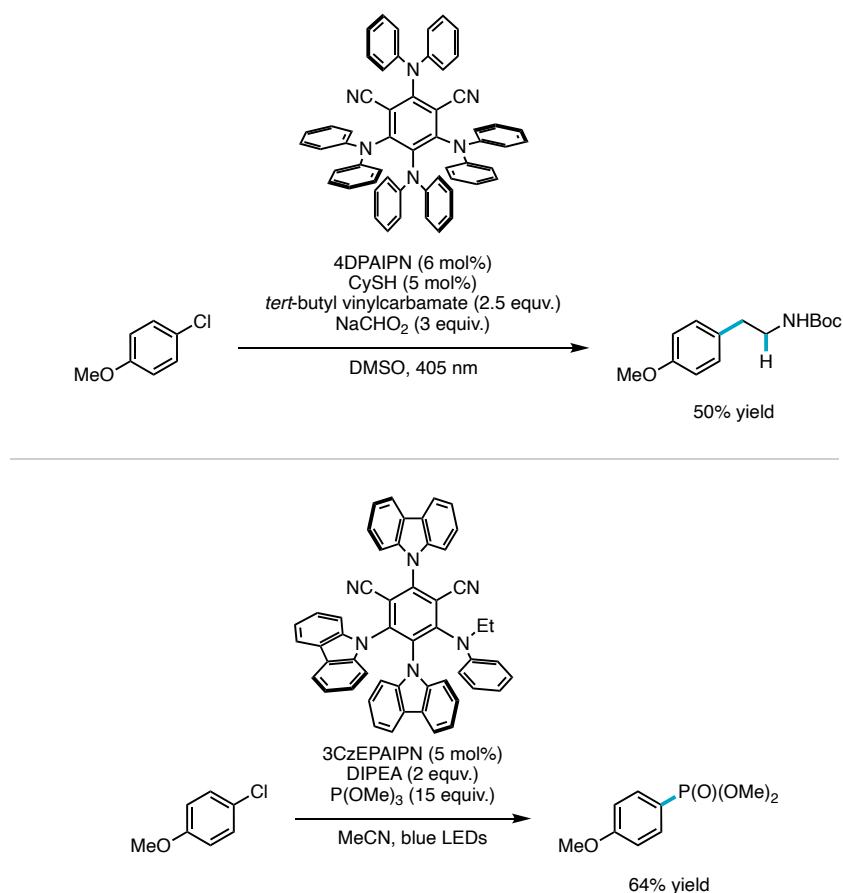


Figure 1.9 Reductions of electron-rich aryl chlorides via two-photon processes with cyanoarene donor-acceptor catalysts.

Combining the energy of two photons is not unique to small organic molecules and has been demonstrated by the Weix group to apply to quantum dots (Figure 1.10).³¹ Due to the unique electronic states accessible to these semiconductor nanocrystals, they can be charged with multiple electrons at once without decomposing. In this example charge accumulation is achieved via a photochemical process. These electronically activated states can then be further excited via a second photon absorption event, analogous to the excitation of electronically destabilized states of small molecules. Relaxation of these excited anionic states by Auger processes allows access to highly reducing intermediates.³² This strategy enables access to reductants capable of reducing exceedingly electron rich aryl chlorides (≤ -3.4 V vs. SCE). Although proceeding via different

elementary steps, the fundamental concepts are the same – using one photon to create an electronically destabilized state, then further exciting that intermediate with a second photon.

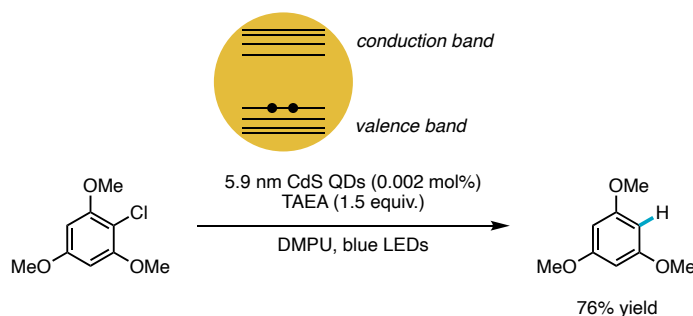


Figure 1.10 Reduction of electron rich aryl chlorides with cadmium-sulfide quantum dots via a two-photon process. QD = quantum dot. TAEA = tris(2-aminoethyl)amine.

All previously discussed two-photon reactions concerned reductive processes. Wickens discovered that unexpected potent photooxidant behavior can be observed by treating a classic highly reducing triaryl amine photocatalyst with terminal oxidants. The first photoexcitation promotes reduction of the terminal oxidant and generates an oxidized form of the catalyst. That electronically destabilized species can then be subsequently excited and enable the oxidation of unactivated arenes (+2.5 V vs. SCE for benzene) (Figure 1.11).³³ This is analogous to Nicewicz's work inverting the behavior of classically highly oxidizing acridiniums to potent photoreductants.²⁷ Key to Wickens' work was employing O₂ as the terminal oxidant along with a Lewis acid cocatalyst that consumed the inhibitory terminal redox reagent byproduct, i.e. superoxide. This cocatalytic system thus enabled the two-photon process by limiting back electron transfer (BET) and driving catalyst speciation toward electronically activated states.

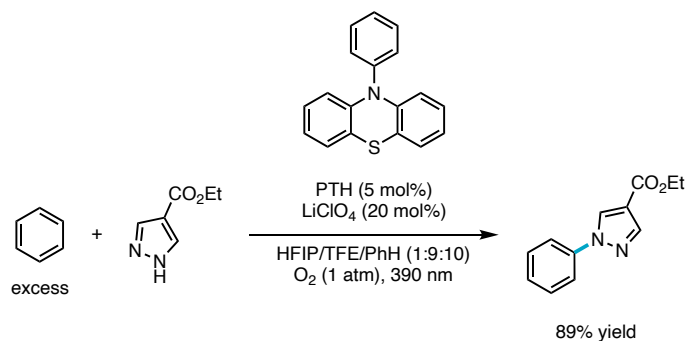


Figure 1.11 Use of a classic photoreductant for oxidation of electron neutral arenes via a two-photon process.

These proposed two-photon cycles have not come without controversy, a major point of contention being the characterized short excited state lifetimes (often on the picosecond time scale) of organic radicals,³⁴ which effectively rules out diffusional quenching. Short lifetimes may rule out diffusional quenching, but they do not rule out electron transfer in general and several alternative mechanistic explanations are available. For example, Miyake disclosed a new benzo[*ghi*]perylene monoamide (BPI) catalyst structurally related to the perylene diimide PDI catalyst first reported by König.³⁵ This catalyst is also proposed to function via a two-photon cycle, in this case promoting the Birch-type reduction of arenes.³⁵ The excited catalyst radical anion lifetime was measured to be hundreds of microseconds, which is more than sufficient for diffusional quenching. This long-lived species was tentatively assigned as the lowest quartet excited state, which arises from intersystem crossing from the doublet manifold. Importantly, quenching studies determined that the excited state quartet species was insufficiently reactive to engage with the arene substrate. Furthermore, the energy of the excited doublet state was computed to be approximately one volt insufficient to reduce the arene substrate. Alternatively, electron transfer from higher lying excited states could feasibly provide a favorable thermodynamic driving force, although intermolecular electron transfer in this fashion is unlikely to occur. They instead proposed the generation of solvated electrons, which can be generated on

picosecond timescales competitive with excited radical anion relaxation (Figure 1.12) This proposal of catalyst radical anion excitation followed by rapid electron ejection provides an alternative to diffusional single electron transfer (SET) and reconciles the observed challenging redox with rapid relaxation from sufficiently energetic high lying excited states. Weix also reports short lifetimes of anionic quantum dot excited states.³¹ They consider solvent redox and subsequent mediation as reasonable alternative mechanism. Like the solvated electrons proposed by Miyake, charge carrying by solvent circumvents short catalyst lifetimes because diffusion is not required for the catalyst excited state to encounter a solvent molecule. A third mechanism that does not require diffusion and long excited state lifetimes is preassociation of the substrate to the catalyst. Weix also suggests this as a viable mechanism in their quantum dot catalyzed system.³¹ These processes (electron ejection/solvated electron generation, solvent redox and mediation, and preassociation) as well as covalent catalyst modification in situ may be more generally occurring in photoredox reactions than currently appreciated. Although typically short lifetimes of organic radical excited states motivate consideration of alternative mechanisms, radical anions have been reported to possess sufficiently long-lived excited states for intermolecular ET. In a notable example from Wu, a lifetime of 12.95 ns was assigned to the doublet excited state of their modified cyanoarene donor-acceptor catalyst.³⁰ Lifetimes on the nanosecond timescale are sufficiently long to make diffusional quenching feasible. However, ability of this long-lived excited state to promote challenging redox events has yet to be evaluated.

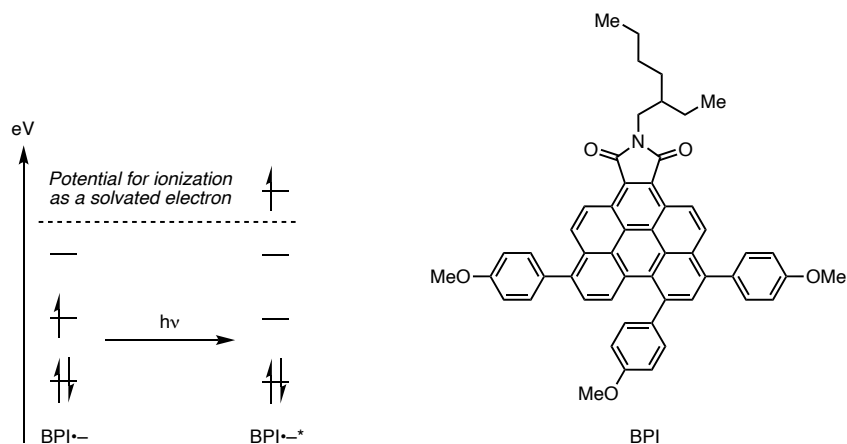


Figure 1.12 Energetic diagram for solvated electron formation from a polycyclic aromatic hydrocarbon imide catalyst.

At its core this strategy represents the summing of two energy inputs, in this case two photons, to achieve a challenging redox event. Conceptually, this strategy relates to catalyst destabilization in general. To achieve a challenging redox event, an already reactive ground state catalyst can be excited, a stable ground state catalyst can be modified in situ to generate a destabilized catalyst that can then be excited, or a catalyst can sum the energy of two photons proceeding through an electronically destabilized intermediate.

1. 4. Electrochemical generation of potent photoredox catalysts

The crux of the previous section was the concept of electronically destabilized states being active for PET. The generation of such states can simply proceed via a redox event, which can be achieved with other means beyond PET. Electrochemically promoted redox is particularly appealing due to continuously available potentials, contrasting to the discrete potentials of chemical redox reagents. Thus, a catalyst should be able to be destabilized via an electrochemical redox event and subsequently excited (Figure 1.13). Lambert first described this process in the context of organic synthesis, in which a trisaminocyclopropenium (TAC) catalyst was

demonstrated to be capable of oxidizing arenes using the combination of light and electricity.³⁶ In this system, the redox active TAC cation catalyst was first electrochemically oxidized. Visible light excitation of the TAC radical dication (estimated +3.33 V vs. SCE) then affected PET from arene substrates (+2.61 V vs. SCE for chlorobenzene) (Figure 1.14). Interestingly, TAC neither functions as a conventional photocatalyst nor as an electrochemical mediator capable of arene oxidation. Instead, it was chosen due to its redox ability and light absorbing capability in its oxidized state. The lack of TAC's ability to function as a conventional photocatalyst in addition to the potential of the substrates that were oxidized compared to the $E_{1/2}$ of TAC (1.22 vs. SCE) indicates that the anode is not simply turning over a photocatalyst in a conventional cycle. Thus, the synergistic combination of electrochemical oxidation and photochemical excitation enables new reactivity through an uncommon light absorbing electronically destabilized intermediate.

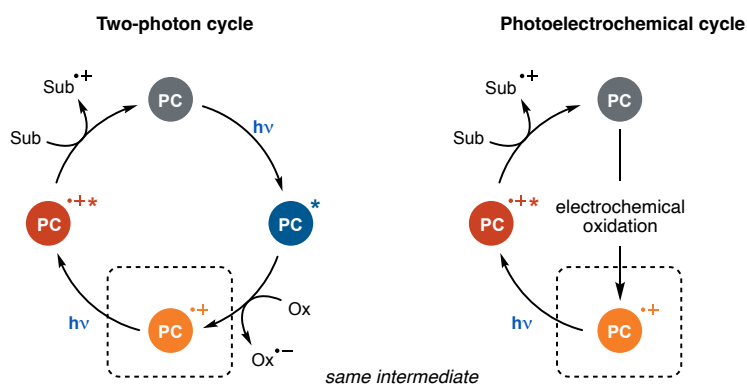


Figure 1.13 Two-photon and photoelectrochemical strategies offer complementary approaches to access the same electronically destabilized catalytic intermediates.

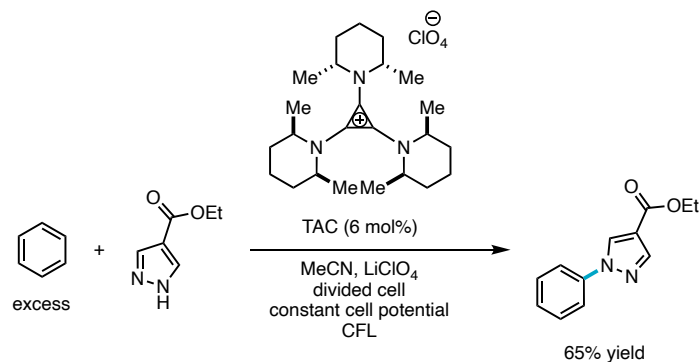


Figure 1.14 Photoelectrochemical oxidation of electron neutral arenes.

Barham reported a similar system combining electricity and light for catalytic arene oxidation (Figure 1.15).³⁷ Again, a catalyst without established ground state photoredox activity but with well-behaved redox properties was employed. Akin to the Lambert work, the triaryl amine catalysts were not effective electrochemical mediators for electron-neutral arene oxidation (+2.61 V vs. SCE for chlorobenzene) and required irradiation for product formation. The authors suggest that the extended π surface of the catalyst was a key design feature as it caused preassociation to the arene substrate via π - π interactions, allowing for redox without long doublet excited state lifetimes.

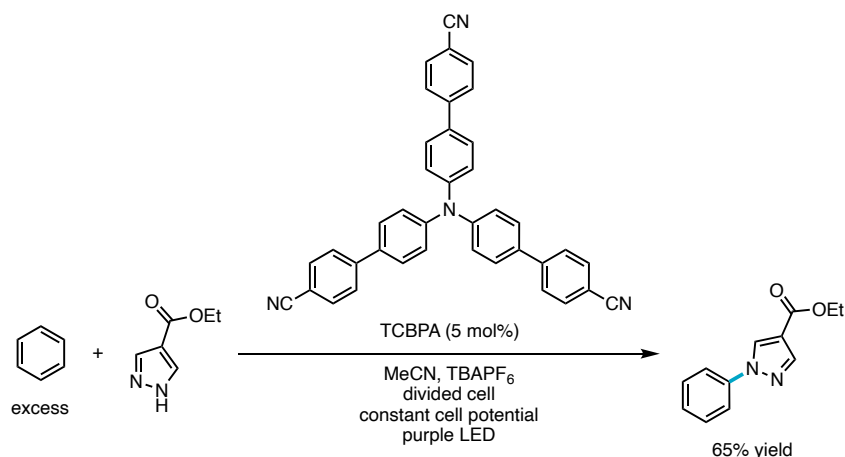


Figure 1.15 Photoelectrochemical oxidation of electron neutral arenes using a catalyst designed for preassociation.

In the context of reductive transformations, Lambert and Lin together reported the use of 9,10-dicyanoanthracene (DCA) as a catalyst whose electrochemically reduced state can be used as a photoreductant for the generation of aryl radicals from electron rich aryl chlorides (-2.9 V vs. SCE for 4-chloroanisole).³⁸ This is an interesting case in which a precedent two-photon catalyst³⁹ (Figure 1.16 A) is shown to function also via electrochemical generation of the key photoreducing intermediate (Figure 1.16 B). Comparing these two strategies reveals the crucial role of terminal reductant identity. The conditions primarily differ in the use of an amine reductant versus a cathode in a divided cell. Yet, the reaction outcome is dramatically different even though the same photoreductant is presumably being generated under highly similar reaction conditions. One possibility for this stark difference is that the redox byproduct of the amine terminal reductant can act as an oxidant and accept an electron back from the reduced photoactive catalyst, thus decreasing active catalyst concentration. This BET process is expected not to be problematic at electrodes because they maintain reducing potentials after electron transfer.

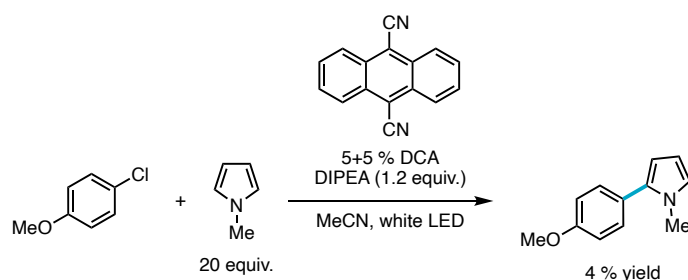
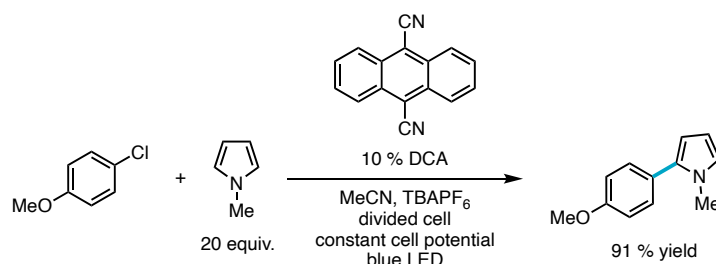
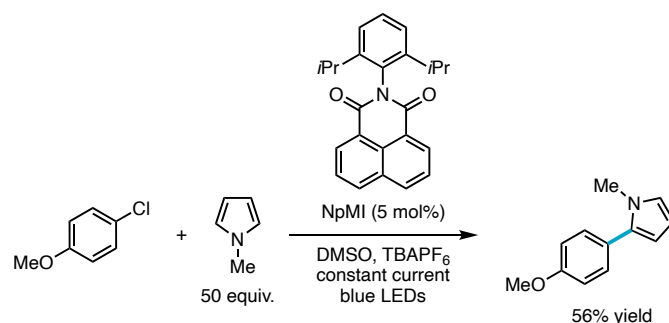
A Two photon process catalyzed by dicyanoanthracene**B** Photoelectrochemical process catalyzed by dicyanoanthracene

Figure: 1.16 Comparison of two-photon and photoelectrochemical electron rich aryl chloride reductions using the same catalyst.

Contemporaneously to the Lambert Lin discovery of an electrochemically generated photoreductant, Wickens disclosed a distinct catalyst structure capable of similar reductive behavior (Figure 1.17 A).⁴⁰ Electrochemical data suggested catalyst decomposition during the reaction. Combined with these data and the commonly accepted dogma that organic radical excited states have short lifetimes, Nocera was inspired to further study the system. Their studies revealed that a species resulting from formal hydride addition was a competent photoreductant (Figure 1.17 B).⁴¹ This provides in situ modification of the photocatalyst to a destabilized anionic closed shell conventional photocatalyst as an alternative mechanism that does not invoke excited states with short lifetimes.

A Photoelectrochemical transformation catalyzed by NpMI



B Active catalyst formed in situ

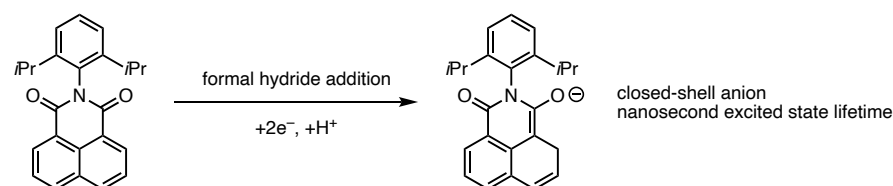


Figure 1.17 Photoelectrochemical reduction of electron-rich aryl chlorides catalyzed by a naphthalene imide. Active closed-shell naphthalene imide catalyst formed in situ.

Building from Wickens' discovery, Barham disclosed a modified version of the naphthalene imide catalyst that proved to be more general for their benzylic phosphate Csp³–O bond cleaving reaction (approximately -2.2 to -2.6 V vs. SCE) (Figure 1.18 A).⁴² Study of the optimal catalyst revealed almost identical electrochemical and photophysical characteristics to the original catalyst. Barham asserts that the key difference between catalyst performance is the ability of the modified catalyst to preassociate with the arene substrates (Figure 1.18 B). As discussed above, this provides a mechanism that obviates the need for long catalyst excited state lifetimes. Stability and possible in situ modification of this version of the catalyst has not yet been evaluated.

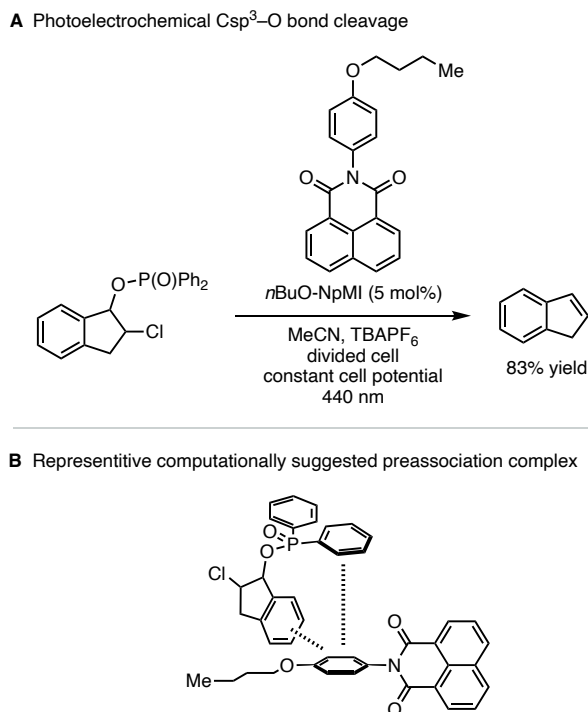


Figure 1.18 Photoelectrochemical Csp³–O bond cleavage catalyzed by a naphthalene imide designed for preassociation.

In a quest to find more stable catalysts compatible with this combined electrochemical and photochemical approach Wickens discovered that many structures with stable electrochemically generated radical anions function as photoreductants. Of the catalysts examined 4DPAIPN proved to be exceptionally effective, enabling the reduction of aryl phosphates (≤ -2.7 V vs. SCE) (Figure 1.19).²⁸ Reactivity onset commensurate with the catalyst reduction potential provides strong evidence for excitation of a cathodically generated species being responsible for product formation. This does not exclude the possibility of cathodic catalyst modification to a more strongly reducing conventional photocatalyst. However, reaction progress kinetic analysis as monitored by current output clearly demonstrated instability of the naphthalene imide catalyst in contrast to the stability of 4DPAIPN. This increased stability presumably translated to greater effectiveness at promoting reductive cleavage reactions.

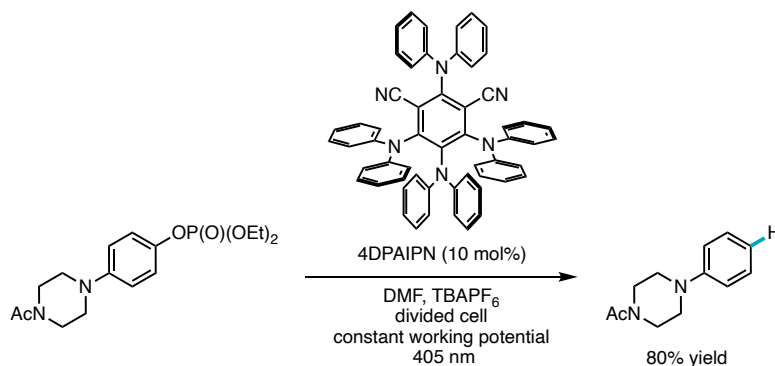


Figure 1.19 Photoelectrochemical aryl phosphate reduction catalyzed by a cyanoarene donor-acceptor catalyst.

This combination of electrochemistry and photochemistry draws strong analogy to the previously discussed two-photon processes. Either via PET or direct electrolysis, an electronically destabilized catalyst is generated that can then act as a potent photoredox catalyst. Although these approaches are simply different ways to access similar intermediates, drastic reaction outcomes have been observed under comparable conditions. A major difference, particularly when using divided cells, is a spatial separation of the active photocatalyst from the terminal redox reagent byproducts. In addition, electrodes with their modular potentials act as effectively limitless sources or sinks of electrons allowing for catalyst speciation to be driven to the electronically activated state. These differences limit BET and provide high concentrations of active catalyst in the electrochemical systems, enabling often more effective reactions.

1. 5. Terminal redox reagent byproducts that promote reactions

As discussed in the previous sections, potent photoredox activity can be elicited from catalysts by first destabilizing them either covalently or electronically. PET or direct electrolysis can both be used to accomplish electronic destabilization. However, whenever the catalyst can

be in contact with the redox reagent byproducts, active catalyst generation can be hampered via BET (notably this problem is alleviated when deploying divided cells as the terminal redox reagents and their byproducts are spatially separated in the counter electrode chamber). For example, amine radical cations are the direct single electron oxidation products of commonly employed amine terminal reductants and are expected to spontaneously oxidize reduced catalysts (Figure 1.20 A). This is however not the case when formate is used as a terminal reductant. Following single electron oxidation, the direct redox byproduct of formate can be consumed via a bimolecular decomposition with another equivalent of formate to generate formic acid and carbon dioxide radical anion ($\text{CO}_2^{\bullet-}$) (Figure 1.20 B).⁴³ Based on the reported potential of -2.2 V vs SCE ,⁴⁴ the generation $\text{CO}_2^{\bullet-}$ from formate represents an intriguing scenario wherein oxidation of a mild reductant generates a far more reducing species. Jui leveraged the generation of $\text{CO}_2^{\bullet-}$ from formate in a photocatalytic system for the reduction of aryl halides (Figure 1.20 C).⁴⁵ Photocatalyst selection parameters suggest that the photocatalyst used in this report should be ineffective (most reducing couple, -1.24 V vs. SCE). However, the available pathway to generate $\text{CO}_2^{\bullet-}$ from formate enables reduction of aryl halides surprisingly outside the reach of the employed photocatalyst (-2.1 V vs. SCE for methyl-2-chloro benzoate).

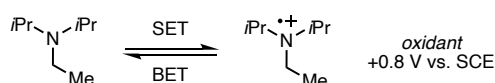
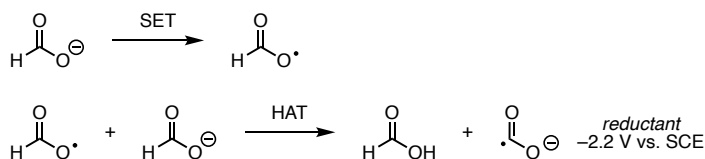
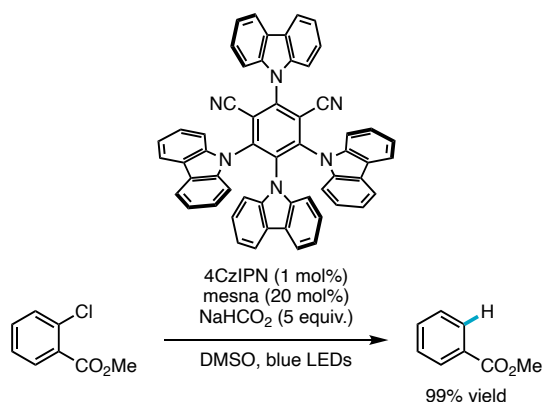
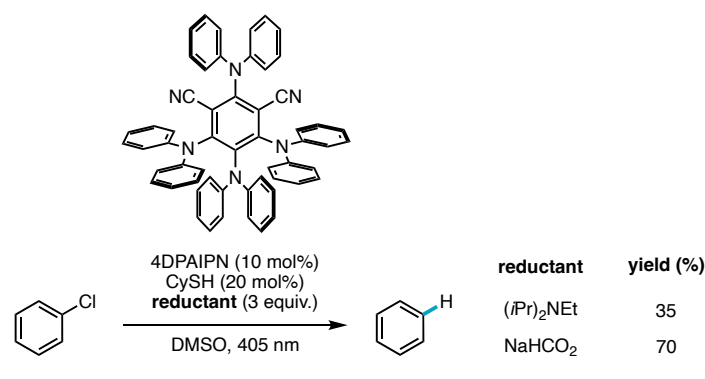
A Formation of oxidizing amine byproduct**B** Formation of highly reducing formate byproduct**C** Photochemical generation of carbon dioxide radical anion from formate for aryl halide reduction

Figure 1.20 Aryl chloride reduction using formate to generate carbon dioxide radical anion.

Wickens, having recently discovered the highly effective diphenyl amine based cyanoarene donor-acceptor catalyst in a combined electrochemical and photochemical mode,²⁸ was interested in adapting the catalyst to a two-photon platform. Initial experiments with amine reductants were unsatisfactory, presumably due to the BET problem that plagues two-photon systems. However, when employing formate as the terminal reductant a dramatic enhancement of reactivity was observed (Figure 1.21 A).²⁹ Beyond hampering BET, the use of formate provides parallel pathways for substrate reduction. CO₂•[−] is itself a potent reductant and can directly reduce some substrates. For more inert substrates, CO₂•[−] can instead reduce and activate the photocatalyst, whose reduced form is an established potent photoreductant.²⁸ Competency of the second pathway is reflected in the substrate scope wherein many substrates that possess

reduction potentials hundreds of millivolts past the reach of $\text{CO}_2^{\bullet-}$ are successfully engaged by the system (Figure 1.21 B).

A Unique effectiveness of formate as a terminal reductant



B Reductive potency beyond the range of carbon dioxide radical anion

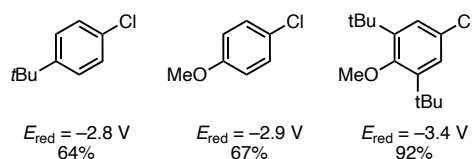


Figure 1.21 Electron-rich aryl chloride reduction using formate to promote a two-photon cycle.

A conceptually related report comes from Leonori in which 4CzIPN is seemingly effective for the reduction of alkyl halides.⁴⁶ This is surprising considering the most reducing redox couple of 4CzIPN (-1.24 V vs. SCE) is insufficient to explain this reactivity by an SET mode (unactivated alkyl halides $< -2 \text{ V}$ vs. SCE). In this report the use of alkyl amine reductants was critical for reactivity and mechanistic studies suggested that carbon-halogen bond cleavage was occurring via a halogen atom transfer pathway with an α -amino radical intermediate (Figure 1.22 A). Like how $\text{CO}_2^{\bullet-}$ can be generated from formate, α -amino radicals can be generated via the oxidation of amines. This discovery provides an alternative mechanism to consider for photoredox reactions in general, particularly those involving the reductive cleavage of halogens. Beyond α -amino radicals displaying this kind of atom transfer behavior, the Leonori group has also reported

cyclohexadienyl radicals to be remarkably effective reductants that proceed through group transfer mechanisms (Figure 1.22 B).⁴⁷ Although not an electron transfer event, this type of behavior is a good example of how a seemingly classic photoredox reactions can function in unexpected ways.

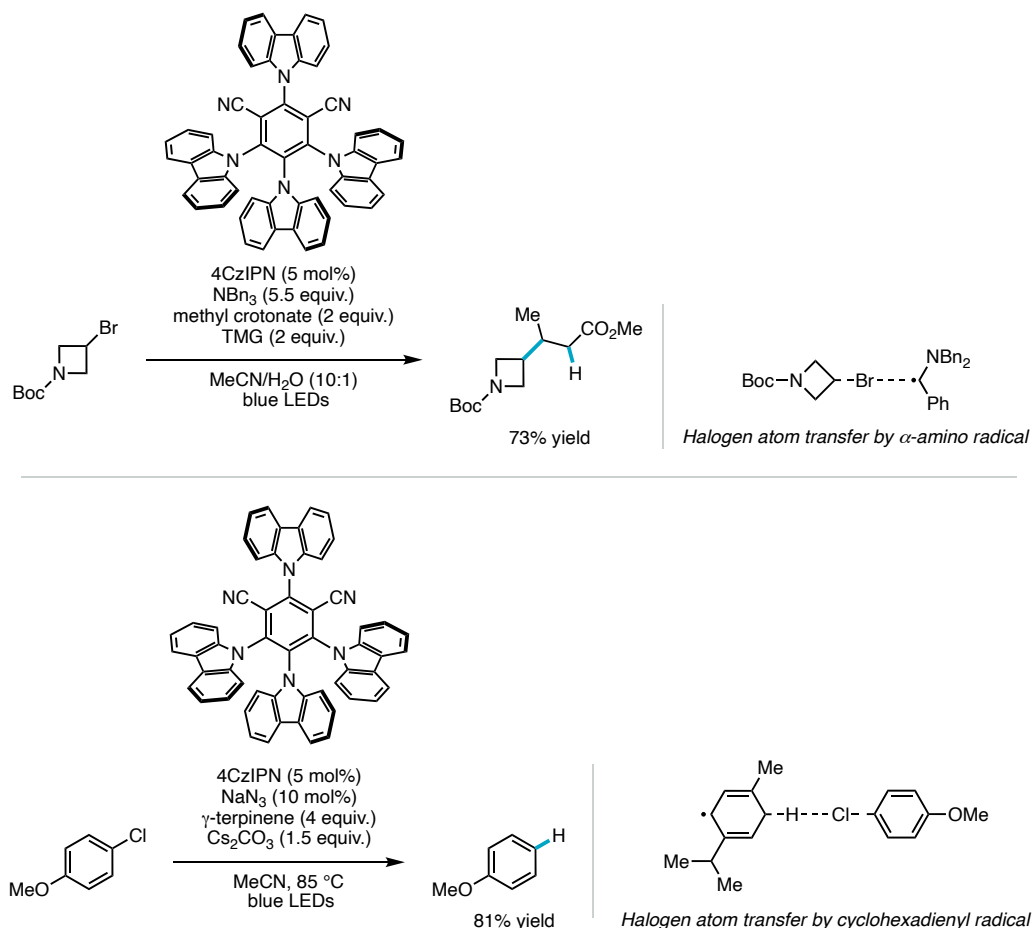


Figure 1.22 Alkyl bromide reduction by photochemically generated α -amino radicals and electron-rich aryl chloride reduction by photochemically generated cyclohexadienyl radicals.

Photoredox reactions that provide surprising results considering classic selection parameters can often be explained by considering other photochemically active species beyond the catalyst that was initially deployed. However, this last section reveals how terminal redox

reagents can be modified by photoredox catalysts into potent redox active species themselves and how they can work in concert to enable unforeseen reactivity.

The enclosed thesis research describes systems in which the classic photoredox paradigm has been broken and how these systems are able to promote challenging redox events. The first chapter will describe how catalysts that function in combined electrochemical/photochemical platforms can be made amenable to purely photochemical process while maintaining the same potent reactivity and radical selectivity. Building from catalysts discovered with electrochemical techniques, this second chapter sharply focuses in on the role of the terminal reductant. These lessons of the non-innocent role of terminal redox reagent byproducts inform the second chapter, which describes the design and development of a highly oxidizing purely photochemical system. The lack of catalysts that promote challenging oxidations in combined electrochemical/photochemical systems that also absorb light before electrochemical oxidation necessitated the identification of a competent catalyst structure. In addition, reaction inhibition by inextricably generated terminal oxidant byproducts necessitated discovery of a cocatalyst capable of inoculating these problematic species. The third and final chapter will describe how terminal reductants that can decompose into a far more potent reductants can be leveraged for challenging reductive chemistry. A major focus of this chapter will be how strong SET reductants are not always sufficient to promote challenging reductive reactions because these transformations consist of elementary steps in addition to ET. Specifically, this chapter will discuss how challenging SET and bond fragmentation can be promoted in concert to enable a challenging reductive cleavage reaction.

1. 6. References

- (1) Narayanam, J. M. R.; Stephenson, C. R. J. Visible Light Photoredox Catalysis: Applications in Organic Synthesis. *Chem. Soc. Rev.* **2010**, *40* (1), 102–113.
- (2) Prier, C. K.; Rankic, D. A.; MacMillan, D. W. C. Visible Light Photoredox Catalysis with Transition Metal Complexes: Applications in Organic Synthesis. *Chem. Rev.* **2013**, *113* (7), 5322–5363.
- (3) Shaw, M. H.; Twilton, J.; MacMillan, D. W. C. Photoredox Catalysis in Organic Chemistry. *J. Org. Chem.* **2016**, *81* (16), 6898–6926.
- (4) Skubi, K. L.; Blum, T. R.; Yoon, T. P. Dual Catalysis Strategies in Photochemical Synthesis. *Chem. Rev.* **2016**, *116* (17), 10035–10074.
- (5) Romero, N. A.; Nicewicz, D. A. Organic Photoredox Catalysis. *Chem. Rev.* **2016**, *116* (17), 10075–10166.
- (6) Marzo, L.; Pagire, S. K.; Reiser, O.; König, B. Visible-Light Photocatalysis: Does It Make a Difference in Organic Synthesis? *Angewandte Chemie International Edition* **2018**, *57* (32), 10034–10072.
- (7) Arias-Rotondo, D. M.; McCusker, J. K. The Photophysics of Photoredox Catalysis: A Roadmap for Catalyst Design. *Chem. Soc. Rev.* **2016**, *45* (21), 5803–5820.
- (8) Wu, C.; Corrigan, N.; Lim, C.-H.; Liu, W.; Miyake, G.; Boyer, C. Rational Design of Photocatalysts for Controlled Polymerization: Effect of Structures on Photocatalytic Activities. *Chem. Rev.* **2022**, *122* (6), 5476–5518.
- (9) McCarthy, B. G.; Pearson, R. M.; Lim, C.-H.; Sartor, S. M.; Damrauer, N. H.; Miyake, G. M. Structure–Property Relationships for Tailoring Phenoxazines as Reducing Photoredox Catalysts. *J. Am. Chem. Soc.* **2018**, *140* (15), 5088–5101.
- (10) Joshi-Pangu, A.; Lévesque, F.; Roth, H. G.; Oliver, S. F.; Campeau, L.-C.; Nicewicz, D.; DiRocco, D. A. Acridinium-Based Photocatalysts: A Sustainable Option in Photoredox Catalysis. *J. Org. Chem.* **2016**, *81* (16), 7244–7249.
- (11) Pistritto, V. A.; Schutzbach-Horton, M. E.; Nicewicz, D. A. Nucleophilic Aromatic Substitution of Unactivated Fluoroarenes Enabled by Organic Photoredox Catalysis. *J. Am. Chem. Soc.* **2020**, *142* (40), 17187–17194.
- (12) Seo, H.; Jamison, T. F. Catalytic Generation and Use of Ketyl Radical from Unactivated Aliphatic Carbonyl Compounds. *Org. Lett.* **2019**, *21* (24), 10159–10163.
- (13) Goldschmid, S. L.; Soon Tay, N. E.; Joe, C. L.; Lainhart, B. C.; Sherwood, T. C.; Simmons, E. M.; Sezen-Edmonds, M.; Rovis, T. Overcoming Photochemical Limitations in Metallaphotoredox Catalysis: Red-Light-Driven C–N Cross-Coupling. *J. Am. Chem. Soc.* **2022**, *144* (49), 22409–22415.
- (14) Schmalzbauer, M.; Marcon, M.; König, B. Excited State Anions in Organic Transformations. *Angewandte Chemie International Edition* **2021**, *60* (12), 6270–6292.
- (15) Das, S.; Natarajan, P.; König, B. Teaching Old Compounds New Tricks: DDQ-Photocatalyzed C–H Amination of Arenes with Carbamates, Urea, and N-Heterocycles. *Chemistry – A European Journal* **2017**, *23* (72), 18161–18165.

- (16) Natarajan, P.; König, B. Excited-State 2,3-Dichloro-5,6-Dicyano-1,4-Benzoquinone (DDQ*) Initiated Organic Synthetic Transformations under Visible-Light Irradiation. *European Journal of Organic Chemistry* **2021**, 2021 (15), 2145–2161.
- (17) Vogt, D. B.; Seath, C. P.; Wang, H.; Jui, N. T. Selective C–F Functionalization of Unactivated Trifluoromethylarenes. *J. Am. Chem. Soc.* **2019**, 141 (33), 13203–13211.
- (18) Ill, J. J. D.; Douglas, J. J.; Nguyen, J. D.; Cole, K. P.; Il, R. A. F.; Stephenson, C. R. J. Ligand Functionalization as a Deactivation Pathway in a Fac-Ir(Ppy)₃-Mediated Radical Addition. *Chem. Sci.* **2014**, 6 (1), 537–541.
- (19) Donabauer, K.; Maity, M.; Berger, A. L.; Huff, G. S.; Crespi, S.; König, B. Photocatalytic Carbanion Generation – Benzylolation of Aliphatic Aldehydes to Secondary Alcohols. *Chem. Sci.* **2019**, 10 (19), 5162–5166.
- (20) Kong, D.; Munch, M.; Qiqige, Q.; Cooze, C. J. C.; Rotstein, B. H.; Lundgren, R. J. Fast Carbon Isotope Exchange of Carboxylic Acids Enabled by Organic Photoredox Catalysis. *J. Am. Chem. Soc.* **2021**, 143 (5), 2200–2206.
- (21) Connell, T. U.; Fraser, C. L.; Czyz, M. L.; Smith, Z. M.; Hayne, D. J.; Doeven, E. H.; Agugiaro, J.; Wilson, D. J. D.; Adcock, J. L.; Scully, A. D.; Gómez, D. E.; Barnett, N. W.; Polyzos, A.; Francis, P. S. The Tandem Photoredox Catalysis Mechanism of [Ir(Ppy)₂(Dtb-Bpy)]⁺ Enabling Access to Energy Demanding Organic Substrates. *J. Am. Chem. Soc.* **2019**, 141 (44), 17646–17658.
- (22) Wang, S.; Wang, H.; König, B. Photo-Induced Thiolate Catalytic Activation of Inert Caryl-Hetero Bonds for Radical Borylation. *Chem* **2021**, 7 (6), 1653–1665.
- (23) Liu, B.; Lim, C.-H.; Miyake, G. M. Visible-Light-Promoted C–S Cross-Coupling via Intermolecular Charge Transfer. *J. Am. Chem. Soc.* **2017**, 139 (39), 13616–13619.
- (24) Jin, S.; Dang, Hang. T.; Haug, G. C.; He, R.; Nguyen, V. D.; Nguyen, V. T.; Arman, H. D.; Schanze, K. S.; Larionov, O. V. Visible Light-Induced Borylation of C–O, C–N, and C–X Bonds. *J. Am. Chem. Soc.* **2020**, 142 (3), 1603–1613.
- (25) Zhang, L.; Jiao, L. Visible-Light-Induced Organocatalytic Borylation of Aryl Chlorides. *J. Am. Chem. Soc.* **2019**, 141 (23), 9124–9128.
- (26) Ghosh, I.; Ghosh, T.; Bardagi, J. I.; König, B. Reduction of Aryl Halides by Consecutive Visible Light-Induced Electron Transfer Processes. *Science* **2014**, 346 (6210), 725–728.
- (27) MacKenzie, I. A.; Wang, L.; Onuska, N. P. R.; Williams, O. F.; Begam, K.; Moran, A. M.; Dunietz, B. D.; Nicewicz, D. A. Discovery and Characterization of an Acridine Radical Photoreductant. *Nature* **2020**, 580 (7801), 76–80.
- (28) Chernowsky, C. P.; Chmiel, A. F.; Wickens, Z. K. Electrochemical Activation of Diverse Conventional Photoredox Catalysts Induces Potent Photoreductant Activity**. *Angewandte Chemie International Edition* **2021**, 60 (39), 21418–21425.
- (29) Chmiel, A. F.; Williams, O. P.; Chernowsky, C. P.; Yeung, C. S.; Wickens, Z. K. Non-Innocent Radical Ion Intermediates in Photoredox Catalysis: Parallel Reduction Modes Enable Coupling of Diverse Aryl Chlorides. *J. Am. Chem. Soc.* **2021**, 143 (29), 10882–10889.
- (30) Xu, J.; Cao, J.; Wu, X.; Wang, H.; Yang, X.; Tang, X.; Toh, R. W.; Zhou, R.; Yeow, E. K. L.; Wu, J. Unveiling Extreme Photoreduction Potentials of Donor–Acceptor Cyanoarenes to Access Aryl Radicals from Aryl Chlorides. *J. Am. Chem. Soc.* **2021**, 143 (33), 13266–13273.

- (31) Widness, J. K.; Enny, D. G.; McFarlane-Connelly, K. S.; Miedenbauer, M. T.; Krauss, T. D.; Weix, D. J. CdS Quantum Dots as Potent Photoreductants for Organic Chemistry Enabled by Auger Processes. *J. Am. Chem. Soc.* **2022**, *144* (27), 12229–12246.
- (32) Melnychuk, C.; Guyot-Sionnest, P. Multicarrier Dynamics in Quantum Dots. *Chem. Rev.* **2021**, *121* (4), 2325–2372.
- (33) Targos, K.; Williams, O. P.; Wickens, Z. K. Unveiling Potent Photooxidation Behavior of Catalytic Photoreductants. *J. Am. Chem. Soc.* **2021**, *143* (11), 4125–4132.
- (34) Gosztola, D.; Niemczyk, M. P.; Svec, W.; Lukas, A. S.; Wasielewski, M. R. Excited Doublet States of Electrochemically Generated Aromatic Imide and Diimide Radical Anions. *J. Phys. Chem. A* **2000**, *104* (28), 6545–6551.
- (35) Cole, J. P.; Chen, D.-F.; Kudisch, M.; Pearson, R. M.; Lim, C.-H.; Miyake, G. M. Organocatalyzed Birch Reduction Driven by Visible Light. *J. Am. Chem. Soc.* **2020**, *142* (31), 13573–13581.
- (36) Huang, H.; Strater, Z. M.; Rauch, M.; Shee, J.; Sisto, T. J.; Nuckolls, C.; Lambert, T. H. Electrophotocatalysis with a Trisaminocyclopropenium Radical Dication. *Angewandte Chemie International Edition* **2019**, *58* (38), 13318–13322.
- (37) Wu, S.; Žurauskas, J.; Domański, M.; S. Hitzfeld, P.; Butera, V.; J. Scott, D.; Rehbein, J.; Kumar, A.; Thyraug, E.; Hauer, J.; P. Barham, J. Hole-Mediated Photoredox Catalysis: Tris(*p*-Substituted)Biarylammonium Radical Cations as Tunable, Precomplexing and Potent Photooxidants. *Organic Chemistry Frontiers* **2021**, *8* (6), 1132–1142.
- (38) Kim, H.; Kim, H.; Lambert, T. H.; Lin, S. Reductive Electrophotocatalysis: Merging Electricity and Light To Achieve Extreme Reduction Potentials. *J. Am. Chem. Soc.* **2020**, *142* (5), 2087–2092.
- (39) Neumeier, M.; Sampedro, D.; Májek, M.; de la Peña O'Shea, V. A.; Jacobi von Wangelin, A.; Pérez-Ruiz, R. Dichromatic Photocatalytic Substitutions of Aryl Halides with a Small Organic Dye. *Chem. Eur. J.* **2018**, *24* (1), 105–108.
- (40) Cowper, N. G. W.; Chernowsky, C. P.; Williams, O. P.; Wickens, Z. K. Potent Reductants via Electron-Primed Photoredox Catalysis: Unlocking Aryl Chlorides for Radical Coupling. *J. Am. Chem. Soc.* **2020**, *142* (5), 2093–2099.
- (41) Rieth, A. J.; Gonzalez, M. I.; Kudisch, B.; Nava, M.; Nocera, D. G. How Radical Are “Radical” Photocatalysts? A Closed-Shell Meisenheimer Complex Is Identified as a Super-Reducing Photoreagent. *J. Am. Chem. Soc.* **2021**, *143* (35), 14352–14359.
- (42) Tian, X.; Karl, T. A.; Reiter, S.; Yakubov, S.; de Vivie-Riedle, R.; König, B.; Barham, J. P. Electro-Mediated PhotoRedox Catalysis for Selective C(Sp³)–O Cleavages of Phosphinated Alcohols to Carbanions. *Angewandte Chemie International Edition* **2021**, *60* (38), 20817–20825.
- (43) Jacobsen, E.; Roberts, J. L.; Sawyer, D. T. Electrochemical Oxidation of Formate in Dimethylsulfoxide at Gold and Platinum Electrodes. *Journal of Electroanalytical Chemistry and Interfacial Electrochemistry* **1968**, *16* (3), 351–360.
- (44) Koppenol, W. H.; Rush, J. D. Reduction Potential of the Carbon Dioxide/Carbon Dioxide Radical Anion: A Comparison with Other C1 Radicals. *J. Phys. Chem.* **1987**, *91* (16), 4429–4430.
- (45) Hendy, C. M.; Smith, G. C.; Xu, Z.; Lian, T.; Jui, N. T. Radical Chain Reduction via Carbon Dioxide Radical Anion (CO₂^{•-}). *J. Am. Chem. Soc.* **2021**, *143* (24), 8987–8992.

- (46) Constantin, T.; Zanini, M.; Regni, A.; Sheikh, N. S.; Juliá, F.; Leonori, D. Aminoalkyl Radicals as Halogen-Atom Transfer Agents for Activation of Alkyl and Aryl Halides. *Science* **2020**, 367 (6481), 1021–1026.
- (47) Constantin, T.; Górski, B.; Tilby, M. J.; Chelli, S.; Juliá, F.; Llaveria, J.; Gillen, K. J.; Zipse, H.; Lakhdar, S.; Leonori, D. Halogen-Atom and Group Transfer Reactivity Enabled by Hydrogen Tunneling. *Science* **2022**, 377 (6612), 1323–1328.

**Chapter 2: Non-innocent radical ion intermediates in
photoredox catalysis: parallel reduction modes enable
coupling of diverse aryl chlorides**

Adapted with permission from Alyah F. Chmiel, **Oliver P. Williams**, Colleen P. Chernowsky, Charles S. Yeung, and Zachary K. Wickens. Non-innocent Radical Ion Intermediates in Photoredox Catalysis: Parallel Reduction Modes Enable Coupling of Diverse Aryl Chlorides. *J. Am. Chem. Soc.* **2021**, 143, 29, 10882–10889. Copyright 2021 American Chemical Society.

2. 1. Abstract

We describe a photocatalytic system that elicits potent photoreductant activity from conventional photocatalysts by leveraging radical anion intermediates generated in situ. The combination of an isophthalonitrile photocatalyst and sodium formate promotes diverse aryl radical coupling reactions from abundant but difficult to reduce aryl chloride substrates. Mechanistic studies reveal two parallel pathways for substrate reduction both enabled by a key terminal reductant byproduct, carbon dioxide radical anion.

2. 2. Introduction

Reductive activation of organic molecules via single electron transfer (SET) is a fundamental elementary step that underpins diverse and powerful synthetic transformations.¹⁻⁴ Photoredox catalysis promotes SET through conversion of energy from visible light into chemical redox potential and has enabled a suite of carbon-carbon and carbon-heteroatom bond-forming reactions.⁵⁻⁹ When considering whether a substrate will be suitable for photoredox reduction, two primary catalyst parameters are initially considered: (1) $E_{1/2}(\text{PC}^{*+}/\text{PC}^*)$ and (2) $E_{1/2}(\text{PC}/\text{PC}^{\cdot-})$.^{7,10,11} These values reflect redox potentials bounded by the energy of photons in the visible region, a limitation compounded by energy losses to intersystem crossing.¹² As a result, many abundant but challenging to reduce substrates are excluded from photoredox activation based on these guidelines (Figure 2.1 A).¹³⁻¹⁵

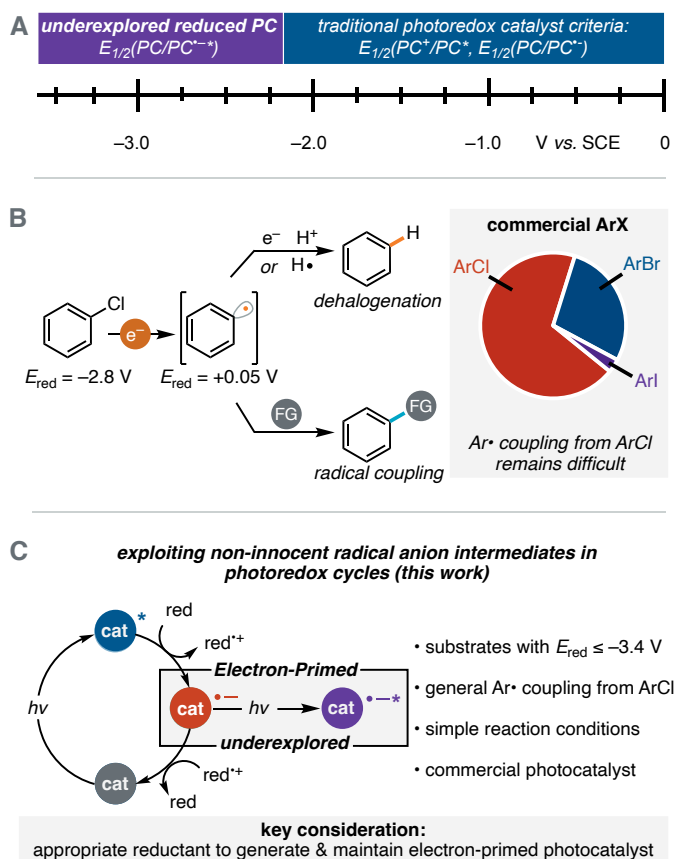


Figure 2.1 **A** Energy limitations for photoredox catalysis and electron-primed photoredox catalysis. **B** Aryl chlorides abundance and reactivity as aryl radical precursors. **C** Strategy employing chemical reductants to exploit electron-primed photoredox catalysis. All V vs. SCE.

Aryl radicals are reactive intermediates that engage in a myriad of synthetically valuable transformations.^{16–18} Classically, aryl radical intermediates are generated from aryl diazonium salts, iodides, or bromides.^{19–29} Aryl chlorides are rarely used as radical precursors despite the fact they comprise over two thirds³⁰ of commercially available aryl halides (Figure 2.1 B).^{31–35} This is a consequence of their resistance to reductive activation,¹³ and high $\text{C}(\text{sp}^2)\text{--Cl}$ BDE.^{36,37} König recently pioneered an elegant strategy, termed consecutive photoinduced electron transfer (conPET), wherein a photochemically generated radical anion is subsequently excited.^{38,39} This approach primes the photocatalyst with an electron prior to excitation and, in principle, can generate much deeper reduction potentials through $E_{1/2}(\text{PC}/\text{PC}^{\bullet-})$. Indeed, later implementations

of this conPET strategy unlocked exceptionally challenging reductions.^{40,41} However, all recent advances in visible light photoredox methods that reduce electronically diverse chloroarenes have been limited to proteodefunctionalization and borylation reactions.^{40,42–45} Recent electrophotocatalytic^{46–49} approaches have directly generated these electron-primed photocatalysts cathodically.^{50,51} While this strategy has begun to expand the range of radical coupling reactions that engage aryl chlorides, a general approach to leverage the expansive pool of aryl chloride substrates in radical couplings has remained elusive and the need for electrochemical equipment remains a barrier in some settings.^{52,53} In particular, net-reductive radical coupling processes, such as alkene hydroarylation,^{54–56} have remained elusive for aryl chloride substrates for all modern methods. We suspect that the paucity of net-reductive processes is a consequence of the intrinsic challenges of circumventing premature reduction of the aryl radical intermediate ($E_{\text{red}}(\text{Ph}^\bullet/\text{Ph}^-) = +0.05 \text{ V vs. SCE}$)⁵⁷ in the presence of a stoichiometric reductant.

Our group recently used electrochemistry to examine a diverse set of organic radical anions for photocatalytic activity in the reductive cleavage of strong $\text{C}(\text{sp}^2)\text{--O}$ and $\text{C}(\text{sp}^2)\text{--N}$ bonds.⁵⁸ These experiments revealed that numerous radical anions, including those derived from commonly employed photoredox catalysts, can serve as potent photocatalytic reductants upon cathodic reduction. These data fit into a growing body of literature from our group⁵⁹ and others^{40,60} that suggest photocatalyst-based redox events can engender more potent activity from conventional photocatalysts. Taken together, these data led us to consider whether we could redesign a photocatalytic system to favor formation of photoactive radical anion intermediates to elicit deeply reducing potentials and expand the repertoire of coupling reactions available from aryl chlorides under operationally simple conditions (Figure 2.1 C). Herein, we disclose that selection of an appropriate reductant to generate and maintain an active electron-primed photoredox catalyst in situ enables reduction potentials far beyond those expected from

conventional catalyst selection criteria. These new reduction conditions promote a diverse array of intermolecular coupling reactions, including net-reductive coupling processes, from readily available aryl chloride substrates.

2. 3. Results and Discussion

We first evaluated a suite of organic compounds recently found to possess photocatalytically active radical anion congeners⁵⁸ for activity in the dehalogenation of PhCl ($E_{\text{red}} = -2.8 \text{ V vs. SCE}$). Considering only conventional photoredox catalyst selection parameters (PC/PC^- and $\text{PC}^+/\text{PC}^{++}$), this reduction would be exceedingly endothermic ($>1 \text{ V}$) for the photocatalysts under investigation. Therefore, activity in this assay would implicate in situ formation of a distinct and potent reductant. Initially, we examined a range of trialkylamine reductants because these are common reductants in photoredox catalysis, including in conPET strategies (Figure 2.2 A).^{38,40,61} We found that each catalyst modestly promoted this energetically demanding dehalogenation reaction. The isophthalonitrile catalysts, which are both excellent neutral chromophores⁶² as well as electron-primed photoredox catalysts,⁵⁸ promoted the reaction most efficiently albeit still in poor yield. To exclude halogen atom transfer (XAT) aryl radical generation,⁶³⁻⁶⁵ we examined the reductive defunctionalization of anilinium and aryl phosphate salts (Figure 2.3). These are each challenging reductive cleavage reactions^{66,67} of non-polarizable leaving groups unlikely to undergo XAT processes. We found both substrates underwent productive defunctionalization, albeit in diminished yield (Figure S13).

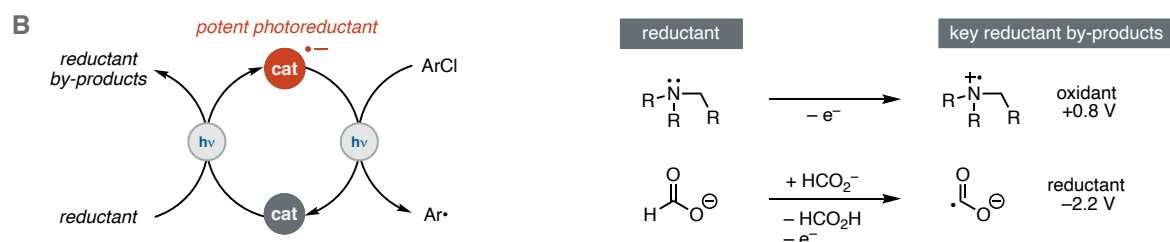
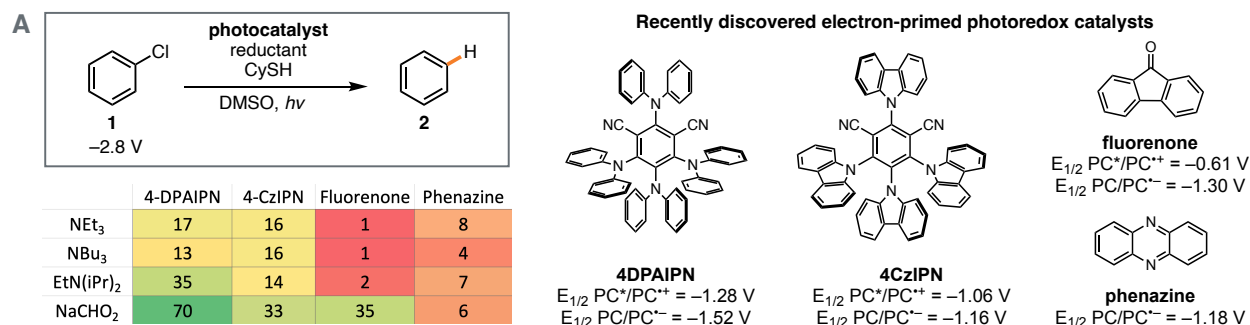


Figure 2.2 A Unlocking radical anion photocatalyst reactivity by evaluation of reductant for catalyst activation. Reactions were conducted on 0.1 mmol scale with 10 mol % 4DPAIPN and 3 equiv. NaCHO₂. Reactions were analyzed via gas chromatography. **B** Overview of key considerations for chemical reductants as catalyst activators. All V vs. SCE.

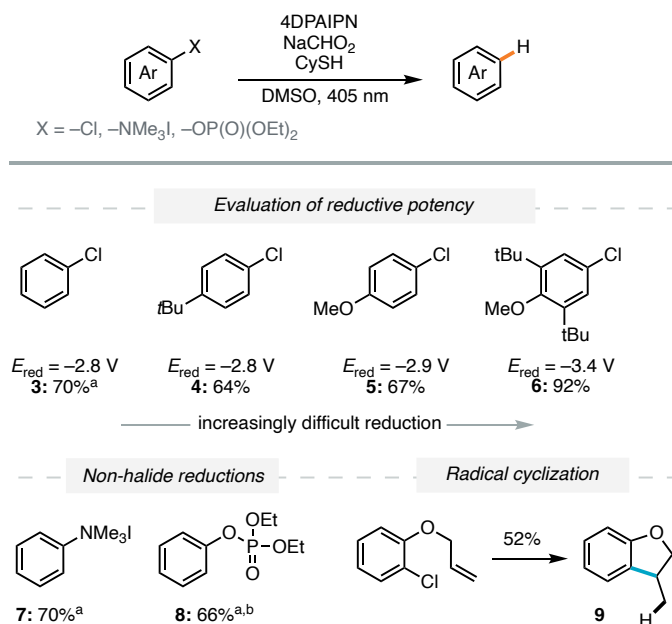


Figure 2.3 Evaluation of catalytic system. Reactions were run on 0.1 mmol scale with 10 mol % 4DPAIPN, 3 equiv NaCHO₂ and 5 mol % CySH. All V vs. SCE. NMR yields. ^aGC yield. ^b 15 mol % 4DPAIPN.

A broader survey of reductants less commonly employed in photoredox catalysis (Figure S14) revealed that sodium formate substantially enhanced the photoreductant activity of 4DPAIPN (Figure 2.2 A). We suspect this improvement occurs because formate salts undergo a second-order hydrogen atom transfer (HAT) process upon oxidation⁶⁸ that results in formic acid and carbon dioxide radical anion.⁶⁹⁻⁷² As a consequence, a second reducing equivalent is liberated from formate after initial oxidation. We suspect that the carbon dioxide radical anion can either reduce another equivalent of photocatalyst or promote the reaction by direct reduction of substrate ($E_{1/2}(\text{CO}_2/\text{CO}_2^{\cdot-}) = -2.2 \text{ V vs. SCE}$).⁷³ In each mechanistic manifold, the SET is rendered irreversible by the release of CO_2 gas. This scenario contrasts starkly with the trialkylamine reductants, which result in oxidizing amine radical cation intermediates ($E_{1/2}(\text{NR}_3^{\cdot+}/\text{NR}_3) = <1 \text{ V vs. SCE}$) that could deactivate the radical anion photocatalyst via back electron transfer (Figure 2.2 B).^{61,74,75}

We next evaluated the potency of this new catalytic system. Having established that chlorobenzene could be reduced (-2.8 V vs. SCE), we probed dehalogenation of increasingly electron-rich aryl chlorides. These experiments revealed that substrates with reduction potentials as low as -3.4 V vs. SCE are efficiently reduced. Additionally, these conditions promoted the challenging reductive cleavage of both an anilinium and aryl phosphate substrate. Taken together, these data clearly implicate processes beyond a conventional photoredox manifold. For example, the reduction of **6** would be predicted to be endothermic by nearly 2 V ($>40 \text{ kcal/mol}$ at room temperature) based on the most reducing conventional redox couple of 4DPAIPN ($E_{1/2}(\text{PC}/\text{PC}^{\cdot-}) = -1.5 \text{ V vs. SCE}$).⁷⁶ We next attempted to validate the intermediacy of an aryl radical in this formate driven system. As anticipated, these conditions furnished the five-membered ring product **9** in high selectivity for radical cyclization. Despite its exceptionally reducing potentials, we suspected that this operationally simple procedure would be amenable to high-throughput techniques widely employed in medicinal chemistry. To this end, we rapidly evaluated the

tolerance of complex drug-like scaffolds using a commercially available informer plate designed to challenge modern cross-coupling technology. We found that not only was photocatalytic activity retained in the well-plate format but that several of these functional group rich molecules were effectively transformed (Figure S16).

Although, in principle, aryl radicals are highly versatile synthetic intermediates, premature reduction precludes radical coupling reactions in many cases. This is particularly problematic when potent reductants are required. To evaluate selectivity for radical coupling, we targeted redox-neutral photo-Arbuzov and radical borylation processes. These established aryl radical transformations produce biologically relevant aryl phosphonates⁷⁷ and versatile organoboron products.⁷⁸ In both cases, we found that chloroarene substrates readily underwent the desired radical coupling process.⁷⁹ We found that both difficult to reduce electron-rich aryl chlorides and substrates bearing potentially reducible functional groups such as esters and amides were well-tolerated (Figure 2.4). Furthermore, the catalytic system tolerated medically relevant heterocycles.

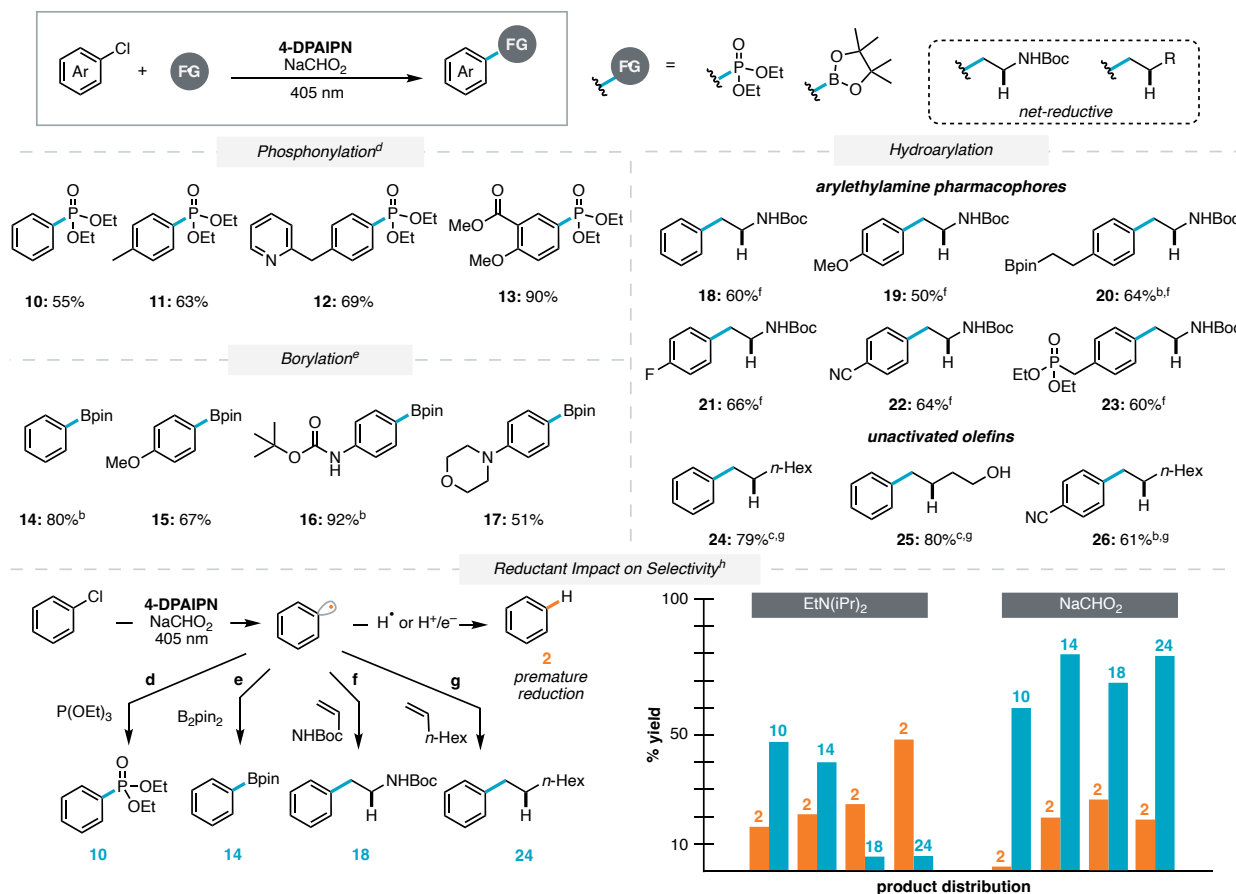


Figure 2.4 Intermolecular couplings from challenging aryl chloride precursors. ^aReactions were run on 0.4 mmol scale. Isolated yield unless otherwise noted. ^bNMR yield. ^cGC yield. ^dReactions were run with 4DPAIPN (12-15 mol %), NaCHO₂ (3 equiv), P(OEt)₃ (5 equiv). ^eReactions were run with 4DPAIPN (5 mol %), NaCHO₂ (3 equiv), B₂pin₂ (3 equiv) and Cs₂CO₃ (3 equiv). ^fReactions were run with 4DPAIPN (6 mol %), NaCHO₂ (3 equiv), N-vinyl carbamate (2.5 equiv) and CySH (5 mol %). ^gReactions were run with 4DPAIPN (6 mol %), NaCHO₂ (3 equiv), alkene (5 equiv) and CySH (5 mol %). ^hReactions were run with conditions d-g, using either EtN(iPr)₂ or NaCHO₂ as the reductant. See SI for details.

Next, we evaluated the reductive hydroarylation of alkenes. This challenging aryl radical reaction requires precise control over the relative rates of radical coupling versus proteodehalogenation. HAT is mechanistically required to furnish product and cannot be simply suppressed. Initially, we targeted the synthesis of arylethylamines via hydroarylation. Recently, Jui and coworkers reported that aryl radical intermediates productively couple with vinyl carbamates to produce the arylethylamine pharmacophore.⁵⁶ Although one of the most reducing

conventional photocatalysts was employed, the majority of the reaction scope was comprised of aryl iodide substrates and only aryl chloride substrates bearing withdrawing groups were viable. Intriguingly, we found that although the vinylcarbamate substrate is thermodynamically easier to reduce than most chloroarenes ($E_{\text{red}} = -2.2 \text{ V vs. SCE}$), these potent reductive conditions selectively transformed chlorobenzene into *N*-Boc phenethylamine in high yield. Even as the gap between the chloroarene and vinyl carbamate coupling partner widens, synthetically useful aryloethylamine yields are still observed. Similar to the other radical couplings, we found aryl chlorides bearing reductively sensitive functional groups were tolerated. We also found these conditions promoted the coupling of aryl chlorides and unactivated alkenes despite the fact that such a hydroarylation remains challenging with any aryl radical precursor.⁸⁰ Finally, we questioned whether formate was uniquely effective for each of these radical coupling reactions or whether alkylamines were suitable terminal reductants. While $\text{EtN}(i\text{-Pr})_2$ and 4DPAIPN promote photoreduction of chlorobenzene, both reactivity and radical selectivity were diminished in each coupling reaction. Of note, competitive proteodehalogenation nearly precluded net-reductive hydroarylation when alkylamines were used.⁸¹

Having established a generally applicable catalytic system to engage aryl chloride substrates in radical coupling reactions, we next conducted a preliminary mechanistic investigation into the process. First, we probed whether an electron-primed photoredox mechanism—wherein the 4DPAIPN radical anion is generated and subsequently excited—was feasible under these conditions. We irradiated a mixture of 4DPAIPN and sodium formate while monitoring speciation by UV–Vis (Figure 2.5 A). This resulted in a decrease in 4DPAIPN features and growth of new features consistent with electrochemically reduced 4DPAIPN (Figure S20). Next, we probed the photoreduction of aryl chlorides. Chlorobenzene was added to the reaction mixture and, upon irradiation, the UV–Vis features of 4DPAIPN were restored (Figure 2.5 B). As expected based on the $>1 \text{ V}$ underpotential, no return of 4DPAIPN was observed upon addition

of chlorobenzene to 4DPAIPN radical anion in the absence of light. Consistent with this mechanistic picture, Stern–Volmer analysis resulted in no measurable quenching of excited 4DPAIPN by chlorobenzene. In contrast, formate salts did quench the excited state. Cyclohexane thiol, which was added to the net-reductive transformations as an HAT co-catalyst, also quenches the excited state and likely mediates the electron-transfer events in these systems by an analogous mechanism (Figure S18). Taken together, these experiments are consistent with our working hypothesis that photooxidation of formate results in the 4DPAIPN radical anion which can be subsequently excited to photoreduce chlorobenzene and return 4DPAIPN.

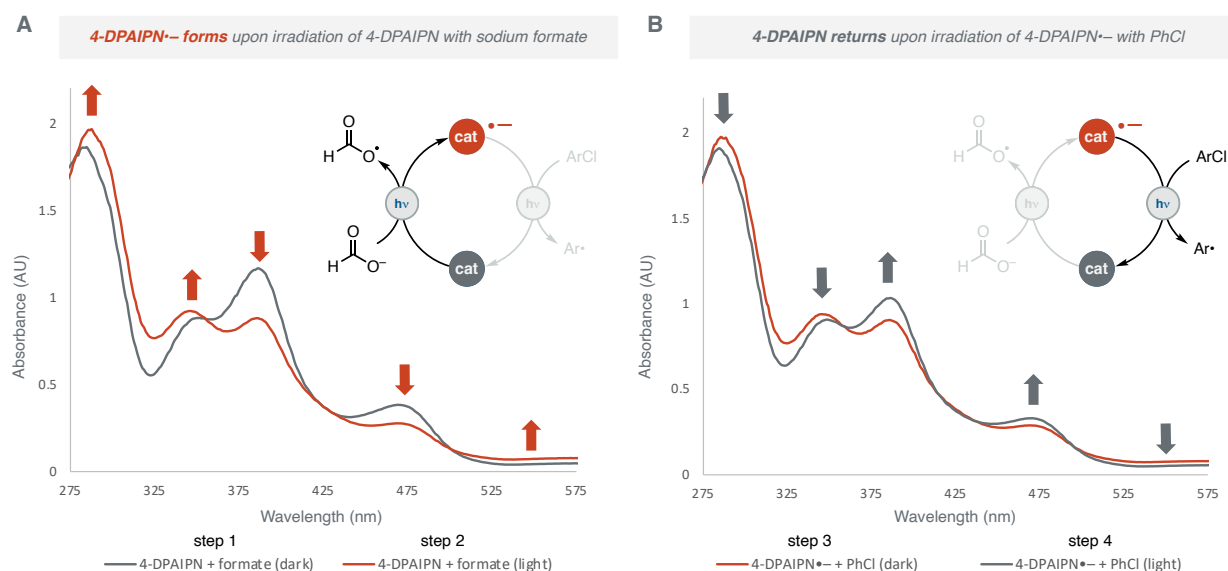


Figure 2.5 **A** UV–vis spectrum demonstrating 4DPAIPN•- generation in the presence of sodium formate and light. **B** UV–vis spectrum demonstrating that 4-DPAIPN•- reverts to 4-DPAIPN upon exposure to PhCl and subsequent irradiation.

While the UV–Vis experiments indicate that an electron-primed photoredox mechanism is feasible, we recognized that carbon dioxide radical anion is sufficiently reducing ($E_{\text{red}}(\text{CO}_2/\text{CO}_2^{\bullet-}) = -2.2 \text{ V vs. SCE}$)⁷³ to promote reductive fragmentation of some of the aryl chloride substrates studied without the intervention of an electron-primed photoredox manifold. To evaluate the

relative contribution of direct substrate reduction by $\text{CO}_2^{\bullet-}$, we attempted to generate this radical anion directly by homolysis of $(\text{PhS})_2$ under 370 nm light in the absence of 4DPAIPN.⁸² We envisioned thiyl radical could abstract a hydrogen atom from formate to directly generate $\text{CO}_2^{\bullet-}$ in situ (Figure S23).^{71,83,84} These conditions resulted in quantitative conversion of 4-chlorobenzonitrile ($E_{\text{red}} = -2.1$ V vs. SCE). However, only 9% conversion of chlorobenzene ($E_{\text{red}} = -2.8$ V vs. SCE) and <5% conversion of 4-chloroanisole ($E_{\text{red}} = -2.9$ V vs. SCE) were observed under these photocatalyst-free conditions. In contrast, all three of these substrates are dehalogenated in comparable efficiency through use of the 4DPAIPN conditions. We suspect both mechanisms operate in parallel for substrates within the bound of the potency of $\text{CO}_2^{\bullet-}$ (-2.2 V vs. SCE) but that an electron-primed photoredox manifold supports more thermodynamically demanding reductions. In both cases, the $\text{CO}_2^{\bullet-}$ reductant byproduct plays an active role either (a) reducing the substrate directly or (b) reducing the photocatalyst to reactivate it without requiring persistent multiphoton excitation (Figure 2.6).

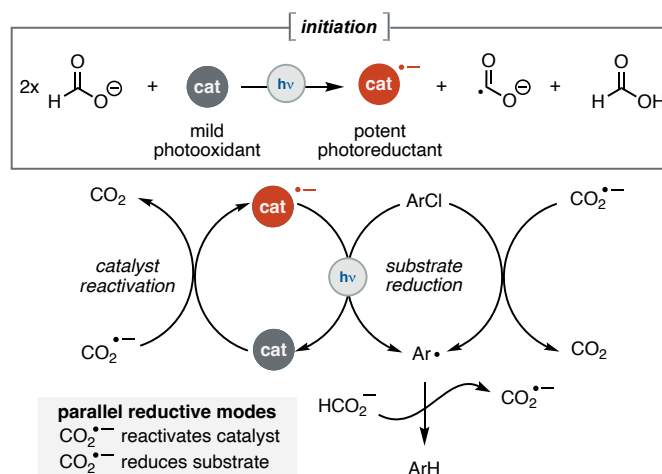


Figure 2.6 Plausible mechanism for aryl chloride reduction and the roles of formate and its by-products.

2. 4. Conclusions

Overall, we have illustrated that use of a formate-based terminal reductant in combination with an isophthalonitrile photocatalyst can engage aryl chlorides in diverse synthetically useful coupling reactions. We anticipate that these operationally simple reaction conditions comprise a broadly useful approach to photochemically induce difficult reductive processes. Beyond the immediate synthetic utility, these results are important because they challenge the notion that the terminal reductant can be viewed as merely an electron-source to turn over the photocatalyst. These data fit within a growing body of literature that suggests terminal reductant byproducts can play a non-innocent role in photoredox catalysis.^{64,65,74} We suspect that these results could also offer an alternative explanation for recent examples wherein isophthalonitrile catalysts have appeared to reduce substrates beyond their expected redox potentials^{65,85} and, more broadly, illustrate the importance of radical ion intermediates in photoredox catalysis.

2. 5. Experimental

2. 5. 1. General Methods and Materials

Unless otherwise noted, reactions were performed under an inert N₂ atmosphere in anhydrous DMSO thoroughly degassed by freeze-pump-thaw. Anhydrous DMSO was purchased from DriSolv. Crude mixtures were evaluated by thin-layer chromatography using EMD/Merck silica gel 60 F254 pre-coated plates (0.25 mm) and were visualized by UV, CAM, p- anisaldehyde, or KMnO₄ staining. Flash chromatography was performed with a Biotage Isolera One automated chromatography system with re-packed silica columns (technical grade silica, pore size 60 Å, 230-400 mesh particle size, 40-63 particle size). Purified materials were dried in vacuo (0.050 Torr) to remove trace solvent. ¹H, ¹³C, ³¹P Spectra were taken using a Bruker Avance-400

with a BBFO Probe or a Bruker Avance-500 with a DCH Cryoprobe. NMR data are reported relative to residual CHCl_3 (1 H, $\delta = 7.26$ ppm), CDCl_3 (13 C, $\delta = 77.16$ ppm). Data for 1 H NMR spectra are reported as follows: chemical shift (δ ppm) (multiplicity, coupling constant (Hz), integration). Multiplicity and qualifier abbreviations are as follows: s = singlet, d = doublet, t = triplet, q = quartet, m = multiplet, br = broad. GC traces were taken on an Agilent 7890A GC with dual DB-5 columns (20 m \times 180 μm \times 0.18 μm), dual FID detectors, and hydrogen as the carrier gas.

2. 5. 2. Experimental Setup

LEDs used in this study were purchased from HepatoChem (PAR20- 18W LG 405 nm) and Kessil (KSPR160L-390, KSPR160L-440, KSPR160L-370).

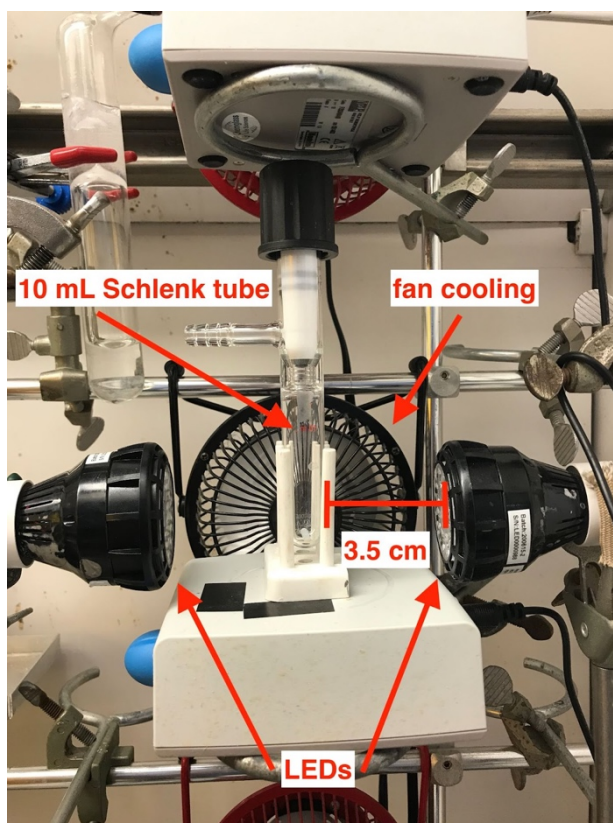
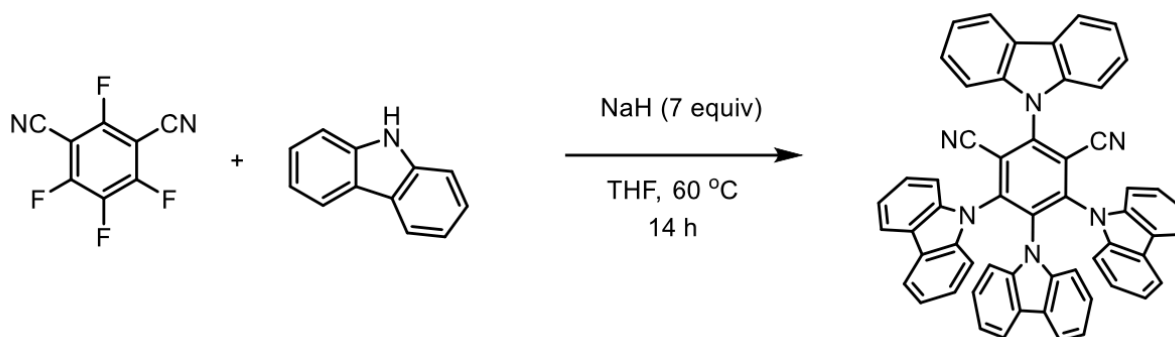


Figure 2. S1. Standard setup for photoredox reactions with either 1 or 2 LEDs depending on the transformation. See **General Experimental Procedures for Photoredox Reductions** for details.

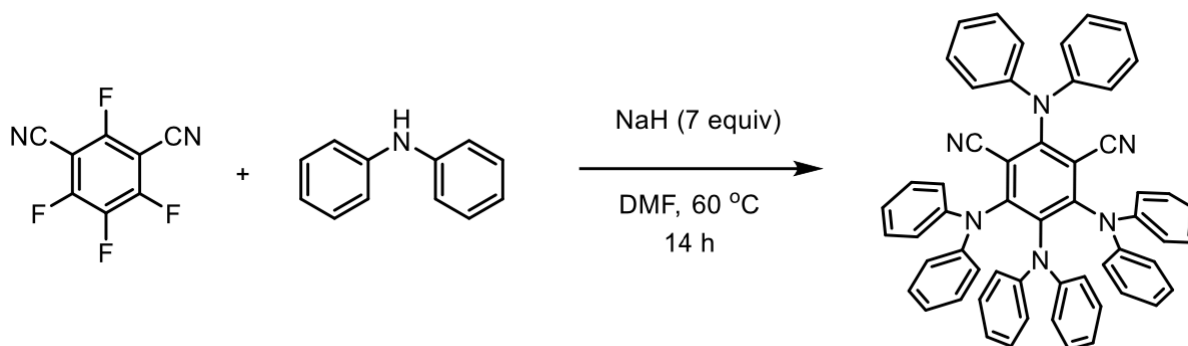
2. 5. 3. Preparation of Catalysts and Starting Materials

2,4,5,6-tetra(9H-carbazol-9-yl)isophthalonitrile (**4-CzIPN**)

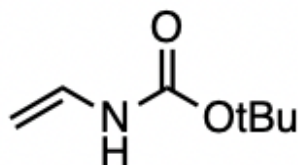


To a flame-dried flask under N₂, NaH (60% dispersion, 3.0 g, 75 mmol, 7 equiv) was added and evacuated then backfilled with N₂ three times. THF (100 mL) was added to the flask followed by 1-H-carbazole (8.4 g, 50 mmol, 5 equiv) in THF (25 mL). The carbazole solution was slowly added to the flask then heated to 60 °C and stirred for 1 hour. 2,4,5,6-tetrafluoroisophthalonitrile (2.0 g, 10 mmol, 1 equiv) in THF (25 mL) was slowly added to the reaction mixture. The solution was then cooled and stirred at 40 °C overnight. After cooling the reaction to room temperature, excess NaH was quenched with isopropanol. Water (200 mL) was then added to precipitate the crude product. The precipitate was filtered then washed with excess water and dried *in vacuo*. The crude product dissolved in DCM then filtered through a silica plug and recrystallized from DCM hexanes to provide pure product as a yellow solid (6.2 g, 8.2 mmol, 82 %). ¹H NMR (500 MHz, CDCl₃) δ 8.24 (d, J = 7.8 Hz, 2H), 7.73 (m, 8H), 7.51 (ddd, J = 8.0, 6.7, 1.5 Hz, 2H) 7.35 (m, 2H), 7.25 (dd, J = 7.8, 1.4 Hz, 4H), 7.11 (tt, J = 7.4, 5.8 Hz, 8H), 6.85 (m, 4H), 6.65 (td, J = 7.7, 1.2 Hz, 2H), consistent with reported spectrum (Chem. Eur. J. 2016, 22, 4889-4898).

2,4,5,6-tetrakis(diphenylamino)isophthalonitrile (4-DPAIPN)

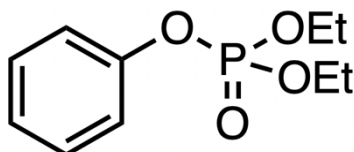


To a flame-dried flask under N₂, NaH (60% dispersion, 3.0 g, 75 mmol, 7 equiv) was added and evacuated then backfilled with N₂ three times. THF (100 mL) was added to the flask followed by diphenylamine (8.5 g, 50 mmol, 5 equiv) in THF (25 mL). The diphenylamine solution was slowly added to the flask then heated to 60 °C and stirred for 1 hour. 2,4,5,6-tetrafluoroisophthalonitrile (2.0 g, 10 mmol, 1 equiv) in THF (25 mL) was slowly added to the reaction mixture. The solution was then cooled and stirred at 40 °C overnight. After cooling the reaction to room temperature, excess NaH was quenched with isopropanol. Water (200 mL) was then added to precipitate the crude product. The precipitate was filtered then washed with excess water and dried *in vacuo*. The crude product dissolved in DCM then filtered through a silica plug and recrystallized from DCM hexanes to provide pure product as a yellow solid (5.0 g, 6.2 mmol, 62%). ¹H NMR (400 MHz, CDCl₃) δ 7.31 – 7.23 (m, 4H), 7.14 – 6.97 (m, 14H), 6.95 – 6.83 (m, 8H), 6.73 – 6.65 (m, 10H), 6.59 – 6.51 (m, 4H), consistent with reported spectrum (Angew. Chem. Int. Ed. 2019, 131, 8266-8270).



tert-butyl vinyl carbamate: Compound was synthesized according to a previous report (*J. Am. Chem. Soc.* 2019, 141, 9, 4147–4153) and 70% yield was obtained as a white crystalline solid.

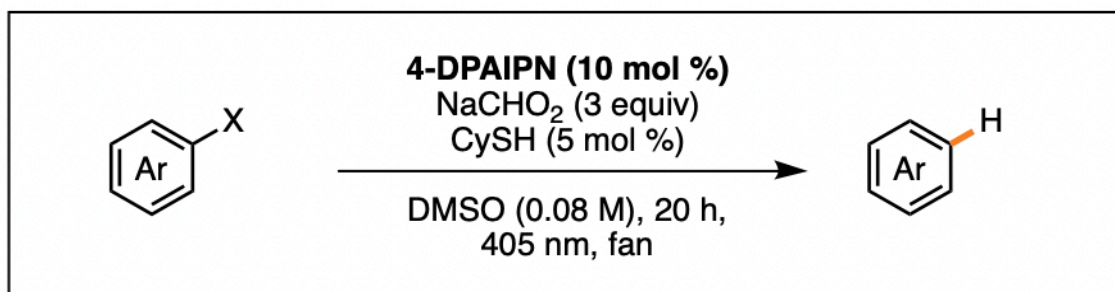
^1H NMR (400 MHz, CDCl_3) δ 6.66 (s, 1H), 6.28 (s, 1H), 4.40 (d, J = 15.7 Hz, 1H), 4.21 (d, J = 8.8 Hz, 1H), 1.47 (s, 9H).



diethyl phenyl phosphate: Compound was synthesized according to a previous report (Chernowsky, Colleen; Chmiel, Alyah; Wickens, Zachary (2021): Photocatalytic Activity of Diverse Organic Radical Anions: Catalyst Discovery Enables Cleavage of Strong $\text{C}(\text{sp}^2)\text{--N}$ and $\text{C}(\text{sp}^2)\text{--O}$ Bonds. ChemRxiv. Preprint. <https://doi.org/10.26434/chemrxiv.14710398.v1>) and 68% yield was obtained as a colorless oil. **^1H NMR** (400 MHz, CDCl_3) δ 7.33 (dd, J = 8.6, 7.2 Hz, 2H), 7.24 – 7.19 (m, 2H), 7.16 (t, J = 7.2 Hz, 1H), 4.29 – 4.14 (m, 4H), 1.34 (td, J = 7.1, 1.1 Hz, 6H).

2. 5. 4. General Experimental Procedures for Photoredox Reductions

General Procedure A — Dehalogenation



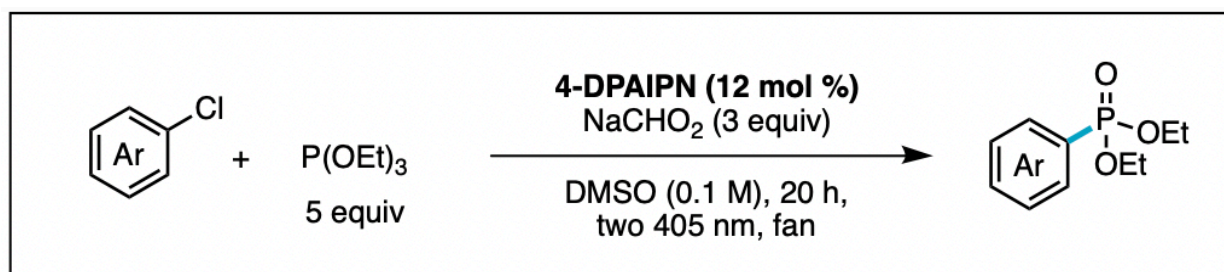
To an oven-dried 10 mL schlenk tube equipped with a stir bar, 4-DPAIPN (0.01 mmol, 10 mol %) and sodium formate (0.3 mmol, 3 equiv) were added. The tube was evacuated and backfilled with N_2 three times. While under active N_2 , cyclohexylthiol (0.005 mmol, 5 mol %) and chlorobenzene (0.1 mmol, 1 equiv) were added to the schlenk tube followed by DMSO (1.25 mL, 0.08 M). The

schlenk tube was sealed under N₂ then stirred and irradiated with a 405 nm LED (3.5 cm from glass surface with fan cooling for 20 hours.

For GC analyses: After reaction completion, mesitylene (14 μ L, 0.1 mmol, 1 equiv) was added as the internal standard to the crude mixture. 0.1 mL aliquot was removed from the crude and quenched with 1 mL water then extracted with 1 mL diethyl ether. Diethyl ether layer was filtered through a silica pipette plug then ran on the GC.

For NMR analyses: Added CH₂Br₂ as the internal standard (7 μ L, 0.1 mmol, 1 equiv) to crude reaction mixture. Took 0.1 mL aliquot and quenched with 1 mL water then extracted with 1 mL CDCl₃. Reactions were analyzed via ¹H NMR of the CDCl₃ layer.

General Procedure B — Phosphonylation

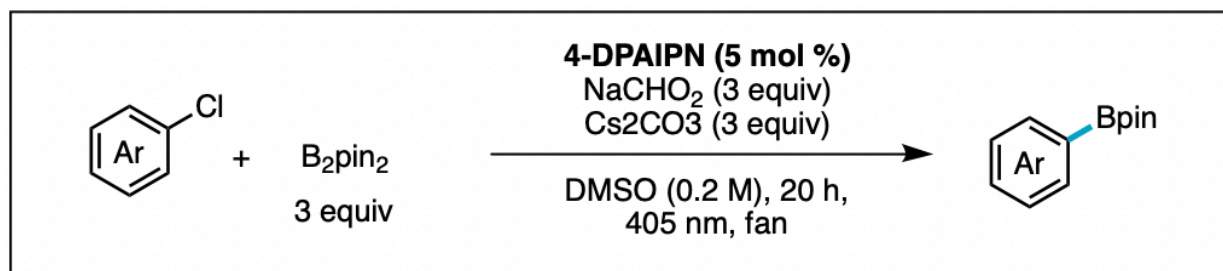


To an oven-dried 10 mL schlenk tube equipped with a stir bar, 4-DPAIPN (0.048 mmol, 12 mol %) and sodium formate (1.2 mmol, 3 equiv) were added. Aryl chloride (0.4 mmol, 1 equiv) and triethyl phosphite (2.0 mmol, 5 equiv) were added to the schlenk tube followed by DMSO (4 mL, 0.1 M). The reaction mixture was freeze-pump-thawed then sealed under N₂ and stirred and irradiated with two 405 nm LEDs (4.5 cm from glass surface on each side of the tube with fan

cooling) for 20 hours. After reaction completion, the reaction was quenched with 50 mL NaHCO_3 (aq) and extracted with 30 mL EtOAc three times. The combined EtOAc layer was washed with 50 mL brine then dried over Na_2SO_4 . The mixture was filtered and concentrated in vacuo then purified by flash chromatography with silica.

For NMR analyses: After reaction completion, CH_2Br_2 was added as the internal standard to crude reaction mixture. 0.1 mL aliquot was removed and quenched with 1 mL water then extracted with 1 mL CDCl_3 . Reactions were analyzed via ^1H NMR of the CDCl_3 layer.

General Procedure C — Borylation

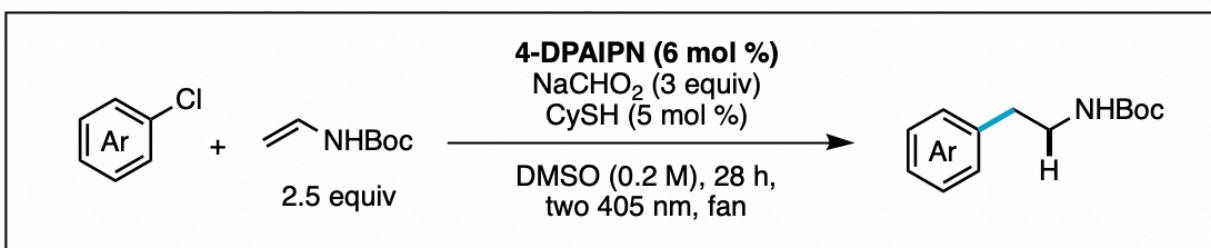


To an oven-dried 10 mL schlenk tube equipped with stir bar, 4-DPAIPN (0.01 mmol, 2.5 mol %), sodium formate (1.2 mmol, 3 equiv), B_2pin_2 (1.2 mmol, 3 equiv), and Cs_2CO_3 (1.2 mmol, 3 equiv) were added. The tube was evacuated and backfilled with N_2 three times. While under active N_2 , aryl chloride (0.4 mmol, 1 equiv) was added to the schlenk tube followed by DMSO (2 mL, 0.2 M). The schlenk tube was sealed under N_2 . Stirred and irradiated with two 405 nm LEDs (4.5 cm from glass surface on each side of the tube with fan cooling) for 20 hours total. At the 6 hour mark, an additional 2.5 mol % 4-DPAIPN was added as a stock solution (2.5 mol % 4-DPAIPN dissolved in 400 μL DMSO — then to the reaction vessel, evacuated and backfilled with N_2 on the side arm then while under active N_2 , added the stock solution). The tube was resealed under N_2 and stirred

while irradiating for the remaining 14 hours. After reaction completion, the reaction was quenched with 50 mL NaHCO₃ (aq) and extracted with 30 mL EtOAc three times. The combined EtOAc layer was washed with 50 mL brine then dried over Na₂SO₄. The mixture was filtered and concentrated in vacuo then purified by flash chromatography with silica.

For NMR analyses: After reaction completion, CH₂Br₂ was added as the internal standard to crude reaction mixture. Took 0.1 mL aliquot and quenched with 1 mL water then extracted with 1 mL CDCl₃. Reactions were analyzed via ¹H NMR of the CDCl₃ layer.

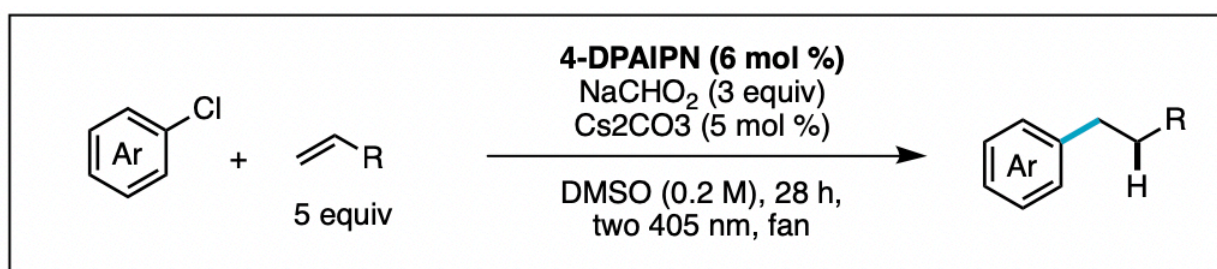
General Procedure D — Hydroarylation of Vinyl Carbamate



To an oven-dried 10 mL schlenk tube equipped with a stir bar, 4-DPAIPN (0.012 mmol, 3 mol %), sodium formate (1.2 mmol, 3 equiv), and vinyl carbamate (1.0 mmol, 2.5 equiv) were added. The tube was evacuated and backfilled with N₂ three times. While under active N₂, added cyclohexylthiol (0.02 mmol, 5 mol %) and aryl chloride (0.4 mmol, 1 equiv) to vial then DMSO (2 mL, 0.2 M). The tube was sealed under N₂ then stirred and irradiated with two 405 nm lamps (4.5 cm from glass surface on each side with fan cooling) for 28 hours total. At the 6 hour mark, an additional 3 mol % 4-DPAIPN was added as a stock solution (3 mol % 4-DPAIPN dissolved in 400 uL DMSO — then to the reaction vessel, evacuated and backfilled with N₂ on the side arm then while under active N₂, added the stock solution). The tube was resealed under N₂ and stirred

while irradiating for the remaining 22 hours. After reaction completion, the reaction was quenched with 50 mL NaHCO_3 (aq) and extracted with 30 mL EtOAc three times. The combined EtOAc layer was washed with 50 mL brine then dried over Na_2SO_4 . The mixture was filtered and concentrated in vacuo then purified by flash chromatography with silica.

General Procedure E — Hydroarylation of Unactivated Alkenes



To an oven-dried 10 mL schlenk tube equipped with a stir bar, 4-DPAIPN (0.012 mmol, 3 mol %) and sodium formate (1.2 mmol, 3 equiv) were added. The tube was evacuated and backfilled with N_2 three times. While under active N_2 , cyclohexylthiol (0.02 mmol, 5 mol %), aryl chloride (0.4 mmol, 1 equiv), and alkene (2.0 mmol, 5 equiv) were added to the vial then DMSO (2 mL, 0.2 M). The tube was sealed under N_2 then stirred and irradiated with two 405 nm lamps (4.5 cm from glass surface on each side with fan cooling) for 28 hours total. At the 6 hour mark, an additional 3 mol % 4-DPAIPN was added as a stock solution (3 mol % 4-DPAIPN dissolved in 400 μL DMSO — then to the reaction vessel, evacuated and backfilled with N_2 on the side arm then while under active N_2 , added the stock solution). The tube was resealed under N_2 and stirred while irradiating for the remaining 22 hours.

For GC analyses: After reaction completion, mesitylene was added as the internal standard to the crude mixture. 0.1 mL aliquot was removed from the crude and quenched with 1 mL water and

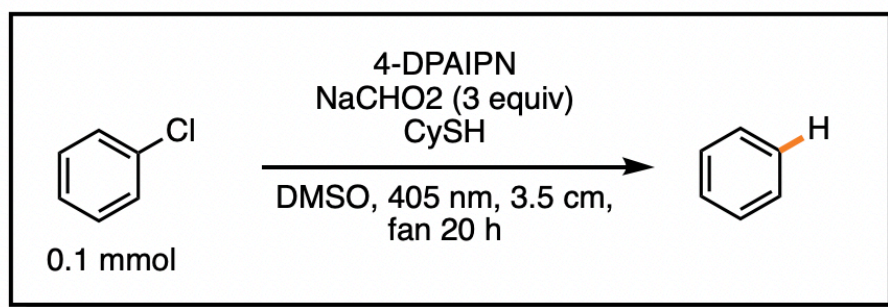
extracted with 1 mL diethyl ether. The diethyl ether layer was filtered through a silica pipette plug then ran on the GC.

For NMR analyses: CH₂Br₂ was added as the internal standard to crude reaction mixture. 0.1 mL aliquot was removed and quenched with 1 mL water then extracted with 1 mL CDCl₃. Took Reactions were analyzed via ¹H NMR of the CDCl₃ layer.

2. 5. 5. Reaction Optimization

Dehalogenation

Following General Procedure A on 0.1 mmol scale, the following parameters were evaluated during optimization of this reaction. Reactions were analyzed via GCMS.



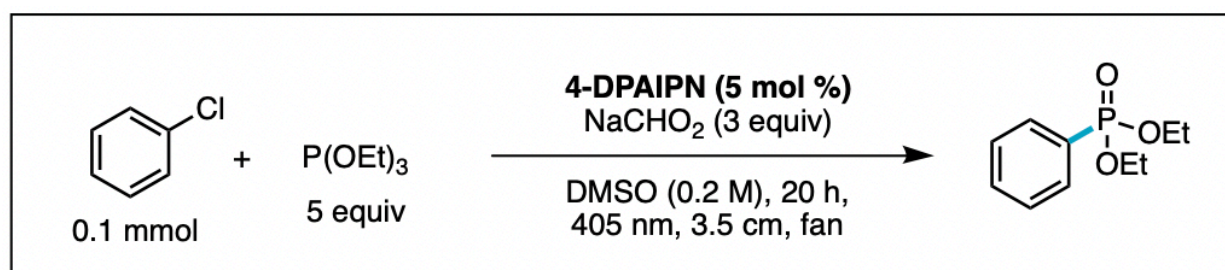
	PhH %
0.2 M DMSO, 5 mol % 4-DPAIPN (two 2.5 mol % batches)	62
0.08 M DMSO, 5 mol % 4-DPAIPN	62
0.08 M DMSO, 10 mol % 4-DPAIPN	74
0.2 M DMSO, 5 mol % 4-DPAIPN (two 2.5 mol % batches), no CySH	57
0.2 M DMF, 5 mol % 4-DPAIPN, no CySH	14
0.2 M THF, 5 mol % 4-DPAIPN (two 2.5 mol % batches), no CySH	0

Figure 2. S2: Dehalogenation optimization.

Phosphonylation

Following General Procedure B, the conditions below were used as the initial standard conditions.

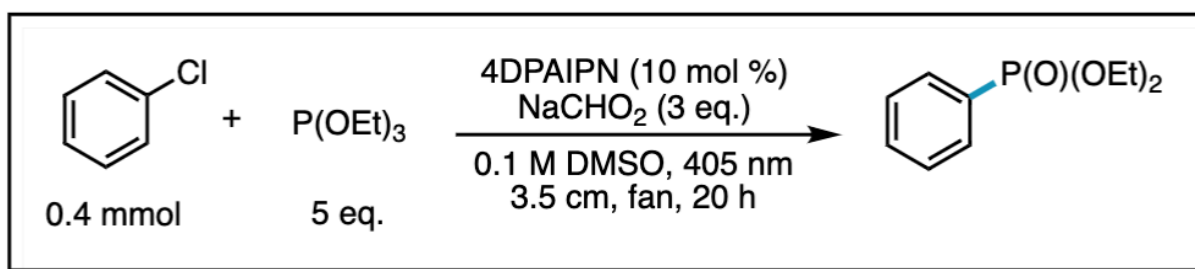
The following parameters were evaluated during optimization of this reaction. Reactions were analyzed via ^1H NMR using CH_2Br_2 as the internal standard.



	prdt
standard	30
2.5 mol % 4-DPAIPN	33
0.1 M DMSO, 2.5 mol % 4-DPAIPN	25
0.1 M DMSO, 5 mol % DPA (no batch addition)	40
0.1 M DMSO, 10 mol % DPA	55
0.1 M DMSO, 10 mol % DPA, FPT	53
10 eq phos, 2.5 mol % 4-DPAIPN	36
15 eq phos, 2.5 mol % 4-DPAIPN	36
0.067 M DMSO, 10 mol % 4-DPAIPN	30
0.1 M DMSO, 10 mol % 4-DPAIPN, 10 eq phos	50
0.067 M DMSO, 10 mol % 4-DPAIPN, 10 eq phos	46
0.1 M, 5 mol % 4-DPAIPN, 10 eq phos (no batch addition)	37

Figure 2. S3: Phosphonylation optimization.

The remainder of optimization for the phosphonylation was performed on 0.4 mmol scale with the following standard conditions.

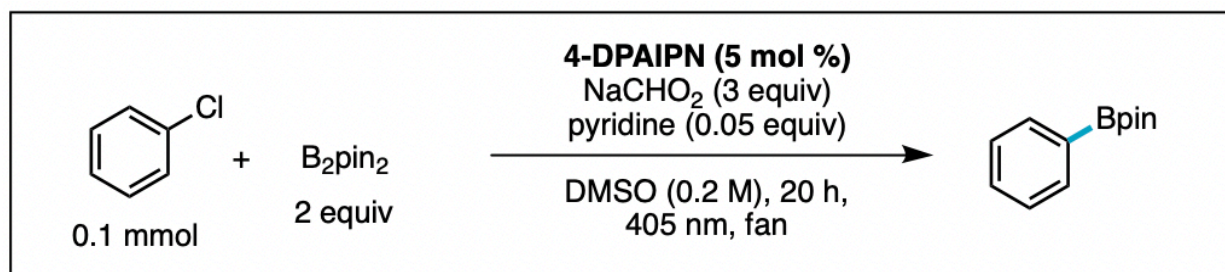


	prdt	rsm
standard	51	yes
2 lights	55	yes
photobox	51	yes
12 mol % DPA	60	yes
15 mol % DPA	61	yes
12 mol % DPA, 0.08 M	50	yes
15 mol % DPA, 0.08 M	63	yes
12 mol % DPA, 0.05 M	47	yes
15 mol % DPA, 0.05 M	52	yes

Figure 2. S4: Phosphonylation optimization on 0.4 mmol scale.

Borylation

Following General Procedure C on 0.1 mmol scale, the following parameters were evaluated during optimization of this reaction. Reactions were analyzed via ^1H NMR using CH_2Br_2 as the internal standard.



	prdt	PhH	prdt/PhH
standard	60	20	3
2.5 mol % 4-DPAIPN	50	15	3.33333333
0 eq pyr	50	28	1.78571429
0.05 eq pyr	68	27	2.51851852
0.5 eq pyr	68	22	3.09090909
1 eq B2pin2	54	18	3
3 eq B2pin2	67	25	2.68
4 eq B2pin2	67	11	6.09090909
5 eq B2pin2	70	15	4.66666667
0.1 M, 10 mol % 4-DPAIPN, 3 eq B2pin2, no batch	60	23	2.60869565
0.15 M, 5 mol % 4-DPAIPN, 3 eq B2pin2	68	19	3.57894737
DMF	15	10	1.5

Figure 2. S5: Borylation optimization.

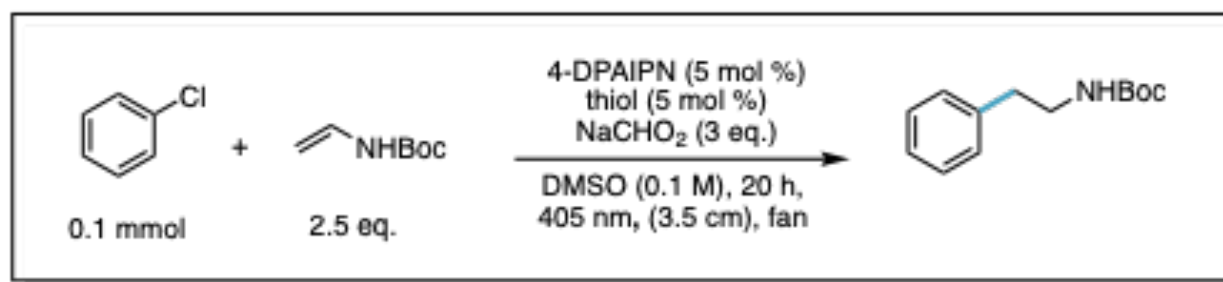
The remainder of borylation optimization was performed with chloroanisole as the substrate because electron-rich substrates were more challenging.

	prdt	Ar-H	rsm	prdt/Ar-H
standard	57	20	26	2.85
0.5 eq pyridine	54	22	30	2.45455
0.5 eq DMAP	58	25	14	2.32
no fan, 5 eq B2pin2, 0.5 eq pyridine	41	9	52	4.55556
10 mol % 4-DPAIPN, 0.08 M DMSO, 0.05 eq pyridine	50	32	21	1.5625
10 mol % 4-DPAIPN, 0.08 M DMSO, 1 eq pyridine	29	20	42	1.45
10 mol % 4-DPAIPN, 0.08 M DMSO, 1 eq DMAP	45	22	34	2.04545
10 mol % 4-DPAIPN, 0.08 M DMSO, 1 eq Cs2CO3	51	30	18	1.7
10 mol % 4-DPAIPN, 0.08 M DMSO, 1 eq tBuOK	41	29	8	1.41379
10 mol % 4-DPAIPN, 0.08 M DMSO, 1 eq K3PO4	37	24	26	1.54167
10 mol % 4-DPAIPN, 0.08 M DMSO, 1 eq pyridine, 5 eq B2pin2	34	9	54	3.77778
0.5 eq Cs2CO3	41	23	21	1.78261
1 eq Cs2CO3	49	20	18	2.45
2 eq Cs2CO3	61	23	11	2.65217
3 eq Cs2CO3	67	29	0	2.31034
4 eq Cs2CO4	66	33	0	2
3 eq Cs2CO3 with Cs formate	63	33	0	1.90909

Figure 2. S6: Borylation optimization with chloroanisole as the substrate.

Hydroarylation of Vinyl Carbamate

Following General Procedure D on 0.1 mmol scale, the following parameters were evaluated during optimization of this reaction. Reactions were analyzed via GCMS.



catalyst	product %	product/PhH	conversion
NpMI (427 nm)	10	1.3	42
NpDI (467)	0	NA	0
DCA (525 nm)	0	NA	0
4-CzIPN (390 nm)	14	7.7	32
tBu-4-CzIPN	16	5.2	24
4-DPAPN	22	5.1	41
4-DPATPN	17	3.4	32
3-CN-3-Ph	0	NA	0
4-DPAIPN	55	4.2	97

Figure 2. S7. Catalyst evaluation for hydroarylation.

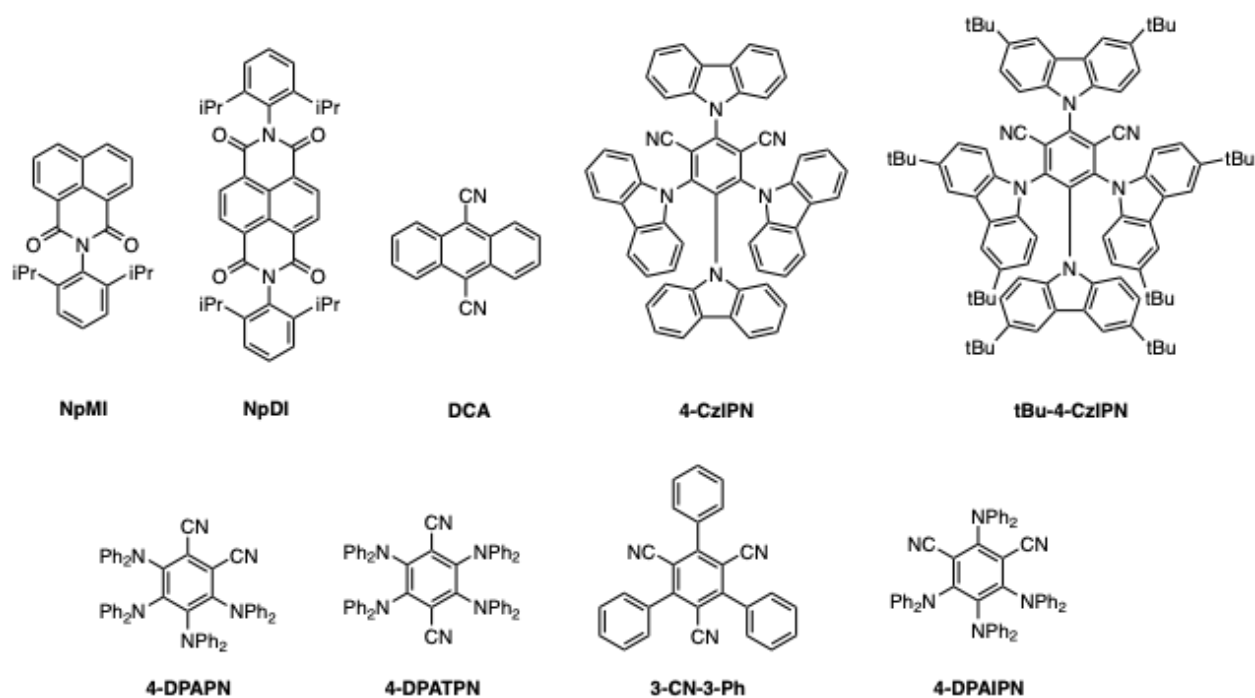


Figure 2. S8: Catalyst structures.

	yield	prdt/PhH	conversion
DMSO	55	2.4	90
MeCN	18	1.6	46
DMF	21	0.7	52
acetone	4	0.5	25
HFIP	0	--	0
DCM	0	--	0
THF	0	(40% PhH)	58
0.05 M	32	0.8	85
0.10 M	50	2.4	90
0.20 M	27	6.2	35

Figure 2. S9: Solvent evaluation for hydroarylation. All solvents tested were run 1:1 with DMSO.

		yield	prdt/PhH	conversion	MB
	no HAT	5	0.6	31	81
	2,6-di-tBu-4-OMe-PhOH	2	0.3	20	87
thiophenols	PhSH	41	2.4	80	83
	4-OMe-PhSH	53	2.4	89	87
alkyl thiols	decanethiol	54	2.1	89	91
	CySH	55	2.4	90	92
	tert-dodecylthiol	57	2.1	89	95

Figure 2. S10: Thiol evaluation for hydroarylation.

	reductant (3 equiv)	prdt	PhH	prdt/PhH
hydroAr of enamines	DIPEA	6	37	0.4
	NPh ₃	0	0	--
	Na-ascorbate	0	0	--
	Li-formate	18	31	0.6
	Cs-formate	53	24	2.3
	K-formate	33	27	1.2
	Na-formate	50	21	2.4
	formic acid + NBu ₃	9	2	4.2
	tBuOH	0	0	--
	iPrOH	0	0	--
	H ₂ O	0	0	--
dehalo	Na-oxalate	--	2	--
	PPh ₃	--	7	--
	NAr ₃ -Ome	--	3	--
	Mn	--	1	--
	Na-formate	--	71	--

Figure 2. S11: Reductant evaluation for hydroarylation.

2. 5. 6. Photocatalyst and Reductant Evaluation

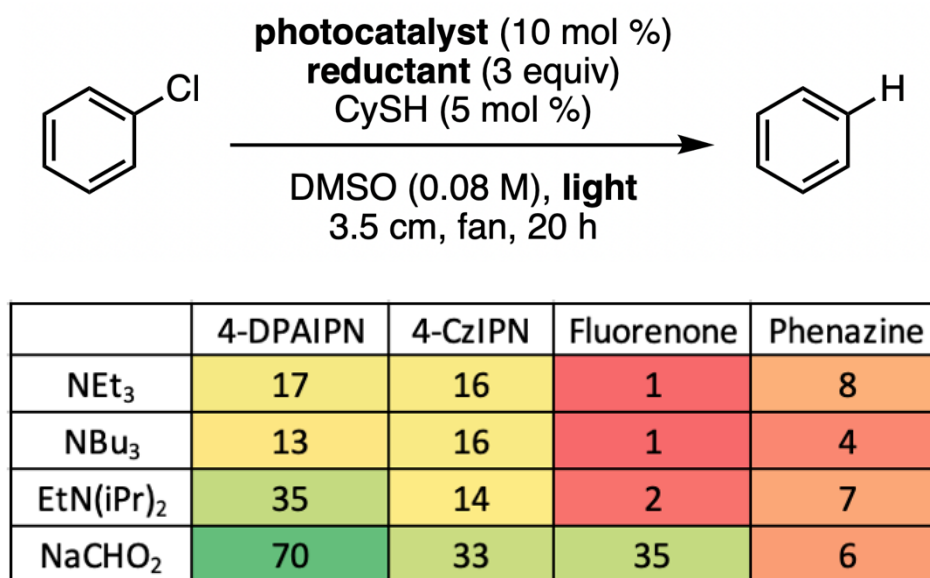


Figure 2. S12. Catalyst and reductant matrix to unlock potent radical anion reactivity.

Following General Procedure A except varying the photocatalyst, reductant, and wavelength, the following yields were obtained via GC analysis using mesitylene as the internal standard. The light used for irradiation (4-DPAIPN = 405 nm, 4-CzIPN = 390 nm, fluorenone = 405 nm, phenazine = 440 nm) was determined from the optimal wavelength for the reduced congener of each photocatalyst, discovered in {Chernowsky, Colleen; Chmiel, Alyah; Wickens, Zachary (2021): Photocatalytic Activity of Diverse Organic Radical Anions: Catalyst Discovery Enables Cleavage of Strong C(sp²)-N and C(sp²)-O Bonds. ChemRxiv. Preprint. <https://doi.org/10.26434/chemrxiv.14710398.v1>}.

2. 5. 7. Evaluation of Leaving Groups not Susceptible to XAT

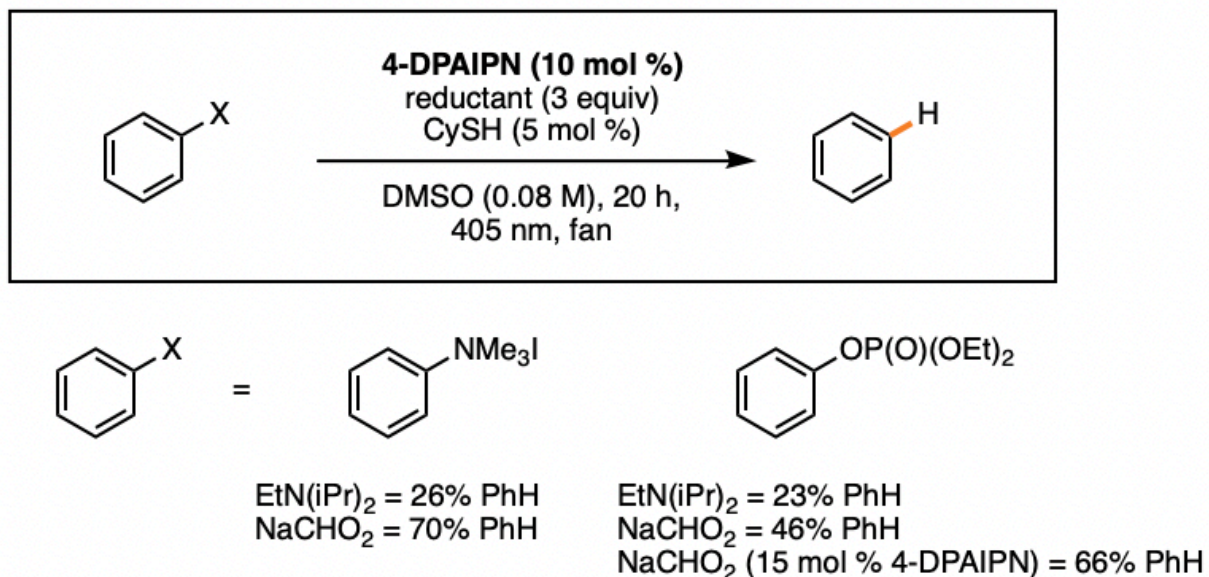


Figure 2. S13. Testing non-halide leaving groups to rule out an XAT mechanism.

Following General Procedure A, the following yields were obtained via GC analysis. The alkyl amine promoted the desired reduction of the anilinium and phosphate in modest yields, supporting an electron-primed mechanism rather than halogen atom transfer (XAT). Furthermore, we see that the reduction becomes much more efficient upon employing sodium formate as the redox activator. Conversion of the phosphate can be increased by employing higher catalyst loading.

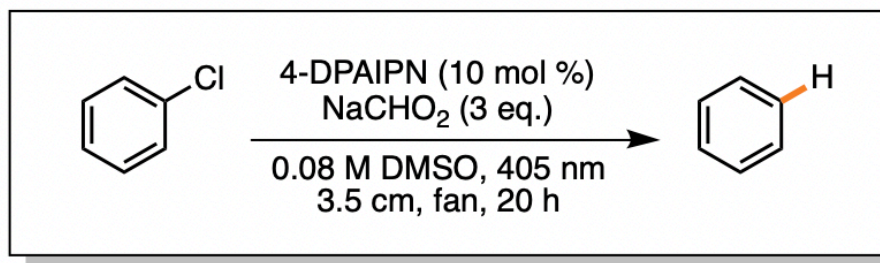
2. 5. 8. Reductants Evaluated with 4-DPAIPN

Below is a complete list of reductants that were tested with 4-DPAIPN as the photocatalyst, using General Procedure A. For reductants that lacked an H-atom (PPh_3 , 4-OMe-NPh₃, Mn(0)), dimethylformamide was used as a co-solvent to act as an H-atom donor to the aryl radical that would be generated upon single electron reduction.

	% prdt
sodium oxalate	2
PPh ₃	7
4-OMe-NPh ₃	3
Mn(0)	1
sodium ascorbate	2
NEt ₃	17
NBu ₃	13
EtN(iPr) ₂	35
NaCHO ₂	70

Figure 2. S14. Reductants tested with 4-DPAIPN for the dehalogenation of chlorobenzene.

2. 5. 9. Control Experiments



alterations	prdt	rsm
none	71	18
no light	< 2	99
no cat	< 2	94
no formate	<i>not detected</i>	98

The following control experiments were run using General Procedure A with the following deviations mentioned above. We see that light, catalyst, and formate are required.

2. 5. 10. Radical Clock Experiment

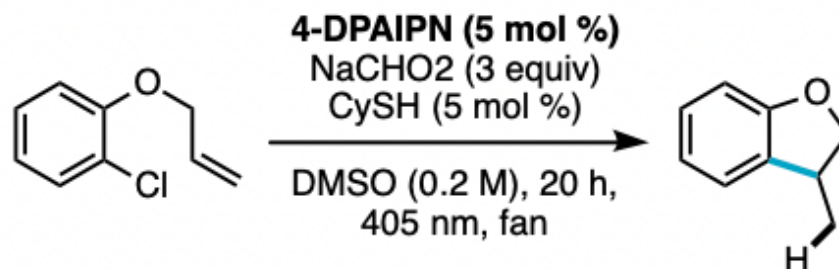
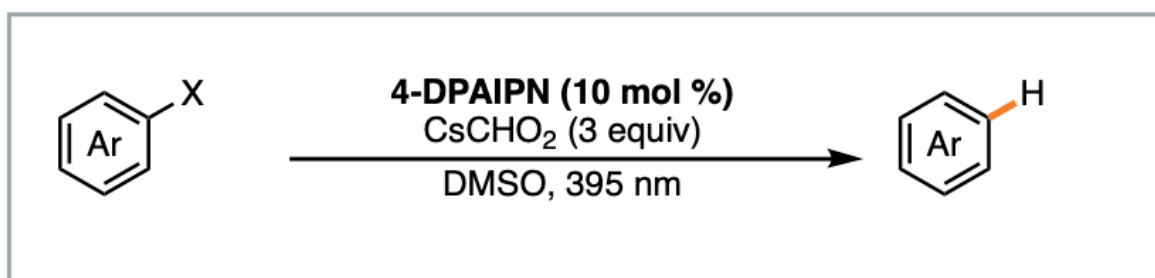


Figure 2. S15. Radical clock experiment to support aryl radical intermediate.

To an oven-dried 10 mL schlenk tube equipped with a stir bar, 4-DPAIPN (0.0025 mmol, 2.5 mol %) and sodium formate (0.3 mmol, 3 equiv) were added. The flask was evacuated and backfilled with N₂ three times. While under active N₂ (if N₂ pressure is too low, then the reaction mixture was freeze-pump-thawed after addition of all reagents), added cyclohexylthiol (0.005 mmol, 5 mol %) and aryl chloride (0.1 mmol, 1 equiv) to vial then DMSO (0.5 mL, 0.2 M). Sealed tube under N₂. The reaction mixture was stirred and irradiated with a 405 nm lamp (3.5 cm from glass surface with fan cooling) for 20 hours total. At the 6 hour mark, an additional 2.5 mol % 4-DPAIPN (for a total of 5 mol % photocatalyst) was added as a stock solution (2.5 mol % 4-DPAIPN dissolved in 100 μ L DMSO — then to the reaction vessel, evacuated and backfilled with N₂ on the side arm then while under active N₂, added the stock solution). The tube was resealed under N₂ and the mixture stirred under irradiation for the remaining 14 hours. CH₂Br₂ (7 μ L, 0.1 mmol, 1 equiv) was added as the internal standard to crude reaction mixture. 0.1 mL aliquot was removed and quenched with 1 mL water then extracted with 1 mL CDCl₃. 52% yield was obtained via ¹H NMR. NMR consistent with reported spectrum (*J. Org. Chem.* 2018, 83, 16, 9381–9390).

2. 5. 11. High-Throughput Experimentation with Aryl Halide Informer Plate



X1	X2	X3	X4	X5	X6
X7	X8	X9	X10	X11	X12
X13	X14	X15	X16	X17	X18

product detected
 no product detected

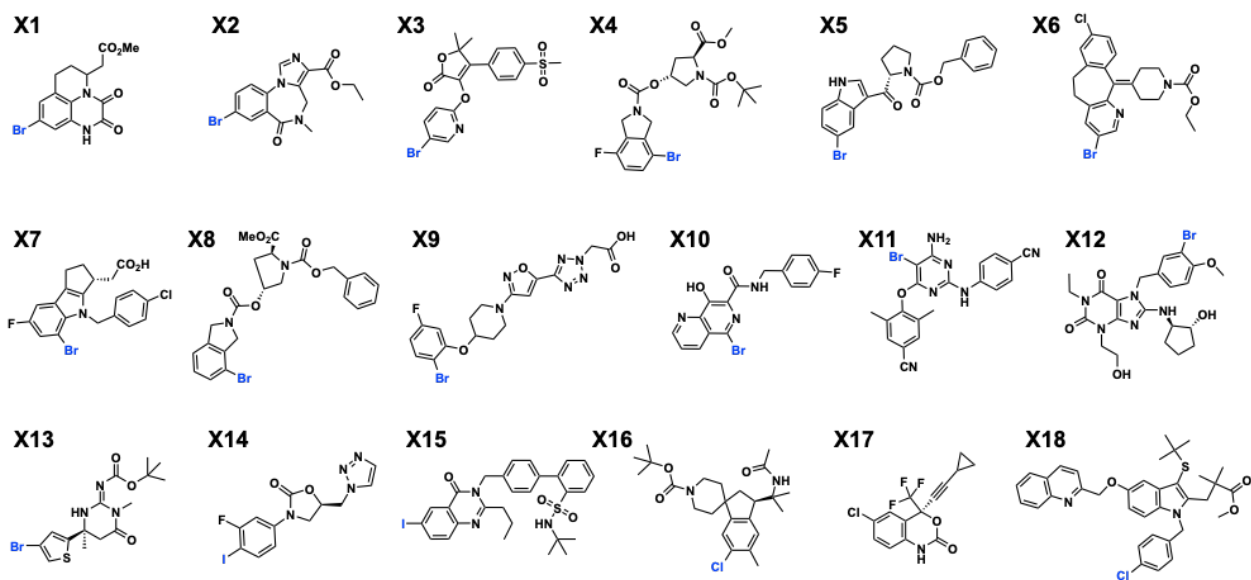


Figure 2. S16. Aryl halide informer plate used in high-throughput experimentation to test the 4-DPAIPN and formate system.

To a 4 mL vial equipped with a stir bar, 4-DPAIPN (23.9 mg, 0.03 mmol) and cesium formate (0.9 mmol, 3 equiv) were added. Under active N₂, DMSO (3.75 mL) previously sparged with nitrogen for 5 min was added. The resulting suspension was vigorously stirred for 5–10 min. In a nitrogen inertion box, to each reaction well of a custom plated kit containing 10 μ mol of the commercially available informers was added 125 μ L of the suspension containing 4-DPAIPN (0.8 mg, 1 μ mol), cesium formate (5.3 mg, 30 μ mol). The reaction block was sealed, and the kit was stirred (by action of a tumble stirrer) under an active stream of nitrogen and irradiated with a 395 nm LED plate (Lumidox II, stage 3, 190 mW/well) equipped with an active cooling base for 8 hours. After completion, each reaction vial was analyzed on an LCMS. The HTE screen afforded hits as depicted in the following graphic showing conversion to the reduction product.

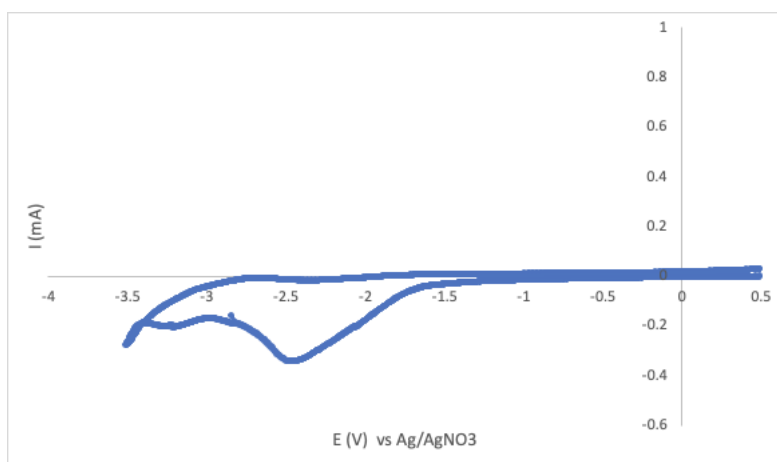
An advantage of using chemical reductants to generate electron-primed catalysts is that it allows for an operationally simple reaction setup as well as allows use of photoredox high-throughput experimentation technology. We demonstrated this using an aryl halide informer plate that contains a unique densely functionalized substrate in each well. Dehalogenation was chosen as the target reaction due to its analytical simplicity. We learned that this electron-primed system can reduce a variety of medicinally-relevant compounds using high-throughput experimentation. These compounds were detected as significant products via LCMS. HTE plate: Lumidox Gen II 24-Position LED Arrays, part no. LUM296DA395. Aryl halide informer plate: <https://www.sigmaaldrich.com/US/en/tech-docs/paper/970033>

To confirm the aforementioned hits, these reactions were repeated on a 0.1 mmol scale using a modified General Procedure A conducted with a Penn PhD Photoreactor M2 equipped with a 405 nm light source without cyclohexylthiol unless otherwise noted. See compounds **27-35**.

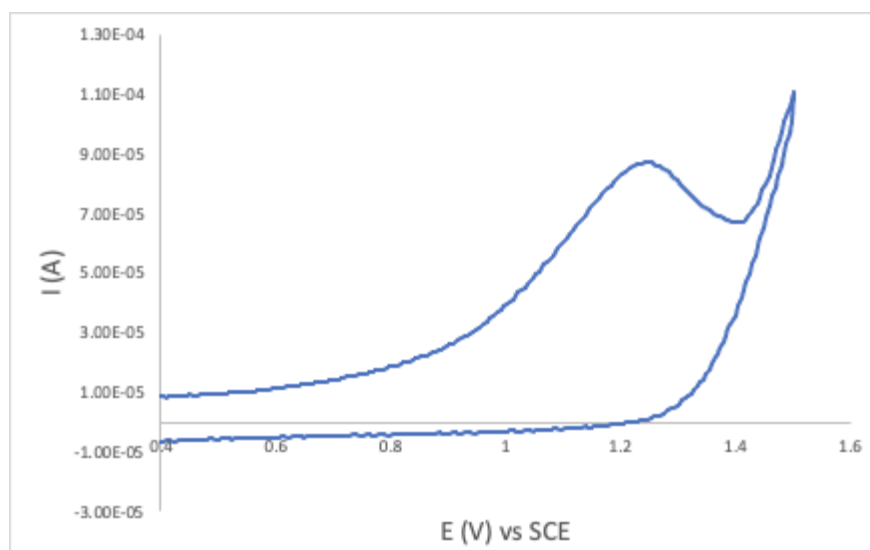
Additionally, a single informer (X2) was reacted on a 0.1 mmol scale using a modified General Procedure E conducted with a Penn PhD Photoreactor M2 equipped with a 405 nm light source. See compound **36**.

2. 5. 12. Cyclic Voltammetry

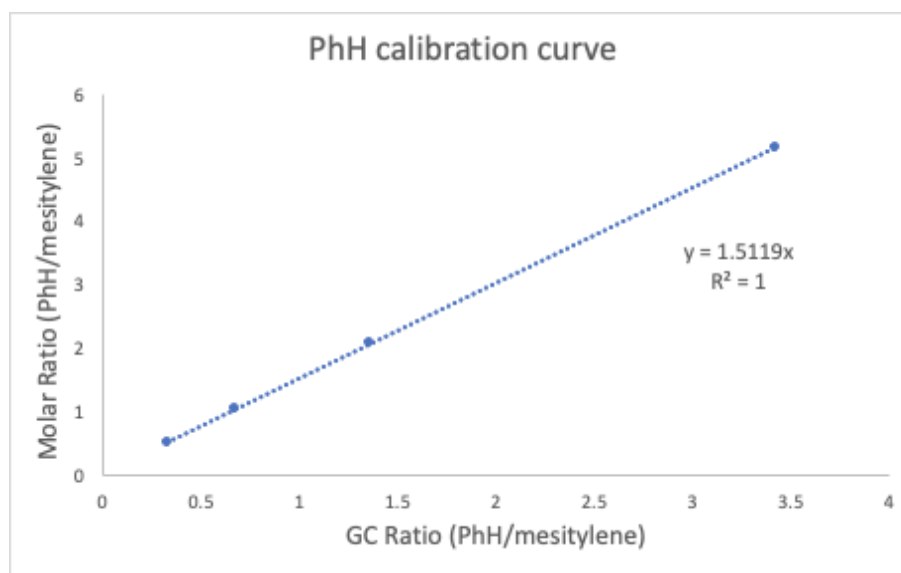
N-vinyl carbamate (0.1 M TBAPF₆) -- $E_{\text{red}} = -2.25 \text{ V vs SCE}$

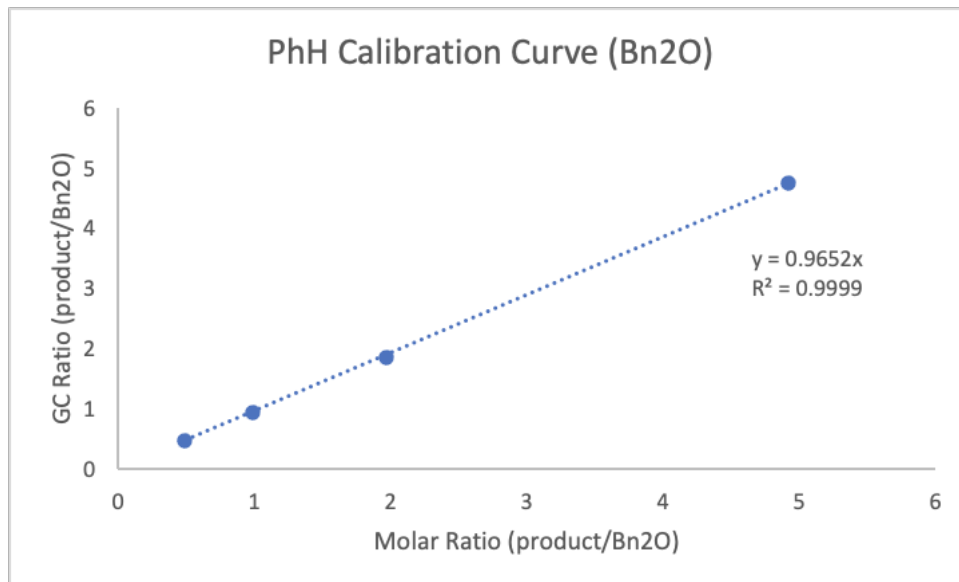
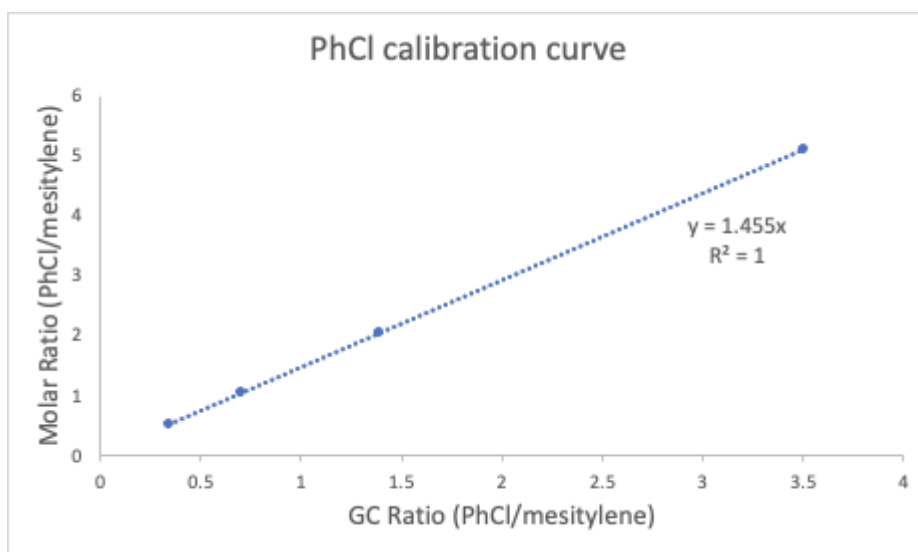


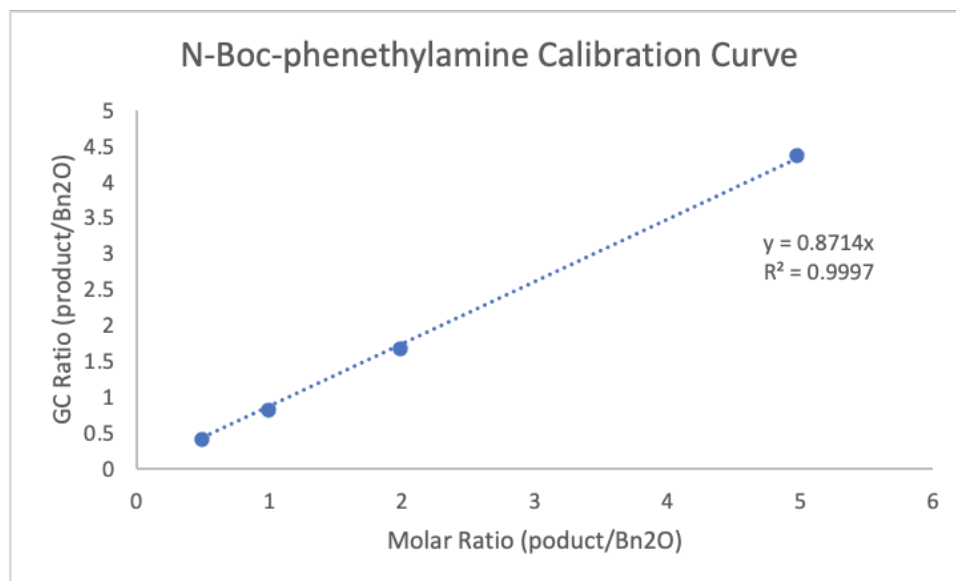
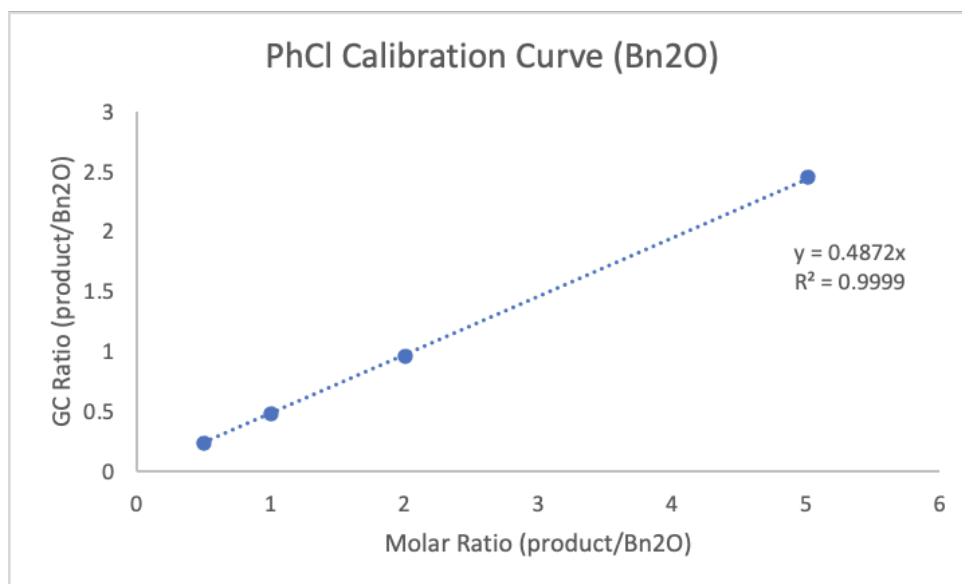
Sodium formate (0.1 M TBAPF₆) -- $E_{\text{ox}} = +1.25 \text{ V vs SCE}$

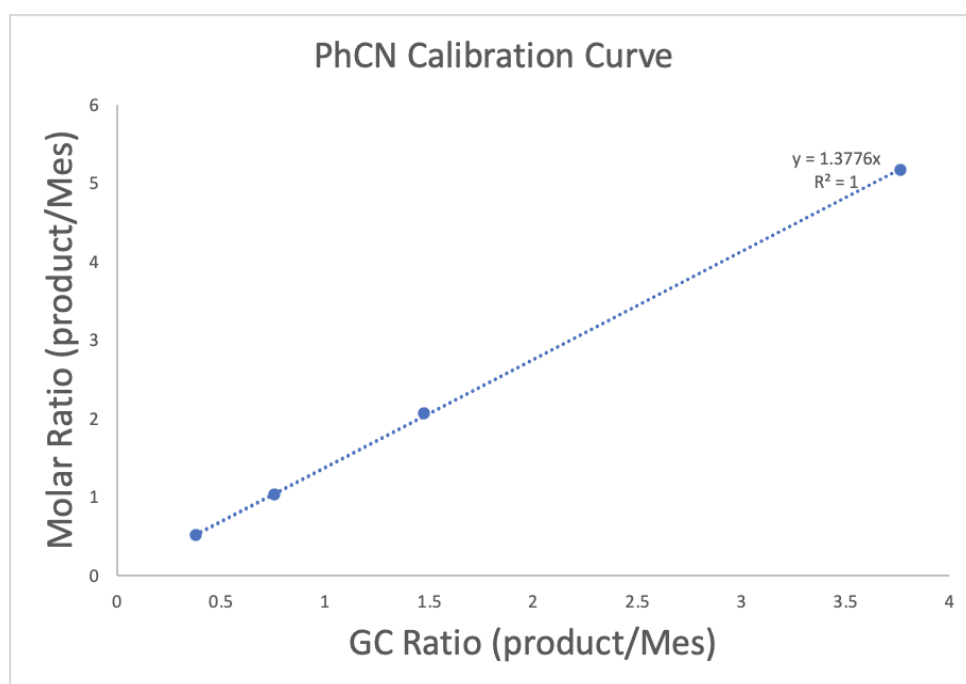
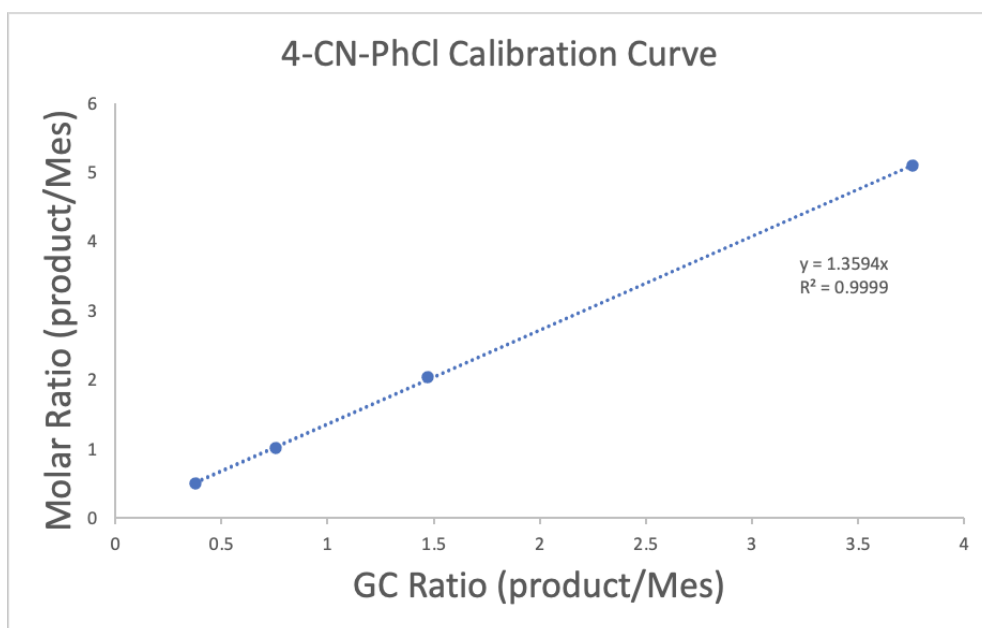


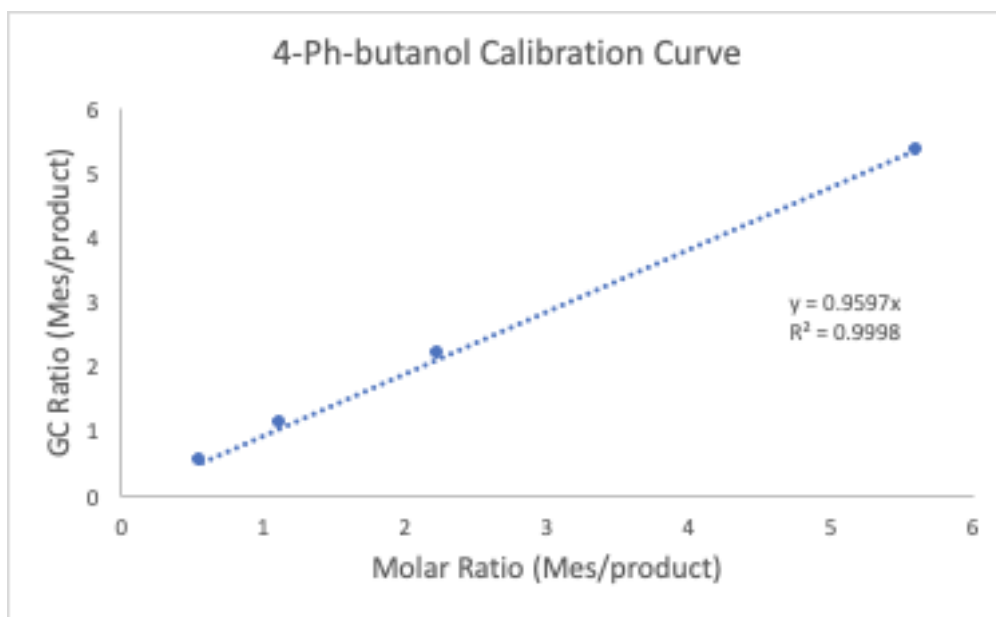
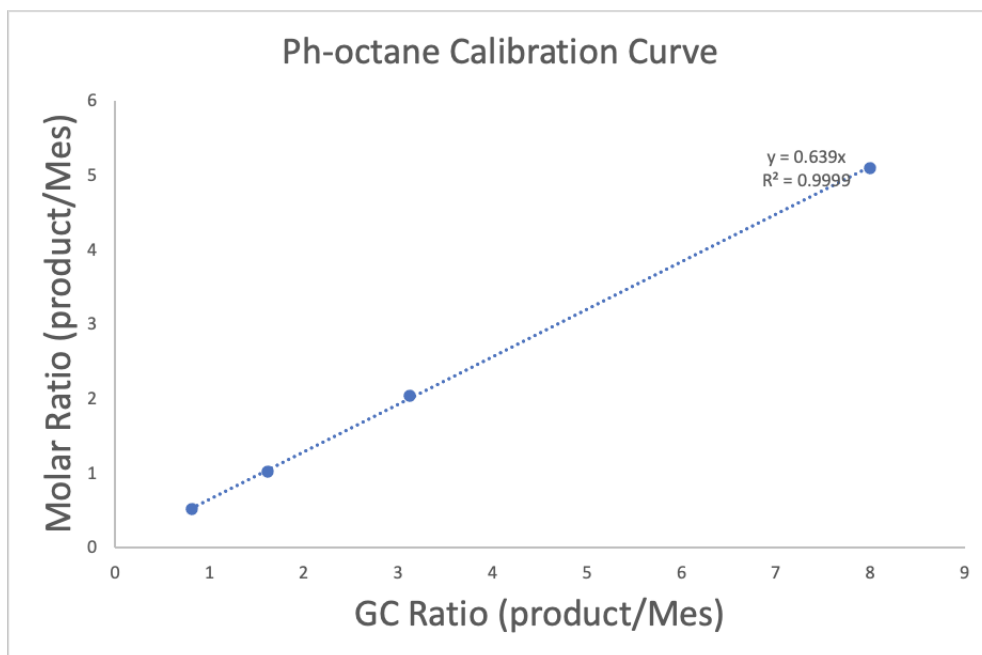
2. 5. 13. Calibration Curves











2. 5. 14. Stern Volmer and UV/Vis Data

Stern Volmer

In the glovebox, a 25 μM solution of 4-DPAIPN in DMSO was prepared with a given concentration of the quencher. The samples were irradiated at 435 nm and emission peak was measured at 525 nm. Quenching of 4-DPAIPN* was observed with tetrabutylammonium (TBA) formate and cyclohexylthiol, however no quenching was observed with chlorobenzene.

Note: TBA-formate was used instead of Na-formate because of poor solubility of the sodium counter ion. TBA-formate was tested as a reductant in the hydroarylation of the vinyl carbamate (General Procedure D) to validate its reactivity. Lower conversion was observed (65% conversion) with undesired over-reduction (PhH) as the major by-product (55%).

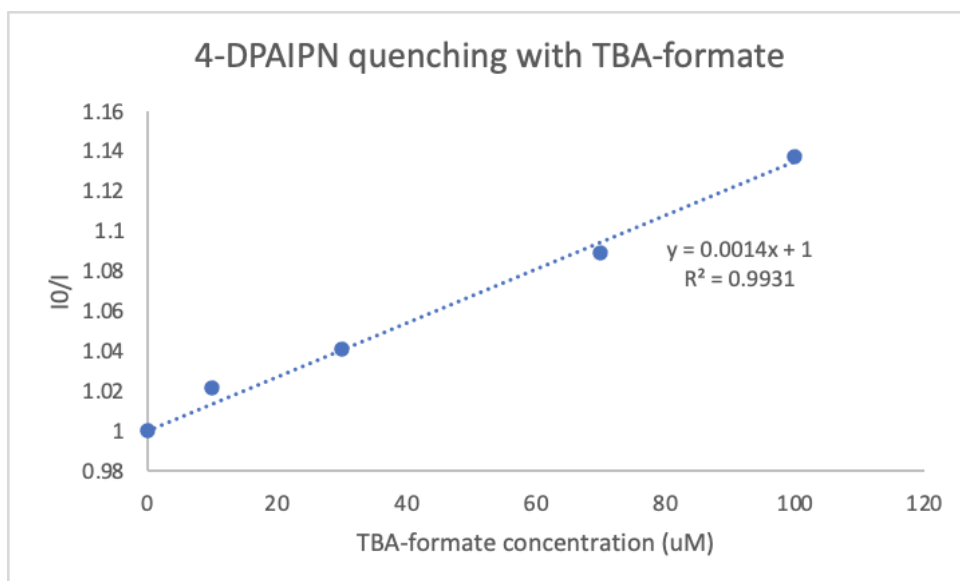


Figure 2. S17. Stern-Volmer quenching of 4-DPAIPN with tetrabutylammonium formate.

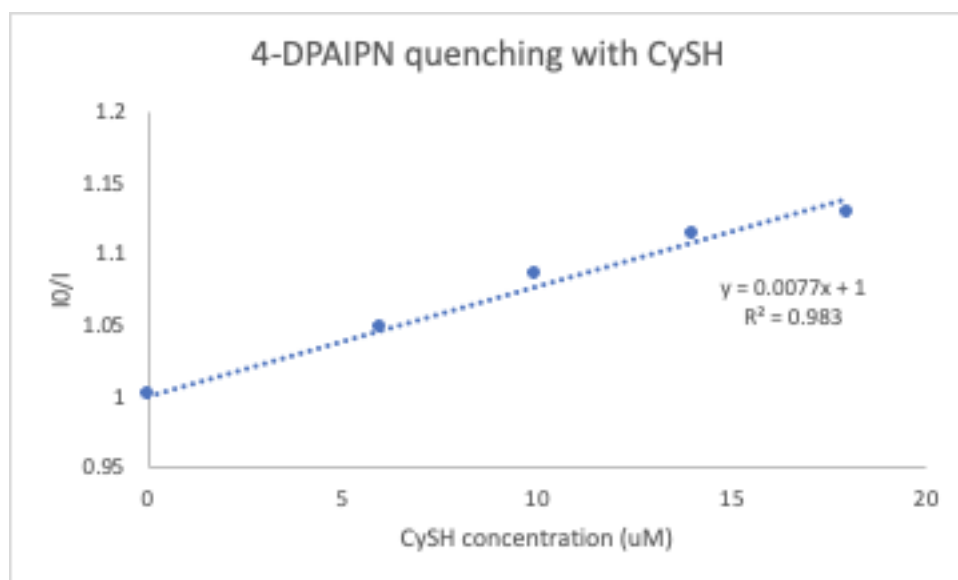


Figure 2. S18. Stern-Volmer quenching of 4-DPAIPN with cyclohexylthiol.

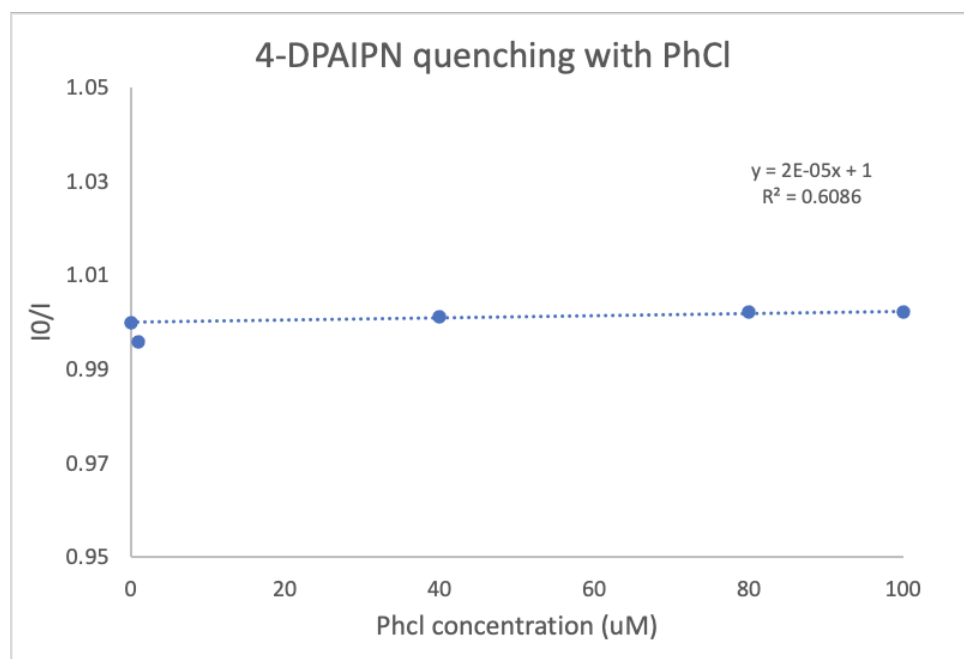


Figure 2. S19. Stern-Volmer quenching of 4-DPAIPN with chlorobenzene.

UV/vis

Under argon, a 25 μM solution of 4-DPAIPN and sodium formate in DMSO was prepared. The first UV/vis spectrum was taken. To the sample cuvette, a 405 nm LED was used to irradiate the mixture for 15 seconds while shaking. Following irradiation, the second UV/vis spectrum was taken which showed 4-DPAIPN \bullet^- features grow in. Next, chlorobenzene was added to the cuvette through the septum cap to give a 100 μM solution of chlorobenzene with the catalyst and formate mixture. The third UV/vis spectrum was recorded which showed no change in features, suggesting that 4-DPAIPN \bullet^- does not react on this time scale with chlorobenzene in the dark. Finally, the mixture was irradiated for 15 seconds with a 405 nm LED while shaking. The fourth UV/vis spectrum was taken and showed the 4-DPAIPN features grow in while the 4-DPAIPN \bullet^- features shrunk, suggesting that light is required for 4-DPAIPN \bullet^- to reduce chlorobenzene and revert to 4-DPAIPN.

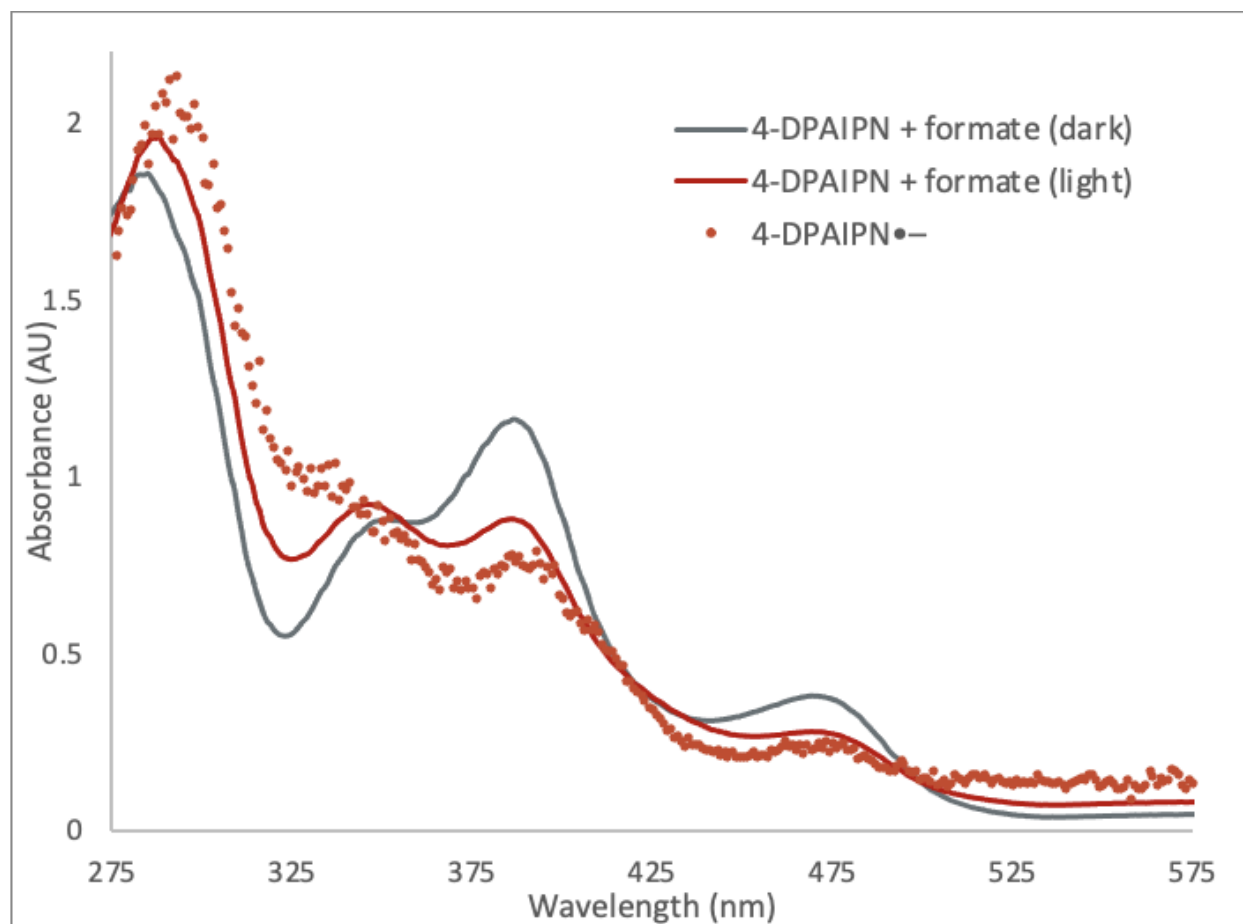


Figure 2. S20. UV/vis of 4-DPAIPN•⁻ generated with formate + light, and electrochemically.

For electrochemically generated 4-DPAIPN:

An oven-dried divided electrochemical cell under N₂ was equipped with an electrode assembly consisting of rubber septa as caps with stainless steel wire and RVC for the cathode, a sacrificial zinc anode, and Ag/AgNO₃ reference electrode. TBAPF₆ (0.1 M in DMF) was added to the cell followed by 4-DPAIPN to make a 25 μ M solution. Using a dip-probe, the solution was electrolyzed at -2 V vs Ag/AgNO₃. The solution changed from bright yellow to dark green/brown/black. The UV/vis spectrum was then recorded.

2. 5. 15. NMR Experiment for 4-DPAIPN•⁻ Generation

In the glovebox, 4-DPAIPN (8 mg, 1 μ mol) and sodium formate (0.7 mg, 1 μ mol) were added to a J-young tube, followed by D₆-DMSO (0.4 mL) to give a bright yellow solution. The NMR tube was wrapped in foil during transport then the first NMR spectrum was recorded. The NMR tube was then irradiated with a 405 nm LED and shaken for 45 seconds until the solution turned brown/black. The NMR spectrum was recorded and revealed significant broadening on the catalyst signals, indicative of a radical species being generated. Finally, the NMR tube was opened to air to presumably oxidize the 4-DPAIPN•⁻ back to neutral 4-DPAIPN. The solution returned to bright yellow and the NMR spectrum was recorded, revealing the neutral 4-DPAIPN features had returned.

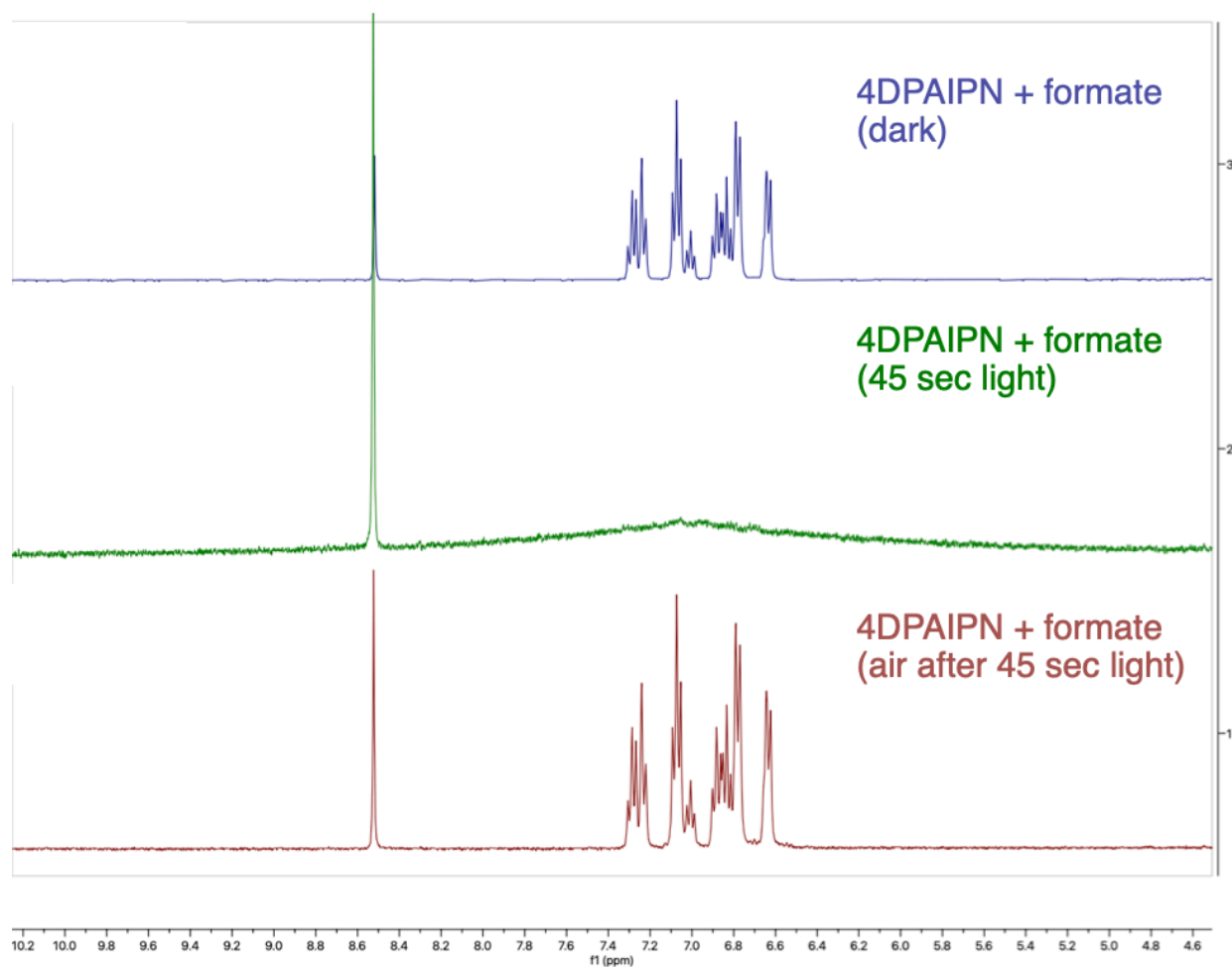


Figure 2. S21: NMR experiment revealing evidence of 4-DPAIPN•– generation in the presence of formate and light.

2. 5. 16. Plausible Mechanism for $\text{CO}_2^{\bullet-}$ Generation from Thiyl Radical

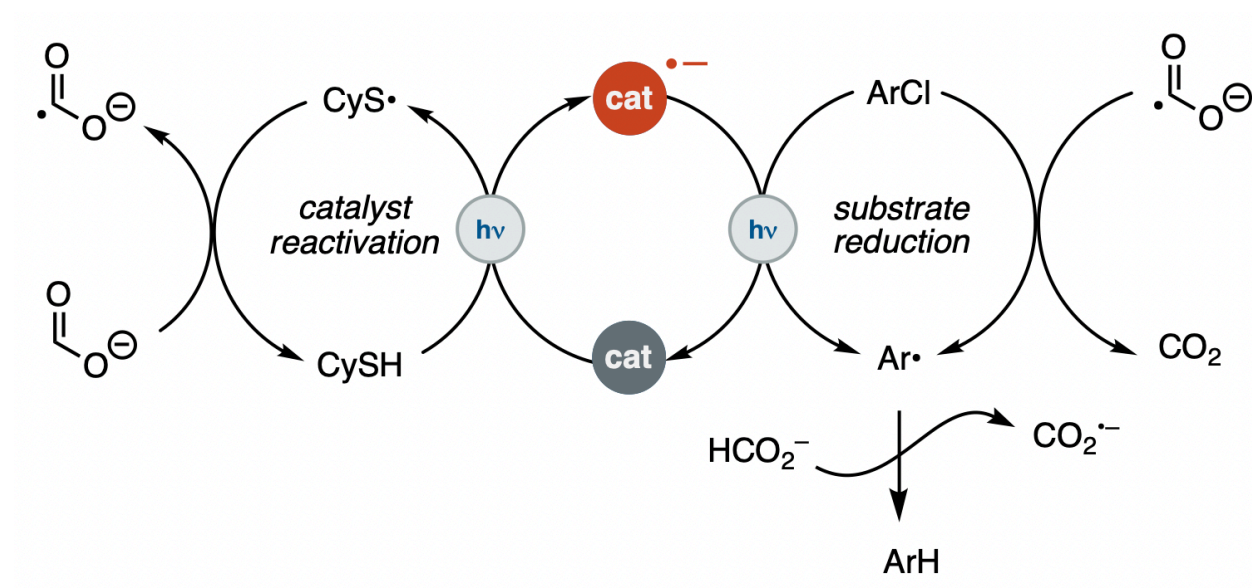


Figure 2. S22. Mechanism of thiol generating $\text{CO}_2^{\bullet-}$

Based on quenching in Stern-Volmer experiments, a plausible mechanism when thiol is present in the net-reductive reactions could be oxidation of the thiol by the 4-DPAIPN* followed by electron-transfer/proton-transfer (ETPT) to generate a thiyl radical. That thiyl radical could then abstract an H^\bullet atom from formate to generate the $\text{CO}_2^{\bullet-}$ that can promote the reaction as shown in Scheme 1.

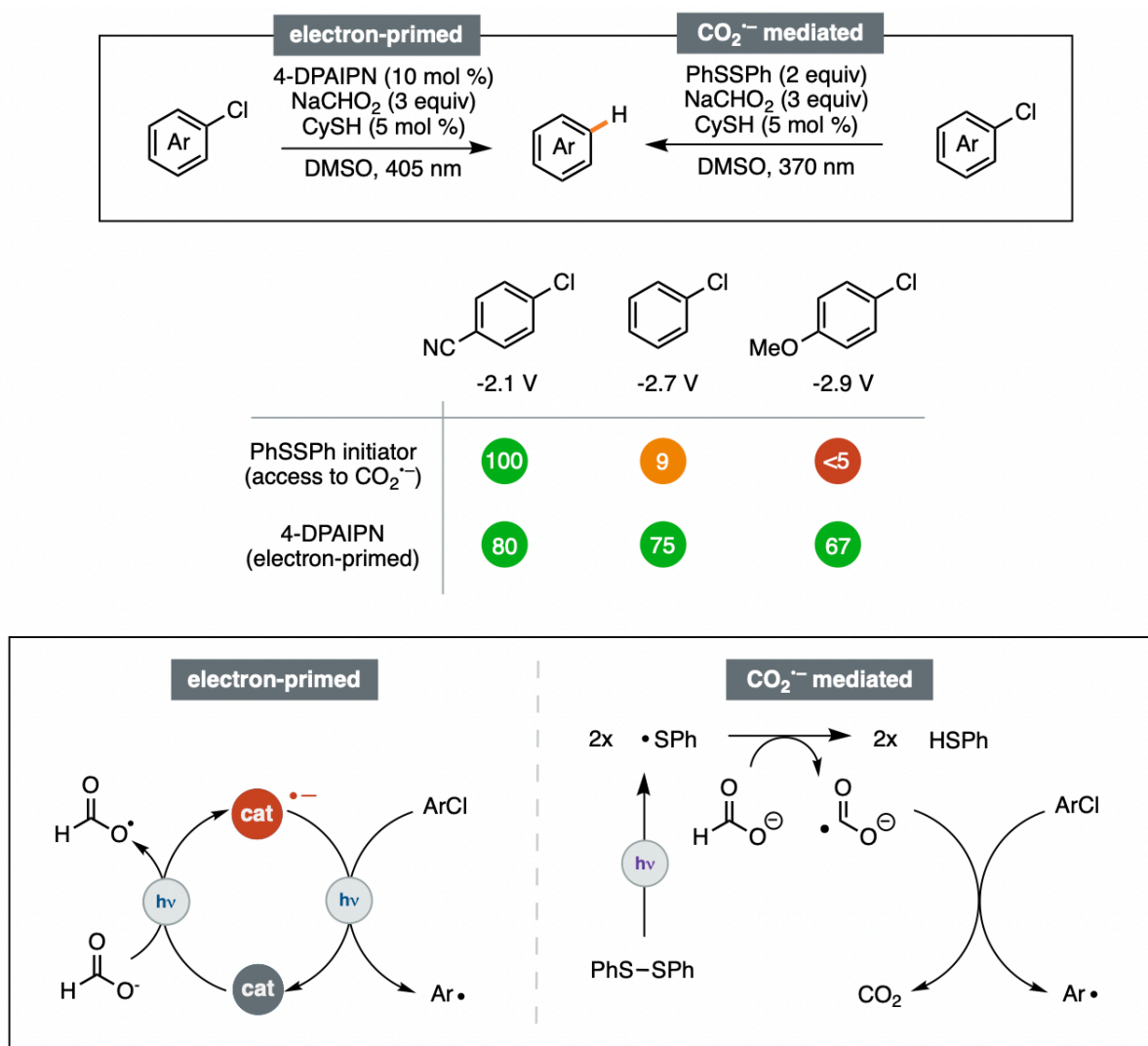
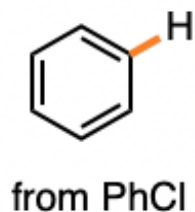
2. 5. 17 Probing Substrate Reduction by $\text{CO}_2^{\bullet-}$ 

Figure 2. S23. Evidence for $\text{CO}_2^{\bullet-}$ promoting substrate reduction at milder substrate E_{red} and electron-primed catalysis promoting substrate reduction at more challenging substrate E_{red} .

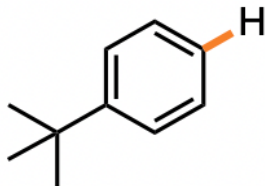
In an attempt to discriminate reduction of substrate via 4-DPAIPN radical anion excited state vs. CO_2 radical anion, the homolysis of the S–S bond of phenyl disulfide was explored as an alternative route to access $\text{CO}_2^{\bullet-}$ from formate. Conditions similar to the 4-DPAIPN-promoted reaction (General Procedure A) were used, replacing 4-DPAIPN with phenyl disulfide (2

equiv) and using 370 nm irradiation to homolyze the S–S bond, instead of 405 nm. The reactions were analyzed by measuring conversion of the aryl chloride via GCMS.

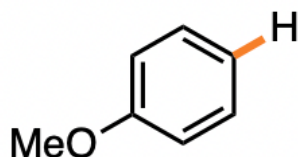
2. 5. 18 Product Characterization



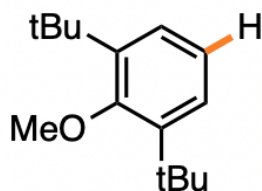
Benzene (3): 70% was obtained following General Procedure A, analyzed via GC analysis.



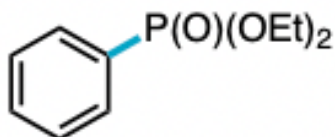
Tert-butylbenzene (4): 64% was obtained following General Procedure A, analyzed via ¹H NMR analysis. NMR consistent with reported spectrum (*J. Am. Chem. Soc.* 2013, 135, 2, 624–627).



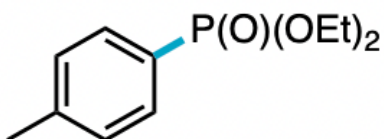
Anisole (5): 67% was obtained following General Procedure A, analyzed via ¹H NMR analysis. NMR consistent with reported spectrum (*Angew. Chem. Int. Ed.* 2018, 57, 12906 –12910).



1,3-di-tert-butyl-2-methoxybenzene (6): 92% was obtained following General Procedure A, analyzed via ^1H NMR analysis. NMR consistent with reported spectrum (*Tetrahedron*, 69, 3, 2013, 1105-1111).

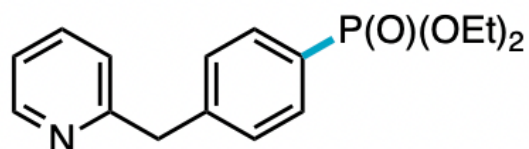


diethyl phenylphosphonate (10): 47 mg (55%) was obtained as a colorless oil following General Procedure B. Product was isolated via flash chromatography on silica using 2:1 hexanes/acetone. ^1H NMR (400 MHz, CDCl_3) δ 7.81 – 7.67 (m, 2H), 7.51 – 7.43 (m, 1H), 7.39 (tdd, J = 8.3, 4.2, 1.0 Hz, 2H), 4.19 – 3.90 (m, 4H), 1.25 (t, J = 7.1 Hz, 6H), consistent with reported spectrum (*Org. Lett.* 2013, 15, 20, 5362–5365).

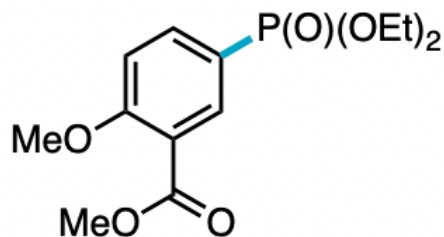


diethyl *p*-tolylphosphonate (11): 58 mg (63%) was obtained as a colorless oil following General Procedure B with the modification that 15 mol % 4-DPAIPN was used, first with the addition of 10

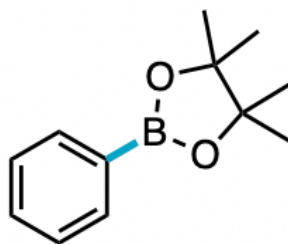
mol % photocatalyst followed by a batch of 5 mol % after 20 hours, giving a total 36 hour reaction time. Product was isolated via flash chromatography on silica using 2:1 hexanes/acetone. **¹H NMR** (400 MHz, CDCl₃) δ 7.63 (dd, J = 13.2, 8.1 Hz, 2H), 7.32 – 7.10 (m, 2H), 4.19 – 3.88 (m, 4H), 2.33 (s, 3H), 1.24 (t, J = 7.1 Hz, 6H), consistent with reported spectrum (*Org. Lett.* 2018, 20, 14, 4164–4167).



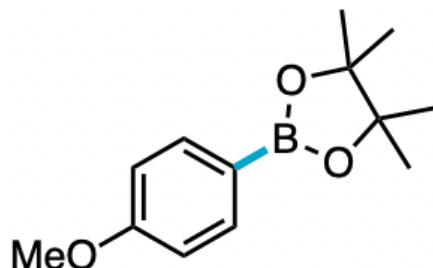
diethyl (4-(pyridin-2-ylmethyl)phenyl)phosphonate (12): 84 mg (69%) was obtained as a pale yellow oil following General Procedure B with the modification that 15 mol % 4-DPAIPN was used, first with the addition of 10 mol % photocatalyst followed by a batch of 5 mol % after 20 hours, giving a total 36 hour reaction time. Product was isolated via flash chromatography on silica using 20% MeOH in DCM. **¹H NMR** (400 MHz, CDCl₃) δ 8.55 – 8.49 (m, 1H), 7.76 – 7.66 (m, 2H), 7.57 (td, J = 7.7, 1.9 Hz, 1H), 7.33 (dd, J = 8.0, 3.9 Hz, 2H), 7.09 (dd, J = 7.8, 2.5 Hz, 2H), 4.16 (s, 2H), 4.15 – 3.96 (m, 4H), 1.27 (t, J = 7.1 Hz, 6H). **¹³C NMR** (101 MHz, CDCl₃) δ 159.83, 149.51, 144.26 (d, J = 3.2 Hz), 136.73, 132.11 (d, J = 10.3 Hz), 129.18 (d, J = 15.3 Hz), 126.17 (d, J = 189.7 Hz), 123.28, 121.57, 62.03 (d, J = 5.4 Hz), 44.60, 16.31 (d, J = 6.5 Hz). **³¹P NMR** (162 MHz, CDCl₃) δ 19.05. **HRMS** (ESI⁺) Calc: [M+H]⁺ (C₁₆H₂₀NO₃P) 306.1253; measured 306.1247 = 2.0 ppm difference.



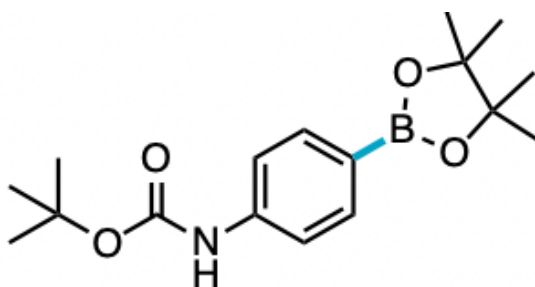
methyl 5-(diethoxyphosphoryl)-2-methoxybenzoate (13): 109 mg (90%) was obtained as a pale yellow oil following General Procedure B. Product was isolated via flash chromatography on silica using 30-60% acetone in hexanes. **¹H NMR** (400 MHz, CDCl₃) δ 8.15 (dd, J = 13.4, 2.1 Hz, 1H), 7.85 (ddd, J = 12.5, 8.6, 2.1 Hz, 1H), 6.99 (dd, J = 8.6, 3.2 Hz, 1H), 4.15 – 3.95 (m, 4H), 3.89 (s, 3H), 3.83 (s, 3H), 1.25 (t, J = 7.1 Hz, 6H). **¹³C NMR** (101 MHz, CDCl₃) δ 165.67, 162.03 (d, J = 3.3 Hz), 137.28 (d, J = 11.1 Hz), 135.60 (d, J = 12.2 Hz), 120.32 (d, J = 15.5 Hz), 119.65 (d, J = 196.4 Hz), 111.93 (d, J = 15.8 Hz), 62.16 (d, J = 5.4 Hz), 56.19, 52.21, 16.32 (d, J = 6.5 Hz). **³¹P NMR** (162 MHz, CDCl₃) δ 18.00. **HRMS** (ESI⁺) Calc: [M+H]⁺ (C₁₃H₁₉O₆P) 303.0992; measured 303.0987 = 1.6 ppm difference.



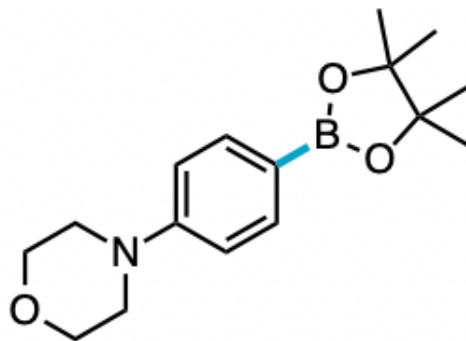
4,4,5,5-tetramethyl-2-phenyl-1,3,2-dioxaborolane (14): 80% was obtained following General Procedure C, analyzed via ¹H NMR analysis. NMR consistent with reported spectrum (*Org. Lett.* 2012, 14, 17, 4560–4563).



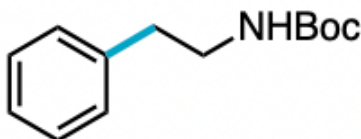
2-(4-methoxyphenyl)-4,4,5,5-tetramethyl-1,3,2-dioxaborolane (15): 63 mg (67%) was obtained as a white solid following General Procedure C. Product was isolated via flash chromatography on silica using 10 % ethyl acetate in hexanes. $^1\text{H NMR}$ (400 MHz, CDCl_3) δ 7.76 (d, $J = 8.6$ Hz, 2H), 6.90 (d, $J = 8.6$ Hz, 2H), 3.83 (s, 3H), 1.34 (s, 12H), consistent with reported spectrum (*Org. Lett.* 2012, 14, 17, 4560–4563).



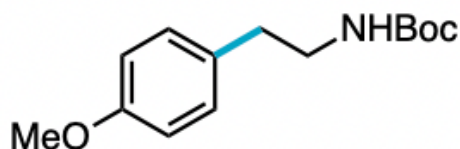
tert-butyl (4-(4,4,5,5-tetramethyl-1,3,2-dioxaborolan-2-yl)phenyl)carbamate (16): 92% was obtained following General Procedure C, analyzed via $^1\text{H NMR}$ analysis. NMR consistent with reported spectrum (*J. Am. Chem. Soc.* 2020, 142, 5, 2087–2092).



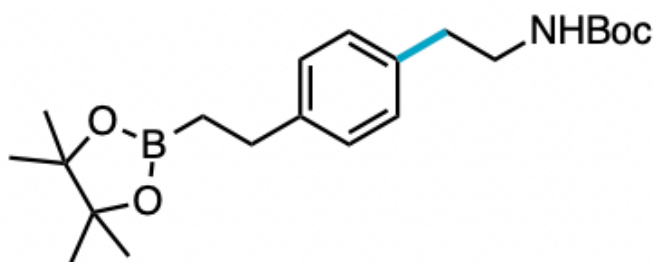
4-(4-(4,4,5,5-tetramethyl-1,3,2-dioxaborolan-2-yl)phenyl)morpholine (17): 59 mg (51%) was obtained as a white solid following General Procedure C. Product was isolated via flash chromatography on silica using 30% ethyl acetate in hexanes. $^1\text{H NMR}$ (400 MHz, CDCl_3) δ 7.73 (d, $J = 8.6$ Hz, 2H), 6.88 (d, $J = 8.7$ Hz, 2H), 3.92 – 3.78 (m, 4H), 3.34 – 3.17 (m, 4H), 1.33 (s, 12H), consistent with reported spectrum (*Org. Lett.* 2016, 18, 11, 2758–2761).



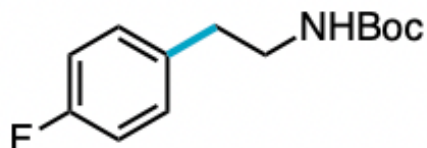
tert-butyl phenethylcarbamate (18): 53 mg (60%) was obtained following General Procedure D. Product was isolated via flash chromatography on silica using hexanes ethyl acetate. $^1\text{H NMR}$ (400 MHz, CDCl_3) δ 7.31 (dd, $J = 8.0, 6.6$ Hz, 2H), 7.20 (dd, $J = 8.6, 7.1$ Hz, 3H), 4.53 (s, 1H), 3.38 (q, $J = 6.8$ Hz, 2H), 2.80 (t, $J = 7.0$ Hz, 2H), 1.44 (s, 9H), consistent with reported spectrum (*Org. Lett.* 2019, 21, 8, 2818–2822).



tert-butyl (4-methoxyphenethyl)carbamate (19): 50 mg (50%) was obtained following General Procedure D. Product was isolated via flash chromatography on silica using hexanes ethyl acetate. $^1\text{H NMR}$ (400 MHz, CDCl_3) δ 7.11 (d, J = 8.6 Hz, 2H), 6.84 (d, J = 8.6 Hz, 2H), 4.52 (s, 1H), 3.79 (s, 3H), 3.33 (t, J = 6.8 Hz, 2H), 2.73 (t, J = 7.0 Hz, 2H), 1.43 (s, 9H), consistent with reported spectrum (*Org. Lett.* 2019, 21, 8, 2818–2822).

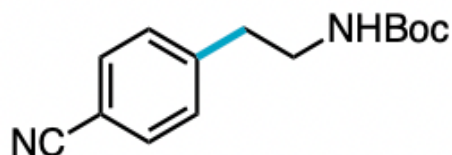


tert-butyl (4-(2-(4,4,5,5-tetramethyl-1,3,2-dioxaborolan-2-yl)ethyl)phenethyl)carbamate (20): 64% was obtained following General Procedure D. The product was partially purified on silica using hexanes ethyl acetate to verify product identity. $^1\text{H NMR}$ (400 MHz, CDCl_3) δ 7.08 (d, J = 7.8 Hz, 2H), 7.01 (d, J = 7.7 Hz, 2H), 3.28 (d, J = 8.7 Hz, 2H), 2.66 (dt, J = 12.4, 7.5 Hz, 4H), 1.36 (s, 9H), 1.15 (s, 12H), 1.06 (t, J = 8.2 Hz, 2H). $^{13}\text{C NMR}$ (126 MHz, CDCl_3) δ 155.89, 142.50, 136.02, 128.61, 128.21, 83.09, 63.63, 41.83, 38.80, 35.73, 34.25, 29.53, 28.42, 24.80. **HRMS** (ESI $^+$) Calc: $[\text{M}+\text{Na}]^+$ ($\text{C}_{21}\text{H}_{34}\text{BNO}_4$) 398.2477; measured 398.2469 = 2.0 ppm difference.

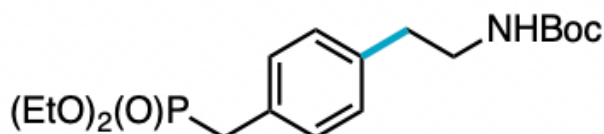


tert-butyl (4-fluorophenethyl)carbamate (21): 66% was obtained following General Procedure D and was analyzed via NMR analysis. The product was partially purified on silica using hexanes

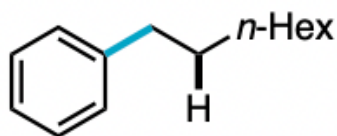
ethyl acetate to verify product identity. ^1H NMR was consistent with reported spectrum (*Molecules* 2016, 21(9), 1160).



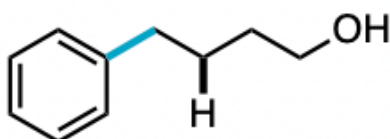
tert-butyl (4-cyanophenethyl)carbamate (22): 63 mg (64%) was obtained following General Procedure D. Product was isolated via flash chromatography on silica using hexanes ethyl acetate. ^1H NMR (400 MHz, CDCl_3) δ 7.60 (d, J = 8.0 Hz, 2H), 7.30 (d, J = 8.0 Hz, 2H), 3.39 (d, J = 7.0 Hz, 2H), 2.87 (t, J = 7.0 Hz, 2H), 1.43 (s, 9H), consistent with reported spectrum (*J. Med. Chem.* 2018, 61, 18, 8457–8467).



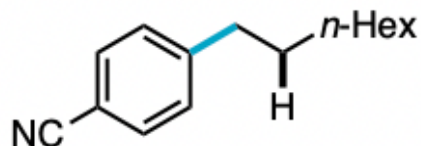
tert-butyl (4-((diethoxyphosphoryl)methyl)phenethyl)carbamate (23): 89 mg (60%) was obtained following General Procedure D. Product was isolated via flash chromatography on silica using hexanes ethyl acetate. ^1H NMR (400 MHz, CDCl_3) δ 7.24 (dd, J = 8.1, 2.5 Hz, 2H), 7.13 (d, J = 7.8 Hz, 2H), 4.51 (s, 1H), 4.10 – 3.95 (m, 4H), 3.36 (d, J = 6.7 Hz, 2H), 3.12 (d, J = 21.5 Hz, 2H), 2.77 (t, J = 7.1 Hz, 2H), 1.43 (s, 9H), 1.24 (t, J = 7.1 Hz, 6H), consistent with reported spectrum (*Angew. Chem. Int. Ed.* 2021, 60, 2393– 2397).



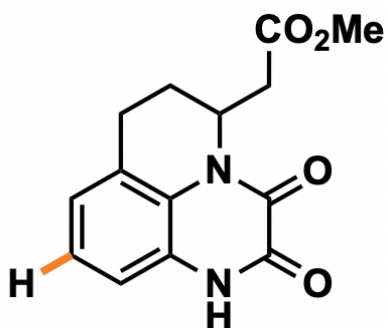
1-phenyloctane (24): 72% was obtained following General Procedure E and analyzed via GC.



4-phenylbutan-1-ol (25): 80% was obtained following General Procedure E and analyzed via GC.

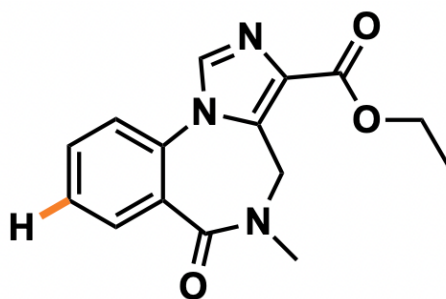


4-octylbenzonitrile (26): 61% was obtained following General Procedure E and analyzed via NMR analysis. Product confirmed with ^1H NMR of partial purification, consistent with reported spectrum (*J. Org. Chem.* 2013, 78, 15, 7436–7444). **HRMS** (ESI $^+$) Calc: $[\text{M}+\text{H}]^+$ ($\text{C}_{15}\text{H}_{21}\text{N}$) 216.1747; measured 216.1744 = 1.3 ppm difference.



methyl 2-(2,3-dioxo-2,3,6,7-tetrahydro-1H,5H-pyrido[1,2,3-de]quinoxalin-5-yl)acetate (27):

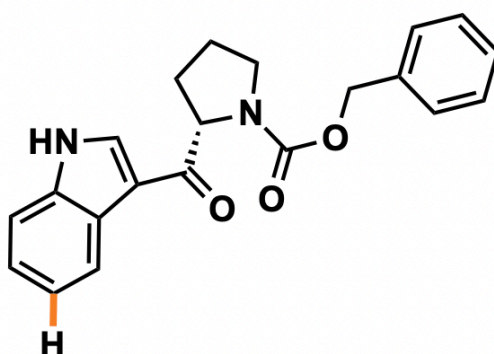
From **X1**, 16 mg (58%) was obtained following General Procedure A with the modification that a Penn PhD Photoreactor M2 equipped with a 405 nm light source was used to irradiate and no cyclohexylthiol was added. Product was isolated via mass-directed reversed phase chromatography using MeCN/H₂O with an NH₄OH modifier. **¹H NMR** (600 MHz, DMSO-d₆) δ 11.82 (s, 1H), 7.09 – 7.05 (m, 1H), 7.03 – 7.00 (m, 1H), 7.00 – 6.98 (m, 1H), 5.16 – 5.08 (m, 1H), 3.62 (s, 3H), 3.00 – 2.89 (m, 1H), 2.82 – 2.74 (m, 1H), 2.67 – 2.56 (m, 2H), 2.15 – 2.07 (m, 1H), 1.91 (tt, J = 13.9, 4.6 Hz, 1H). **¹³C NMR** (151 MHz, DMSO-d₆) δ 170.77, 154.19, 153.55, 125.64, 124.41, 123.25, 123.10, 122.56, 113.46, 51.69, 47.04, 34.96, 22.75, 21.08. **HRMS** (ESI+) Calc: [M+H]⁺ (C₁₄H₁₄N₂O₄) 275.1032; measured 275.1035 = 1.1 ppm difference.



ethyl 5-methyl-6-oxo-5,6-dihydro-4H-benzo[f]imidazo[1,5-a][1,4]diazepine-3-carboxylate

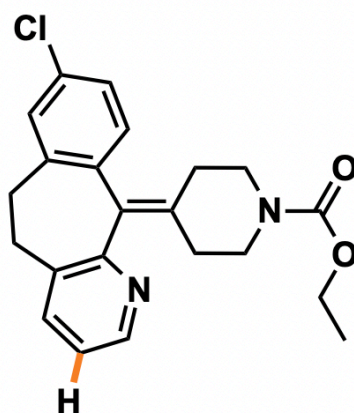
(28): From **X2**, 13 mg (45%) was obtained as a white solid following General Procedure A with

the modification that a Penn PhD Photoreactor M2 equipped with a 405 nm light source was used to irradiate and no cyclohexylthiol was added. Product was isolated via mass-directed reversed phase chromatography using MeCN/H₂O with an NH₄OH modifier. **¹H NMR** (600 MHz, DMSO-d₆) δ 8.37 (s, 1H), 7.93 – 7.89 (m, 1H), 7.76 – 7.72 (m, 2H), 7.61 – 7.55 (m, 1H), 4.98 (s, 1H), 4.47 (s, 1H), 4.32 (s, 2H), 3.10 (s, 3H), 1.33 (t, J = 7.1 Hz, 3H); consistent with reported spectrum (*Organic and Biomolecular Chemistry*, 2011, 9, 24, 8346–8355). **¹³C NMR** (151 MHz, DMSO-d₆) δ 165.74, 162.37, 136.42, 135.51, 132.68, 131.83, 131.73, 128.57, 128.16, 127.63, 122.82, 60.10, 42.00, 35.06, 14.22. **HRMS** (ESI+) Calc: [M+H]⁺ (C₁₅H₁₅N₃O₃) 286.1191; measured 286.1190 = –0.3 ppm difference.



benzyl (S)-2-(1H-indole-3-carbonyl)pyrrolidine-1-carboxylate (29): From **X5**, 10 mg (22%) was obtained as a white solid following General Procedure A with the modification that a Penn PhD Photoreactor M2 equipped with a 405 nm light source was used to irradiate and 8 mol% cyclohexylthiol was added. Product was isolated via mass-directed reversed phase chromatography using MeCN/H₂O with an NH₄OH modifier. Compound is a roughly 1:1 mixture of two rotamers with distinct NMR signals. Peaks observed are reported (not assigned). **¹H NMR** (600 MHz, DMSO-d₆) δ 12.02 (d, J = 12.6 Hz, 1H), 8.44 (dd, J = 15.2, 3.1 Hz, 1H), 8.20 (dd, J = 30.8, 7.4 Hz, 1H), 7.51 – 7.47 (m, 1H), 7.38 (d, J = 4.6 Hz, 2H), 7.36 – 7.29 (m, 1H), 7.26 – 7.17 (m, 2H), 7.12 – 7.06 (m, 1H), 7.01 (t, J = 7.6 Hz, 1H), 5.22 (ddd, J = 30.3, 8.6, 3.5 Hz, 1H), 5.12

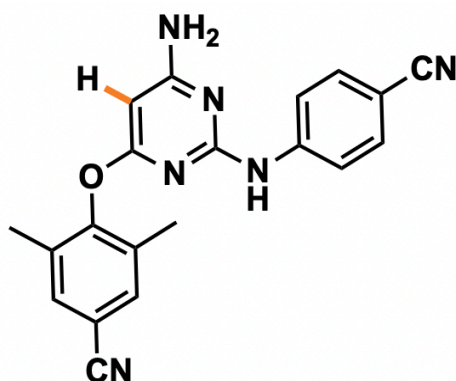
– 5.02 (m, 1H), 5.02 – 4.87 (m, 1H), 3.57 – 3.47 (m, 2H), 2.45 – 2.28 (m, 1H), 1.95 – 1.81 (m, 3H). **¹³C NMR** (151 MHz, DMSO-d₆) δ 193.65, 193.25, 153.83, 153.76, 137.17, 136.87, 136.54, 136.51, 133.87, 133.85, 128.40, 127.87, 127.75, 127.44, 127.23, 126.67, 125.75, 125.68, 122.94, 122.91, 121.85, 121.79, 121.39, 121.35, 113.73, 113.63, 112.15, 112.14, 65.75, 65.59, 61.95, 61.53, 47.27, 46.61, 31.84, 30.77, 23.99, 23.18. **HRMS** (ESI+) Calc: [M+H]⁺ (C₂₁H₂₀N₂O₃) 349.1552; measured 349.1557 = 1.4 ppm difference.



Ethyl 4-(8-chloro-5,6-dihydro-11H-benzo[5,6]cyclohepta[1,2-b]pyridin-11-ylidene)piperidine-1-carboxylate (30): From **X6**, 13 mg (33%) was obtained as an off-white solid following General Procedure A with the modification that a Penn PhD Photoreactor M2 equipped with a 405 nm light source was used to irradiate and no cyclohexylthiol was added. Product was isolated via mass-directed reversed phase chromatography using MeCN/H₂O with an NH₄OH modifier. **¹H NMR** (600 MHz, DMSO-d₆) δ 8.34 (dd, J = 4.6, 1.3 Hz, 1H), 7.60 – 7.55 (m, 1H), 7.30 (d, J = 2.0 Hz, 1H), 7.25 – 7.17 (m, 2H), 7.09 (d, J = 8.2 Hz, 1H), 4.03 (q, J = 7.1 Hz, 2H), 3.67 – 3.55 (m, 2H), 3.33 – 3.24 (m, 2H), 3.23 – 3.12 (m, 2H), 2.81 (dq, J = 13.2, 6.1 Hz, 2H), 2.37 – 2.24 (m, 2H), 2.23 – 2.11 (m, 2H), 1.17 (t, J = 7.1 Hz, 3H); consistent with reported spectrum (*Journal of Organic Chemistry*, 1989. 54, 9, 2242–2244). **¹³C NMR** (151 MHz, DMSO-d₆) δ 156.80, 154.54, 146.37, 140.18, 137.84, 137.48, 136.48, 133.47, 133.25, 131.62, 130.70,

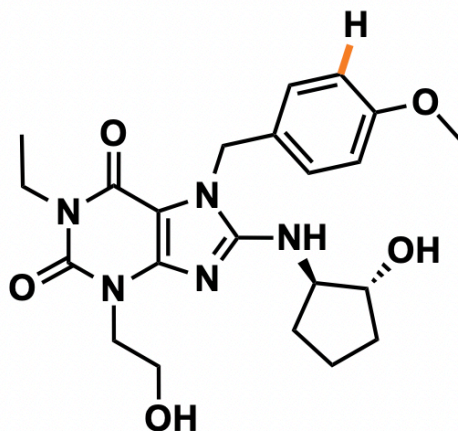
128.96, 125.69, 122.39, 60.69, 44.39, 44.31, 30.96, 30.55, 30.28, 30.18, 14.60. **HRMS** (ESI+)

Calc: [M+H]⁺ (C₂₂H₂₃CIN₂O₂) 383.1526; measured 383.1533 = 1.8 ppm difference.

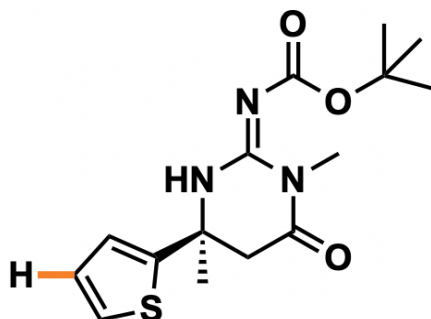


4-((6-amino-2-((4-cyanophenyl)amino)pyrimidin-4-yl)oxy)-3,5-dimethylbenzonitrile (31):

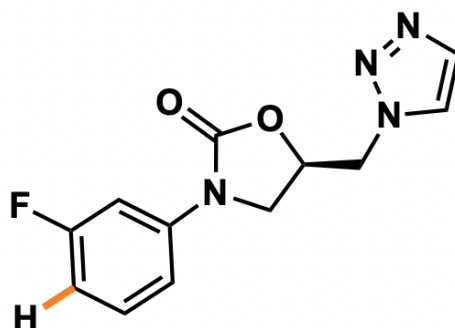
From **X11**, 22 mg (61%) was obtained following General Procedure A with the modification that a Penn PhD Photoreactor M2 equipped with a 405 nm light source was used to irradiate and no cyclohexylthiol was added. Product was isolated via mass-directed reversed phase chromatography using MeCN/H₂O with an NH₄OH modifier. **¹H NMR** (600 MHz, DMSO-d₆) δ 9.54 (s, 1H), 7.71 (s, 2H), 7.65 (d, J = 8.3 Hz, 2H), 7.46 (d, J = 8.8 Hz, 2H), 6.77 (s, 2H), 5.46 (s, 1H), 2.12 (s, 6H); consistent with reported spectrum (*Organic Process Research and Development*, 2010, 14, 3, 657–660). **¹³C NMR** (151 MHz, DMSO-d₆) δ 168.16, 166.41, 158.86, 153.90, 145.32, 132.93, 132.52, 132.45, 119.63, 118.69, 117.99, 108.01, 101.66, 78.66, 15.81. **HRMS** (ESI+) Calc: [M+H]⁺ (C₂₀H₁₆N₆O) 357.1464; measured 357.1474 = 2.7 ppm difference.



1-ethyl-8-(((1R,2R)-2-hydroxycyclopentyl)amino)-3-(2-hydroxyethyl)-7-(4-methoxybenzyl)-3,7-dihydro-1H-purine-2,6-dione (32): From **X12**, 23 mg (53%) was obtained following General Procedure A with the modification that a Penn PhD Photoreactor M2 equipped with a 405 nm light source was used to irradiate and no cyclohexylthiol was added. Product was isolated via mass-directed reversed phase chromatography using MeCN/H₂O with an NH₄OH modifier. **¹H NMR** (600 MHz, DMSO-d₆) δ 7.23 (d, *J* = 8.3 Hz, 2H), 6.94 (d, *J* = 6.6 Hz, 1H), 6.87 (d, *J* = 8.2 Hz, 2H), 5.25 (s, 2H), 4.84 – 4.75 (m, 2H), 3.98 (t, *J* = 6.4 Hz, 3H), 3.87 (dq, *J* = 13.8, 6.5 Hz, 3H), 3.70 (s, 3H), 3.62 (q, *J* = 5.9 Hz, 2H), 2.05 (dq, *J* = 13.4, 7.6 Hz, 1H), 1.84 (dq, *J* = 14.2, 6.8 Hz, 1H), 1.64 (ddt, *J* = 21.7, 13.6, 7.4 Hz, 2H), 1.52 – 1.40 (m, 2H), 1.08 (t, *J* = 6.9 Hz, 3H). **¹³C NMR** (151 MHz, DMSO-d₆) δ 158.62, 153.45, 152.55, 150.42, 148.67, 129.22, 128.82, 113.86, 101.19, 76.10, 61.49, 57.80, 55.05, 44.63, 44.61, 35.13, 32.43, 29.90, 20.53, 13.34. **HRMS** (ESI+) Calc: [M+H]⁺ (C₂₂H₂₉N₅O₅) 444.2247; measured 444.2253 = 1.3 ppm difference.

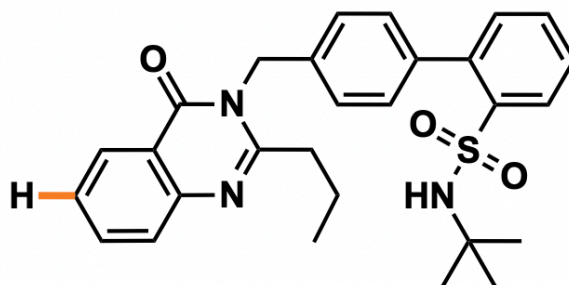


tert-butyl (S,Z)-(1,4-dimethyl-6-oxo-4-(thiophen-2-yl)tetrahydropyrimidin-2(1H)-ylidene)carbamate (33): From **X13**, 12 mg (38%) was obtained as a yellow oil following General Procedure A with the modification that a Penn PhD Photoreactor M2 equipped with a 405 nm light source was used to irradiate and no cyclohexylthiol was added. Product was isolated via mass-directed reversed phase chromatography using MeCN/H₂O with an NH₄OH modifier. **¹H NMR** (600 MHz, DMSO-d₆) δ 10.05 (s, 1H), 7.46 (d, J = 5.0 Hz, 1H), 7.06 – 7.03 (m, 1H), 7.00 (dd, J = 4.9, 3.7 Hz, 1H), 3.24 – 3.12 (m, 2H), 3.04 (s, 3H), 1.70 (s, 3H), 1.43 (s, 9H). **¹³C NMR** (151 MHz, DMSO-d₆) δ 167.63, 163.12, 156.84, 148.47, 127.51, 125.37, 124.09, 78.57, 52.88, 44.54, 31.31, 29.64, 27.92. **HRMS** (ESI+) Calc: [M+H]⁺ (C₁₅H₂₁N₃O₃S) 324.1382; measured 324.1379 = – 0.9 ppm difference.



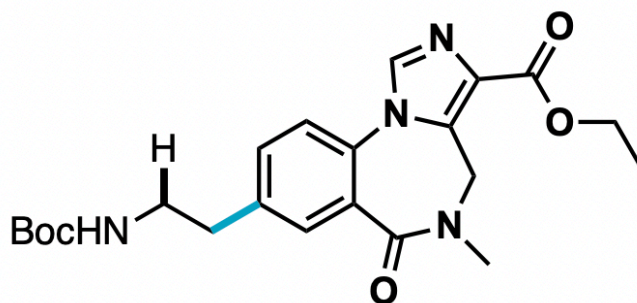
(R)-5-((1H-1,2,3-triazol-1-yl)methyl)-3-(3-fluorophenyl)oxazolidin-2-one (34): From **X14**, 16 mg (42%) was obtained as a white solid following General Procedure A with the modification that

a Penn PhD Photoreactor M2 equipped with a 405 nm light source was used to irradiate and no cyclohexylthiol was added. Product was isolated via mass-directed reversed phase chromatography using MeCN/H₂O with an NH₄OH modifier. Alternatively, on a 0.022 mmol scale, 2.9 mg (50%) was obtained as a white solid following General Procedure A with the same modifications as mentioned above. **¹H NMR** (600 MHz, DMSO-d₆) δ 8.17 (d, J = 0.8 Hz, 1H), 7.77 – 7.75 (m, 1H), 7.46 – 7.39 (m, 2H), 7.26 (dd, J = 8.3, 1.5 Hz, 1H), 6.96 (td, J = 8.2, 2.3 Hz, 1H), 5.15 (dq, J = 10.9, 5.4 Hz, 1H), 4.84 (d, J = 5.2 Hz, 2H), 4.25 (t, J = 9.2 Hz, 1H), 3.91 (dd, J = 9.3, 5.7 Hz, 1H). **¹³C NMR** (151 MHz, DMSO-d₆) δ 162.22 (d, J = 241.8 Hz), 153.44, 139.78 (d, J = 11.0 Hz), 133.41, 130.65 (d, J = 9.5 Hz), 125.87, 113.73, 110.17 (d, J = 21.1 Hz), 105.07 (d, J = 26.9 Hz), 70.93, 51.70, 47.02. **HRMS** (ESI+) Calc: [M+H]⁺ (C₁₂H₁₁FN₄O₂) 263.0944; measured 263.0945 = 0.3 ppm difference.



N-(tert-butyl)-4'-((4-oxo-2-propylquinazolin-3(4H)-yl)methyl)-[1,1'-biphenyl]-2-sulfonamide (35): From **X15**, 19 mg (39%) was obtained following General Procedure A with the modification that a Penn PhD Photoreactor M2 equipped with a 405 nm light source was used to irradiate and no cyclohexylthiol was added. Product was isolated via mass-directed reversed phase chromatography using MeCN/H₂O with an NH₄OH modifier. **¹H NMR** (600 MHz, DMSO-d₆) δ 8.18 (d, J = 7.9 Hz, 1H), 8.03 (d, J = 7.9 Hz, 1H), 7.83 (t, J = 7.7 Hz, 1H), 7.65 (d, J = 8.2 Hz, 1H), 7.61 (t, J = 7.4 Hz, 1H), 7.54 (q, J = 7.8 Hz, 2H), 7.38 (d, J = 6.9 Hz, 2H), 7.29 (d, J = 7.6 Hz, 1H), 7.21 (d, J = 7.3 Hz, 2H), 6.54 (s, 1H), 5.45 (s, 2H), 2.77 (t, J = 7.0 Hz, 2H), 1.76 (h,

$J = 7.2$ Hz, 2H), 0.96 – 0.94 (m, 9H), 0.94 – 0.91 (m, 3H). **^{13}C NMR** (151 MHz, DMSO- d_6) δ 161.66, 157.31, 146.99, 142.07, 139.58, 138.80, 135.78, 134.54, 132.58, 131.76, 129.65, 128.05, 127.74, 126.89, 126.50, 126.45, 125.58, 119.85, 53.35, 45.39, 35.79, 29.30, 19.41, 13.56. **HRMS** (ESI+) Calc: $[\text{M}+\text{H}]^+$ ($\text{C}_{28}\text{H}_{31}\text{N}_3\text{O}_3\text{S}$) 490.2164; measured 490.2172 = 1.6 ppm difference.



ethyl 8-(2-((tert-butoxycarbonyl)amino)ethyl)-5-methyl-6-oxo-5,6-dihydro-4H-benzo[f]imidazo[1,5-a][1,4]diazepine-3-carboxylate (36): From **X2**, 13 mg (29%) was obtained as a white solid following General Procedure E with the modification that a Penn PhD Photoreactor M2 equipped with a 405 nm light source was used to irradiate and 8 mol% cyclohexylthiol was added. In the reaction, an additional 4.4 mg (15%) of the reduction product was obtained as a white solid. Product was isolated via mass-directed reversed phase chromatography using MeCN/ H_2O with an NH_4OH modifier. **^1H NMR** (600 MHz, DMSO- d_6) δ 8.33 (s, 1H), 7.73 (s, 1H), 7.66 (d, $J = 8.2$ Hz, 1H), 7.59 – 7.53 (m, 1H), 6.93 (t, $J = 5.4$ Hz, 1H), 4.98 (s, 1H), 4.41 (s, 1H), 4.32 (s, 2H), 3.20 (q, $J = 6.8$ Hz, 2H), 3.10 (s, 3H), 2.81 (t, $J = 7.1$ Hz, 2H), 1.36 (s, 9H), 1.33 (t, $J = 7.1$ Hz, 3H). **^{13}C NMR** (151 MHz, DMSO- d_6) δ 165.75, 162.37, 155.57, 139.82, 136.31, 135.36, 132.97, 131.75, 130.06, 128.31, 127.54, 122.74, 77.61, 60.08, 42.01, 41.13, 35.09, 34.67, 28.23, 14.23. **HRMS** (ESI+) Calc: $[\text{M}+\text{H}]^+$ ($\text{C}_{22}\text{H}_{28}\text{N}_4\text{O}_5$) 429.2138; measured 429.2146 = 1.8 ppm difference.

2. 6. References

- (1) Ashby, E. C. Single-Electron Transfer, a Major Reaction Pathway in Organic Chemistry. An Answer to Recent Criticisms. *Acc. Chem. Res.* **1988**, 21 (11), 414–421.
- (2) Zhang, N.; Samanta, S. R.; Rosen, B. M.; Percec, V. Single Electron Transfer in Radical Ion and Radical-Mediated Organic, Materials and Polymer Synthesis. *Chem. Rev.* **2014**, 114 (11), 5848–5958.
- (3) Broggi, J.; Terme, T.; Vanelle, P. Organic Electron Donors as Powerful Single-Electron Reducing Agents in Organic Synthesis. *Angew. Chem., Int. Ed.* **2014**, 53 (2), 384–413.
- (4) Eberson, L. Electron-Transfer Reactions in Organic Chemistry. In *Advances in Physical Organic Chemistry*; Gold, V., Bethell, D., Eds.; Academic Press, 1982; Vol. 18, pp 79–185.
- (5) Prier, C. K.; Rankic, D. A.; MacMillan, D. W. C. Visible Light Photoredox Catalysis with Transition Metal Complexes: Applications in Organic Synthesis. *Chem. Rev.* **2013**, 113 (7), 5322–5363.
- (6) Shaw, M. H.; Twilton, J.; MacMillan, D. W. C. Photoredox Catalysis in Organic Chemistry. *J. Org. Chem.* **2016**, 81 (16), 6898–6926.
- (7) Romero, N. A.; Nicewicz, D. A. Organic Photoredox Catalysis. *Chem. Rev.* **2016**, 116 (17), 10075–10166.
- (8) Skubi, K. L.; Blum, T. R.; Yoon, T. P. Dual Catalysis Strategies in Photochemical Synthesis. *Chem. Rev.* **2016**, 116 (17), 10035–10074..
- (9) Narayanam, J. M. R.; Stephenson, C. R. J. Visible Light Photoredox Catalysis: Applications in Organic Synthesis. *Chem. Soc. Rev.* **2010**, 40 (1), 102–113.
- (10) Teegardin, K.; Day, J. I.; Chan, J.; Weaver, J. Advances in Photocatalysis: A Microreview of Visible Light Mediated Ruthenium and Iridium Catalyzed Organic Transformations. *Org. Process Res. Dev.* **2016**, 20 (7), 1156–1163.
- (11) Capaldo, L.; Ravelli, D. The Dark Side of Photocatalysis: One Thousand Ways to Close the Cycle. *Eur. J. Org. Chem.* **2020**, 2020 (19), 2783–2806.
- (12) Arias-Rotondo, D. M.; McCusker, J. K. The Photophysics of Photoredox Catalysis: A Roadmap for Catalyst Design. *Chem. Soc. Rev.* **2016**, 45 (21), 5803–5820.
- (13) Roth, H. G.; Romero, N. A.; Nicewicz, D. A. Experimental and Calculated Electrochemical Potentials of Common Organic Molecules for Applications to Single-Electron Redox Chemistry. *Synlett* **2016**, 27 (05), 714–723.
- (14) For a review on multi-photon excitation, which is not limited by the classic photocatalyst selection criteria, see: Glaser, F.; Kerzig, C.; Wenger, O. S. Multi-Photon Excitation in Photoredox Catalysis: Concepts, Applications, Methods. *Angew. Chem., Int. Ed.* **2020**, 59 (26), 10266–10284.
- (15) For a review on photoelectrochemistry, which is not limited by the classic photocatalyst selection criteria, see: Liu, J.; Lu, L.; Wood, D.; Lin, S. New Redox Strategies in Organic Synthesis by Means of Electrochemistry and Photochemistry. *ACS Cent. Sci.* **2020**, 6 (8), 1317–1340.
- (16) Meerwein, H.; Büchner, E.; Emster, K. van. Über Die Einwirkung Aromatischer Diazoverbindungen Auf α,β -Ungesättigte Carbonylverbindungen. *J. Prakt. Chem.* **1939**, 152 (7–10), 237–266.

- (17) Sainsbury, M. Modern Methods of Aryl-Aryl Bond Formation. *Tetrahedron* **1980**, 36 (23), 3327–3359.
- (18) Hanson, P.; Hammond, R. C.; Goodacre, P. R.; Purcell, J.; Timms, A. W. Sandmeyer Reactions. Part 2. Estimation of Absolute Rate Constants for Some Hydrogen-Transfer Reactions and for the Transfer of Water Ligands on Cu(I) to Aryl Radicals by Use of a Pschorr Radical Clock. *J. Chem. Soc., Perkin Trans. 2* **1994**, No. 4, 691–696.
- (19) Ghosh, I.; Marzo, L.; Das, A.; Shaikh, R.; König, B. Visible Light Mediated Photoredox Catalytic Arylation Reactions. *Acc. Chem. Res.* **2016**, 49 (8), 1566–1577.
- (20) Wang, C.-S.; Dixneuf, P. H.; Soulé, J.-F. Photoredox Catalysis for Building C–C Bonds from C(Sp²)–H Bonds. *Chem. Rev.* **2018**, 118 (16), 7532–7585.
- (21) Discekici, E. H.; Treat, N. J.; Poelma, S. O.; Mattson, K. M.; Hudson, Z. M.; Luo, Y.; Hawker, C. J.; Alaniz, J. R. de. A Highly Reducing Metal-Free Photoredox Catalyst: Design and Application in Radical Dehalogenations. *Chem. Commun.* **2015**, 51 (58), 11705–11708.
- (22) Devery, J. J.; Nguyen, J. D.; Dai, C.; Stephenson, C. R. J. Light-Mediated Reductive Debromination of Unactivated Alkyl and Aryl Bromides. *ACS Catal.* **2016**, 6 (9), 5962–5967.
- (23) Boyington, A. J.; Riu, M.-L. Y.; Jui, N. T. Anti-Markovnikov Hydroarylation of Unactivated Olefins via Pyridyl Radical Intermediates. *J. Am. Chem. Soc.* **2017**, 139 (19), 6582–6585.
- (24) Cheng, Y.; Gu, X.; Li, P. Visible-Light Photoredox in Homolytic Aromatic Substitution: Direct Arylation of Arenes with Aryl Halides. *Org. Lett.* **2013**, 15 (11), 2664–2667.
- (25) Shirakawa, E.; Hayashi, T. Transition-Metal-Free Coupling Reactions of Aryl Halides. *Chem. Lett.* **2012**, 41 (2), 130–134.
- (26) Galli, C. Radical Reactions of Arenediazonium Ions: An Easy Entry into the Chemistry of the Aryl Radical. *Chem. Rev.* **1988**, 88 (5), 765–792.
- (27) Kvasovs, N.; Gevorgyan, V. Contemporary Methods for Generation of Aryl Radicals. *Chem. Soc. Rev.* **2021**, 50 (4), 2244–2259.
- (28) Heinrich, M. R. Intermolecular Olefin Functionalisation Involving Aryl Radicals Generated from Arenediazonium Salts. *Chem. Eur. J.* **2009**, 15 (4), 820–833.
- (29) Raviola, C.; Protti, S. Leaving Groups in Metal-Free Arylations: Make Your Choice! *Eur. J. Org. Chem.* **2020**, 2020 (33), 5292–5304.
- (30) Weix and co-workers conducted an analysis of the commercially available aryl halides and found that aryl chlorides comprise more than two-thirds of the commercial substrates, see: Huang, L.; Ackerman, L. K. G.; Kang, K.; Parsons, A. M.; Weix, D. J. LiCl-Accelerated Multimetallic Cross-Coupling of Aryl Chlorides with Aryl Triflates. *J. Am. Chem. Soc.* **2019**, 141 (28), 10978–10983.
- (31) Electron-deficient aryl chlorides are viable substrates for the most reducing visible light photocatalysts. For examples, see refs 32–35.
- (32) Glaser, F.; Larsen, C. B.; Kerzig, C.; Wenger, O. S. Aryl Dechlorination and Defluorination with an Organic Super-Photoreductant. *Photochem. Photobiol. Sci.* **2020**, 19 (8), 1035–1041.
- (33) Shon, J.-H.; Kim, D.; Rathnayake, M. D.; Sittel, S.; Weaver, J.; Teets, T. S. Photoredox Catalysis on Unactivated Substrates with Strongly Reducing Iridium Photosensitizers. *Chem. Sci.* **2021**, 12 (11), 4069–4078.

- (34) Schmalzbauer, M.; Ghosh, I.; König, B. Utilising Excited State Organic Anions for Photoredox Catalysis: Activation of (Hetero)Aryl Chlorides by Visible Light-Absorbing 9-Anthrolate Anions. *Faraday Discuss.* **2019**, 215 (0), 364–378.
- (35) Ghosh, I.; Shaikh, R. S.; König, B. Sensitization-Initiated Electron Transfer for Photoredox Catalysis. *Angew. Chem., Int. Ed.* **2017**, 56 (29), 8544–8549.
- (36) Blanksby, S. J.; Ellison, G. B. Bond Dissociation Energies of Organic Molecules. *Acc. Chem. Res.* **2003**, 36 (4), 255–263.
- (37) Costentin, C.; Robert, M.; Savéant, J.-M. Fragmentation of Aryl Halide π Anion Radicals. Bending of the Cleaving Bond and Activation vs Driving Force Relationships. *J. Am. Chem. Soc.* **2004**, 126 (49), 16051–16057.
- (38) Ghosh, I.; Ghosh, T.; Bardagi, J. I.; König, B. Reduction of Aryl Halides by Consecutive Visible Light-Induced Electron Transfer Processes. *Science* **2014**, 346 (6210), 725–728.
- (39) For later work introducing a second catalyst structure for conPET, see: Neumeier, M.; Sampedro, D.; Májek, M.; de la Peña O'Shea, V. A.; Jacobi von Wangelin, A.; Pérez-Ruiz, R. Dichromatic Photocatalytic Substitutions of Aryl Halides with a Small Organic Dye. *Chem. Eur. J.* **2018**, 24 (1), 105–108.
- (40) MacKenzie, I. A.; Wang, L.; Onuska, N. P. R.; Williams, O. F.; Begam, K.; Moran, A. M.; Dunietz, B. D.; Nicewicz, D. A. Discovery and Characterization of an Acridine Radical Photoreductant. *Nature* **2020**, 580 (7801), 76–80.
- (41) Cole, J. P.; Chen, D.-F.; Kudisch, M.; Pearson, R. M.; Lim, C.-H.; Miyake, G. M. Organocatalyzed Birch Reduction Driven by Visible Light. *J. Am. Chem. Soc.* **2020**, 142 (31), 13573–13581.
- (42) Wang, S.; Wang, H.; Koenig, B. Photo-Induced Thiolate Catalytic Activation of Inert Caryl-Hetero Bonds for Radical Borylation. *Chem.* **2021**, 7 (6), 1653–1665.
- (43) Jin, S.; Dang, H.; Haug, G. C.; He, R.; Nguyen, V. D.; Nguyen, V. T.; Arman, H. D.; Schanze, K. S.; Larionov, O. V. Visible Light-Induced Borylation of C–O, C–N, and C–X Bonds. *J. Am. Chem. Soc.* **2020**, 142 (3), 1603–1613.
- (44) Zhang, L.; Jiao, L. Visible-Light-Induced Organocatalytic Borylation of Aryl Chlorides. *J. Am. Chem. Soc.* **2019**, 141 (23), 9124–9128.
- (45) Cybularczyk-Cecotka, M.; Szczepanik, J.; Giedyk, M. Photocatalytic Strategies for the Activation of Organic Chlorides. *Nat Catal* **2020**, 3 (11), 872–886.
- (46) Barham, J. P.; König, B. Synthetic Photoelectrochemistry. *Angew. Chem., Int. Ed.* **2020**, 59 (29), 11732–11747.
- (47) Novaes, L. F. T.; Liu, J.; Shen, Y.; Lu, L.; Meinhardt, J. M.; Lin, S. Electrocatalysis as an Enabling Technology for Organic Synthesis. *Chem. Soc. Rev.* **2021**. DOI: 10.1039/d1cs00223f.
- (48) Capaldo, L.; Quadri, L. L.; Ravelli, D. Merging Photocatalysis with Electrochemistry: The Dawn of a New Alliance in Organic Synthesis. *Angew. Chem., Int. Ed.* **2019**, 58 (49), 17508–17510.
- (49) Yu, Y.; Guo, P.; Zhong, J.-S.; Yuan, Y.; Ye, K.-Y. Merging Photochemistry with Electrochemistry in Organic Synthesis. *Org. Chem. Front.* **2019**, 7 (1), 131–135.

- (50) Cowper, N. G. W.; Chernowsky, C. P.; Williams, O. P.; Wickens, Z. K. Potent Reductants via Electron-Primed Photoredox Catalysis: Unlocking Aryl Chlorides for Radical Coupling. *J. Am. Chem. Soc.* **2020**, *142* (5), 2093–2099.
- (51) Kim, H.; Kim, H.; Lambert, T. H.; Lin, S. Reductive Electrophotocatalysis: Merging Electricity and Light To Achieve Extreme Reduction Potentials. *J. Am. Chem. Soc.* **2020**, *142* (5), 2087–2092.
- (52) For example, high-throughput experimentation (HTE) remains particularly difficult for electrochemical processes but is well-established for photochemical systems. Recent work from Lin has advanced an attractive HTE plate for electrophotocatalysis in undivided cells. However, divided cells are required for all reductive electrophotocatalysis reported to-date, which would not be compatible with this technology. See ref 53.
- (53) Rein, J.; Annand, J. R.; Wismer, M. K.; Fu, J.; Siu, J. C.; Klapars, A.; Strotman, N. A.; Kalyani, D.; Lehnher, D.; Lin, S. Unlocking the Potential of High-Throughput Experimentation for Electrochemistry with a Standardized Microscale Reactor. *ChemRxiv*. **2021**. <https://doi.org/10.26434/chemrxiv.14173538.v2>
- (54) Aryl chlorides with electron-withdrawing groups are in these bounds and are viable substrates for the most reducing photoredox catalysts, albeit often in diminished yield. For selected examples, see refs 55 and 56.
- (55) Li, H.; Liu, Y.; Chiba, S. Anti-Markovnikov Hydroarylation of Alkenes via Polysulfide Anion Photocatalysis. *Chem. Commun.* **2021**. <https://doi.org/10.1039/D1CC02185K>.
- (56) Boyington, A. J.; Seath, C. P.; Zearfoss, A. M.; Xu, Z.; Jui, N. T. Catalytic Strategy for Regioselective Arylethylamine Synthesis. *J. Am. Chem. Soc.* **2019**, *141* (9), 4147–4153.
- (57) Andrieux, C. P.; Pinson, J. The Standard Redox Potential of the Phenyl Radical/Anion Couple. *J. Am. Chem. Soc.* **2003**, *125* (48), 14801–14806.
- (58) Chernowsky, C.; Chmiel, A.; Wickens, Z. Photocatalytic Activity of Diverse Organic Radical Anions: Catalyst Discovery Enables Cleavage of Strong C(Sp²)–N and C(Sp²)–O Bonds. *ChemRxiv*. **2021**. <https://doi.org/10.26434/chemrxiv.14710398.v1>
- (59) Targos, K.; Williams, O. P.; Wickens, Z. K. Unveiling Potent Photooxidation Behavior of Catalytic Photoreductants. *J. Am. Chem. Soc.* **2021**, *143* (11), 4125–4132.
- (60) Connell, T. U.; Fraser, C. L.; Czyz, M. L.; Smith, Z. M.; Hayne, D. J.; Doeven, E. H.; Agugiaro, J.; Wilson, D. J. D.; Adcock, J. L.; Scully, A. D.; Gómez, D. E.; Barnett, N. W.; Polyzos, A.; Francis, P. S. The Tandem Photoredox Catalysis Mechanism of [Ir(Ppy)₂(Dtb-Bpy)]⁺ Enabling Access to Energy Demanding Organic Substrates. *J. Am. Chem. Soc.* **2019**, *141*, 17646–17658.
- (61) Hu, J.; Wang, J.; Nguyen, T. H.; Zheng, N. The Chemistry of Amine Radical Cations Produced by Visible Light Photoredox Catalysis. *Beilstein J. Org. Chem.* **2013**, *9* (1), 1977–2001.
- (62) Speckmeier, E.; Fischer, T. G.; Zeitler, K. A Toolbox Approach To Construct Broadly Applicable Metal-Free Catalysts for Photoredox Chemistry: Deliberate Tuning of Redox Potentials and Importance of Halogens in Donor–Acceptor Cyanoarenes. *J. Am. Chem. Soc.* **2018**, *140* (45), 15353–15365.
- (63) Recent reports from Leonori and co-workers have illustrated that α -amino radicals formed in situ from alkylamine oxidation promote aryl radical reactions from aryl iodides and bromides via halogen atom transfer (XAT). However, the stronger and less polarizable

C(sp²)–Cl bonds are expected to be less amenable to such a mechanism; see refs 64 and 65.

- (64) Constantin, T.; Zanini, M.; Regni, A.; Sheikh, N. S.; Juliá, F.; Leonori, D. Aminoalkyl Radicals as Halogen-Atom Transfer Agents for Activation of Alkyl and Aryl Halides. *Science* **2020**, 367 (6481), 1021–1026.
- (65) Constantin, T.; Juliá, F.; Sheikh, N. S.; Leonori, D. A Case of Chain Propagation: α -Aminoalkyl Radicals as Initiators for Aryl Radical Chemistry. *Chem. Sci.* **2020**, 11 (47), 12822–12828.
- (66) Azzena, U.; Denurra, T.; Melloni, G.; Fenude, E.; Rassu, G. Electron-Transfer-Induced Reductive Demethoxylation of Anisole: Evidence for Cleavage of a Radical Anion. *J. Org. Chem.* **1992**, 57 (5), 1444–1448. <https://doi.org/10.1021/jo00031a022>.
- (67) Xu, H.; Yu, B.; Zhang, H.; Zhao, Y.; Yang, Z.; Xu, J.; Han, B.; Liu, Z. Reductive Cleavage of Inert Aryl C–O Bonds to Produce Arenes. *Chem. Commun.* **2015**, 51 (61), 12212–12215.
- (68) The oxidation potential of formate, +1.25 V vs SCE, is within the bound of the excited state reduction potential of each catalyst. For the potential of formate, see supporting information.
- (69) Gu, X.; Lu, S.; Fu, X.; Qiu, Z.; Sui, Q.; Guo, X. Carbon Dioxide Radical Anion-Based UV/S2O8²⁻/HCOOH Reductive Process for Carbon Tetrachloride Degradation in Aqueous Solution. *Sep. Purif. Technol.* **2017**, 172, 211–216.
- (70) Jacobsen, E.; Roberts, J. L.; Sawyer, D. T. Electrochemical Oxidation of Formate in Dimethylsulfoxide at Gold and Platinum Electrodes. *J. Electroanal. Chem. Interf. Electrochem.* **1968**, 16 (3), 351–360.
- (71) Grills, D. C.; Lyman, S. V. Radiolytic Formation of the Carbon Dioxide Radical Anion in Acetonitrile Revealed by Transient IR Spectroscopy. *Phys. Chem. Chem. Phys.* **2018**, 20 (15), 10011–10017.
- (72) Rosso, J. A.; Bertolotti, S. G.; Braun, A. M.; Mártire, D. O.; Gonzalez, M. C. Reactions of Carbon Dioxide Radical Anion with Substituted Benzenes. *J. Phys. Org. Chem.* **2001**, 14 (5), 300–309.
- (73) Koppenol, W. H.; Rush, J. D. Reduction Potential of the Carbon Dioxide/Carbon Dioxide Radical Anion: A Comparison with Other C1 Radicals. *J. Phys. Chem.* **1987**, 91 (16), 4429–4430.
- (74) Sevrin, M. J.; Furst, L.; Nguyen, J. D.; Collins, J. L.; Stephenson, C. R. J. Lithium Bis-Catechol Borate as an Effective Reductive Quencher in Photoredox Catalysis. *Tetrahedron* **2018**, 74 (26), 3246–3252.
- (75) Beatty, J. W.; Stephenson, C. R. J. Amine Functionalization via Oxidative Photoredox Catalysis: Methodology Development and Complex Molecule Synthesis. *Acc. Chem. Res.* **2015**, 48 (5), 1474–1484.
- (76) Singh, P. P.; Srivastava, V. Recent Advances in Using 4DPAIPN in Photocatalytic Transformations. *Org. Biomol. Chem.* **2021**, 19 (2), 313–321.
- (77) Németh, G.; Greff, Z.; Sipos, A.; Varga, Z.; Székely, R.; Sebestyén, M.; Jászay, Z.; Béni, S.; Nemes, Z.; Pirat, J.-L.; Volle, J.-N.; Virieux, D.; Gyuris, Á.; Kelemenics, K.; Áy, É.; Minarovits, J.; Szathmary, S.; Kéri, G.; Órfi, L. Synthesis and Evaluation of Phosphorus Containing, Specific CDK9/CycT1 Inhibitors. *J. Med. Chem.* **2014**, 57 (10), 3939–3965.
- (78) Fyfe, J. W. B.; Watson, A. J. B. Recent Developments in Organoboron Chemistry: Old Dogs, New Tricks. *Chem* **2017**, 3 (1), 31–55.

- (79) We found for most of the reactions studied herein that the photocatalyst bleached over the course of the reaction and that adding photocatalyst in two batches provided improved yields, see the Supporting information for details. At this stage, a photocatalytically active decomposition product, either closed or open shell, cannot be excluded as a possibility. For an example of isophthalonitrile catalysts being attacked by radical intermediates, see: Grotjahn, S.; König, B. *Org. Lett.* **2021**, 23, 3146–3150.
- (80) For an example of unactivated alkene hydroarylation, see: ref 55.
- (81) While both alkylamine and formate reductants can act as hydrogen atom sources, we noted that sodium formate exhibits limited solubility under the reaction conditions. We suspect that the limited concentration of the reductant diminishes premature HAT to the aryl radical relative to homogeneous alkylamine reductants.
- (82) Ito, O. Flash Photolysis Study on Reversible Addition Reactions of Thiyl Radicals. *Res. Chem. Intermed.* **1995**, 21 (1), 69–93.
- (83) For a proposed mechanism for $\text{CO}_2^{\bullet-}$ generation from PhSSPh, see the supporting information. PhSSPh was used as the thiyl radical source to initiate the slightly endothermic HAT (BDE PhSH = 79 kcal/mol, BDE HCO_2^- = 86 kcal/mol; see ref 84.
- (84) Dénès, F.; Pichowicz, M.; Povie, G.; Renaud, P. Thiyl Radicals in Organic Synthesis. *Chem. Rev.* **2014**, 114 (5), 2587–2693.
- (85) McDaniel, K. A.; Blood, A. R.; Smith, G. C.; Jui, N. T. Dearomatization of Unactivated Arenes via Catalytic Hydroalkylation. *ACS Catal.* **2021**, 11 (9), 4968–4972.

Chapter 3: Unveiling Potent Photooxidation Behavior of Catalytic Photoreductants

Adapted with permission from Karina Targos,[†] **Oliver P. Williams**,[†] and Zachary K. Wickens. Unveiling Potent Photooxidation Behavior of Catalytic Photoreductants. *J. Am. Chem. Soc.* **2021**, 143, 11, 4125–4132. Copyright 2021 American Chemical Society." [†]K.T. and O.P.W. contributed equally.

3. 1. Abstract

We describe a photocatalytic system that reveals latent photooxidant behavior from one of the most reducing conventional photoredox catalysts, *N*-phenylphenothiazine (PTH). This aerobic photochemical reaction engages difficult to oxidize feedstocks, such as benzene, in C(sp²)-N coupling reactions through direct oxidation. Mechanistic studies are consistent with activation of PTH via photooxidation and that Lewis acid co-catalysts scavenge inhibitors formed upon catalyst activation.

3. 2. Introduction

Reactions driven by single electron transfer (SET) are pervasive in organic chemistry. Consequently, new strategies to induce redox events are poised to profoundly impact synthetic chemistry.¹⁻⁴ Photoredox catalysis has unlocked a broad range of attractive new transformations through conversion of energy from readily accessible LEDs into chemical redox potential.⁵⁻⁸ However, only a portion of this energy⁹ can be harnessed due to inevitable energy losses from vibrational relaxation, internal conversion, and intersystem crossing.¹⁰ Despite tremendous effort in photoredox catalyst design,¹⁰⁻¹⁷ excited state potentials beyond roughly -2 and +2 V vs. SCE remain difficult to achieve using conventional photocatalyst design principles wherein a single photon from commercial LEDs is used as the primary energy source (Figure 3.1 A). Unfortunately,¹⁸⁻²² this redox window excludes numerous abundant hydrocarbon feedstocks from facile photoinduced electron transfer.²³

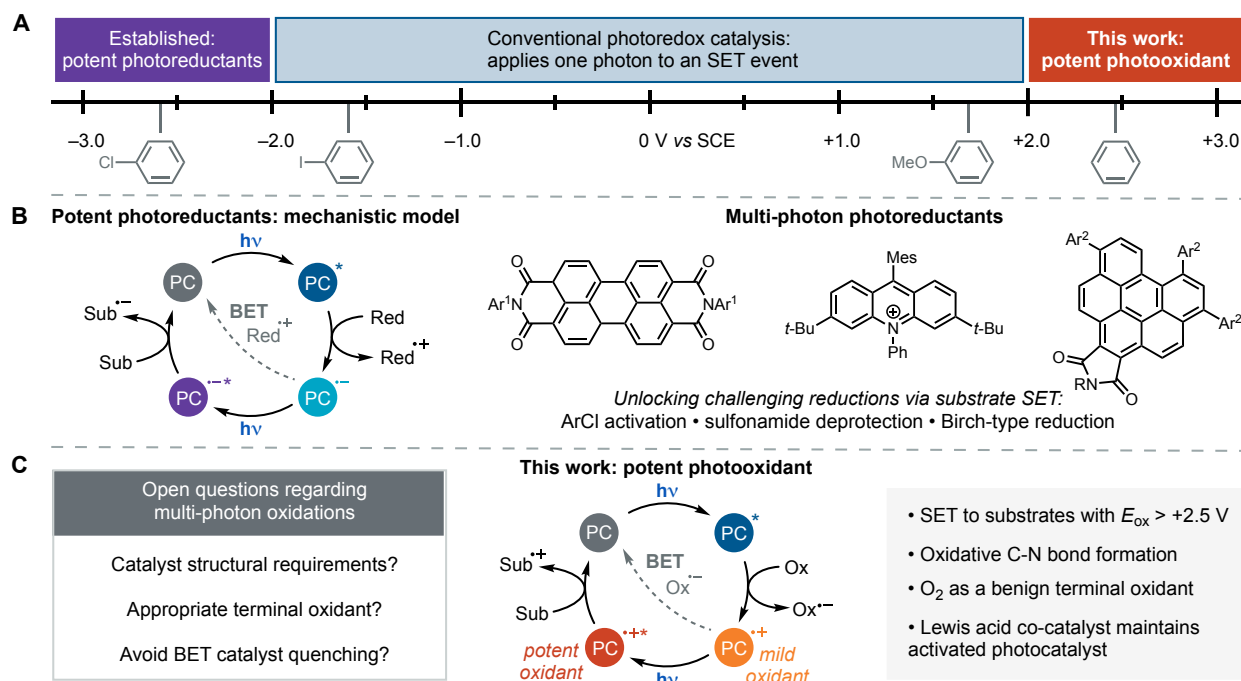


Figure 3.1 **A** Overview of redox potentials in photoredox catalysis. **B** Overview of multi-photon photoreductants. Full catalyst structures available in SI. **C** Overview of research described herein.

To overcome the energetic limitations intrinsic to conventional photoredox catalysis, König and coworkers recently designed a photocatalytic system that drives challenging reductive SET events using the energy of two photons rather than one. This consecutive photoninduced electron transfer (conPET)^{24,25} strategy relies on a catalytic photooxidant and sacrificial reductant that, upon irradiation, result in a potent radical anion photoreductant (Figure 3.1 B). Despite its mechanistic complexity, this approach is practical and operationally simple; it leverages inexpensive and safe LEDs to accomplish reactions that otherwise require UV photoreactors or harsh chemical reductants. Following proof-of-concept aryl halide reductions,^{24,26–33} this approach has enabled photochemical alternatives to alkali metal reductants in reactions such as Birch reductions³⁴ and sulfonamide cleavage.³⁵

In contrast to the progress in photoreductions, oxidations driven by the consumption of multiple photons have remained elusive. We suspect that this is the consequence of two

inextricable challenges: (1) the catalyst must be a competent photocatalyst in both the closed shell and radical cation states^{5,25} and (2) the terminal oxidant must efficiently activate the catalyst but not otherwise interfere with the reaction (Figure 3.1 C).³⁶ Given the difficulty applying multiple photons towards a challenging SET oxidation, photoredox reactions initiated by SET oxidation are typically limited to electron-rich hydrocarbon substrates.^{6,37–42}

We questioned whether conventional photoreductants, which typically possess persistent radical cation states, could be repurposed as strong photooxidants using a conPET strategy.⁴³ We hypothesized photochemical conditions designed to drive these photocatalysts towards their oxidized congeners could reveal potent photooxidation behavior. To probe this hypothesis, we targeted cyclic triarylamine photoreductants. These are a well-established and modular family of photocatalysts^{21,44} and photophysical studies conducted by Wasilewski and coworkers indicate that their radical cation congeners exhibit photochemical activity.⁴⁵ Furthermore, intriguing studies from Wagenknecht and coworkers have implicated photoexcitation of triarylamine radical cations formed via SF₆ reduction in alkene pentafluorosulfonylation processes.^{46,47} We envisioned that photochemically accessing these radical cations using a bystander oxidant would offer an ideal avenue to explore the potency of these radical cation photooxidants.

We selected the Nicewicz-type⁴¹ oxidative coupling of arenes and *N*-heterocyclic nucleophiles as a model reaction. This synthetically valuable transformation is representative of the general challenges in oxidative photoredox catalysis. It has been predominantly limited to electron-rich arene substrates, such as anisole derivatives⁴⁸ and also requires a bystander terminal oxidant. Difficult to oxidize arene substrates, such as benzene, typically mandate high energy UV light (UVB or shorter)¹⁸ or strong ground state oxidants (e.g. DDQ) that absorb visible light.^{49,50} Recent progress by Lambert and coworkers has introduced an alternative electrophotocatalytic approach that employs electrochemistry and photochemistry in concert to accomplish this energetically demanding oxidation.^{51–53} However, while electrophotocatalysis is

an exciting emerging area of research,^{51,52,54–63} these reactions require specialized electrochemical equipment (e.g. divided cells, electrodes, and power supplies) and are technically complex relative to purely photochemical processes.⁶⁴ Thus, we envisioned that promoting this transformation using a bench stable and commercially available photocatalyst simply with inexpensive LEDs would be a synthetically useful complement to existing methods. Accordingly, this constitutes an appealing context for our proof-of-concept experiments.

3. 3. Results and Discussion

First, we examined three distinct photoreductants^{21,65,66} and a range of oxidants for activity in the oxidative coupling of benzene ($E_{\text{ox}} = 2.5 \text{ V vs. SCE}$)⁶⁷ and pyrazole **1** (Figure 3.2). We initially aimed to generate the catalyst radical cation congener via photoreduction of reagents that undergo irreversible decomposition after SET to avoid catalyst deactivation via back electron transfer (BET). Excitingly, these data revealed that *N*-phenylphenothiazine (**PTH**), the most reducing photocatalyst of the series, could promote this challenging oxidative coupling in low yield using organohalides as the oxidant. A sufficiently strong oxidant to oxidize each catalyst to the corresponding radical cation without additional energy from light, NOPF₆,⁶⁸ provided low yield of benzene oxidation products using all three catalysts. However, under one atmosphere of O₂, **PTH** promoted oxidative coupling in promising yield (14%). Given the enhanced stability of radical cations in fluorinated alcohol solvents,^{19,53,69–71} we substituted MeCN for trifluoroethanol (TFE). This resulted in a modest increase in reaction yield with **PTH** but only traces of product with the other two catalysts. Of note, while most photoredox catalysts undergo rapid intersystem crossing to a long-lived triplet,^{5,13} **PTH** is a singlet excited state reductant.⁷² This property circumvents photocatalyst deactivation by triplet-triplet annihilation with O₂.

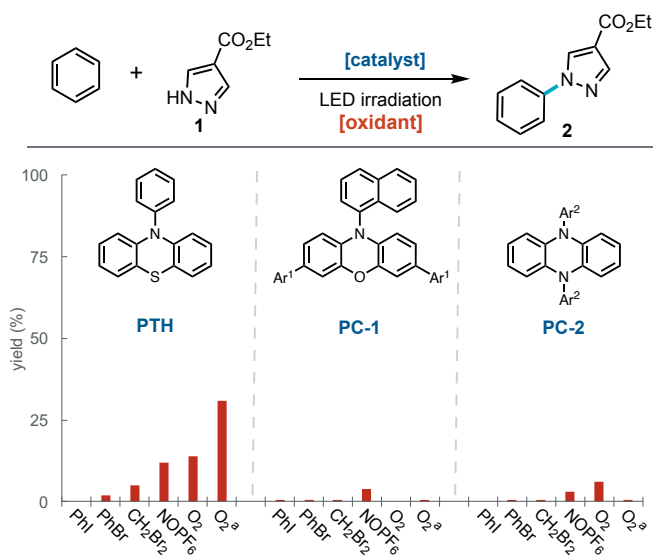


Figure 3.2 Survey of oxidants and photoreductants. Reactions were conducted on a 0.05 mmol scale in 1:1 MeCN:PhH for 24h, unless noted otherwise, using 2 equiv. oxidant or 1 atm O₂. Ar₁ = 4-biphenyl. Ar₂ = 2-naphthyl. PTH irradiated using 390 nm Kessil lamp. PC-1 and PC-2 irradiated using Tuna Blue Kessil lamp. a:1:1 TFE:PhH.

We suspected that BET between **PTH** radical cation and superoxide⁷³ might attenuate reactivity under these conditions (Figure 3.3).⁷⁴ Indeed, when synthetically prepared **PTH** radical cation is treated with KO₂, we observe a rapid color change and reformation of **PTH** by ¹H-NMR. Given that superoxide generation is inextricable from aerobic catalyst activation, this observation could account for the modest reactivity of this catalytic system (Figure 3.4, entry 1). As expected, addition of 5 mol % KO₂ to the reaction mixture completely suppressed product formation (entry 2). We hypothesized that additives capable of sequestering or scavenging this inhibitor would enhance the observed reactivity. Guided by this model, we found addition of one equivalent of an inexpensive, redox innocent Lewis acid, LiClO₄, dramatically improved the yield of oxidative coupling product (entry 3). Reduction of the LiClO₄ loading to a substoichiometric quantity (20 mol %) retained the benefits of the additive, suggesting a co-catalytic role for LiClO₄ rather than it purely sequestering stoichiometric byproducts (entry 4). In principle, the lithium co-catalyst could mitigate BET by promoting superoxide disproportionation.^{75,76} Consistent with this proposed Lewis

acidic role, alkylammonium salts had no impact on the reaction (entry 5); whereas, other Lewis acidic lithium salts retained the catalytic effect (entries 6 and 7). Final tuning of the reaction parameters revealed adjusting the solvent mixture to include a small amount of hexafluoroisopropanol (HFIP) delivered the desired product in 89% yield (entry 8). Substitution of **PTH** with other triarylamine photoreductants or a classic metal-based photoreductant, Ir(ppy)₃, resulted in only trace yield of oxidation product under these otherwise optimal conditions (entries 9–11).

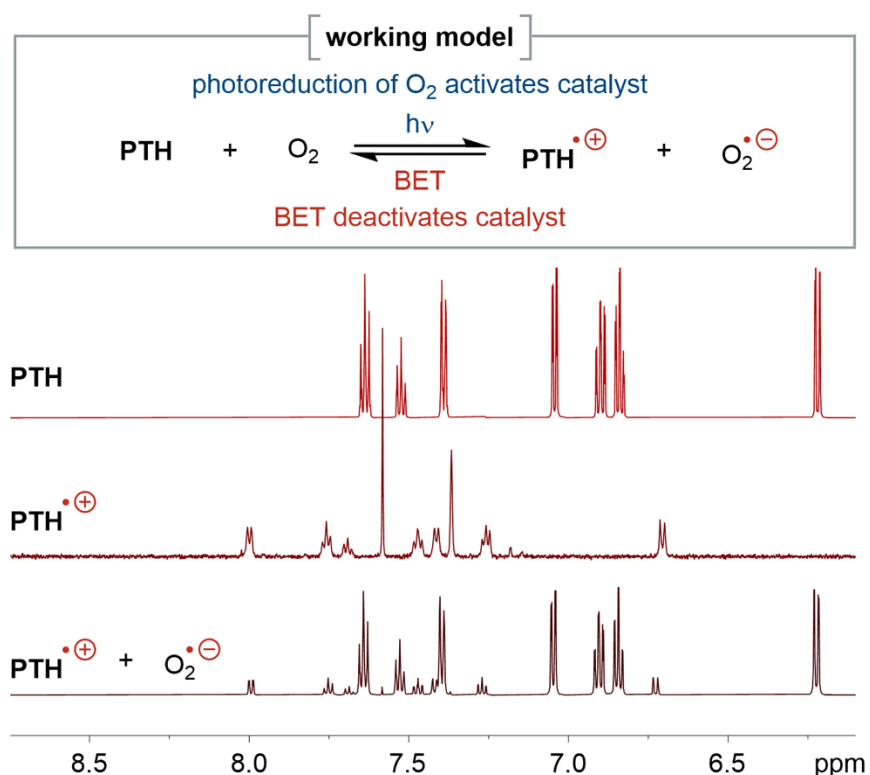


Figure 3.3 ¹H NMR spectroscopic evidence supporting working model for catalyst deactivation pathways.

entry	additive	yield (%)
1	none	31
2	KO ₂ (5 mol %)	<2
3	LiClO ₄ (1 equiv)	86
4	LiClO ₄ (20 mol %)	73
5	<i>n</i> -Bu ₄ NClO ₄ (20 mol %)	29
6	LiPF ₆ (20 mol %)	64
7	LiOTf (20 mol %)	56
8	LiClO ₄ (20 mol %) ^b	89
9	PC-1 (5 mol %), LiClO ₄ (20 mol %) ^{a,b}	<2
10	PC-2 (5 mol %), LiClO ₄ (20 mol %) ^{a,b}	<2
11	Ir(ppy) ₃ (1 mol %), LiClO ₄ (20 mol %) ^{a,b}	<2

Figure 3.4 Reaction optimization. Reactions were conducted on a 0.05 mmol scale in 1:1 TFE:PhH for 24h. See SI for details. ^a9:1:10 TFE:HFIP:PhH solvent mixture. ^bTuna Blue Kessil lamp irradiation.

Having identified a promising catalytic system, we examined the scope of this new process (Figure 3.5). Pyrazole nucleophiles bearing a range of electron-withdrawing moieties, including ketones (**3**), aldehydes (**4**), nitriles (**5**), and trifluoromethyl groups (**6**) were oxidatively coupled to benzene. Halogenated pyrazoles (**7** and **8**) were also productively coupled despite the fact that **PTH** is a potent photoreductant. Prior approaches capable of oxidizing benzene have not been readily amenable to the arylation of neutral heterocyclic substrates.⁷⁷ In contrast, we observed coupling of both parent pyrazole (**9**) and even an electron-rich analog (**10**), albeit in diminished yield relative to the electron deficient heterocyclic coupling partners. In addition to pyrazole derivatives, we found that 1,2,3-triazoles (**11** and **12**) were amenable to oxidative coupling with benzene. Even an exceptionally challenging to oxidize electron-deficient arene, chlorobenzene, could be engaged in productive C(sp²)–N coupling via arene photooxidation (**13**). To probe the limits of what this catalytic system can oxidize, we evaluated acetophenone as an arene substrate and detected at most traces of oxidative coupling products. This result indicates that this arene is too electronically deactivated for oxidation under these conditions. We recognized that benzylic

C–H bonds could be a liability under these aerobic conditions; however, we found reasonable C(sp²)–N coupling yields could be obtained from toluene using our standard conditions and these yields could be further improved by tuning the reaction conditions to mitigate benzylic oxidation processes.⁷⁸ Under these modified conditions, **PTH** promoted the photochemical coupling of toluene, *m*-xylene, and mesitylene with pyrazole derivatives in high yield (**14–21**). The oxidation of *m*-xylene and mesitylene could be achieved using a smaller excess of arene, presumably due to the significantly lower oxidation potential relative to benzene.⁷⁹ Of note, while the scope and reagent stoichiometries required for this approach are similar to prior electrophotocatalytic systems, these photocatalytic conditions exclusively require commercially available catalysts and no specialized equipment outside of LED lamps. Furthermore, this simple photocatalytic system delivers coupling products with substantially shorter reaction times.⁸⁰ Overall, these data illustrate that the scope of this photochemical process described herein is on par with complementary electrophotocatalytic approaches.^{51,52}

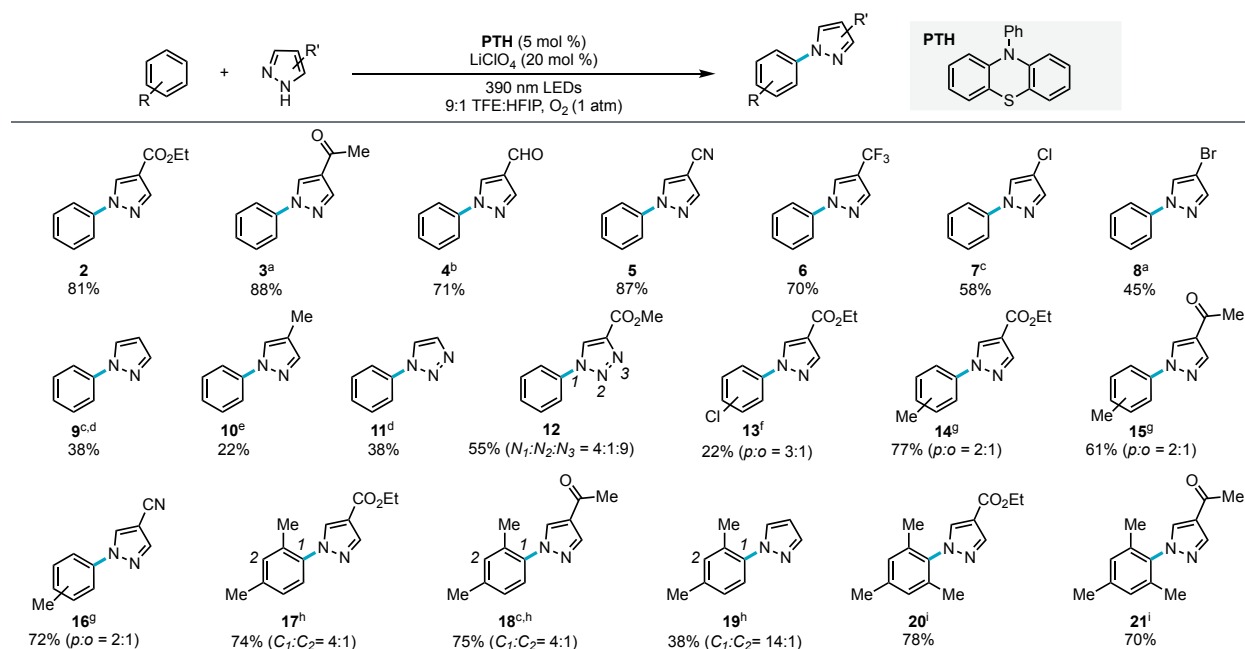


Figure 3.5 Scope of arene C–H amination. Reactions conducted using 0.4 mmol of heterocycle, 8 mL of arene, and irradiated with two 390 nm Kessil lamps for 24h with fan cooling. See the SI for further experimental details. Isolated yields. ^a 20% LiPF₆. ^b 1:1 HFIP:PhH solvent. ^c NMR yield. ^d 0% r.s.m. ^e 31% r.s.m. ^f 10% r.s.m. ^g 1:1:2 MeCN:HFIP:arene solvent with 10% *t*-dodecyl mercaptan. ^h 10 equiv arene, 0.1 M in 1:1 MeCN:HFIP, 10% *t*-dodecyl mercaptan. ⁱ 5 equiv arene, 0.1 M in 1:1 MeCN:HFIP, 10% *t*-dodecyl mercaptan.

Next, we aimed to uncover preliminary mechanistic insight into this new and unusually oxidizing photocatalytic system. First, we collected the full reaction profile by monitoring the yield of coupling product **2** as a function of time (Figure 3.6 A). These data revealed an induction period, wherein only a trace amount of product is formed, followed by 0th order formation of product that continues until nearly all of the pyrazole is consumed (see SI for complete reaction profile). If irradiation is temporarily suspended during the induction period, the onset of product formation is correspondingly delayed (Figure 3.6 B). Similarly, when irradiation is halted during the product-forming regime, the reaction ceases until irradiation resumes (Figure 3.6 C). Overall, these data are consistent with a mechanism involving an initial photochemical catalyst activation step (*e.g.* photooxidation of **PTH** to the radical cation) followed by a product-forming regime with either rate-limiting catalyst oxidation or benzene oxidation, given both benzene and O₂ are present in excess throughout the reaction. Additionally, we determined the O₂ stoichiometry of the reaction by measuring gas consumption within a sealed reaction vessel equipped with a pressure transducer (Figure S16).⁸¹ These data indicate that just over 2 equivalents of O₂ are consumed over the course of the reaction, consistent with O₂ acting as only a one-electron oxidant.⁸² As anticipated, we found that only minimal oxygen is consumed during the induction period.

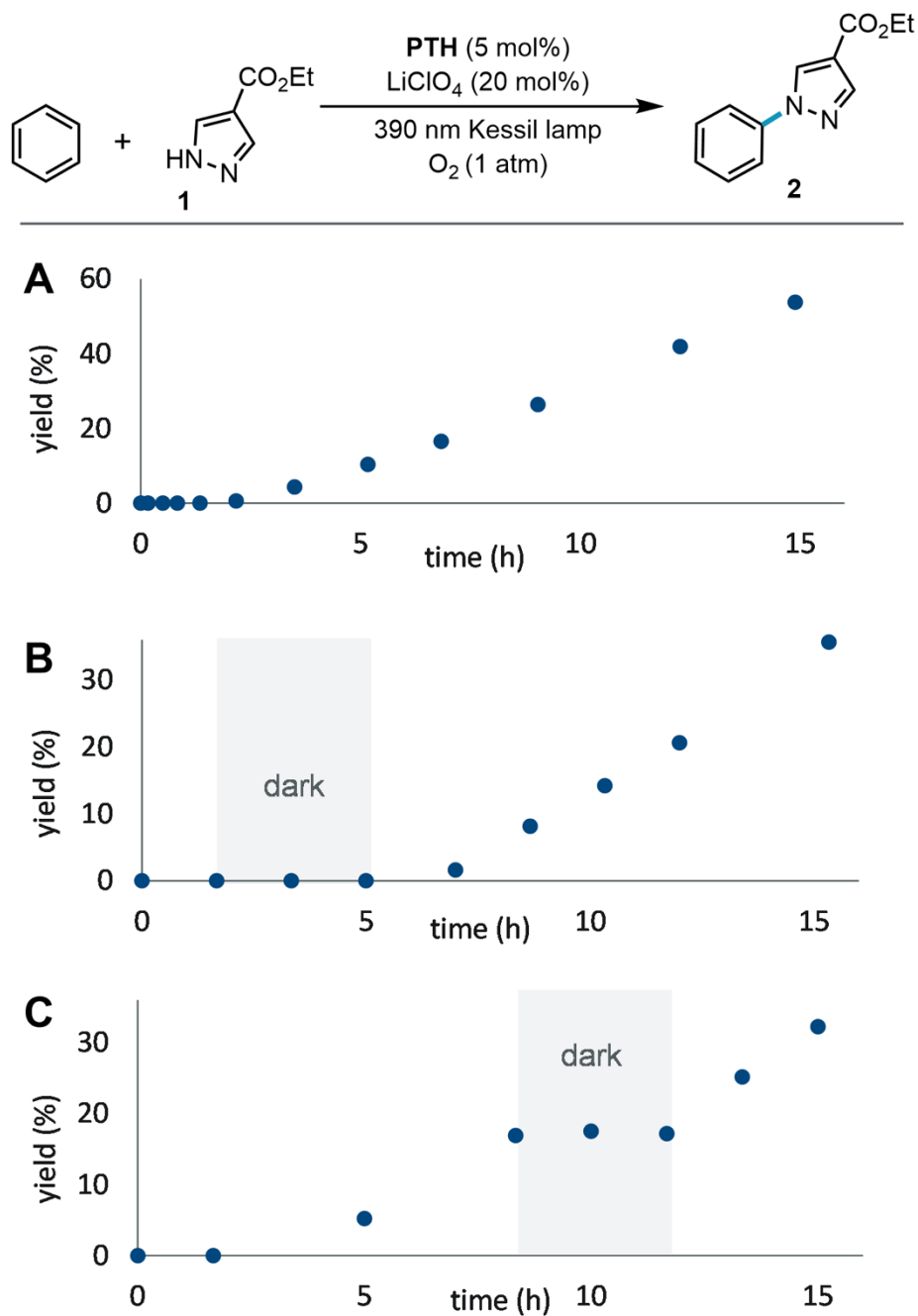


Figure 3.6 Light-dependence on induction period and product formation regimes. **A** Standard reaction profile with continuous irradiation; **B** suspended irradiation during induction period; **C** suspended irradiation during product formation. Reactions were conducted on a 0.05 mmol scale in 9:1:10 TFE:HFIP:PhH. See the SI for overlays of total irradiation time.

Given the initially unanticipated co-catalytic role of LiClO₄ in this system, we next carefully investigated the origin of its impact on the reaction. Omission of this additive resulted in a modest

elongation of the induction period and, subsequently, slower product formation (see SI for details). Systematic variation of the concentration of LiClO_4 revealed that the impact of this reaction component on rate saturates at roughly 20 mol % (Figure 3.7). These data are consistent with our working model wherein LiClO_4 catalytically scavenges inhibitory reactive oxygen species produced through photochemical O_2 reduction. Once the inhibitor is scavenged at a sufficiently rapid rate, its steady state concentration will approach zero and additional increase in co-catalyst loading is expected to have no impact on the process. When the reaction is charged with 5 mol % KO_2 shortly after the induction period, we observe that the reaction halts thereafter in the absence of LiClO_4 . In stark contrast, a reaction containing 2 equivalents of LiClO_4 was unperturbed by direct addition of this inhibitor (Figure 3.8).⁸³

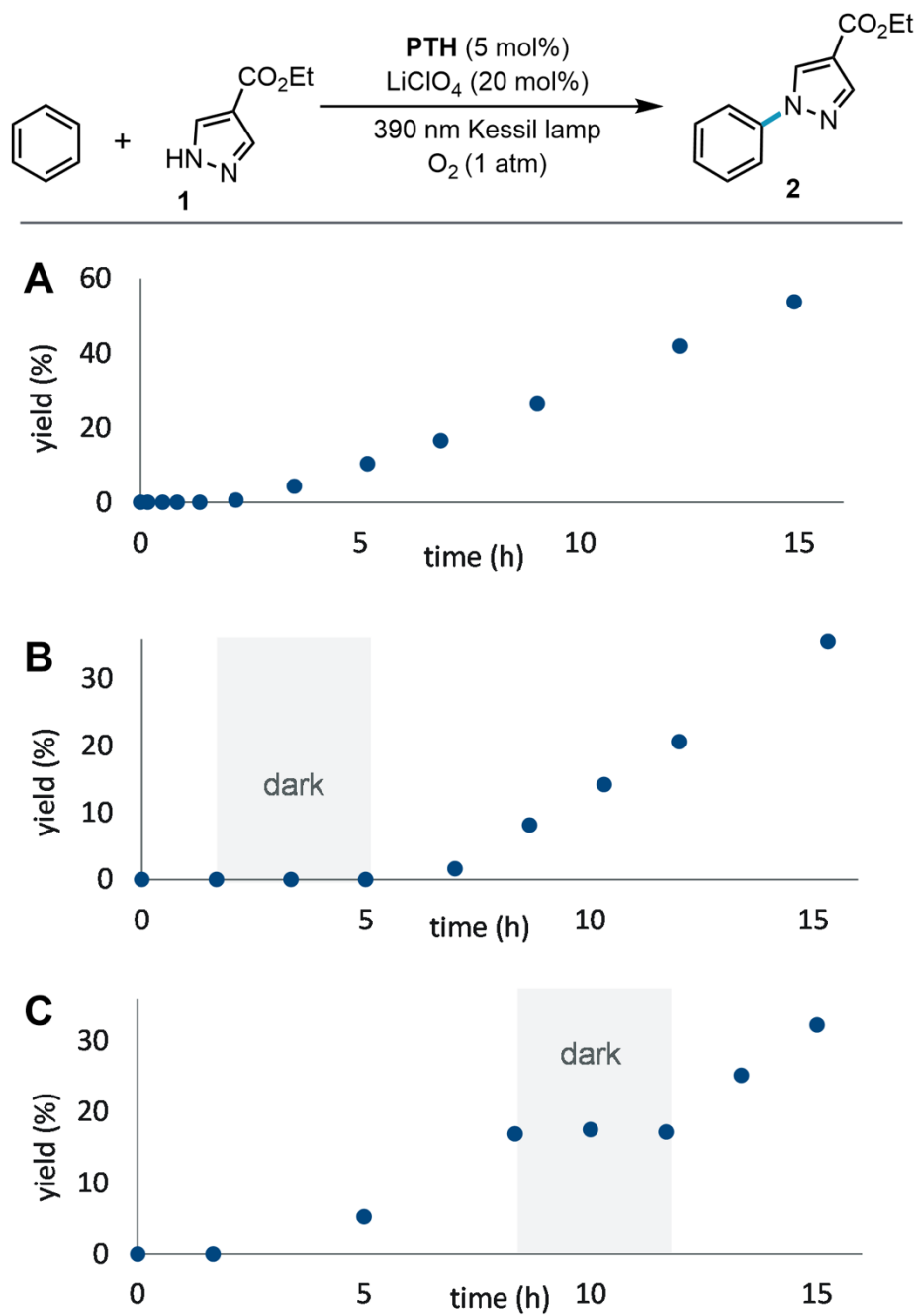


Figure 3.7 Saturation in lithium co-catalyst. Reactions were conducted on a 0.05 mmol scale in 9:1:10 TFE:HFIP:PhH.

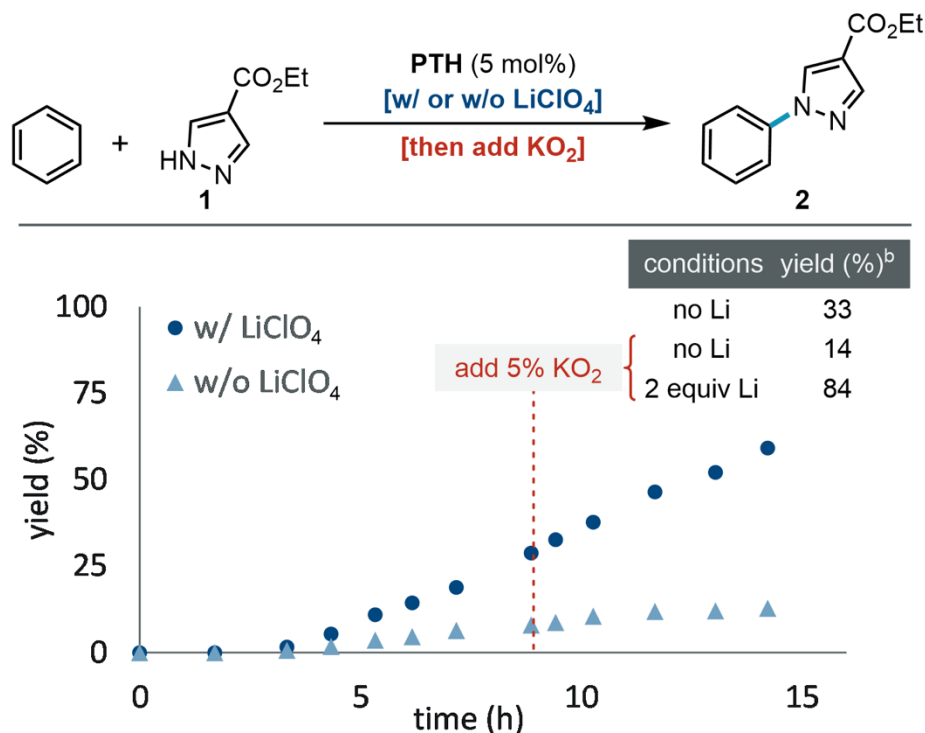


Figure 3.8 Impact of added substoichiometric KO_2 on rate with and without LiClO_4 . Reactions were conducted on a 0.05 mmol scale in 9:1:10 TFE:HFIP:PhH. See the SI for further details.
^bFinal yield after 22h.

Based on the data presented herein, we have constructed a plausible mechanistic model, which involves: (1) initial oxidative activation of **PTH** via photoreduction of O_2 ; (2) photoexcitation of a triarylamine radical cation to oxidize the arene substrate;^{84,85} (3) trapping of arene radical cation with pyrazole nucleophile. While lithium salts are not mechanistically necessary to promote the photocatalytic transformation, we suspect that these Lewis acidic co-catalysts accelerate the reaction by promoting the disproportionation of superoxide, an inhibitor inextricably formed in the aerobic catalyst activation step. We envision the lithium co-catalyst is turned over by protonation of Li_2O_2 by HFIP.⁸⁶

3. 4. Conclusions

Overall, we have identified a catalytic system that unlocks potent photooxidant behavior from one of the most reducing conventional photoredox catalysts, **PTH**. This approach enables oxidative C(sp²)–N coupling via photooxidation of arene substrates outside of the redox window of reported photoredox approaches. Preliminary mechanistic studies are fully consistent with photocatalyst activation via photoreduction of O₂. Intriguingly, we found that Lewis acid co-catalysts could promote and maintain catalyst activation. Beyond providing the first example of purely photochemical benzene oxidation using inexpensive LEDs, this study provides a roadmap to exploit known photocatalysts in new and unconventional ways. We anticipate that continued examination of reaction conditions that force photocatalysts into destabilized oxidation states will dramatically expand the scope of oxidative photoredox catalysis.

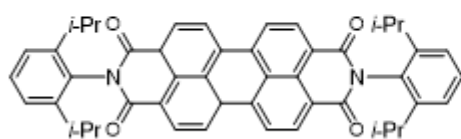
3. 5. Experimental

3. 5. 1. General Methods and Materials

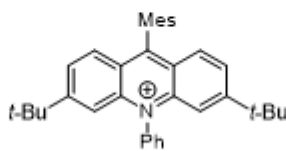
Unless otherwise noted, reactions were performed under 1 atm O₂ in an anhydrous solvent. MeCN was dried by passing through activated alumina columns. Unless otherwise noted, commercially-available reagents were used as received. LiClO₄ was recrystallized from MeCN and dried under vacuum. Irradiation of photochemical reactions was carried out using Kessil LED lamps (390 nm [KSPR160L-390]; Tuna Blue [A160WE]). Crude mixtures were evaluated by thin-layer chromatography using EMD/Merck silica gel 60 F254 pre-coated plates (0.25 mm) and were visualized by UV. Flash chromatography was performed with a Biotage Isolera One automated chromatography system with re-packed silica columns (technical grade silica, pore size 60 Å, 230-400 mesh particle size, 40-63 particle size). Purified materials were dried *in vacuo* (0.050 Torr) to remove trace solvent. ¹H and ¹³C Spectra were

collected using a Bruker Avance-400 with a BBFO Probe, Bruker Avance-500 with a DCH Cryoprobe, or a Bruker Avance-600 with a TCI-F Cryoprobe. NMR data are reported relative to residual CHCl_3 (^1H , $\delta = 7.26$ ppm), CDCl_3 (^{13}C , $\delta = 77.16$ ppm), $\text{DMSO}-d_6$ (^1H , $\delta = 2.50$ ppm), C_6D_6 (^1H , $\delta = 7.16$ ppm), or $\text{MeCN}-d_3$ (^1H , $\delta = 1.94$ ppm). Data for ^1H NMR spectra are reported as follows: chemical shift (δ ppm) (multiplicity, coupling constant (Hz), integration). Multiplicity and qualifier abbreviations are as follows: s = singlet, d = doublet, t = triplet, q = quartet, m = multiplet, br = broad. All NMR yields were determined via reference against an internal standard (dibromomethane for ^1H NMR). GC traces were taken on an Agilent 7890A GC with dual DB-5 columns ($20\text{ m} \times 180\text{ }\mu\text{m} \times 0.18\text{ }\mu\text{m}$), dual FID detectors, and hydrogen as the carrier gas. A sample volume of $1\text{ }\mu\text{L}$ was injected at a temperature of $300\text{ }^\circ\text{C}$ and a 100:1 split ratio. The initial inlet pressure was 20.3 psi but varied as the column flow was held constant at 1.8 mL/min for the duration of the run, FID temperature was $325\text{ }^\circ\text{C}$.

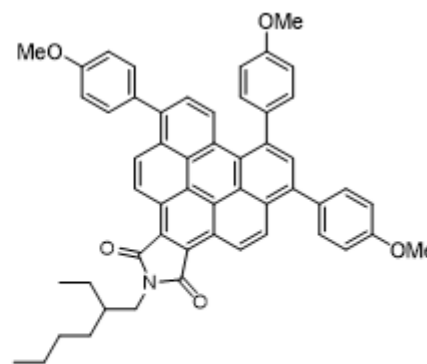
Abbreviations: BET–back electron transfer, DCM– dichloromethane, EtOAc–ethyl acetate, HFIP–1,1,1,3,3,3-hexafluoro-2-propanol, MeCN–acetonitrile, Mes–mesityl, Ph–phenyl, PTH–10-phenyl-10H-phenothiazine, TFE–2,2,2-trifluoroethanol, TFA–trifluoroacetate, GC–gas chromatography



König
Science **2014**,
346 (6210), 725–728.



Nicewicz
Nature **2020**,
580 (7801), 76–80.



Miyake
J. Am. Chem. Soc. **2020**,
142 (31), 13573–13581.

Figure 3. S1: Established multi-photon photoreductants; complete catalyst structures for Figure 3.1.

3. 5. 2. Photochemical Experimental Set-Ups

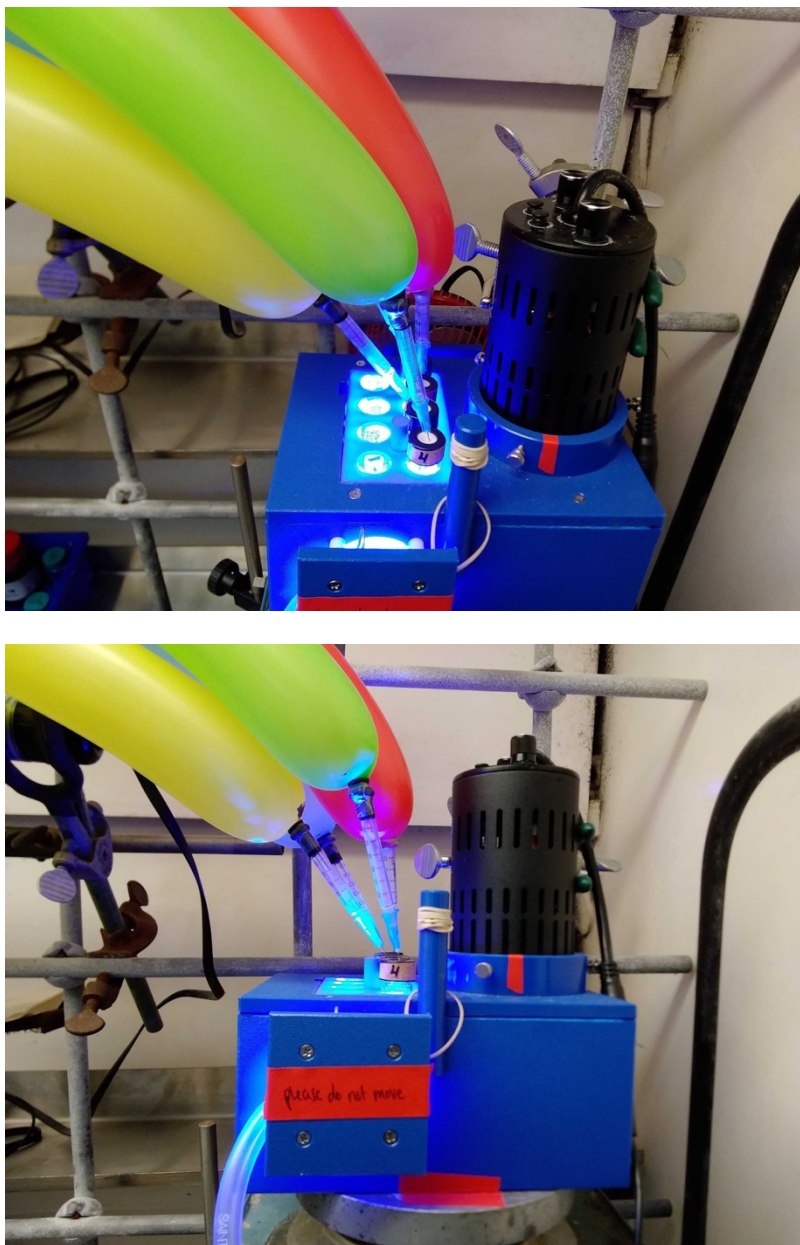


Figure 3. S2: Photochemical experimental set-up for reaction optimization experiments using a HepatoChem EvoluChem™ PhotoRedOx Box [HCK1006-01-016] fitted with a Kessil LED lamp and compressed air cooling.

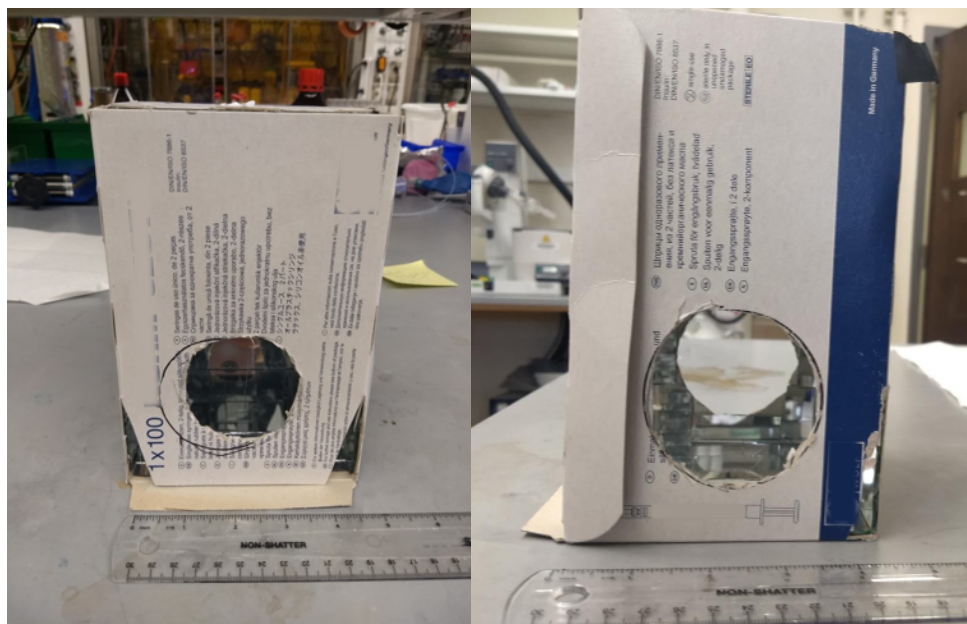


Figure 3. S3. Homemade photobox for scaling up reactions. Circular cut-out in front “door” and triangular slits on side and top for fan cooling and air flow; two circular openings fit Kessil LED lamps for side-on irradiation; angled mirrors at top to reflect light downwards; rectangular opening in back wall for clamp to hold reaction tube; circular hole on top for balloon needle.

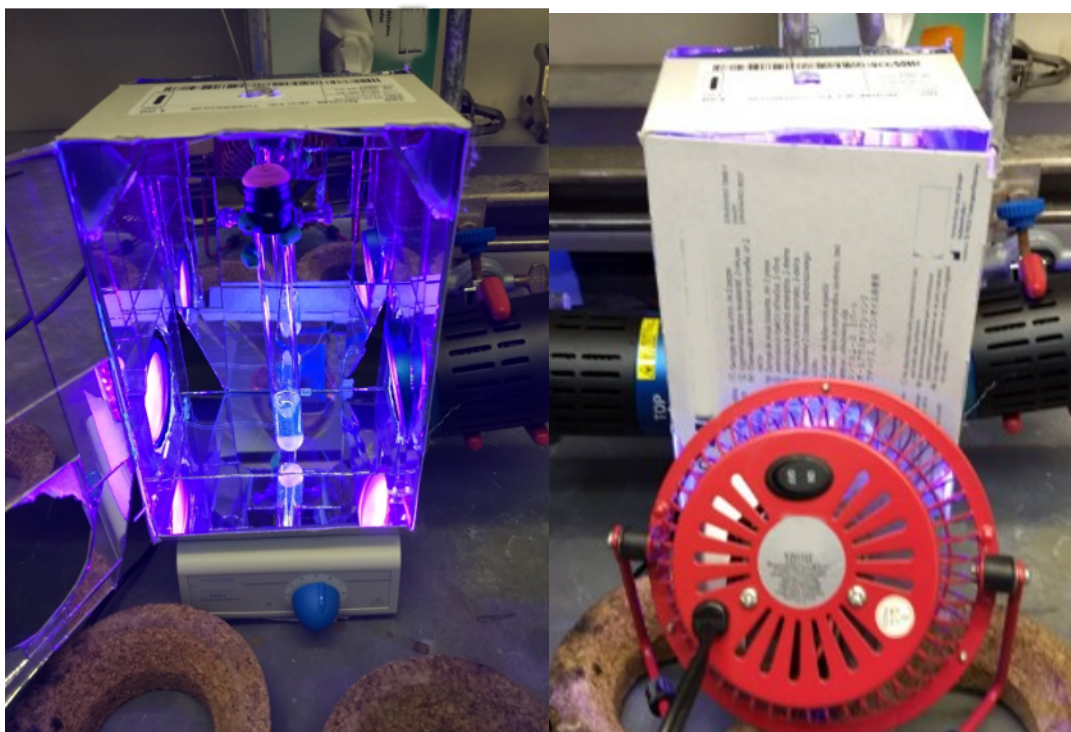
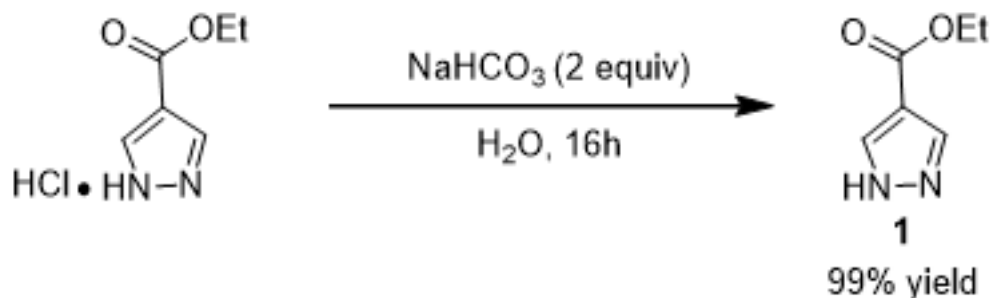


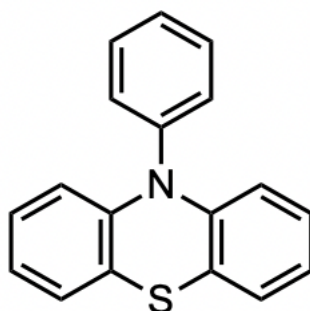
Figure 3. S4. Scale up photobox in action. End reactions measure ca. 35°C.

3. 5. 3. Preparation of Ester Pyrazole 1



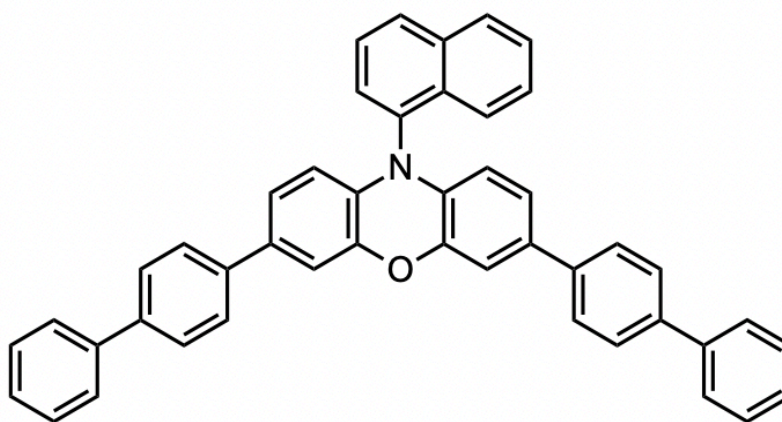
Ethyl 1H-pyrazole-4-carboxylate hydrochloride (2.649 g, 15.0 mmol, 1.0 equiv) and sodium bicarbonate (2.520 g, 30.0 mmol, 2.0 equiv) were dissolved in water (160 mL). The reaction mixture was stirred under ambient conditions for 16 h. The aqueous phase was extracted with 3 × 200 mL DCM. The combined organic phases were dried over Na₂SO₄, filtered, and the solvent evaporated to afford ester pyrazole **1** as a white solid (2.0877 g, 99%). ¹H NMR (500 MHz, CDCl₃) δ 11.68 (br s, 1H), 8.09 (s, 2H), 4.33 (qd, J = 7.1, 0.8 Hz, 2H), 1.36 (td, J = 7.1, 0.9 Hz, 3H). Consistent with reported spectra (*Synthetic Communications*, **2008**, 38, 5, 674 - 683).

3. 5. 4. Preparation of Photocatalysts

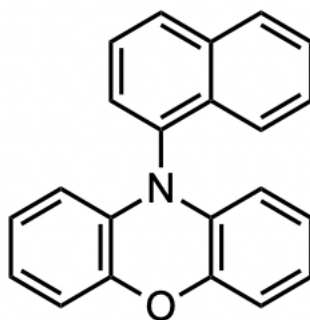


10-phenyl-10H-phenothiazine (PTH) – prepared according to *Beilstein J. Org. Chem.* **2019**, 15, 52–59. 10H-phenothiazine (1.49 g, 7.50 mmol, 1.0 equiv), potassium tert-butoxide (1.09 g, 9.67

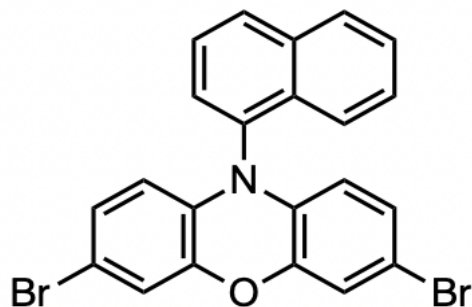
mmol, 1.29 equiv), tri-tert-butylphosphoniumtetrafluoroborate (131 mg, 450 μ mol, 0.06 equiv), and bis(dibenzylideneacetone)palladium (129 mg, 225 μ mol, 0.03 equiv) were combined and placed under an atmosphere of nitrogen. The solids were then dissolved in anhydrous toluene (14 mL). Bromobenzene (1.44 g, 964 μ L, 9.15 mmol, 1.22 equiv) was added. The reaction mixture was stirred under reflux for 20 h. After reaching room temperature, the reaction contents were filtered, then 200 mL EtOAc and 100 mL water were added to the reaction mixture. After phase separation, the aqueous phase was extracted additionally with 3 \times 200 mL EtOAc followed by 1 \times 100 mL brine. The combined organic phases were dried over Na₂SO₄, the solvent evaporated, and the crude product purified by column chromatography (2.01 g, 97%); ¹H NMR (400 MHz, DMSO) δ 7.67 (t, *J* = 7.6 Hz, 2H), 7.54 (t, *J* = 7.5 Hz, 1H), 7.45 – 7.38 (m, 2H), 7.08 (dd, *J* = 7.5, 1.6 Hz, 2H), 6.93 (ddd, *J* = 8.4, 7.3, 1.7 Hz, 2H), 6.89 – 6.81 (m, 2H), 6.16 (dd, *J* = 8.1, 1.3 Hz, 2H); consistent with reported spectra (*Eur. J. Org. Chem.*, **2019**: 5807-5811)



3,7-di([1,1'-biphenyl]-4-yl)-10-(naphthalen-1-yl)-10H-phenoxazine (PC-1) – prepared in three steps according to *J. Am. Chem. Soc.* **2016**, 138, 35, 11399–11407.

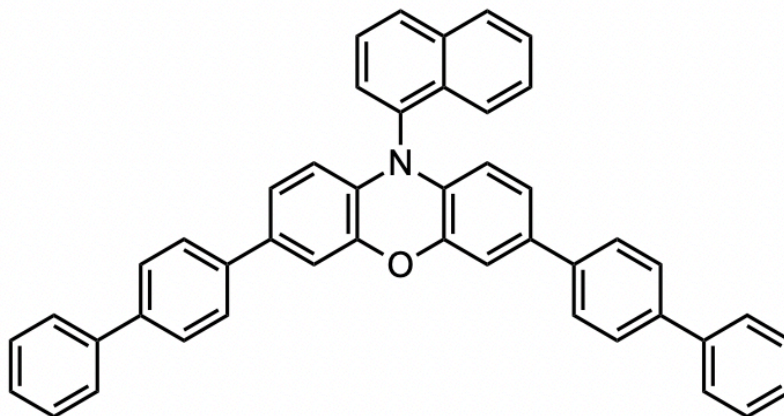


Step 1: Synthesis of 1-Naphthalene-10-phenoxazine – A stir bar was placed into a 100 mL storage flask, flame dried under vacuum and then back filled with nitrogen three times. The flask was then charged with 10H-phenoxazine (500 mg, 2.73 mmol, 1.0 equiv), sodium tert-butoxide (525 mg, 5.46 mmol, 2.0 equiv), 2-dicyclohexylphosphino-2',6'-diisopropoxybiphenyl (RuPhos, 38.2 mg, 81.9 μ mol, 0.03 equiv), (2-dicyclohexylphosphino-2',6'-diisopropoxy-1,1'-biphenyl)[2-(2'-amino-1,1'-biphenyl)]palladium(II) methanesulfonate (RuPhos Pd G3, 68.5 mg, 81.9 μ mol, 0.03 equiv), 1,4-dioxane (3 mL), and 1-bromonaphthalene (1.13 g, 764 μ L, 5.46 mmol, 2.0 equiv). The flask was heated at 130 °C while stirring for 48 hours. The flask was then cooled to room temperature, diluted with CH₂Cl₂, and the solution was washed with water three times, brine once, dried over MgSO₄ and purified by recrystallization from CH₂Cl₂ layered with hexanes on top at -25°C to yield the product as yellow crystals (615 mg, 73% yield). **¹H NMR** (400 MHz, CDCl₃) δ 8.08 (dt, J = 8.2, 1.0 Hz, 1H), 8.02 – 7.95 (m, 2H), 7.65 (dd, J = 8.3, 7.2 Hz, 1H), 7.59 – 7.51 (m, 2H), 7.47 (ddd, J = 8.2, 6.8, 1.3 Hz, 1H), 7.26 (s, 1H), 6.73 (dd, J = 7.9, 1.5 Hz, 2H), 6.63 (td, J = 7.7, 1.5 Hz, 2H), 6.49 (td, J = 7.7, 1.5 Hz, 2H), 5.70 (dd, J = 8.0, 1.5 Hz, 2H); consistent with reported spectra (*J. Am. Chem. Soc.* **2016**, 138, 35, 11399–11407)

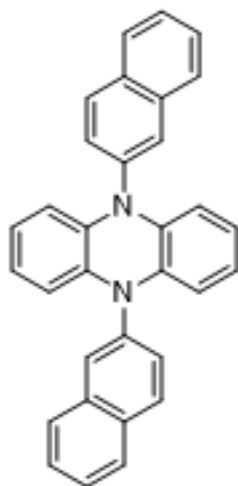


Step 2: Synthesis of 3,7-Dibromo-1-Naphthalene-10-phenoxazine – 10-(naphthalen-1-yl)-10H-phenoxazine (515 mg, 1.66 mmol, 1.0 equiv) was dissolved in chloroform (51.5 mL). Acetic acid (51.5 mL) was then added to the stirring mixture. Aluminum foil was thoroughly wrapped around to cover the reaction vial, blocking out light. In the dark, powdered *N*-bromosuccinimide (607 mg, 3.41 mmol, 2.05 equiv) was added in small portions over a 20 minute period. After 2 hours at room temperature the reaction mixture was concentrated under vacuum. The resulting solid was washed three times with water, brine, then dried with MgSO_4 . A light tan powder (688 mg, 88% yield) was collected. This was used for the Suzuki coupling without further purification.

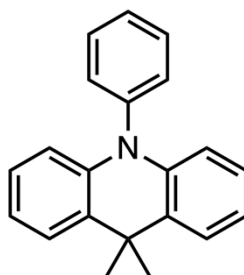
^1H NMR (400 MHz, C_6D_6) δ 7.82 (d, J = 8.4 Hz, 1H), 7.58 (dd, J = 19.0, 8.2 Hz, 2H), 7.20 (d, J = 7.4 Hz, 1H), 7.13 – 7.07 (m, 2H), 6.90 (d, J = 7.2 Hz, 1H), 6.84 (d, J = 2.3 Hz, 2H), 6.37 (dd, J = 8.6, 2.3 Hz, 2H), 5.31 (d, J = 8.4 Hz, 2H); consistent with reported spectra (*J. Am. Chem. Soc.* **2016**, 138, 35, 11399–11407)



Step 3: Synthesis of 3,7-Di(4-biphenyl) 1-Naphthalene-10-Phenoxazine (PC-1) – A 200 mL schlenk flask was flame dried, filled with nitrogen, and equipped with a stir bar and reflux condenser before 3,7-dibromo-10-(naphthalen-1-yl)-10H-phenoxazine (225 mg, 482 μmol , 1.0 equiv), [1,1'-biphenyl]-4-ylboronic acid (382 mg, 1.93 mmol, 4.0 equiv) was added, then dissolved in 20 mL of THF. 6 mL of aqueous K_2CO_3 (2M) was syringed into the solution and then heated to 80 $^\circ\text{C}$ and stirred for 20 minutes. After which, tetrakis(triphenylphosphine)-palladium(0) (167 mg, 144 μmol , 0.3 equiv) in a 20 mL solution of THF was added then heated to 100 $^\circ\text{C}$ and left to run for 24 hours. Once complete, the reaction was concentrated under vacuum, dissolved in DCM, and washed with water two times, brine, then dried with MgSO_4 . A bright yellow powder was collected (128 mg, 43% yield) after recrystallization in DCM/MeOH. $^1\text{H NMR}$ (400 MHz, C_6D_6) δ 8.18 (d, $J = 8.3$ Hz, 1H), 7.69 (d, $J = 8.6$ Hz, 2H), 7.68 – 7.63 (m, 1H), 7.61 – 7.54 (m, 1H), 7.54 – 7.49 (m, 4H), 7.46 (s, 8H), 7.36 (d, $J = 2.0$ Hz, 2H), 7.25 (td, $J = 7.8, 7.3, 4.9$ Hz, 8H), 6.73 (dd, $J = 8.3, 2.1$ Hz, 2H), 5.88 (d, $J = 8.3$ Hz, 2H); consistent with reported spectra (*J. Am. Chem. Soc.* **2016**, 138, 35, 11399–11407)

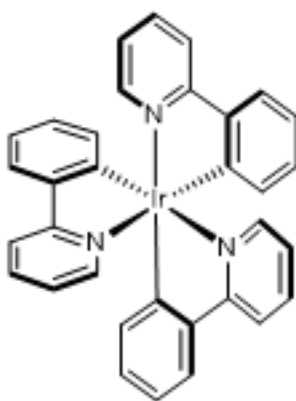


N,N-5,10-di(2-naphthalene)-5,10-dihydrophenazine (PC-2) – Commercially available material from MilliporeSigma was used. For preparation, see *Science*, **2016**, 352, 6289, 1082-1086.



[9,9-dimethyl-10-phenyl-9,10-dihydroacridine] (PC-3) – In a three-neck flask, bromobenzene (0.23 mL, 2.2 mmol, 1.1 equiv), 9-dimethyl-9,10-dihydroacridine (419 mg, 2.0 mol), and sodium tert-butoxide (577 mg, 6.0 mol, 3.0 equiv) were introduced. Everything was kept under an inert atmosphere and the solids were dissolved in 10 mL of toluene. The catalyst was prepared in a flask, by mixing Pd(dba)₂ (73.3 mg, 0.08 mmol, 0.04 equiv) and HP(tBu)₃ BF₄ (46.4 mg, 0.16 mmol, 0.08 equiv) in 2 ml of toluene. This catalyst solution was added to the reaction medium and heated overnight at reflux. After complete conversion, the reaction medium was filtered through a celite pad and the solvent was removed under vacuum. The crude product purified by column chromatography (550 mg, 96%); ¹H NMR (400 MHz, CDCl₃) δ 7.63 (t, *J* = 7.6 Hz, 2H), 7.51 (t, *J*

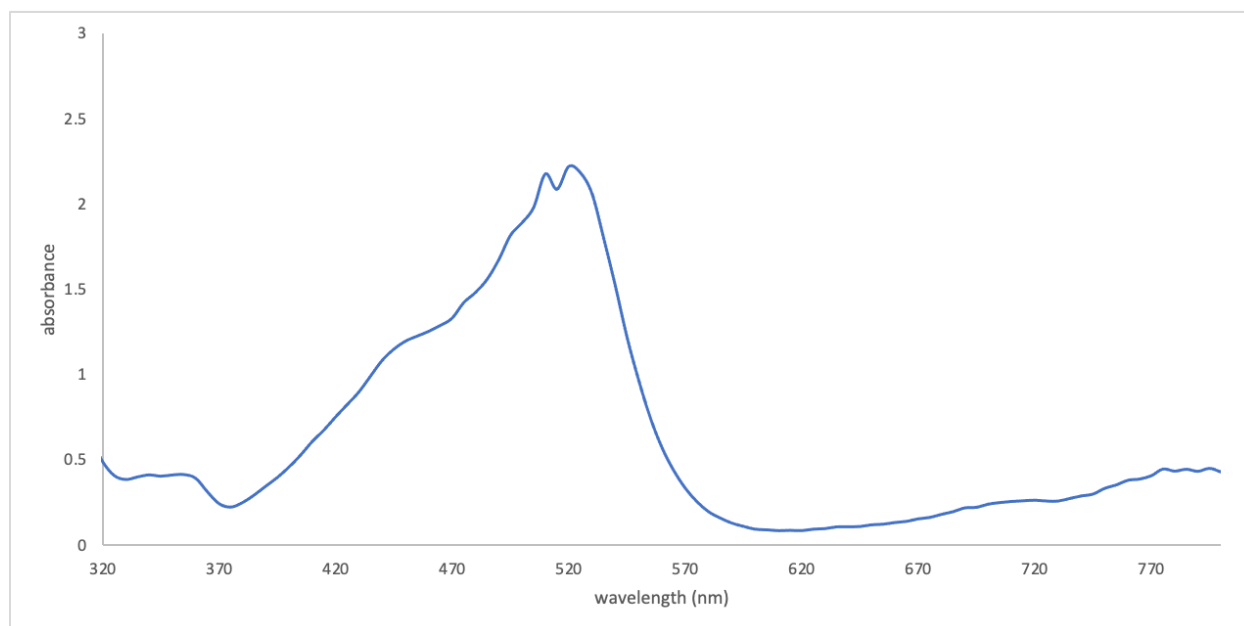
= 7.5 Hz, 1H), 7.46 (dd, J = 7.5, 1.8 Hz, 2H), 7.34 (d, J = 7.0 Hz, 2H), 6.97 (td, J = 8.0, 7.6, 1.8 Hz, 2H), 6.92 (td, J = 7.4, 1.5 Hz, 2H), 6.26 (dd, J = 7.9, 1.5 Hz, 2H), 1.70 (s, 6H); consistent with reported spectra (*Organic Electronics* **2018**, 57, 327–334)



Ir(ppy)₃ - sample generously donated from the Yoon group. For preparation see *J. Am. Chem. Soc.* **2003**, 125, 24, 7377–7387.

3. 5. 5. Preparation of PTH•PF₆ Radical Cation

Preparation adapted from *ChemCatChem* **2018**, 10, 2955 –2961. In a Schlenk tube 82.5 mg (0.300 mmol, 1.00 equiv) 10-phenyl-10H-phenothiazine was dissolved in 1mL anhydrous MeCN. Then the mixture was cooled to 0 °C and 47.2 mg (0.270 mmol, 0.90 equiv) NOPF₆ was slowly added to the mixture as a concentrated MeCN solution. The mixture turned deep red immediately and was stirred for a further 20 min. The mixture was freeze-pump-thawed for three cycles to remove the generated NO. Then the mixture was let come to room temperature and the solvent removed. The solid was then dissolved in DCM. A red solid precipitated upon addition of hexanes. The red solid was washed with hexanes three times to remove excess PTH then dried under reduced pressure. PTH•PF₆ radical cation was characterized by its absorption spectrum.



Spectrum and distinct feature at 520 nm is consistent with literature (*Bulletin of the Chemical Society of Japan*, **1999**, vol. 72, # 2, p. 253 - 257). ^1H NMR confirmed no residual PTH, although a trace amount of PTH S-oxide is observed.

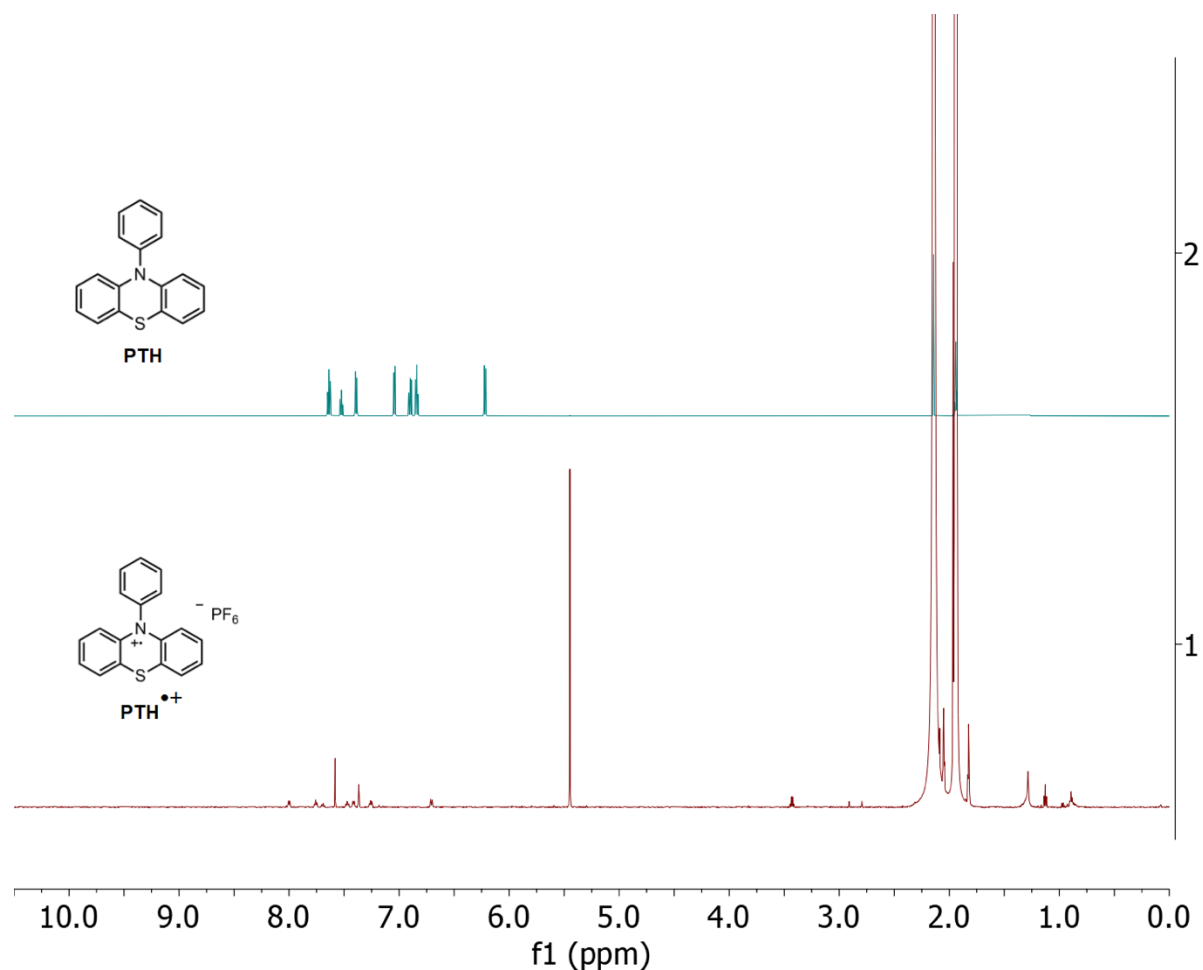


Figure 3. S5: ^1H NMR (600 MHz, $\text{MeCN}-d_3$) spectrum shows no residual PTH.

3. 5. 6. General Experimental Procedures for Redox-Primed Photocatalysis

General Procedure A – Add PTH (5.5 mg, 0.02 mmol, 5 mol %) and LiClO_4 (1.1 mg, 0.08 mmol, 20 mol %) to a 16x150 mm fraction tube equipped with a stir bar. If a solid, add pyrazole (0.4 mmol, 1.0 equiv) to the tube. Add arene (8 mL), TFE (7.2 mL), and HFIP (0.8 mL) to the tube. Affix the reaction vessel to the photoreactor (see fig. S3 and S4 photobox description). Sparge the solution for 20 minutes with oxygen from a balloon (1 atm). If liquid, add pyrazole (0.4 mmol, 1.0 equiv) to the tube. Irradiate using two 390 nm Kessil lamps for 20 h under 1 atm O_2 and with fan cooling. Concentrate crude product for purification by flash chromatography with silica.

General Procedure B – Following General Procedure A, but with the following modification: following irradiation, concentrate crude product. Add dibromomethane internal standard to the residue and dilute with CDCl₃. Take up the solution in an NMR tube. Cross coupling product yield was determined via ¹H NMR using dibromomethane as an internal standard.

General Procedure C – Add PTH (5.5 mg, 0.02 mmol, 5 mol %) to a 16x150 mm fraction tube equipped with a stir bar. If a solid, add pyrazole (0.4 mmol, 1.0 equiv) to the tube. Add arene (8 mL), MeCN (4 mL), and HFIP (4 mL) to the tube. Affix the reaction vessel to the photoreactor (see fig. S3 and S4 photobox description). Sparge the solution for 20 minutes with oxygen from a balloon (1 atm). If liquid, add pyrazole (0.4 mmol, 1.0 equiv) to the tube. Add *t*-dodecyl mercaptan (9.4 μL, 0.04 mmol, 10 mol %) to the tube. Irradiate using two 390 nm Kessil lamps for 20h under 1 atm O₂ and with fan cooling. Concentrate crude product for purification by flash chromatography with silica.

General Procedure D – Add PTH (5.5 mg, 0.02 mmol, 5 mol %) to a 16x150 mm fraction tube equipped with a stir bar. If a solid, add pyrazole (0.4 mmol, 1.0 equiv) to the tube. Add MeCN (2 mL) and HFIP (2 mL) to the tube. Affix the reaction vessel to the photoreactor (see fig. S3 and S4 photobox description). Sparge the solution for 7 minutes with oxygen from a balloon (1 atm). If liquid, add pyrazole (0.4 mmol, 1.0 equiv) to the tube. Add *t*-dodecyl mercaptan (9.4 μL, 0.04 mmol, 10 mol %) to the tube. Irradiate using two 390 nm Kessil lamps for 20h under 1 atm O₂ and with fan cooling. Concentrate crude product for purification by flash chromatography with silica.

3. 5. 7. Reaction Optimization and Control Experiments (Tables 1 and 2)

Add solid reaction components (catalyst, pyrazole, co-catalyst) to a 1-dram vial equipped with a stir bar. Add arene (1 mL) and solvent (1 mL) to the vial. Seal with a septum-containing cap. Pierce septum with a needle attached to a balloon filled with the gas of choice and purge the headspace of the vial for two minutes. Tighten the cap and place the vial into the photobox, which itself is on a magnetic stirring plate. Commence the reactions by turning on the Kessil lamp and compressed air cooling. Experiments performed on a 0.05 mmol scale with the pyrazole as the limiting reagent.

For NMR analyses – Following irradiation, concentrate crude product. Add dibromomethane internal standard to the residue and dilute with CDCl_3 . Take up the solution in an NMR tube. Oxidative coupling product yield was determined via ^1H NMR using dibromomethane as an internal standard.

For GC analyses – Following irradiation, add dodecane internal standard to crude reaction and remove a 0.1 mL aliquot. Filter the aliquot through a celite plug pre-wetted with EtOAc to remove solids and dilute the filtrate (0.2 mL) with ethyl acetate (1.0 mL).

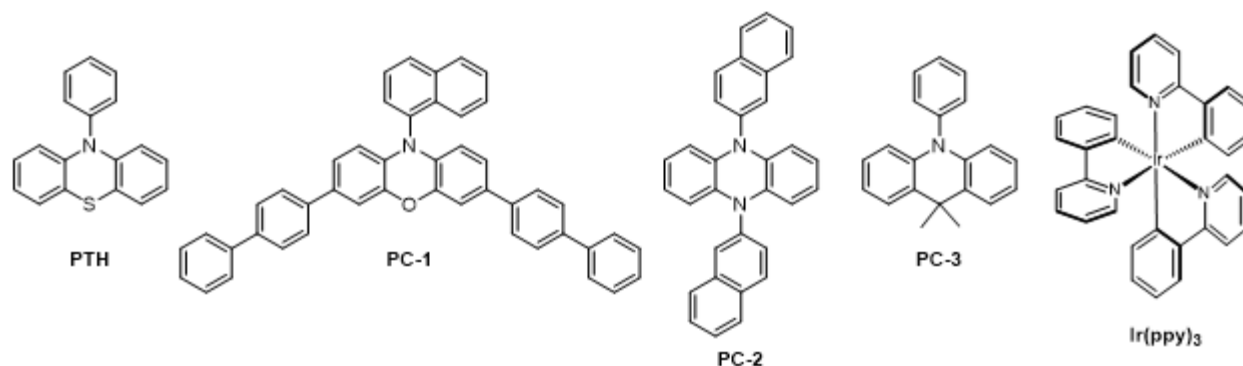


Figure 3. S6: Catalysts used for reaction development.

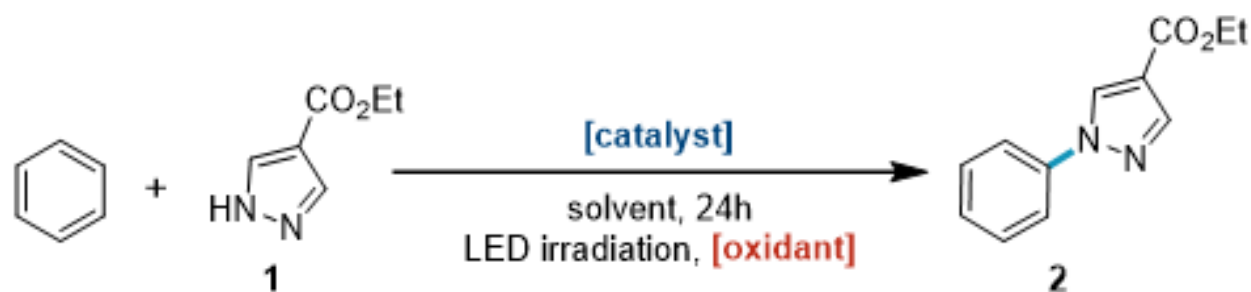


Table 3. S1: Optimization of photocatalyst and terminal oxidant for oxidative coupling of benzene with pyrazole **1**.^{a-d}

entry	catalyst	solvent	oxidant	yield (%)
1	PTH (5%)	MeCN	none	n.d.
2	PTH (5%)	MeCN	PhI (2 equiv)	n.d.
3	PTH (5%)	MeCN	PhBr (2 equiv)	2%
4	PTH (5%)	MeCN	CH ₂ Br ₂ (2 equiv)	5
5	PTH (5%)	MeCN	NOPF ₆ (2 equiv)	12
6	PTH (5%)	MeCN	Cu(TFA) ₂ (2 equiv)	n.d.
7	PTH (5%)	MeCN	O ₂ (1 atm)	14
8	PTH (5%)	TFE	O ₂ (1 atm)	31
9 ^e	PTH (5%)	9:1 TFE:HFIP	O ₂ (1 atm)	89

10	PC-1 (5%)	MeCN	PhI (2 equiv)	<2%
11	PC-1 (5%)	MeCN	PhBr (2 equiv)	<2%
12	PC-1 (5%)	MeCN	CH ₂ Br ₂ (2 equiv)	<2%
13	PC-1 (5%)	MeCN	NOPF ₆ (2 equiv)	4
14	PC-1 (5%)	MeCN	Cu(TFA) ₂ (2 equiv)	n.d.
15	PC-1 (5%)	MeCN	O ₂ (1 atm)	n.d.
16	PC-1 (5%)	TFE	O ₂ (1 atm)	<2%
17 ^e	PC-1 (5%)	9:1 TFE:HFIP	O ₂ (1 atm)	<2%
18	PC-2 (5%)	MeCN	PhI (2 equiv)	n.d.
19	PC-2 (5%)	MeCN	PhBr (2 equiv)	<2%
20	PC-2 (5%)	MeCN	CH ₂ Br ₂ (2 equiv)	<2%
21	PC-2 (5%)	MeCN	NOPF ₆ (2 equiv)	3
23	PC-2 (5%)	MeCN	Cu(TFA) ₂ (2 equiv)	n.d.
24	PC-2 (5%)	MeCN	O ₂ (1 atm)	6

25	PC-2 (5%)	TFE	O ₂ (1 atm)	<2%
26 ^e	PC-2 (5%)	9:1 TFE:HFIP	O ₂ (1 atm)	<2%
27 ^f	PC-2 (5%)	MeCN	NOPF ₆ (2 equiv)	<2%
28 ^f	PC-2 (5%)	MeCN	O ₂ (1 atm)	<2%
29 ^f	PC-2 (5%)	TFE	O ₂ (1 atm)	2%
30 ^{e,f}	PC-2 (5%)	9:1 TFE:HFIP	O ₂ (1 atm)	8%
<hr/>				
31 ^{f,g}	PC-3 (5%)	MeCN	O ₂ (1 atm)	37%
<hr/>				
32	Ir(ppy) ₃ (1%)	MeCN	PhI (2 equiv)	n.d.
33	Ir(ppy) ₃ (1%)	MeCN	PhBr (2 equiv)	n.d.
34	Ir(ppy) ₃ (1%)	MeCN	CH ₂ Br ₂ (2 equiv)	<2%
35	Ir(ppy) ₃ (1%)	MeCN	NOPF ₆ (2 equiv)	6
36	Ir(ppy) ₃ (1%)	MeCN	Cu(TFA) ₂ (2 equiv)	n.d.
37	Ir(ppy) ₃ (1%)	MeCN	O ₂ (1 atm)	n.d.
38	Ir(ppy) ₃ (1%)	TFE	O ₂ (1 atm)	n.d.

39^e Ir(ppy)₃ (1%) 9:1 TFE:HFIP O₂ (1 atm) <2%

^aPTH irradiated using 390 nm Kessil lamp; **PC-1**, **PC-2**, and Ir(ppy)₃ irradiated using Tuna Blue Kessil lamp. ^bConducted under an argon atmosphere (1 atm) unless noted otherwise. ^cGC yields.

^dn.d. = not detected. ^e20 mol % LiClO₄. ^f390 nm Kessil lamp used. ^g10% *t*-dodecyl mercaptan.

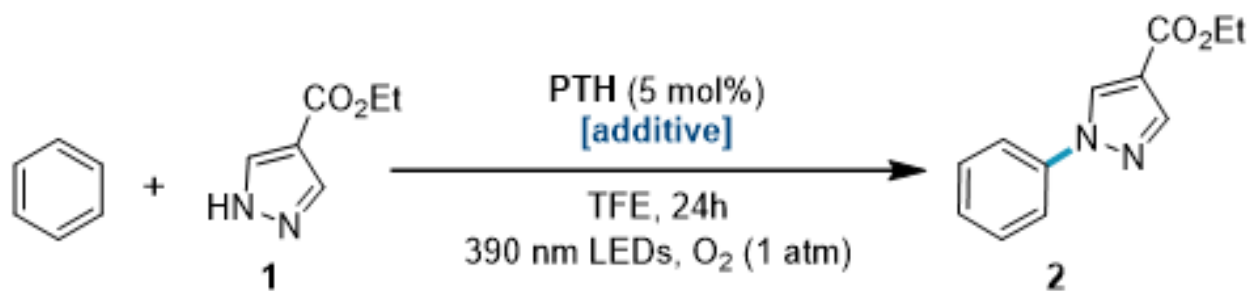


Table 3. S2: effect of superoxide and optimization of Li additive.^a

entry	additive	yield (%)
1	none	31
2	KO ₂ (5 mol %)	<2%
3	LiClO ₄ (1 equiv)	86
4	LiClO ₄ (20 mol %)	73
5	TBAClO ₄ (20 mol %)	29
6	LiPF ₆ (20 mol %)	64

7 LiOTf (20 mol %) 56

8^b LiClO₄ (20 mol %) 89

^aGC yields. ^b9:1 TFE:HFIP solvent.

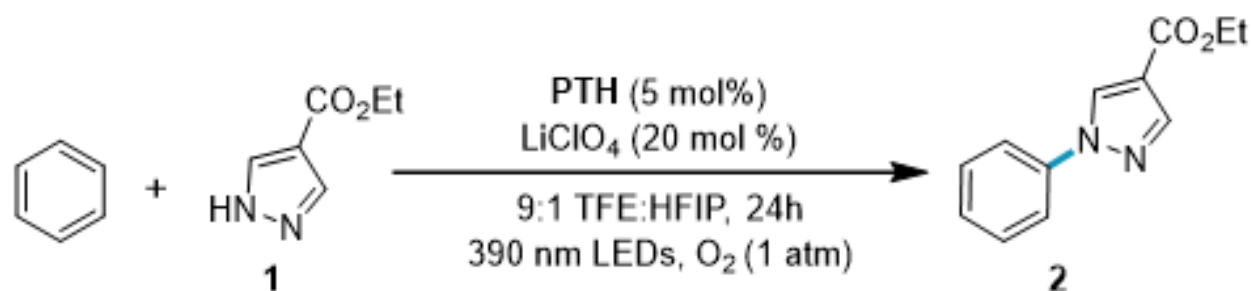


Table 3. S3: control experiments for optimized reaction condition.^{a,b}

entry	variation	yield (%)
1	no change	89
2	no catalyst	n.d.
3	no irradiation	n.d.
4 ^{c,d}	no oxidant	n.d.
5	air instead of O ₂ balloon	21
6 ^c	no LiClO ₄	33
7	0.1 M instead of 0.025 M	45

^aNMR yields. ^bn.d.=not detected. ^cGC yield using dodecane internal standard. ^dConducted under an argon atmosphere (1 atm).

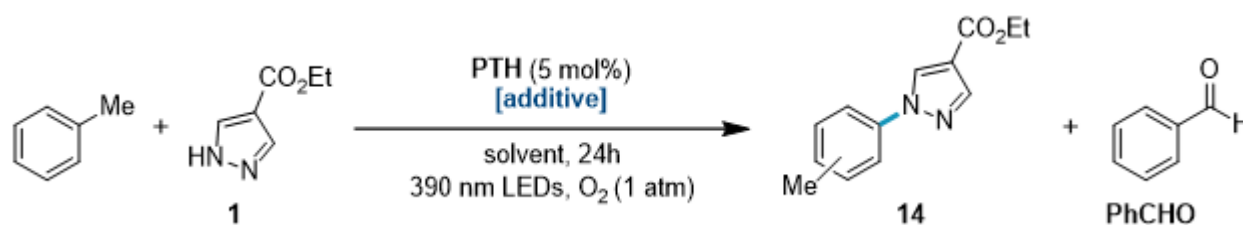


Table 3. S4: optimization oxidative coupling of toluene as model alkyl arene.^{a,b}

entry	solvent	additive	yield (%) (<i>p:o</i>)	PhCHO (%) ^c
1	9:1 TFE:HFIP	LiClO ₄ (20%)	70 (1:1)	91
2	1:1 MeCN:HFIP	LiClO ₄ (1 equiv)	73 (1:1)	55
3	1:1 MeCN:HFIP	<i>t</i> -dodecyl mercaptan (10%)	75 (1:1)	31

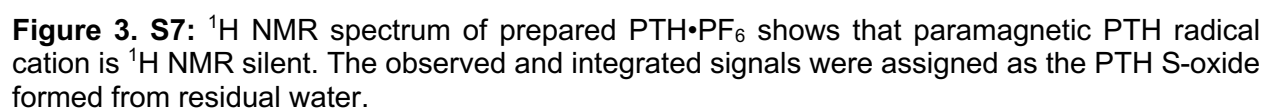
^aReactions conducted using 0.4 mmol of pyrazole **1**, 8 mL of toluene, and irradiated with two 390 nm Kessil lamps for 24h with fan cooling. ^bNMR yields. ^cRelative to pyrazole **1**.

The optimized conditions for benzene applied to alkyl arenes afforded significant oxygenation of the benzylic position (table S10, entry 1). We found increasing the LiClO₄ to stoichiometric quantity and adjusting the solvent system decreased undesired reactivity in the presence of O₂ atmosphere (entry 2). However, we wondered if other additives might serve the co-catalytic role of Li in catalyzing the decomposition of reduced O₂ byproducts arising from catalyst photooxidative activation. Addition of co-catalytic thiol decreased benzylic oxygenation side products while retaining oxidative coupling product yield (entry 3). Superoxide may undergo HAT

with thiol to generate hydroperoxy radical and thus prevent BET to deactivate catalyst. The resulting thiyl radical may formally abstract a hydrogen atom from the distonic radical cation adduct between pyrazole and benzene to regenerate the thiol co-catalyst and form the final product. Alternative roles of thiol are also possible.

3. 5. 8 BET ^1H NMR Experiment (Figure 2)

Add PTH•PF₆ (9.0 mg, 0.021 mmol) and KO₂ (3.3 mg, 0.046 mmol, 2.2 equiv) to a 1-dram vial equipped with a stir bar. Add MeCN-d₃ (2 mL) and stir for 40 min. Transfer 0.5 mL of the solution to an NMR tube. ^1H NMR spectra were acquired 5 h after sample preparation.



¹H NMR (600 MHz, CD₃CN) δ 8.00 (d, J = 7.4 Hz, 2H), 7.76 (t, J = 7.3 Hz, 1H), 7.69 (t, J = 7.6 Hz, 1H), 7.47 (t, J = 7.7 Hz, 1H), 7.41 (d, J = 7.4 Hz, 1H), 7.29 – 7.23 (m, 1H), 6.71 (d, J = 8.5 Hz, 1H); consistent with reported spectra (*J. Chem. Soc., Perkin Trans. 1*, **1995**, No. 8, 1057-1064).

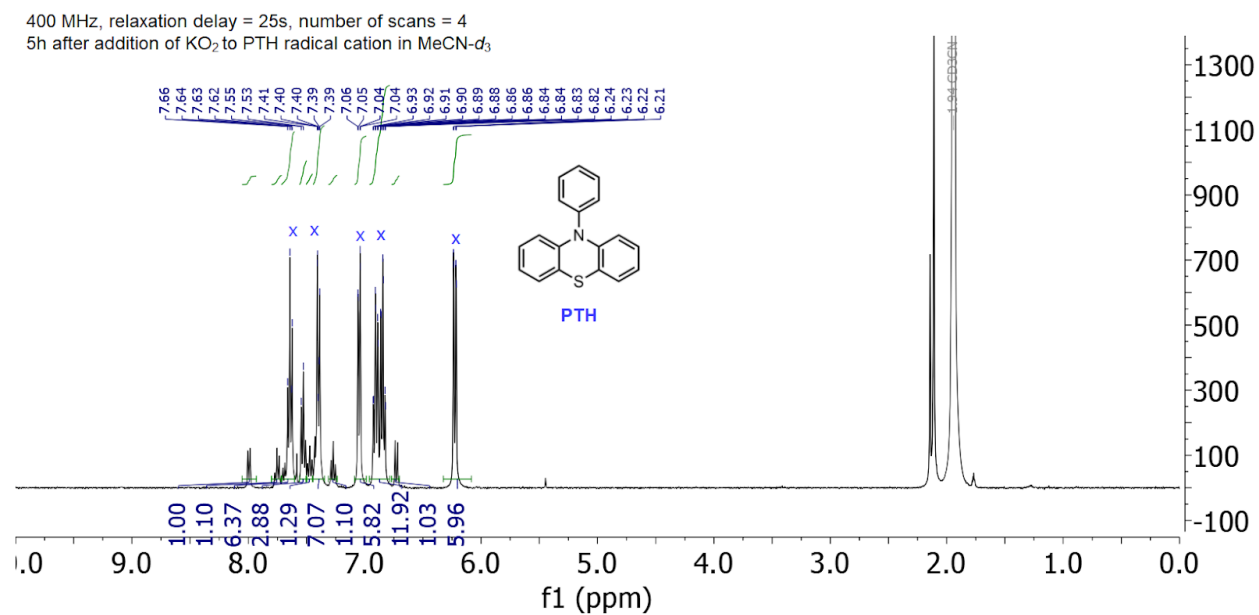


Figure 3. S8: Formation of closed-shell PTH from $\text{PTH}\cdot\text{PF}_6$ in MeCN-d_3 upon addition of KO_2 .

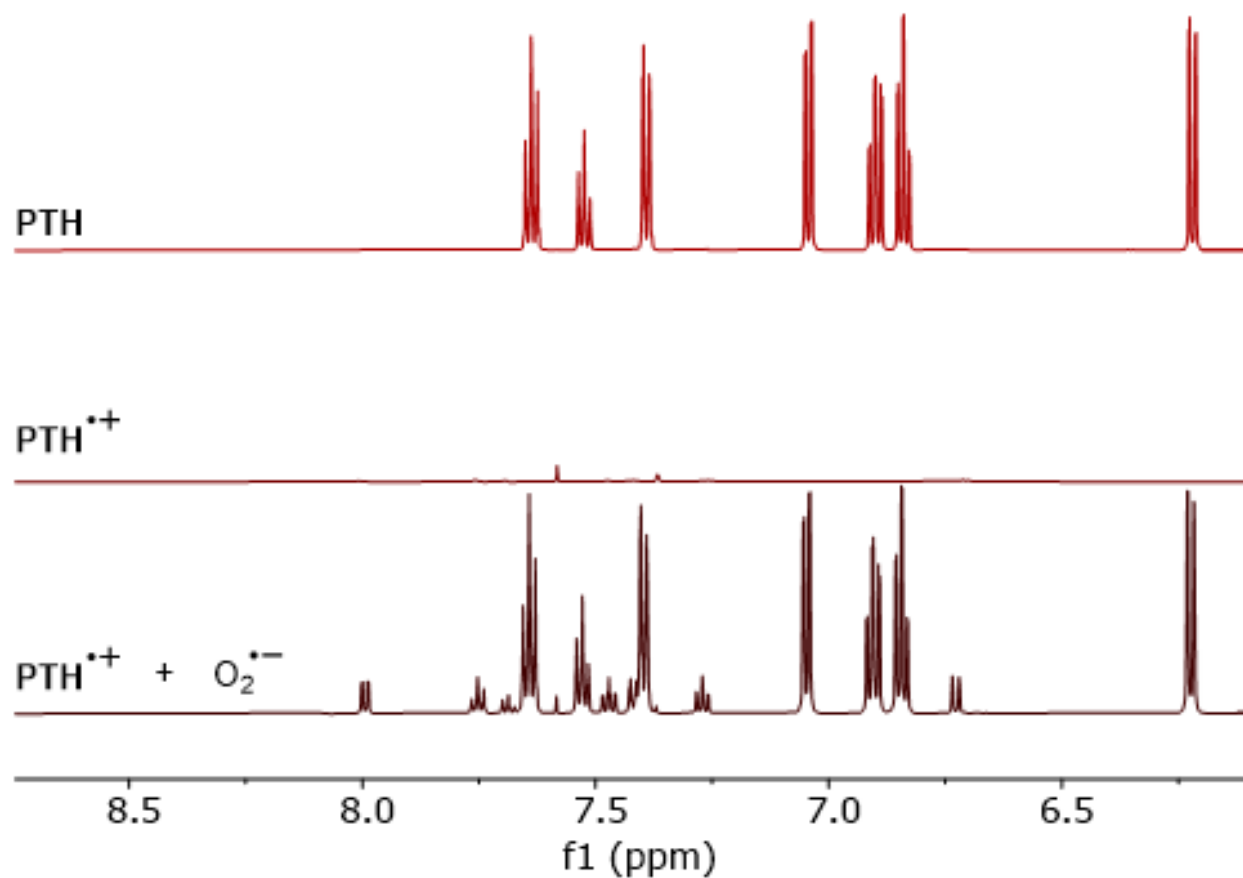


Figure 3. S9: ^1H NMR spectroscopic evidence supporting the working model for catalyst deactivation pathways by superoxide.

3. 5. 9. Time Course Experiments

Add ester pyrazole **1** (7.0 mg, 0.05 mmol, 1.0 equiv), PTH (0.7 mg, 0.0025 mmol, 5 mol %), and LiClO_4 (1.1 mg, 0.01 mmol, 20 mol %) to a 1-dram vial equipped with a stir bar and septum-containing cap. Add benzene (1 mL), TFE (0.9 mL), and HFIP (0.1 mL). Pierce the septum with a needle attached to an O_2 balloon. Purge the headspace for 2 min by partially opening the cap of the vial while stirring the solution. Add dodecane (10 μL , 0.044 mmol) via microsyringe and tighten the cap to maintain an O_2 atmosphere. Place vial into a HepatoChem EvoluChemTM PhotoRedOx Box [HCK1006-01-016] and irradiate with a 390 nm Kessil lamp for the duration of the time course experiment.

For GC analyses – Remove 10 μL of reaction solution via microsyringe through the septum cap. Filter the aliquot through a celite plug pre-wetted with EtOAc to remove salts and dilute the filtrate (0.2 mL) with ethyl acetate (1.0 mL).

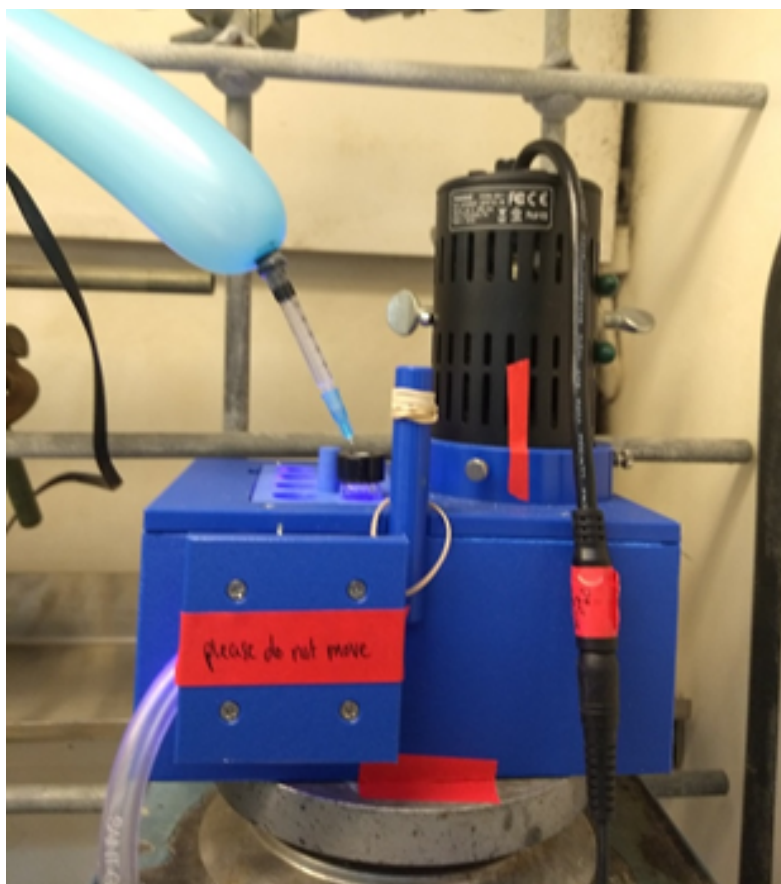


Figure 3. S10: Time course experimental set up.

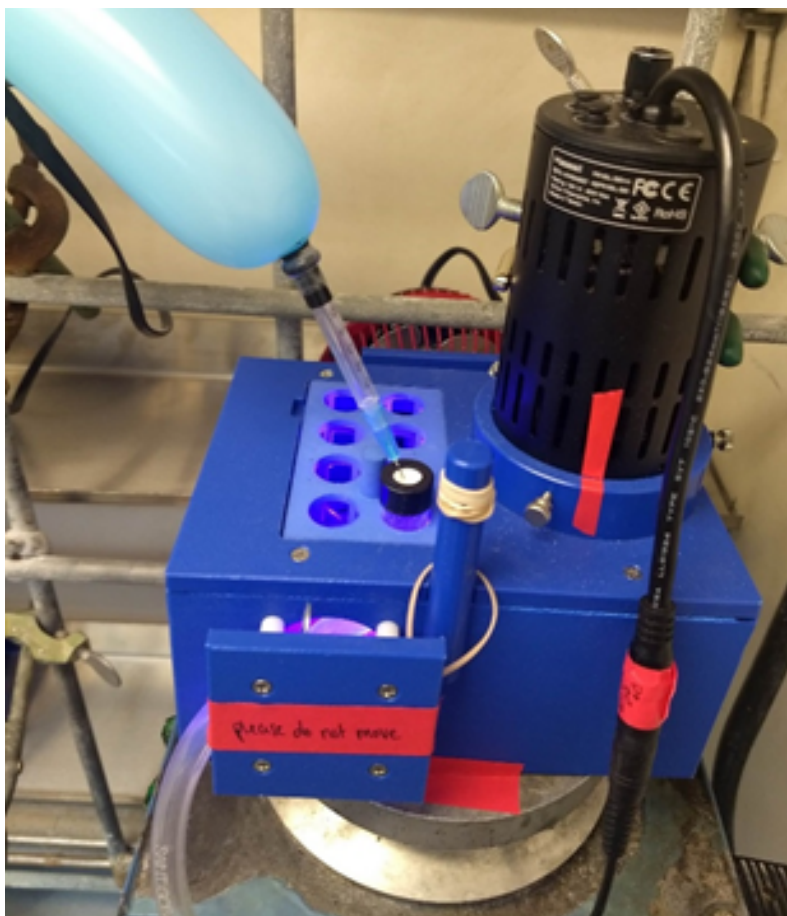


Figure 3. S11: reaction vial in designated position for reproducibility.

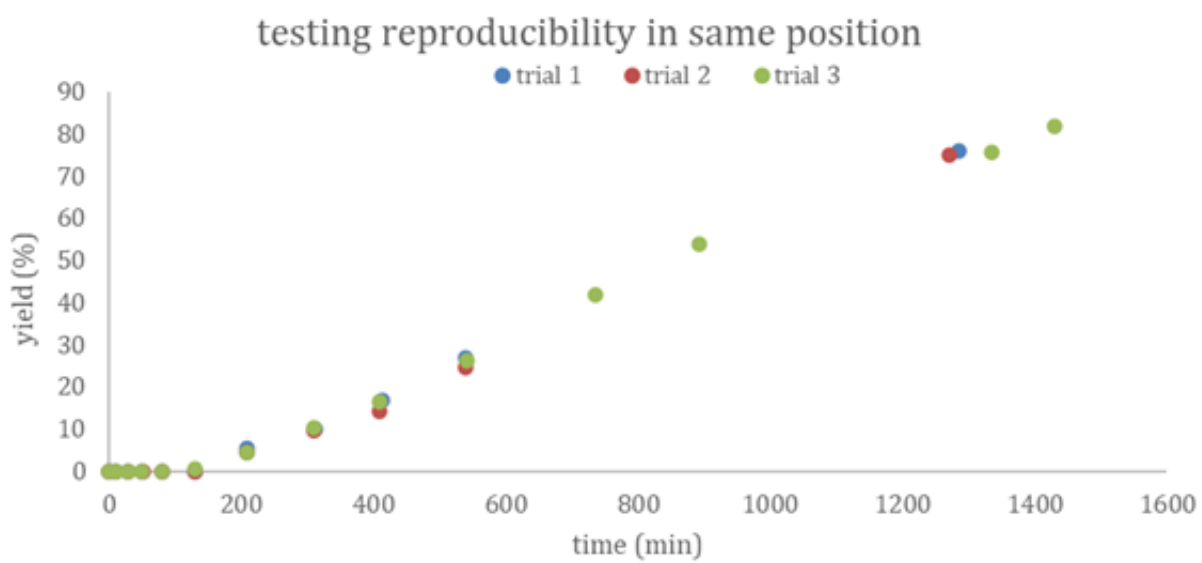


Figure 3. S12: Three trials prepared on separate days using the general procedure led to reproducible reaction rates and final yields.

3. 5. 10. Light Dependence Experiments (Scheme 1)

The procedure for time course experiments was followed, except for the following: during the designated “dark” time points, the reaction vial was wrapped in aluminum foil and kept in the photobox. After the dark period, the foil was removed, and the reaction was allowed to proceed with irradiation.

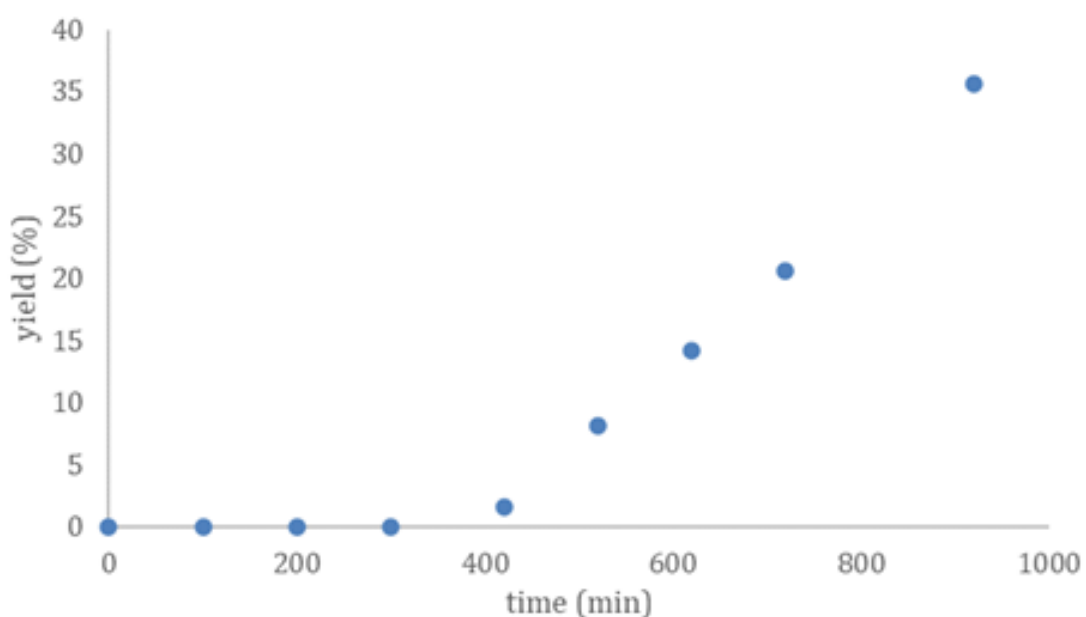


Figure 3. S13: 200 min of dark time during the induction period. Reactions shielded from light between 100 min and 300 min. The induction period lengthened accordingly.

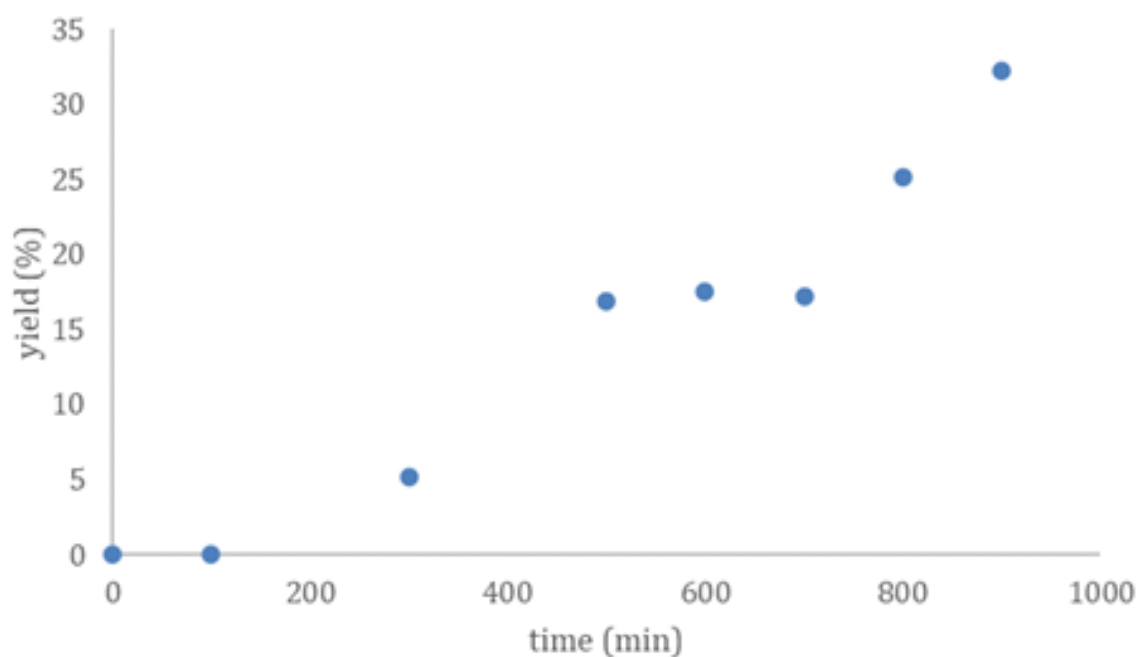


Figure 3. S14: 200 min of dark time during product formation. Reactions shielded from light between 500 min and 700 min. The percent yield of the coupling product did not increase without irradiation.

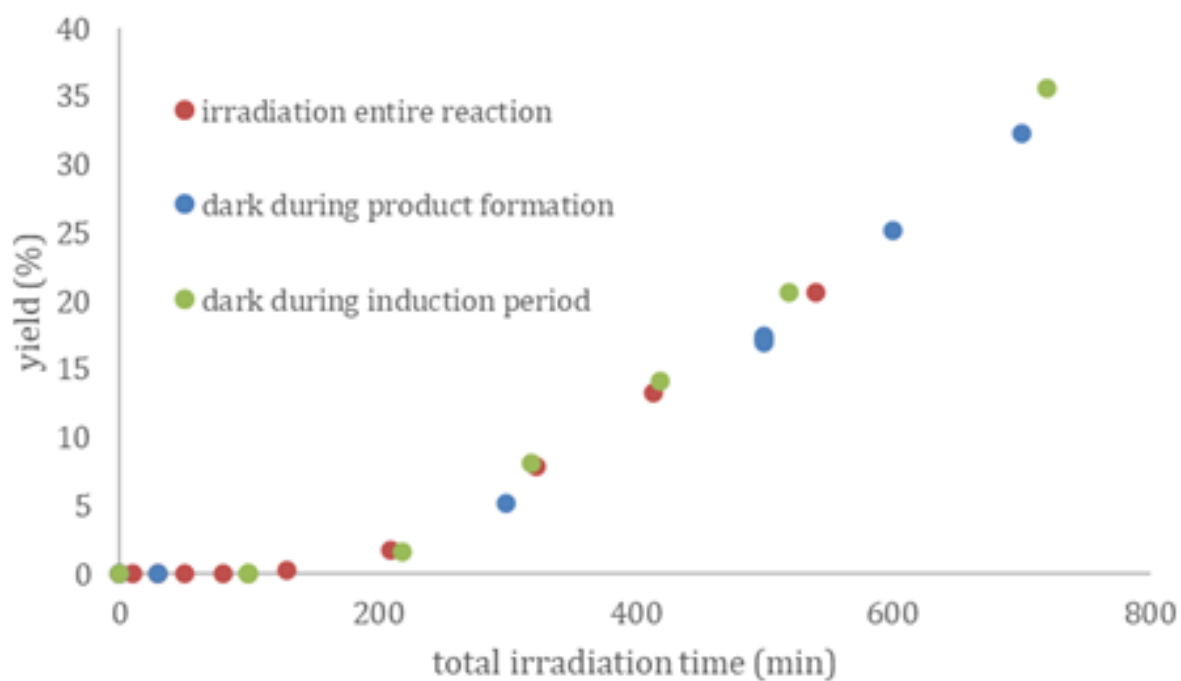


Figure 3. S15: When accounting for total irradiation time (by subtraction of the dark periods), the dark control experiments during the induction period and product forming phase overlay with the standard reaction profile during which irradiation is continuous. This indicates both the induction period and product formation involve light dependent processes.

3. 5. 11. Oxygen Uptake Experiment

Oxygen uptake experiments were performed on an apparatus developed by the Stahl lab – A stock solution of ethyl 1H-pyrazole-4-carboxylate (0.025 M) and LiClO₄ (0.005 M) in 9:1:10 TFE:HFIP:benzene was prepared as well as a stock solution of PTH in benzene (0.00125 M). A heavy walled tube equipped with a stir bar of known volume was attached to a pressure transducer, evacuated and refilled with 1 atm O₂ three times, and then pressurized to 1 atm. The tube was clamped above a stir plate and 2 mL of the ethyl 1H-pyrazole-4-carboxylate stock solution (0.05 mmol) was added to the tube through a thick rubber septum. Magnetic stirring and fan cooling were begun and the 390 nm Kessil lamp was turned on to allow for thermal equilibration over 20 min. Pressure monitoring was commenced, then 0.1 mL of PTH containing stock solution (0.0025 mmol PTH) was injected into the tube through the septum. To facilitate analysis, the uptake was normalized after the 0.1 mL catalyst injection. After pressure monitoring, the final yield of the reaction was measured via gas chromatography using dodecane as an internal standard. The data points were plotted over time to determine the amount of O₂ consumed during different phases of the reaction.

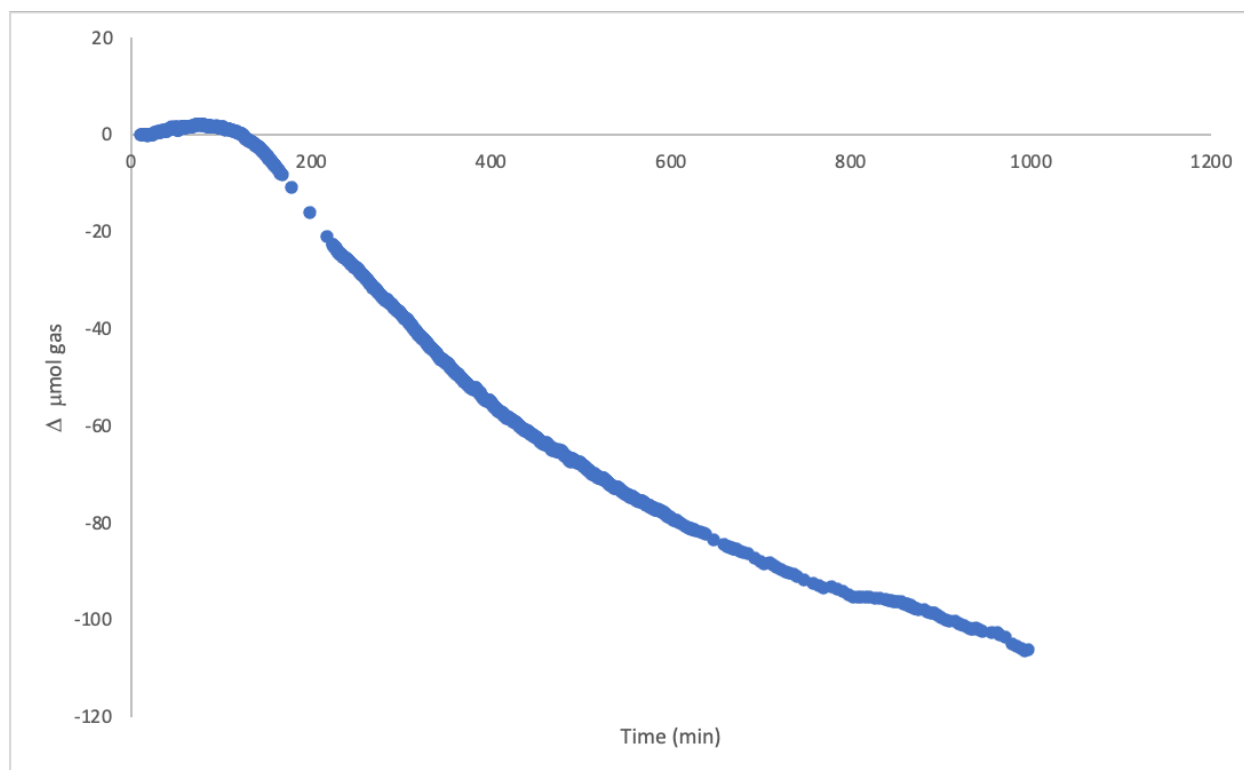


Figure 3. S16: Change in μmol of O_2 over the course of the reaction.

The reaction was run on a 50 μmol scale. 46.5 μmol of product was determined via GC, and 106 μmol of O_2 were consumed during the reaction. Collectively, this indicates that approximately 2.3 equivalents of O_2 are consumed relative to product. Furthermore, this experiment reveals that there is minimal change in pressure during the induction period. However, due to the slightly positive slope (consistent with modest heating from the light source and the system thermally equilibrating), precise quantification of how much O_2 is consumed during catalyst activation is not feasible. Drawing analogy to time course experiments, O_2 is only significantly consumed during the product forming phase of the reaction.

3. 5. 12. Lithium Saturation Curve Experiments (Scheme 2)

The general procedure for time course experiments was followed, except for the following: LiClO_4 concentrations lower than 0.005 M (20 mol%) were prepared from stock solutions.

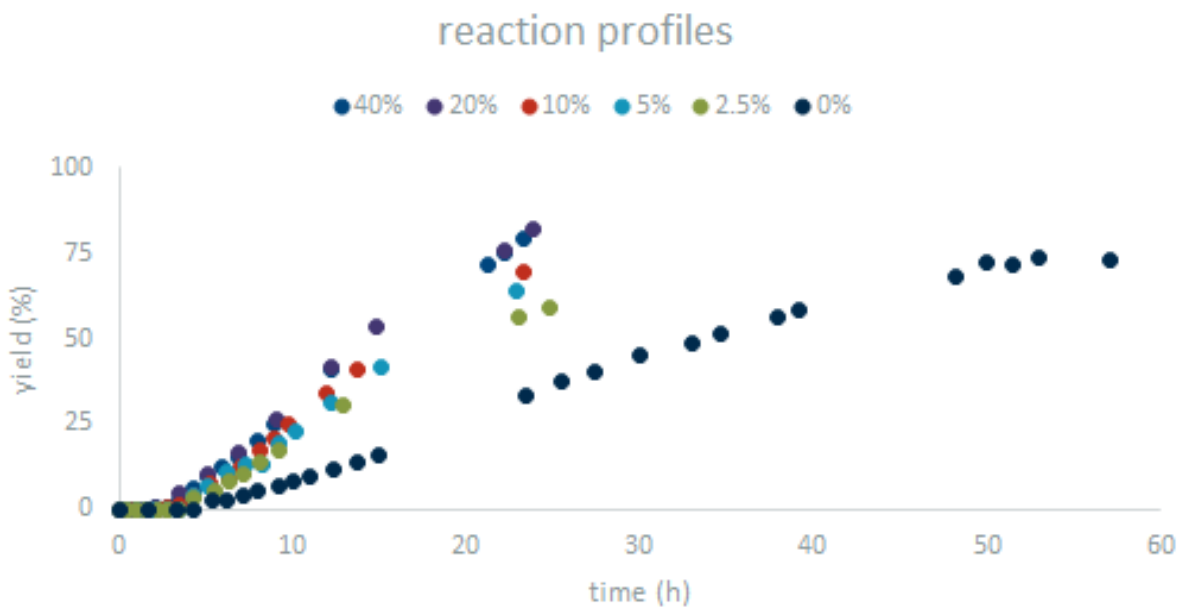


Figure 3. S17: Reaction profiles for varying LiClO_4 concentrations (0 to 40 mol % loading).

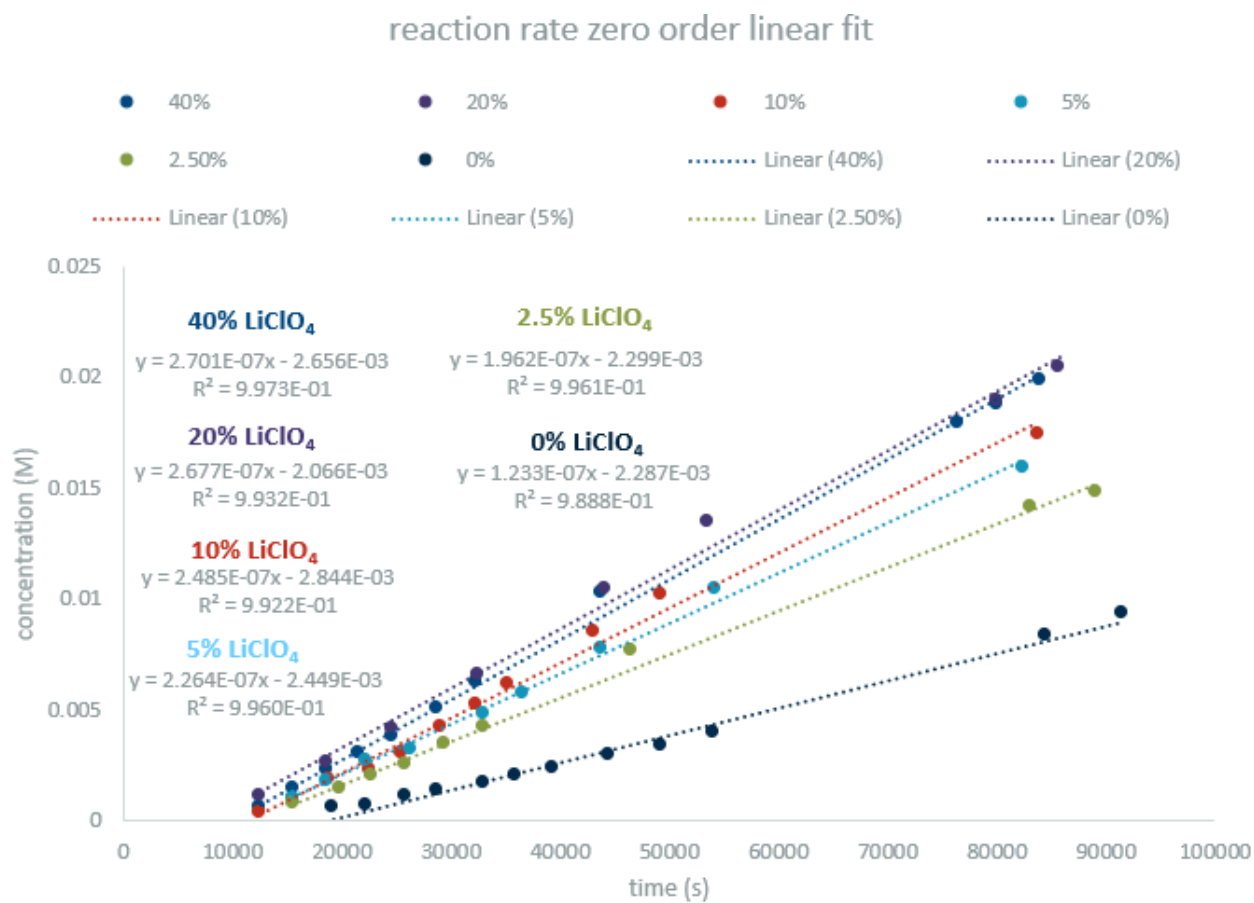


Figure 3. S18: Linear fit of zeroth order product formation regime for varying LiClO_4 concentrations (0 to 40 mol % loading). Slope is the rate of the reaction.

Table 3. S5: Reaction rate for varying Li concentrations. Li = LiClO_4 .

mol % Li	[Li] (mM)	rate ($10^{-5} \text{ M} \cdot \text{s}^{-1}$)
40	10	2.701
20	5	2.677
10	2.5	2.485

5	1.25	2.264
2.5	0.625	1.962
0	0	1.233

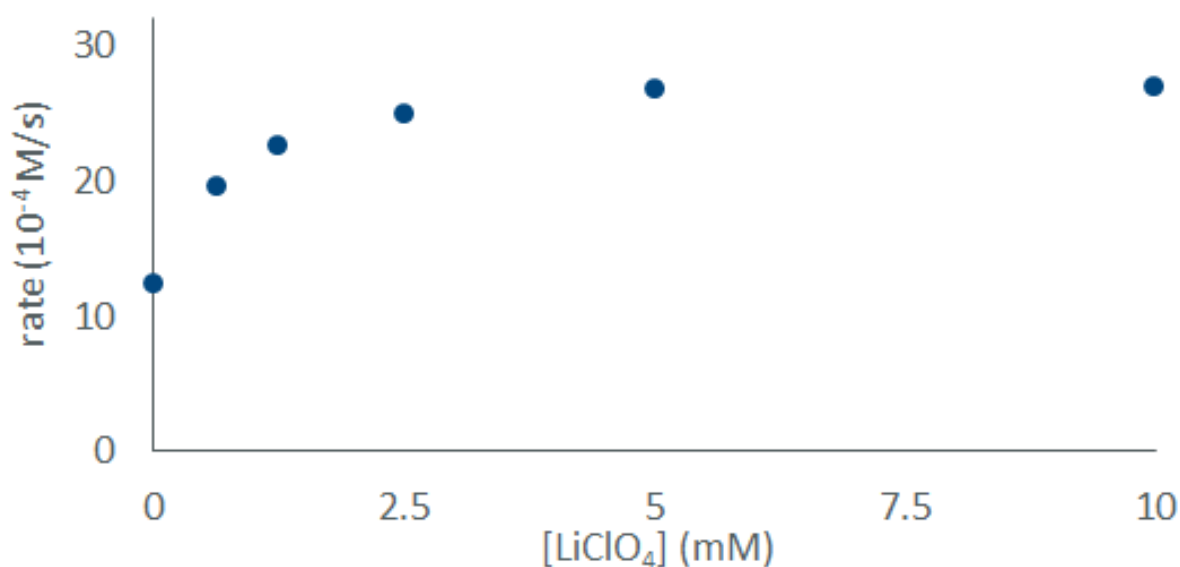


Figure 3. S19: Plot of Li concentration versus reaction rate reveals saturation in Li co-catalyst.

3. 5. 13. Superoxide Inhibition (Scheme 3)

The general procedure for time course experiments was followed, except for the following: working quickly, prepare a stock solution of KO₂ (0.05 M) in TFE and immediately add 50 μ L via microsyringe to the reaction solution that was irradiated for 9.3h (560 min). Continue monitoring the reaction using GC aliquots. No change in reaction outcome is observed due to addition of 50 μ L TFE.

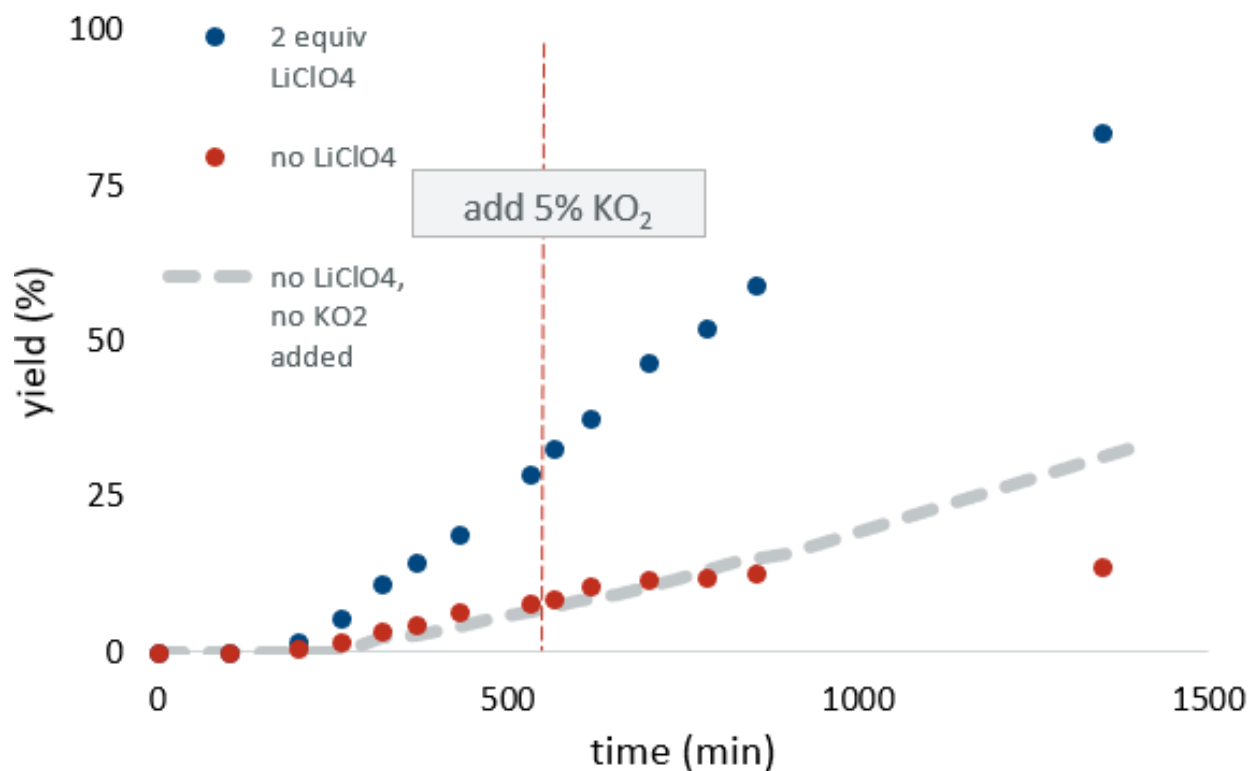


Figure 3. S20: Addition of 5% KO₂ shows an inhibitory effect on product formation (red points vs. grey dash). The presence of sufficient LiClO₄ protects the reaction from KO₂ inhibition (blue points).

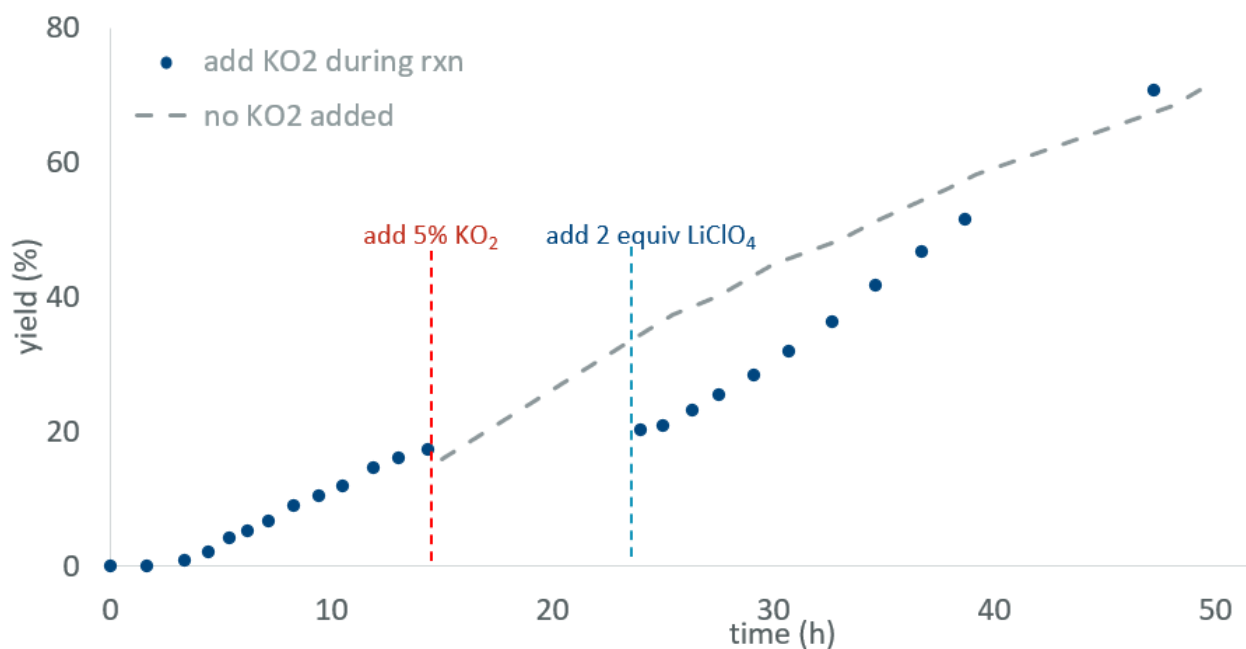
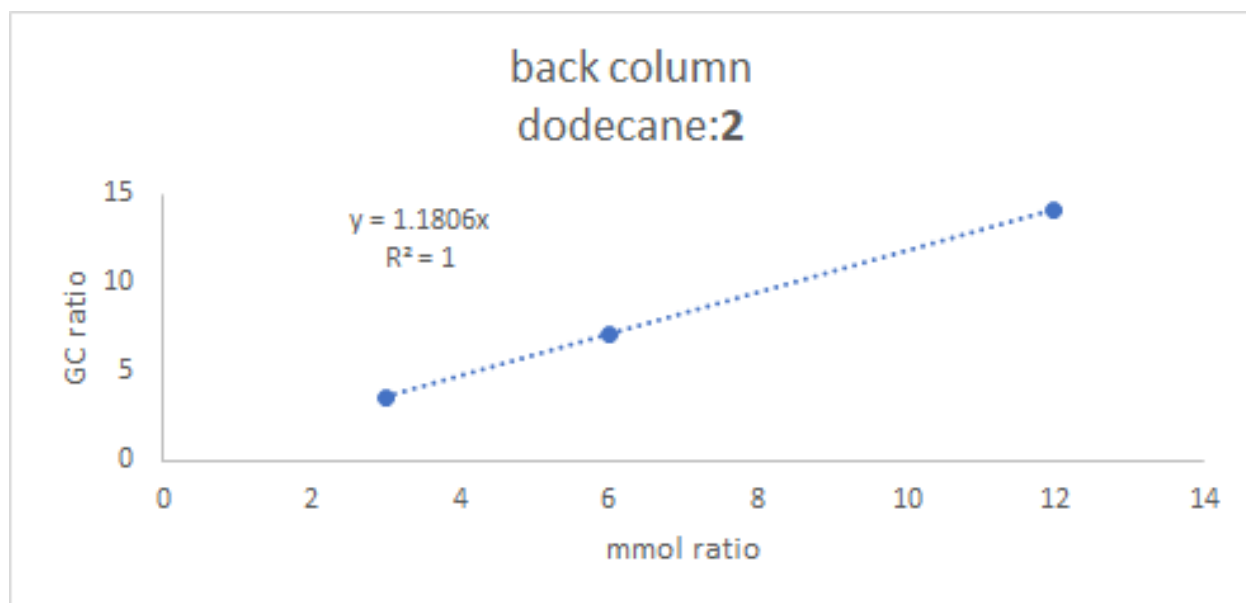
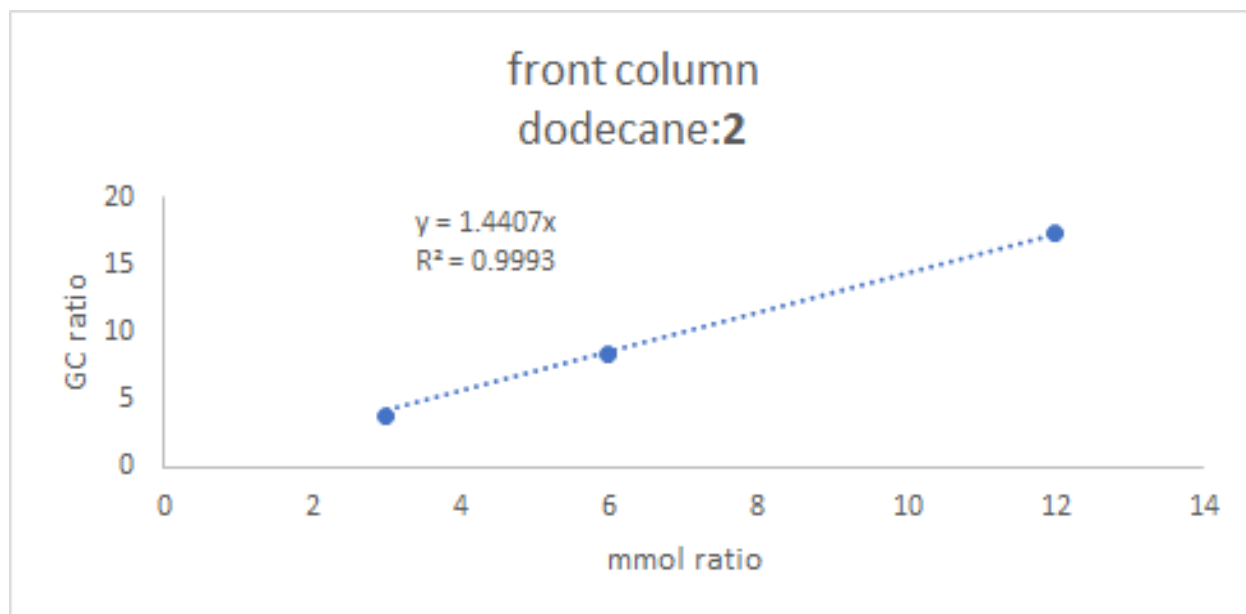


Figure 3. S21: A reaction with no LiClO_4 present is stalled by addition of 5% KO_2 compared to when no KO_2 is added (grey dash); the addition of LiClO_4 restarts the reaction and recovers product formation (blue points).

GC Calibration Curves



3. 5. 14. Investigation of Charge Transfer Complex Formation via UV-Vis

All absorbance spectra were measured on a Varian Cary 50 UV-Vis spectrophotometer instrument using quartz cuvettes. Baseline corrections were made using blanks containing solvent only.

A 50 μM solution of $\text{PTH}\cdot\text{PF}_6$ in TFE was prepared and its absorbance spectrum collected. Absorbance spectra of the same sample were sequentially measured after addition of 100, 1000, and 10000 equivalents of benzene (1.34, 12, 120 μL). The spectra in Figure S22 did not provide definitive evidence of a charge transfer complex between PTH radical cation and benzene. The observed decrease in absorbance is more consistent with either dilution or medium effects than a discrete complex between PTH radical cation and benzene.

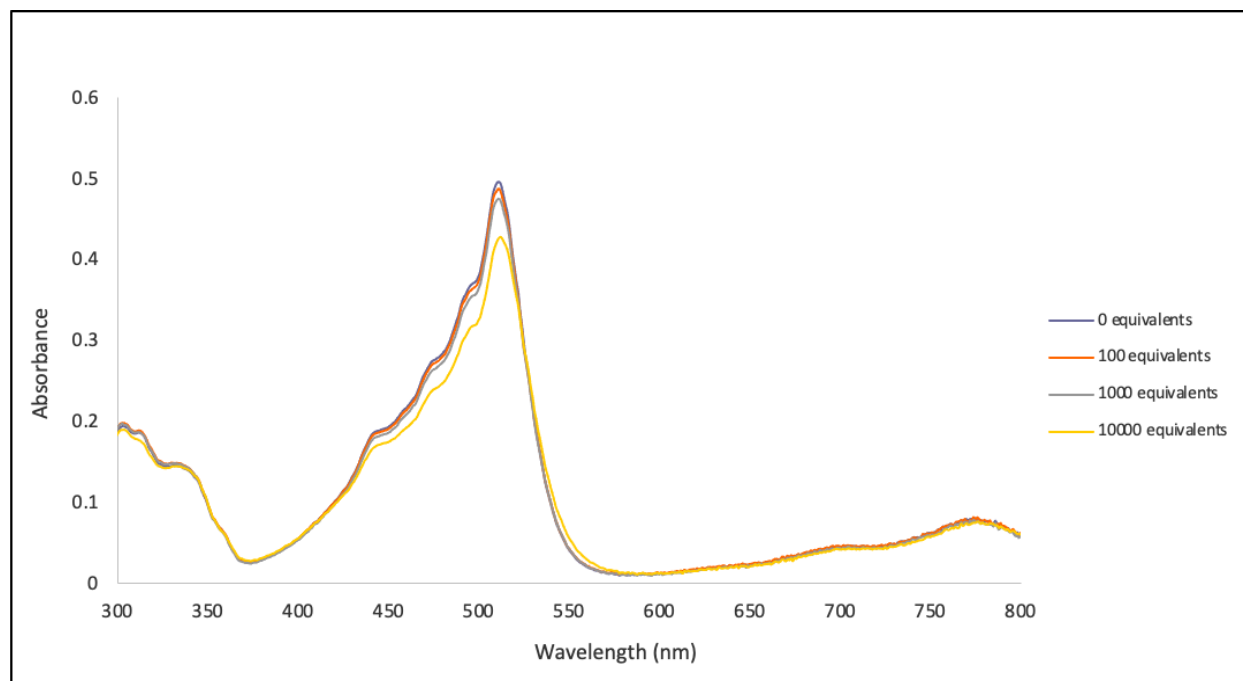


Figure 3. S22: Absorption spectra of PTH radical cation with increasing equivalents of benzene.

Next, to control for dilution, two cuvettes containing a 50 μM $\text{PTH}\cdot\text{PF}_6$ in TFE solution were prepared. To one was added 10000 equivalents of benzene (134 μL), and to the other an

equal volume of TFE. A third cuvette containing a 50 μM $\text{PTH}\cdot\text{PF}_6$ solution in 1:2 TFE:benzene was also prepared. Under these conditions, no clear feature consistent with a charge transfer complex was observed (Figure S23). Based on these data, we conclude that the observed spectral changes are most consistent with a change in solvation.

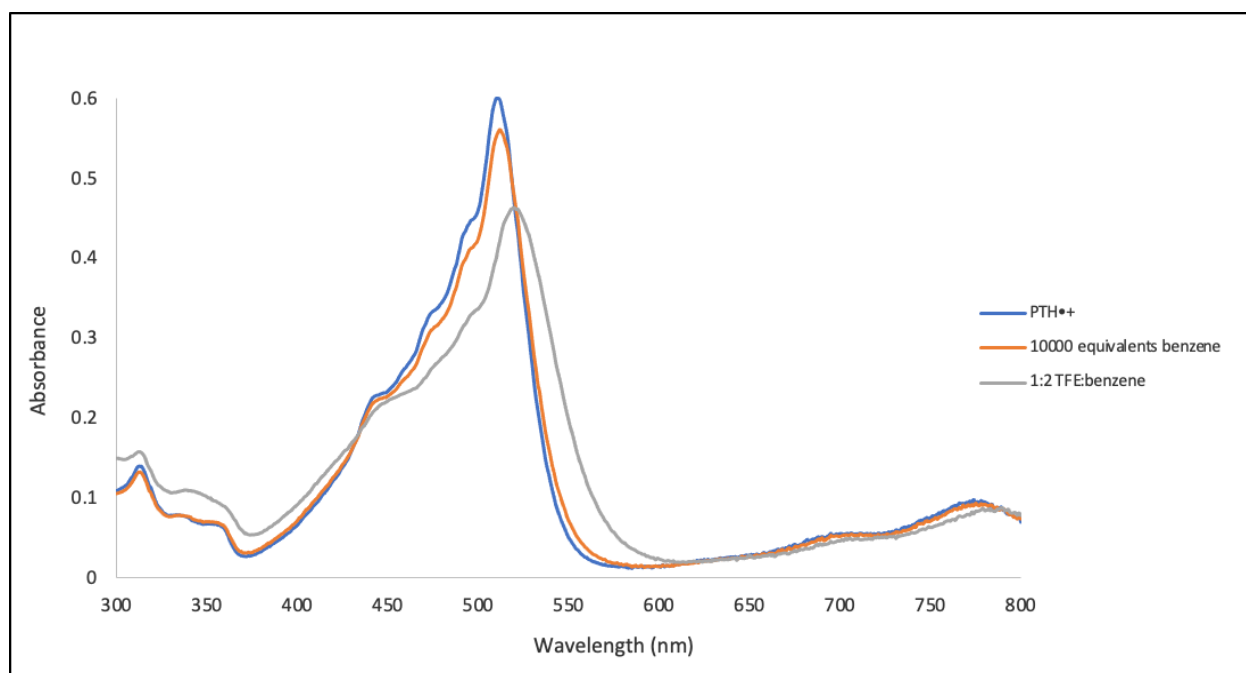


Figure 3. S23: Absorption spectrum of 50 μM PTH radical cation in the presence (orange trace) and absence (blue trace) of benzene. Absorption spectrum of PTH radical cation with benzene as a co-solvent (grey trace).

Finally, UV-Vis spectra of PTH radical cation and mesitylene were collected given that a smaller excess of mesitylene was amenable in the reaction. A 50 μM stock solution of $\text{PTH}\cdot\text{PF}_6$ in MeCN was prepared. To one cuvette was added 10 equivalents of mesitylene (1.50 μmol), via stock solution, and to the other an equal volume of MeCN. No significant change was observed upon addition of mesitylene (Figure S24). Overall, these data (Figures S22–24) are inconsistent with an exergonic association between PTH radical cation and the arene substrates.

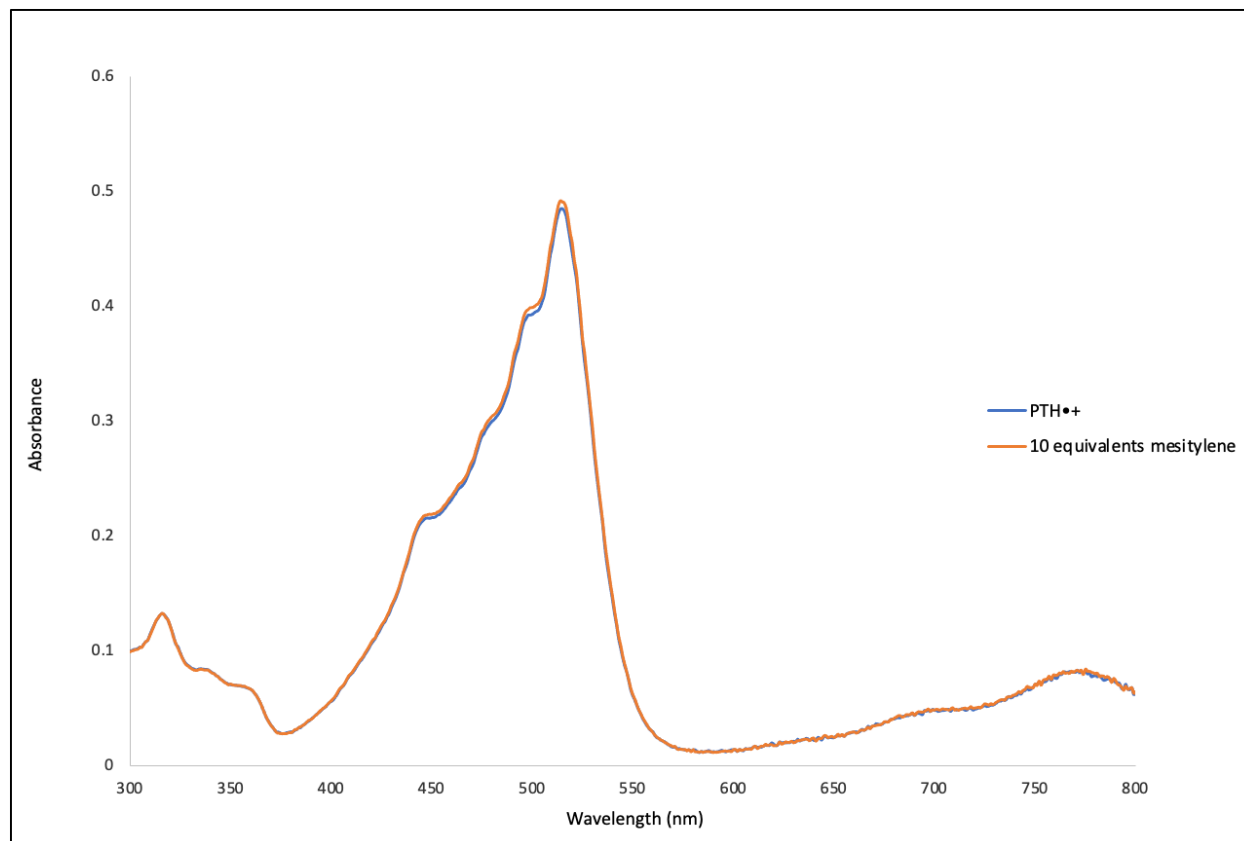
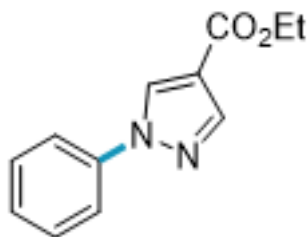


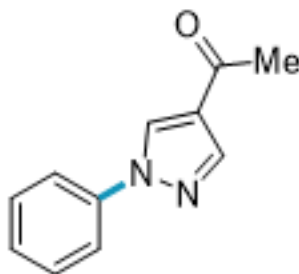
Figure 3. S24: Absorption spectrum of 50 μM PTH radical cation in the presence (orange trace) and absence (blue trace) of mesitylene.

3. 5. 15. Product Isolation and Characterization

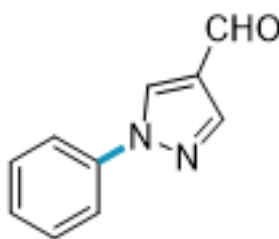


Ethyl 1-phenyl-1H-pyrazole-4-carboxylate (2): Prepared from benzene and ethyl 1H-pyrazole-4-carboxylate; 86.5 mg (81% yield) obtained following General Procedure A. ¹H NMR (500 MHz, CDCl₃) δ 8.41 (s, 1H), 8.10 (s, 1H), 7.74 – 7.68 (m, 2H), 7.52 – 7.44 (m, 2H), 7.36 (td, *J* = 7.4, 1.3

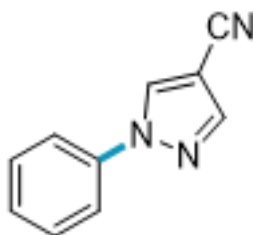
Hz, 1H), 4.34 (q, $J = 7.2$ Hz, 2H), 1.38 (t, $J = 7.1$ Hz, 3H); consistent with reported spectra (*Angew. Chem. Int. Ed.*, **2019**, 58, 13318–13322).



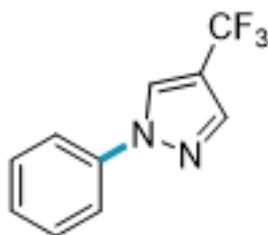
1-(1-phenyl-1H-pyrazol-4-yl)ethanone (3): Prepared from benzene and 1-(1H-pyrazol-4-yl)ethanone; 66.0 mg (88% yield) obtained following General Procedure A using 20 mol % LiPF_6 . $^1\text{H NMR}$ (500 MHz, CDCl_3) δ 8.32 (s, 1H), 8.03 (s, 1H), 7.67 – 7.62 (m, 2H), 7.46 – 7.40 (m, 2H), 7.33 – 7.28 (m, 1H), 2.44 (s, 3H); consistent with reported spectra (*Angew. Chem. Int. Ed.*, **2019**, 58, 13318–13322).



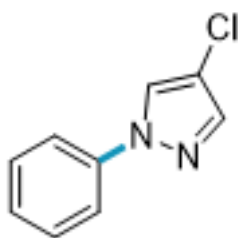
1-phenyl-1H-pyrazole-4-carbaldehyde (4): Prepared from benzene and 1H-pyrazole-4-carbaldehyde; 49.2 mg (71% yield) obtained following General Procedure A using 1:1 HFIP:PhH solvent mixture. $^1\text{H NMR}$ (500 MHz, CDCl_3) δ 9.96 (s, 1H), 8.44 (s, 1H), 8.16 (s, 1H), 7.74 – 7.68 (m, 2H), 7.50 (t, $J = 8.0$ Hz, 2H), 7.42 – 7.35 (m, 1H); consistent with reported spectra (*Angew. Chem. Int. Ed.*, **2019**, 58, 13318–13322).



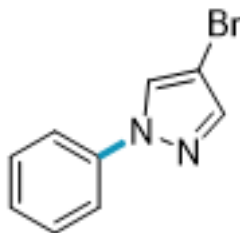
1-phenyl-1H-pyrazole-4-carbonitrile (5): Prepared from benzene and 1H-pyrazole-4-carbonitrile; 58.6 mg (87% yield) obtained following General Procedure A. ^1H NMR (500 MHz, CDCl_3) δ 8.32 (s, 1H), 8.00 (s, 1H), 7.71 – 7.65 (m, 2H), 7.52 (dd, J = 8.7, 7.3 Hz, 2H), 7.42 (td, J = 7.2, 1.3 Hz, 1H); consistent with reported spectra (*Org. Lett.*, **2015**, 17, 2886–2889).



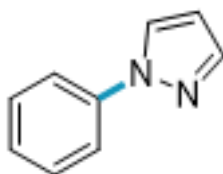
1-phenyl-4-(trifluoromethyl)-1H-pyrazole (6): Prepared from benzene and 4-(trifluoromethyl)-1H-pyrazole; 59.0 mg (70% yield) obtained following General Procedure A. ^1H NMR (500 MHz, CDCl_3) δ 8.19 (s, 1H), 7.92 (s, 1H), 7.72 – 7.66 (m, 2H), 7.50 (dd, J = 8.6, 7.4 Hz, 2H), 7.39 (td, J = 7.3, 1.3 Hz, 1H); ^1H and ^{19}F NMR are consistent with reported spectra (*RSC Advances*, **2019**, 9, 30952–30956).



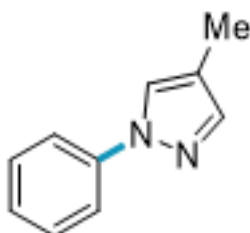
4-chloro-1-phenyl-1H-pyrazole (7): Prepared from benzene and 4-chloro-1H-pyrazole; 58% yield obtained following General Procedure B; consistent with reported spectra (*Angew. Chem. Int. Ed.*, **2019**, 58, 13318–13322).



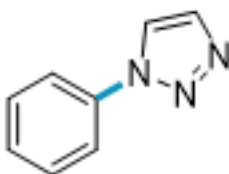
4-bromo-1-phenyl-1H-pyrazole (8): Prepared from benzene and 4-bromo-1H-pyrazole; 40.2 mg (45% yield) obtained following General Procedure A using 20 mol % LiPF_6 . $^1\text{H NMR}$ (500 MHz, CDCl_3) δ 7.94 (s, 1H), 7.68 (s, 1H), 7.67 – 7.62 (m, 2H), 7.51 – 7.42 (m, 2H), 7.35 – 7.31 (m, 1H); consistent with reported spectra (*Chem. - Eur. J.*, **2015**, 21, 11976–11979).



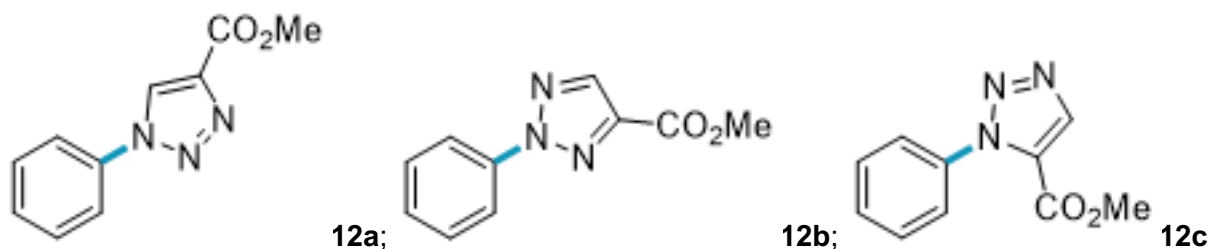
1-phenylpyrazole (9): Prepared from benzene and pyrazole; 38% yield obtained following General Procedure B; consistent with reported spectra (*Tetrahedron*, **2013**, 69 (30), 6230–6233).



4-methyl-1-phenyl-1H-pyrazole (10): Prepared from benzene and 4-methyl-1H-pyrazole; 13.6 mg (22% yield) obtained following General Procedure A. $^1\text{H NMR}$ (500 MHz, CDCl_3) δ 7.71 (s, 1H), 7.70 – 7.63 (m, 2H), 7.54 (s, 1H), 7.48 – 7.40 (m, 2H), 7.29 – 7.22 (m, 1H), 2.17 (s, 3H); consistent with reported spectra (*Chemistry – A European Journal*, **2019**, 26 (1), 155–159).



1-phenyl-1,2,3-triazole (11): Prepared from benzene and 1,2,3-triazole; 22.1 mg (38% yield) obtained following General Procedure A. $^1\text{H NMR}$ (500 MHz, CDCl_3) δ 8.00 (d, $J = 1.1$ Hz, 1H), 7.86 (d, $J = 1.1$ Hz, 1H), 7.80 – 7.72 (m, 2H), 7.58 – 7.50 (m, 2H), 7.49 – 7.42 (m, 1H); consistent with reported spectra (*Angew. Chem. Int. Ed.* **2020**, 59, 1181).

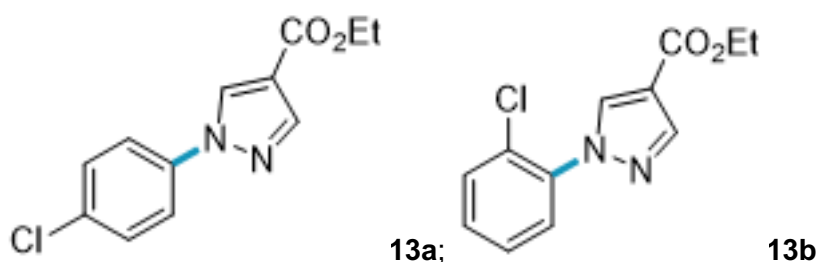


Methyl 1-phenyl-1H-1,2,3-triazole-4-carboxylate (12a), methyl 2-phenyl-2H-1,2,3-triazole-4-carboxylate (12b), and methyl 1-phenyl-1H-1,2,3-triazole-5-carboxylate (12c): Prepared from benzene and methyl 1,2,3-triazole-4-carboxylate; 45.9 mg (55% combined yield, 4:1:9 **12a** to **12b** to **12c** ratio) obtained as a separable mixture following General Procedure A.

12a: $^1\text{H NMR}$ (500 MHz, CDCl_3) δ 8.52 (s, 1H), 7.79 – 7.73 (m, 2H), 7.62 – 7.53 (m, 2H), 7.53 – 7.47 (m, 1H), 4.00 (s, 3H); consistent with reported spectra (*Green Chem.*, **2016**, 18, 2534-2541).

12b: $^1\text{H NMR}$ (500 MHz, CDCl_3) δ 8.25 (s, 1H), 8.18 – 8.12 (m, 2H), 7.55 – 7.47 (m, 2H), 7.46 – 7.39 (m, 1H), 4.01 (s, 3H); consistent with reported spectra (*J. Org. Chem.*, **2014**, 79, 6105-6112).

12c: $^1\text{H NMR}$ (500 MHz, CDCl_3) δ 8.27 (s, 1H), 7.57 – 7.51 (m, 3H), 7.51 – 7.46 (m, 2H), 3.85 (s, 3H); consistent with reported spectra (*Adv. Synth. Catal.* **2018**, 360, 3117).

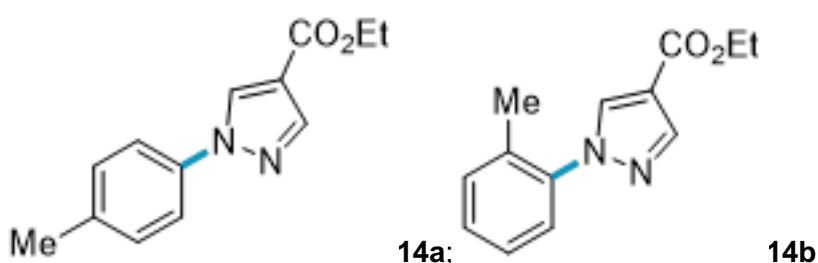


Ethyl 1-(4-chlorophenyl)-1H-pyrazole-4-carboxylate (13a) and ethyl 1-(2-chlorophenyl)-1H-pyrazole-4-carboxylate (13b): Prepared from chlorobenzene and ethyl 1H-pyrazole-4-

carboxylate; 21.8 mg (22% combined yield, 3:1 **13a** to **13b** ratio) obtained as a separable mixture following General Procedure A.

13a: ¹H NMR (400 MHz, CDCl₃) δ 8.37 (s, 1H), 8.09 (s, 1H), 7.70 – 7.62 (m, 2H), 7.49 – 7.39 (m, 2H), 4.34 (q, *J* = 7.1 Hz, 2H), 1.38 (t, *J* = 7.1 Hz, 3H).; consistent with reported spectra (*Angew. Chem. Int. Ed.*, **2020**, 59, 658).

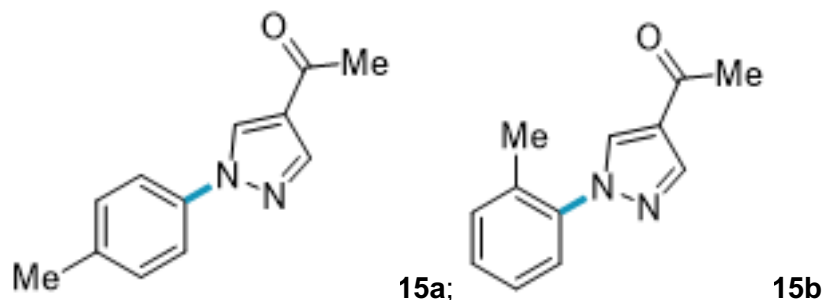
13b: ¹H NMR (400 MHz, CDCl₃) δ 8.35 (s, 1H), 8.13 (s, 1H), 7.63 – 7.50 (m, 2H), 7.46 – 7.34 (m, 2H), 4.34 (q, *J* = 7.2 Hz, 2H), 1.38 (t, *J* = 7.1 Hz, 3H); consistent with reported spectra (*ChemRxiv* **2020**, <https://doi.org/10.26434/chemrxiv.13140053.v1>).



Ethyl 1-(4-methylphenyl)-1H-pyrazole-4-carboxylate (14a) and ethyl 1-(2-methylphenyl)-1H-pyrazole-4-carboxylate (14b): Prepared from toluene and ethyl 1H-pyrazole-4-carboxylate; 71.1 mg (77% yield, 2:1 **14a** to **14b** ratio) obtained as an intractable mixture following General Procedure C.

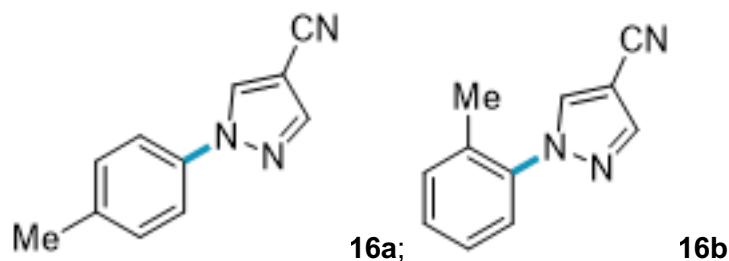
14a: ¹H NMR (500 MHz, CDCl₃) δ 8.29 (s, 1H), 8.01 (s, 1H), 7.53 – 7.47 (m, 2H), 7.32 – 7.17 (m, 2H), 4.26 (q, *J* = 7.1 Hz, 2H), 2.32 (s, 3H), 1.30 (t, *J* = 7.1 Hz, 3H); consistent with reported spectra (*Org. Lett.*, **2015**, *17*, 872–875).

14b: ¹H NMR (500 MHz, CDCl₃) δ 8.03 (s, 1H), 8.01 (s, 1H), 7.55 – 7.49 (m, 1H), 7.51 – 7.46 (m, 1H), 7.37 (t, J = 7.8 Hz, 1H), 7.18 (d, J = 7.6 Hz, 1H), 4.26 (q, J = 7.1 Hz, 2H), 2.17 (s, 3H), 1.30 (t, J = 7.1 Hz, 3H); consistent with reported spectra (*Org. Lett.*, **2015**, 17, 872–875).



1-[1-(4-methylphenyl)pyrazol-4-yl]ethanone (15a) and 1-[1-(2-methylphenyl)pyrazol-4-yl]ethanone (15b): Prepared from toluene and 1-(1H-pyrazol-4-yl)ethanone; 49.2 mg (61% yield, 2:1 **15a** to **15b** ratio) obtained as an intractable mixture following General Procedure C.

¹H NMR (500 MHz, CDCl₃, mixture of **15a** and **15b**) δ 8.31 (s, 1H), 8.06 (s, 1H), 8.03 (s, 2H), 7.57 – 7.50 (m, 2H), 7.36 – 7.20 (m, 6H), 2.45 (s, 6H), 2.36 (s, 3H), 2.21 (s, 3H). **¹³C NMR** (126 MHz, CDCl₃, mixture of **15a** and **15b**) δ 192.23, 192.15, 141.42, 141.05, 139.08, 137.85, 137.14, 133.76, 133.09, 131.57, 130.22, 130.16, 129.36, 129.05, 128.49, 126.86, 126.03, 125.51, 124.85, 119.73, 77.36, 77.10, 76.85, 28.10, 28.08, 21.06, 18.02. **HRMS** (ESI⁺) Calc: [M+H]⁺ (C₁₂H₁₃N₂O) 201.1028; measured: 201.1022 = 0.6 ppm difference.

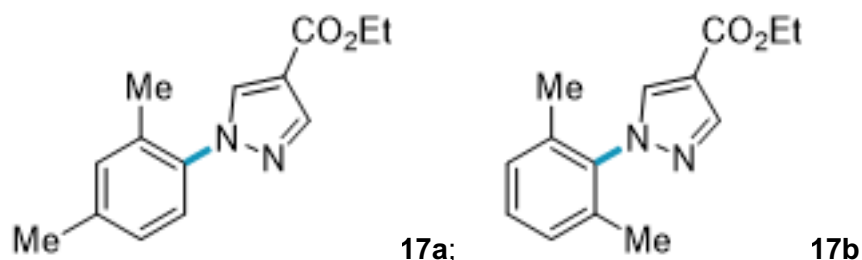


1-(4-methylphenyl)-1H-pyrazole-4-carbonitrile (16a) and 1-(2-methylphenyl)-1H-pyrazole-4-carbonitrile (16b): Prepared from toluene and 1H-pyrazole-4-carbonitrile; 52.8 mg (72% yield, 2:1 **16a** to **16b** ratio) obtained as an intractable mixture following General Procedure C.

16a: **¹H NMR** (500 MHz, CDCl₃) δ 8.26 (s, 1H), 7.98 (s, 1H), 7.60 – 7.54 (m, 2H), 7.34 – 7.29 (m, 2H), 2.42 (s, 3H).

16b: ^1H NMR (500 MHz, CDCl_3) δ 8.29 (s, 1H), 7.99 (s, 1H), 7.54 – 7.50 (m, 1H), 7.46 (dd, J = 7.8, 2.3 Hz, 1H), 7.39 (t, J = 7.8 Hz, 1H), 7.23 (ddt, J = 7.5, 1.7, 0.9 Hz, 1H), 2.45 (s, 3H).

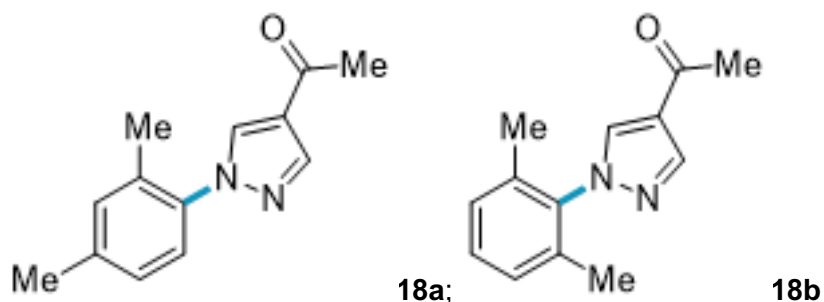
^{13}C NMR (126 MHz, CDCl_3 , mixture of **16a** and **16b**) δ 143.20, 143.13, 140.18, 138.54, 136.66, 131.90, 131.75, 130.37, 129.66, 129.19, 120.77, 119.97, 117.08, 113.22, 113.16, 94.32, 94.18, 77.35, 77.10, 76.85, 21.52, 21.11. **HRMS** (ESI+) Calc: $[\text{M}+\text{H}]^+$ ($\text{C}_{11}\text{H}_{10}\text{N}_3$) 184.0875; measured: 184.0869 = 0.6 ppm difference.



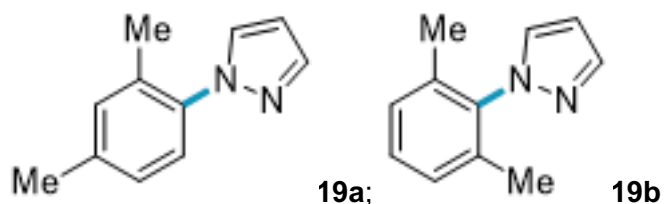
Ethyl 1-(2,4-dimethylphenyl)-1H-pyrazole-4-carboxylate (17a) and ethyl 1-(2,6-dimethylphenyl)-1H-pyrazole-4-carboxylate (17b): Prepared from m-xylene (490 μL , 4 mmol, 10.0 equiv) and ethyl 1H-pyrazole-4-carboxylate; 72.1 mg (74% yield, 4:1 **17a** to **17b** ratio) obtained as an intractable mixture following General Procedure D.

17a: ^1H NMR (500 MHz, CDCl_3) δ 8.11 (s, 1H), 8.07 (s, 1H), 7.21 (d, J = 8.0 Hz, 1H), 7.18 – 7.14 (m, 1H), 7.10 (dd, J = 8.0, 2.0 Hz, 1H), 4.35 (q, J = 7.1 Hz, 2H), 2.39 (s, 3H), 2.21 (s, 3H), 1.37 (t, J = 7.1 Hz, 3H); consistent with reported spectra (*Org. Lett.*, **2015**, 17, 872–875).

17b: ^1H NMR (500 MHz, CDCl_3) δ 8.16 (s, 1H), 7.98 (s, 1H), 7.29 (t, J = 8.0 Hz, 1H), 7.18 – 7.14 (m, 2H), 4.36 (q, J = 7.2 Hz, 2H), 2.04 (s, 6H), 1.38 (t, J = 7.1 Hz, 3H); consistent with reported spectra (*ChemRxiv* **2020**, <https://doi.org/10.26434/chemrxiv.13140053.v1>).



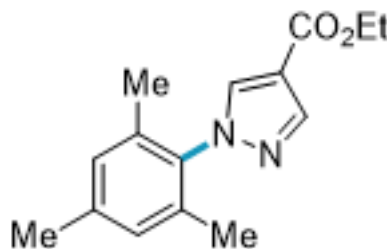
1-[1-(2,4-dimethylphenyl)pyrazol-4-yl]ethanone (18a) and 1-[1-(2,6-dimethylphenyl)pyrazol-4-yl]ethanone (18b): Prepared from m-xylene (490 μ L, 4 mmol, 10.0 equiv) and 1-(1H-pyrazol-4-yl)ethanone; 75% yield (4:1 **18a** to **18b** ratio) obtained following General Procedure B; peaks assigned by analogy to **17a** and **17b**.



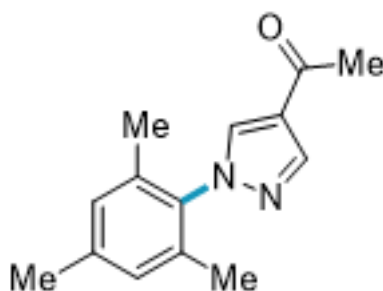
1-(2,4-dimethylphenyl)-1H-pyrazole (19a) and 1-(2,6-dimethylphenyl)-1H-pyrazole (19b): Prepared from m-xylene (490 μ L, 4 mmol, 10.0 equiv) and pyrazole; 26.5 mg (38% yield, 14:1 **19a** to **19b** ratio) obtained as an intractable mixture following General Procedure D.

19a: $^1\text{H NMR}$ (500 MHz, CDCl_3) δ 7.70 (d, J = 1.8 Hz, 1H), 7.56 (d, J = 2.3 Hz, 1H), 7.20 (d, J = 7.9 Hz, 1H), 7.12 (d, J = 2.1 Hz, 1H), 7.10 – 7.04 (m, 1H), 6.42 (t, J = 2.1 Hz, 1H), 2.37 (s, 3H), 2.19 (s, 3H); consistent with reported spectra (*Angew. Chem. Int. Ed.*, **2019**, 58, 13318–13322).

19b: $^1\text{H NMR}$ (500 MHz, CDCl_3) δ 7.74 (d, J = 1.9 Hz, 1H), 7.46 (d, J = 2.3 Hz, 1H), 7.25 – 7.22 (m, 2H), 7.14 (s, 1H), 6.45 (t, J = 2.1 Hz, 1H), 2.01 (s, 6H); consistent with reported spectra (*Angew. Chem. Int. Ed.*, **2019**, 58, 13318–13322).



Ethyl 1-mesityl-1H-pyrazole-4-carboxylate (20): Prepared from mesitylene (278 μL , 2 mmol, 5.0 equiv) and ethyl 1H-pyrazole-4-carboxylate; 80.5 mg (78% yield) obtained following General Procedure D. $^1\text{H NMR}$ (500 MHz, CDCl_3) δ 8.13 (s, 1H), 7.94 (s, 1H), 6.96 (s, 2H), 4.34 (q, J = 7.1 Hz, 2H), 2.35 (s, 3H), 1.99 (s, 6H), 1.38 (t, J = 7.1 Hz, 3H); consistent with reported spectra (*Angew. Chem. Int. Ed.*, **2019**, 58, 13318–13322).



1-(1-mesityl-1H-pyrazol-4-yl)ethanone (21): Prepared from mesitylene (278 μL , 2 mmol, 5.0 equiv) and 1-(1H-pyrazol-4-yl)ethanone; 63.7 mg (70% yield) obtained following General Procedure D. $^1\text{H NMR}$ (500 MHz, CDCl_3) δ 8.12 (s, 1H), 7.93 (s, 1H), 6.96 (s, 2H), 2.50 (s, 3H), 2.34 (s, 3H), 1.98 (s, 6H); consistent with reported spectra (*Angew. Chem. Int. Ed.*, **2019**, 58, 13318–13322).

3. 6. References

- (1) Girard, P.; Namy, J. L.; Kagan, H. B. Divalent Lanthanide Derivatives in Organic Synthesis. 1. Mild Preparation of Samarium Iodide and Ytterbium Iodide and Their Use as Reducing or Coupling Agents. *J. Am. Chem. Soc.* **1980**, 102 (8), 2693–2698.
- (2) Eberson, L. Electron-Transfer Reactions in Organic Chemistry. In *Advances in Physical Organic Chemistry*; Gold, V., Bethell, D., Eds.; Academic Press, 1982; Vol. 18, pp 79–185.

- (3) Zhang, N.; Samanta, S. R.; Rosen, B. M.; Percec, V. Single Electron Transfer in Radical Ion and Radical-Mediated Organic, Materials and Polymer Synthesis. *Chem. Rev.* **2014**, *114* (11), 5848–5958.
- (4) Ashby, E. C. Single-Electron Transfer, a Major Reaction Pathway in Organic Chemistry. An Answer to Recent Criticisms. *Acc. Chem. Res.* **1988**, *21* (11), 414–421.
- (5) Romero, N. A.; Nicewicz, D. A. Organic Photoredox Catalysis. *Chem. Rev.* **2016**, *116* (17), 10075–10166.
- (6) Prier, C. K.; Rankic, D. A.; MacMillan, D. W. C. Visible Light Photoredox Catalysis with Transition Metal Complexes: Applications in Organic Synthesis. *Chem. Rev.* **2013**, *113* (7), 5322–5363.
- (7) Shaw, M. H.; Twilton, J.; MacMillan, D. W. C. Photoredox Catalysis in Organic Chemistry. *J. Org. Chem.* **2016**, *81* (16), 6898–6926.
- (8) Marzo, L.; Pagire, S. K.; Reiser, O.; König, B. Visible-Light Photocatalysis: Does It Make a Difference in Organic Synthesis? *Angewandte Chemie International Edition* **2018**, *57* (32), 10034–10072.
- (9) Photoredox methodologies commonly employ wavelengths between 390 nm and 540 nm due to the widespread availability of inexpensive and safe LEDs in this range. These wavelengths correspond to a maximum energy of 3.2 and 2.3 eV, respectively.
- (10) Arias-Rotondo, D. M.; McCusker, J. K. The Photophysics of Photoredox Catalysis: A Roadmap for Catalyst Design. *Chem. Soc. Rev.* **2016**, *45* (21), 5803–5820.
- (11) Vega-Peñaloza, A.; Mateos, J.; Companyó, X.; Escudero-Casao, M.; Dell'Amico, L. A Rational Approach to Organo-Photocatalysis: Novel Designs and Structure-Property Relationships. *Angew. Chem. Int. Ed.* **2021**, *60*, 1082
- (12) Speckmeier, E.; Fischer, T. G.; Zeitler, K. A Toolbox Approach To Construct Broadly Applicable Metal-Free Catalysts for Photoredox Chemistry: Deliberate Tuning of Redox Potentials and Importance of Halogens in Donor–Acceptor Cyanoarenes. *J. Am. Chem. Soc.* **2018**, *140* (45), 15353–15365.
- (13) Sartor, S. M.; McCarthy, B. G.; Pearson, R. M.; Miyake, G. M.; Damrauer, N. H. Exploiting Charge-Transfer States for Maximizing Intersystem Crossing Yields in Organic Photoredox Catalysts. *J. Am. Chem. Soc.* **2018**, *140* (14), 4778–4781.
- (14) Joshi-Pangu, A.; Lévesque, F.; Roth, H. G.; Oliver, S. F.; Campeau, L.-C.; Nicewicz, D.; DiRocco, D. A. Acridinium-Based Photocatalysts: A Sustainable Option in Photoredox Catalysis. *J. Org. Chem.* **2016**, *81* (16), 7244–7249.
- (15) Lee, Y.; Kwon, M. S. Emerging Organic Photoredox Catalysts for Organic Transformations. *Eur. J. Org. Chem.* **2020**, *38*, 6028–6043.
- (16) Singh, V. K.; Yu, C.; Badgujar, S.; Kim, Y.; Kwon, Y.; Kim, D.; Lee, J.; Akhter, T.; Thangavel, G.; Park, L. S.; Lee, J.; Nandajan, P. C.; Wannemacher, R.; Milián-Medina, B.; Lüer, L.; Kim, K. S.; Gierschner, J.; Kwon, M. S. Highly Efficient Organic Photocatalysts Discovered via a Computer-Aided-Design Strategy for Visible-Light-Driven Atom Transfer Radical Polymerization. *Nature Catalysis* **2018**, *1* (10), 794–804.
- (17) Glaser, F.; Wenger, O. S. Recent Progress in the Development of Transition-Metal Based Photoredox Catalysts. *Coordination Chemistry Reviews* **2020**, *405*, 213129.

- (18) For an example of UV light promoted oxidation of benzene, see: Ohkubo, K.; Kobayashi, T.; Fukuzumi, S. Direct Oxygenation of Benzene to Phenol Using Quinolinium Ions as Homogeneous Photocatalysts. *Angew. Chem.* **2011**, 123 (37), 8811–8814.
- (19) For a recent advance in redox neutral reactions triggered by photocatalytic oxidation of arenes, see: Pistritto, V. A.; Schutzbach-Horton, M. E.; Nicewicz, D. A. Nucleophilic Aromatic Substitution of Unactivated Fluoroarenes Enabled by Organic Photoredox Catalysis. *J. Am. Chem. Soc.* **2020**, 142 (40), 17187–17194.
- (20) Matsubara, R.; Yabuta, T.; Md Idros, U.; Hayashi, M.; Ema, F.; Kobori, Y.; Sakata, K. UVA- and Visible-Light-Mediated Generation of Carbon Radicals from Organochlorides Using Nonmetal Photocatalyst. *J. Org. Chem.* **2018**, 83 (16), 9381–9390.
- (21) Treat, N. J.; Sprafke, H.; Kramer, J. W.; Clark, P. G.; Barton, B. E.; Read de Alaniz, J.; Fors, B. P.; Hawker, C. J. Metal-Free Atom Transfer Radical Polymerization. *J. Am. Chem. Soc.* **2014**, 136 (45), 16096–16101.
- (22) Although not a conventional photoredox catalyst due to its highly oxidizing ground state, DDQ has been employed as an exceptionally potent photooxidant (>3 V vs. SCE). For a recent review, see: Natarajan, P.; König, B. Excited-State 2,3-Dichloro-5,6-Dicyano-1,4-Benzoquinone (DDQ*) Initiated Organic Synthetic Transformations under Visible-Light Irradiation. *Eur. J. Org. Chem.* <https://doi.org/10.1002/ejoc.202100011>.
- (23) For a compilation of potentials of common organic molecules, see: Roth, H.; Romero, N.; Nicewicz, D. Experimental and Calculated Electrochemical Potentials of Common Organic Molecules for Applications to Single-Electron Redox Chemistry. *Synlett* **2016**, 27 (05), 714–723.
- (24) For the seminal example of the conPET strategy, see: Ghosh, I.; Ghosh, T.; Bardagi, J. I.; König, B. Reduction of Aryl Halides by Consecutive Visible Light-Induced Electron Transfer Processes. *Science* **2014**, 346 (6210), 725–728.
- (25) For a recent review of work in conPET, see: Glaser, F.; Kerzig, C.; Wenger, O. S. Multi-Photon Excitation in Photoredox Catalysis: Concepts, Applications, Methods. *Angew. Chem. Int. Ed.* **2020**, 59 (26), 10266–10284.
- (26) Neumeier, M.; Sampedro, D.; Májek, M.; de la Peña O'Shea, V. A.; Jacobi von Wangelin, A.; Pérez-Ruiz, R. Dichromatic Photocatalytic Substitutions of Aryl Halides with a Small Organic Dye. *Chem. Eur. J.* **2018**, 24 (1), 105–108.
- (27) Ghosh, I.; König, B. Chromoselective Photocatalysis: Controlled Bond Activation through Light-Color Regulation of Redox Potentials. *Angewandte Chemie International Edition* **2016**, 55 (27), 7676–7679.
- (28) Bardagi, J. I.; Ghosh, I.; Schmalzbauer, M.; Ghosh, T.; König, B. Anthraquinones as Photoredox Catalysts for the Reductive Activation of Aryl Halides: Anthraquinones as Photoredox Catalysts for the Reductive Activation of Aryl Halides. *Eur. J. Org. Chem.* **2018**, 2018 (1), 34–40.
- (29) Kerzig, C.; Wenger, O. S. Reactivity Control of a Photocatalytic System by Changing the Light Intensity. *Chem. Sci.* **2019**, 10 (48), 11023–11029.
- (30) Connell, T. U.; Fraser, C. L.; Czyz, M. L.; Smith, Z. M.; Hayne, D. J.; Doeven, E. H.; Agugiaro, J.; Wilson, D. J. D.; Adcock, J. L.; Scully, A. D.; Gómez, D. E.; Barnett, N. W.; Polyzos, A.; Francis, P. S. The Tandem Photoredox Catalysis Mechanism of [Ir(Ppy)₂(Dtb-Bpy)]⁺ Enabling Access to Energy Demanding Organic Substrates. *J. Am. Chem. Soc.* **2019**, 141 (44), 17646–17658.

- (31) Naumann, R.; Lehmann, F.; Goetz, M. Micellized Tris(Bipyridine)Ruthenium Catalysts Affording Preparative Amounts of Hydrated Electrons with a Green Light-Emitting Diode. *Chem. Eur. J.* **2018**, *24* (50), 13259–13269.
- (32) Qiao, Y.; Yang, Q.; Schelter, E. J. Photoinduced Miyaura Borylation by a Rare-Earth-Metal Photoreductant: The Hexachloroacetate(III) Anion. *Angewandte Chemie International Edition* **2018**, *57* (34), 10999–11003.
- (33) Majek, M.; Faltermeier, U.; Dick, B.; Pérez-Ruiz, R.; Jacobi von Wangelin, A. Application of Visible-to-UV Photon Upconversion to Photoredox Catalysis: The Activation of Aryl Bromides. *Chem. Eur. J.* **2015**, *21* (44), 15496–15501.
- (34) Cole, J. P.; Chen, D.-F.; Kudisch, M.; Pearson, R. M.; Lim, C.-H.; Miyake, G. M. Organocatalyzed Birch Reduction Driven by Visible Light. *J. Am. Chem. Soc.* **2020**, *142* (31), 13573–13581.
- (35) MacKenzie, I. A.; Wang, L.; Onuska, N. P. R.; Williams, O. F.; Begam, K.; Moran, A. M.; Dunietz, B. D.; Nicewicz, D. A. Discovery and Characterization of an Acridine Radical Photoreductant. *Nature* **2020**, *580* (7801), 76–80.
- (36) While trialkyl amines are commonly employed reductants in both conventional and conPET photoredox processes, the oxidants employed in photoredox catalysis are typically incorporated into the final product and examples of bystander terminal oxidants in photoredox catalysis are less common.
- (37) Margrey, K. A.; Nicewicz, D. A. A General Approach to Catalytic Alkene Anti-Markovnikov Hydrofunctionalization Reactions via Acridinium Photoredox Catalysis. *Acc. Chem. Res.* **2016**, *49* (9), 1997–2006.
- (38) Prier, C. K.; MacMillan, D. W. C. Amine α -Heteroarylation via Photoredox Catalysis: A Homolytic Aromatic Substitution Pathway. *Chem. Sci.* **2014**, *5* (11), 4173–4178.
- (39) Terrett, J. A.; Clift, M. D.; MacMillan, D. W. C. Direct β -Alkylation of Aldehydes via Photoredox Organocatalysis. *J. Am. Chem. Soc.* **2014**, *136* (19), 6858–6861.
- (40) Zuo, Z.; Ahneman, D. T.; Chu, L.; Terrett, J. A.; Doyle, A. G.; MacMillan, D. W. C. Merging Photoredox with Nickel Catalysis: Coupling of α -Carboxyl sp^3 -Carbons with Aryl Halides. *Science* **2014**, *345* (6195), 437–440.
- (41) Romero, N. A.; Margrey, K. A.; Tay, N. E.; Nicewicz, D. A. Site-Selective Arene C-H Amination via Photoredox Catalysis. *Science* **2015**, *349* (6254), 1326–1330.
- (42) Niu, L.; Yi, H.; Wang, S.; Liu, T.; Liu, J.; Lei, A. Photo-Induced Oxidant-Free Oxidative C–H/N–H Cross-Coupling between Arenes and Azoles. *Nature Communications* **2017**, *8* (1), 14226.
- (43) Nicewicz and co-workers recently illustrated that acridinium photooxidants can be transformed into potent photoreductants through photoreduction to the acridine radical. However, it remains unclear whether this inversion of available redox potentials—from a photooxidant to a photoreductant—is a unique feature of acridinium photocatalysts or whether the behavior of other photocatalysts could be similarly manipulated by careful selection of reaction conditions.
- (44) Du, Y.; Pearson, R. M.; Lim, C.-H.; Sartor, S. M.; Ryan, M. D.; Yang, H.; Damrauer, N. H.; Miyake, G. M. Strongly Reducing, Visible-Light Organic Photoredox Catalysts as Sustainable Alternatives to Precious Metals. *Chem. Eur. J.* **2017**, *23* (46), 10962–10968.

- (45) Christensen, J. A.; Phelan, B. T.; Chaudhuri, S.; Acharya, A.; Batista, V. S.; Wasielewski, M. R. Phenothiazine Radical Cation Excited States as Super-Oxidants for Energy-Demanding Reactions. *J. Am. Chem. Soc.* **2018**, *140* (15), 5290–5299.
- (46) Rombach, D.; Wagenknecht, H.-A. Photoredox Catalytic Activation of Sulfur Hexafluoride for Pentafluorosulfanylation of α -Methyl- and α -Phenyl Styrene. *ChemCatChem* **2018**, *10* (14), 2955–2961.
- (47) Rombach, D.; Wagenknecht, H.-A. Photoredox Catalytic α -Alkoxy-pentafluorosulfanylation of α -Methyl- and α -Phenylstyrene Using SF₆. *Angewandte Chemie International Edition* **2020**, *59* (1), 300–303.
- (48) Chan, C.-M.; Chow, Y.-C.; Yu, W.-Y. Recent Advances in Photocatalytic C–N Bond Coupling Reactions. *Synthesis* **2020**, *52*, (20), 2899–2921.
- (49) For examples of DDQ excitation promote the oxidation of benzene, see: Ohkubo, K.; Fujimoto, A.; Fukuzumi, S. Visible-Light-Induced Oxygenation of Benzene by the Triplet Excited State of 2,3-Dichloro-5,6-Dicyano- *p* -Benzoquinone. *J. Am. Chem. Soc.* **2013**, *135* (14), 5368–5371.
- (50) Das, S.; Natarajan, P.; König, B. Teaching Old Compounds New Tricks: DDQ-Photocatalyzed C–H Amination of Arenes with Carbamates, Urea, and N-Heterocycles. *Chemistry – A European Journal* **2017**, *23* (72), 18161–18165.
- (51) Huang, H.; Strater, Z. M.; Rauch, M.; Shee, J.; Sisto, T. J.; Nuckolls, C.; Lambert, T. H. Electrophotocatalysis with a Trisaminocyclopropenium Radical Dication. *Angewandte Chemie International Edition* **2019**, *58* (38), 13318–13322.
- (52) During the review of this manuscript, a second electrophotocatalytic strategy to accomplish this reaction was reported by another group, see: Wu, S.; Žurauskas, J.; Domański, M.; Hitzfeld, P. S.; Butera, V.; Scott, D. J.; Rehbein, J.; Kumar, A.; Thyraug, E.; Hauer, J.; Barham, J. P. Hole-Mediated Photoredox Catalysis: Tris(*p*-Substituted)Biarylammonium Radical Cations as Tunable, Precomplexing and Potent Photooxidants. *Org. Chem. Front.* **2021**, 10.1039.D0QO01609H. <https://doi.org/10.1039/D0QO01609H>.
- (53) Photoanodes have also been used to promote the oxidative coupling of pyrazoles and arenes; however, this approach has an analogous scope to conventional photoredox catalysts and examples are limited to electron-rich systems. For an example, see: Zhang, L.; Liardet, L.; Luo, J.; Ren, D.; Grätzel, M.; Hu, X. Photoelectrocatalytic Arene C–H Amination. *Nat. Catal.* **2019**, *2* (4), 366–373.
- (54) Wang, F.; Stahl, S. S. Merging Photochemistry with Electrochemistry: Functional-Group Tolerant Electrochemical Amination of C(Sp³)–H Bonds. *Angewandte Chemie International Edition* **2019**, *58* (19), 6385–6390.
- (55) Yan, H.; Hou, Z.-W.; Xu, H.-C. Photoelectrochemical C–H Alkylation of Heteroarenes with Organotrifluoroborates. *Angewandte Chemie International Edition* **2019**, *58* (14), 4592–4595.
- (56) Kim, H.; Kim, H.; Lambert, T. H.; Lin, S. Reductive Electrophotocatalysis: Merging Electricity and Light To Achieve Extreme Reduction Potentials. *J. Am. Chem. Soc.* **2020**, *142* (5), 2087–2092.
- (57) Cowper, N. G. W.; Chernowsky, C. P.; Williams, O. P.; Wickens, Z. K. Potent Reductants via Electron-Primed Photoredox Catalysis: Unlocking Aryl Chlorides for Radical Coupling. *J. Am. Chem. Soc.* **2020**, *142* (5), 2093–2099.

- (58) Costentin, C.; Fortage, J.; Collomb, M.-N. Electrophotocatalysis: Cyclic Voltammetry as an Analytical Tool. *J. Phys. Chem. Lett.* **2020**, *11* (15), 6097–6104.
- (59) Zhang, W.; Carpenter, K. L.; Lin, S. Electrochemistry Broadens the Scope of Flavin Photocatalysis: Photoelectrocatalytic Oxidation of Unactivated Alcohols. *Angewandte Chemie International Edition* **2020**, *59* (1), 409–417.
- (60) Shen, T.; Lambert, T. H. Electrophotocatalytic Diamination of Vicinal C–H Bonds. *Science* **2021**, *371* (6529), 620–626.
- (61) Capaldo, L.; Quadri, L. L.; Ravelli, D. Merging Photocatalysis with Electrochemistry: The Dawn of a New Alliance in Organic Synthesis. *Angew. Chem., Int. Ed.* **2019**, *58* (49), 17508–17510.
- (62) Liu, J.; Lu, L.; Wood, D.; Lin, S. New Redox Strategies in Organic Synthesis by Means of Electrochemistry and Photochemistry. *ACS Cent. Sci.* **2020**, *6* (8), 1317–1340.
- (63) Barham, J. P.; König, B. Synthetic Photoelectrochemistry. *Angewandte Chemie International Edition* **2020**, *59* (29), 11732–11747.
- (64) Kingston, C.; Palkowitz, M. D.; Takahira, Y.; Vantourout, J. C.; Peters, B. K.; Kawamata, Y.; Baran, P. S. A Survival Guide for the “Electro-Curious.” *Acc. Chem. Res.* **2020**, *53* (1), 72–83.
- (65) Pearson, R. M.; Lim, C.-H.; McCarthy, B. G.; Musgrave, C. B.; Miyake, G. M. Organocatalyzed Atom Transfer Radical Polymerization Using *N*-Aryl Phenoxazines as Photoredox Catalysts. *J. Am. Chem. Soc.* **2016**, *138* (35), 11399–11407.
- (66) Theriot, J. C.; Lim, C.-H.; Yang, H.; Ryan, M. D.; Musgrave, C. B.; Miyake, G. M. Organocatalyzed Atom Transfer Radical Polymerization Driven by Visible Light. *Science* **2016**, *352* (6289), 1082–1086.
- (67) Merkel, P. B.; Luo, P.; Dinnocenzo, J. P.; Farid, S. Accurate Oxidation Potentials of Benzene and Biphenyl Derivatives via Electron-Transfer Equilibria and Transient Kinetics. *J. Org. Chem.* **2009**, *74* (15), 5163–5173.
- (68) Connelly, N. G.; Geiger, W. E. Chemical Redox Agents for Organometallic Chemistry. *Chem. Rev.* **1996**, *96* (2), 877–910.
- (69) Colomer, I.; Chamberlain, A. E. R.; Haughey, M. B.; Donohoe, T. J. Hexafluoroisopropanol as a Highly Versatile Solvent. *Nature Reviews Chemistry* **2017**, *1* (11), 1–12.
- (70) Shida, N.; Imada, Y.; Nagahara, S.; Okada, Y.; Chiba, K. Interplay of Arene Radical Cations with Anions and Fluorinated Alcohols in Hole Catalysis. *Communications Chemistry* **2019**, *2* (1), 1–8.
- (71) Eberson, L.; Hartshorn, M. P.; Persson, O.; Radner, F. Making Radical Cations Live Longer. *Chem. Commun.* **1996**, No. 18, 2105.
- (72) Discekici, E. H.; Treat, N. J.; Poelma, S. O.; Mattson, K. M.; Hudson, Z. M.; Luo, Y.; Hawker, C. J.; de Alaniz, J. R. A Highly Reducing Metal-Free Photoredox Catalyst: Design and Application in Radical Dehalogenations. *Chem. Commun.* **2015**, *51* (58), 11705–11708.
- (73) On the basis of our working model, superoxide would be formed after O₂ reduction. Other reduced oxygen species could also act as inhibitors for the reaction through either BET or another mechanism.

- (74) For redox potentials of various reactive oxygen species, see: Krumova, K.; Cosa, G. Overview of Reactive Oxygen Species. In *Singlet Oxygen: Applications in Biosciences and Nanomedicines*; Royal Society of Chemistry, **2016**; Chapter 1, Vol. 1, pp 1–21.
- (75) Lu, Y.-C.; Gallant, B. M.; Kwabi, D. G.; Harding, J. R.; Mitchell, R. R.; Whittingham, M. S.; Shao-Horn, Y. Lithium–Oxygen Batteries: Bridging Mechanistic Understanding and Battery Performance. *Energy Environ. Sci.* **2013**, 6 (3), 750.
- (76) Sawyer, D. T.; Chiericato, G.; Angelis, C. T.; Nanni, E. J.; Tsuchiya, T. Effects of Media and Electrode Materials on the Electrochemical Reduction of Dioxigen. *Anal. Chem.* **1982**, 54 (11), 1720–1724.
- (77) For an example of photochemical coupling of benzene and pyrazole in 22% yield, see: ref 50.
- (78) We found that blending MeCN back into the solvent mixture reduced the activity of the system. This change improved the yields for these easier to oxidize substrates. Additionally, *t*-dodecyl mercaptan was employed as a cocatalyst in place of lithium salts; we suspect this cocatalyst could either function similarly by hydrogen atom transfer to superoxide or through an alternative mechanism. See SI for details.
- (79) While benzene possesses an oxidation potential of 2.5 V vs. SCE, *m*-xylene and mesitylene possess oxidation potentials of 2.05 and 2.1 vs. SCE respectively. For further information, see ref 67.
- (80) Typical reaction times were 48–72 h in the electrophotocatalytic approaches reported in ref 51 and ref 52.
- (81) For a recent example using the gas uptake apparatus employed herein, see: Ryan, M. C.; Kim, Y. J.; Gerken, J. B.; Wang, F.; Aristov, M. M.; Martinelli, J. R.; Stahl, S. S. Mechanistic Insights into Copper-Catalyzed Aerobic Oxidative Coupling of N–N Bonds. *Chem. Sci.* **2020**, 11 (4), 1170–1175.
- (82) In principle, O₂ can accept between one and four electrons in oxidative processes, see: Stahl, S. S. Palladium Oxidase Catalysis: Selective Oxidation of Organic Chemicals by Direct Dioxigen-Coupled Turnover. *Angew. Chem. Int. Ed.* **2004**, 43 (26), 3400–3420.
- (83) Adding LiClO₄ could also recover a reaction inhibited by KO₂ (5 mol %) addition. See SI for details.
- (84) While the expected excited state lifetime of the PTH radical cation is <1 ns and likely too short for intermolecular photocatalysis requiring diffusion (based on ref 45), preassociation between the catalyst and the arene may be responsible for photochemical activity. However, preliminary UV-vis data exclude favorable formation of a charge transfer complex (Figure S22–24). Neither endothermic pre-association nor decomposition of PTH to a photocatalyst with a longer excited state lifetime can be excluded. Studies are ongoing into the nature of the active catalytic photooxidant.
- (85) Catalyst decomposition to an active photocatalyst has been suggested as a mechanistic revision in other conPET systems and cannot be excluded here. For an example, see: Marchini, M.; Gualandi, A.; Mengozzi, L.; Franchi, P.; Lucarini, M.; Cozzi, P. G.; Balzani, V.; Ceroni, P. Mechanistic Insights into Two-Photon-Driven Photocatalysis in Organic Synthesis. *Phys. Chem. Chem. Phys.* **2018**, 20 (12), 8071–8076.
- (86) The pK_a of HFIP is 9.3 and the pK_a of H₂O₂ is 11.6.

Chapter 4: Practical and General Alcohol Deoxygenation Protocol

A collaboration with Oliver P. Williams,[†] Alyah F. Chmiel,[†] Myriam Mikhael, Desiree M. Bates, Charles S. Yeung, and Zachary K. Wickens. [†]O.P.W. and A. F. C. contributed equally.

4. 1. Abstract

Herein, we describe a practical protocol for the removal of alcohol functional groups through reductive cleavage of their benzoate ester analogs. This transformation requires a strong single electron transfer (SET) reductant and a means to accelerate slow fragmentation following substrate reduction. To accomplish this, we developed a photocatalytic system that generates a potent reductant from formate salts alongside Brønsted or Lewis acids that promote fragmentation of the reduced intermediate. This deoxygenation procedure is effective across structurally and electronically diverse alcohols and enables a variety of difficult net transformations. This protocol requires no precautions to exclude air or moisture and remains efficient on multigram scale. Finally, the system can be adapted to a one-pot benzoylation-deoxygenation sequence to enable direct alcohol deletion. Mechanistic studies validate that the role of acidic additives is to promote the key C(sp³)–O bond fragmentation step.

4. 2. Introduction

While forging new bonds has been a major focus of synthetic chemistry, selective and efficient covalent bond breaking reactions can be equally valuable synthetic tactics.^[1–7] In particular, development of methods to selectively delete ubiquitous alcohol functional groups from molecules has attracted substantial attention for over half a century (Figure 4.1 A).^[8] Deoxygenation processes are typically deployed in two distinct contexts: (1) removal of oxygen-based functional groups after they enable robust C–C and C–X bond forming reactions (e.g., carbonyl reactivity, Figure 4.1 B)^[9–12] and (2) selective removal of specific oxygen atoms from complex polyoxygenated feedstocks, such as carbohydrates, to access chiral building blocks (Figure 4.1 C).^[13–15] Unfortunately, the current standard protocol to remove alcohols, the Barton-McCombie deoxygenation, relies on stoichiometric trialkyl tin hydride and thiocarbonyl-based activating groups (Figure 4.1 D).^[16] While Barton-McCombie variants designed to reduce or

eliminate trialkyltin reagents have been developed, these approaches remain limited in scope and still require unstable thiocarbonyl activating groups, which can also be difficult to install. As a result, the development of alternative deoxygenation methods continues to be an area of considerable synthetic interest.^[17–35] Specifically, mechanistically distinct polar S_N1 and S_N2 -type substitution processes that exploit silane hydride sources are increasingly favored alternatives.^[36–38] While effective in some cases, these alternative methods suffer the synthetic limitations endemic to standard substitution chemistry; S_N1 requires readily ionizable alcohols and S_N2 proceeds only with unhindered alcohols. Despite the drawbacks of trialkyl tin reagents, the limitations of all alternative methods still regularly force the use of tin-based deoxygenation protocols, from academic settings to large-scale industrial processes.^[39–45] Overall, introduction of a general, nontoxic, and practical method to deoxygenate alcohols would enable broader implementation of alcohol deletion approaches in synthesis.

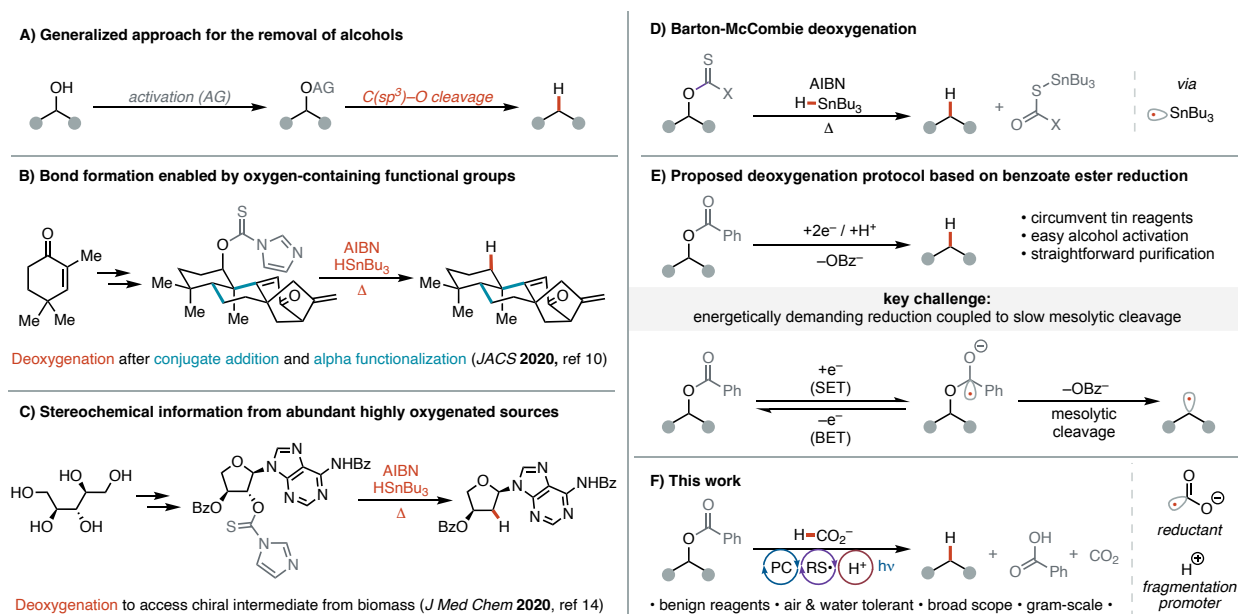


Figure 4.1 **A** Schematic representation of deoxygenation transformations. **B** Representative recent example of using oxygen-based functional groups to build molecular skeletons. **C** Representative recent example of deoxygenation to exploit chiral oxygenated feedstocks to access stereochemically-rich intermediates. **D** Barton-McCombie deoxygenation overview. **E** Proposed deoxygenation strategy based on benzoate ester reduction. **F** Deoxygenation protocol employed in this work. AG = activating group. X = OPh, SME, or imidazole.

We envisioned that a radical deoxygenation approach based around a bench stable activating group that can be installed in a high-fidelity manner would lay the foundation for a general and practical deoxygenation protocol (Figure 4.1 E). Previous work has established that readily accessible benzoylated alcohol derivatives can undergo C(sp³)–O bond cleavage upon single electron reduction.^[46] However, exploiting this reactivity in a synthetic context is challenging because aroyl esters are both difficult to reduce and their radical anion congeners have slow C(sp³)–O bond fragmentation rates. As a consequence, this reductive fragmentation requires potent reductants such as SmI₂,^[47] alkali metals,^[48] stoichiometric UV photosensitizers,^[49] or deeply reducing electrodes,^[50] in combination with elevated temperatures to enable reductive scission. While promoting this process under mild photocatalytic conditions would be an appealing alternative, conventional photoreductants do not possess the requisite reductive potency to promote general alkyl benzoate C(sp³)–O bond fragmentation. Back electron transfer (BET) following substrate reduction is a challenge for all photoredox systems^[51,52] but is expected to be a more significant impediment to productive transformation of substrates with slow mesolytic cleavage steps, such as the targeted aroyl esters. Electron-deficient benzoate esters can be reduced by conventional photoredox catalysts and have been explored in photochemical deoxygenation. However, these procedures are limited to substrates that liberate stabilized alkyl radicals following reduction (e.g. benzhydryl substrates) as a consequence of slow mesolytic cleavage for less activated substrates.^[53–55] Recent work from our group^[56–58] and others^[59–68] has introduced a range of strategies to promote challenging reductions; however, pioneering work employing these new potent reductants in deoxygenation has remained limited to activated benzylic substrates.^{62,65,69} Given the reductive potency of these new systems, we suspect these limitations are, in part, a consequence of the lack of understanding of how mesolytic cleavage steps can be promoted. Herein, we report an operationally simple protocol for formal alcohol deletion that is effective across structurally diverse substrates (primary, secondary, and tertiary

alcohols). This transformation occurs via reductive cleavage of alkyl benzoate esters and hinges on formate salt reductants working in concert with mild acids to trigger C(sp³)–O bond rupture (Figure 4.1 F).

4. 3. Results and Discussion

At the outset of our studies, we outlined a plausible photoinitiated chain reaction for C(sp³)–O bond cleavage using inexpensive formate salts (Figure 4.2 A). In this process, formate plays dual roles as both a potent single electron reductant and hydrogen atom source, releasing only CO₂ as a benign byproduct. The proposed strategy builds on recent reports from Li,^[70] Jui,^[59] and our group^[58,71] that introduced a series of photochemical strategies to generate CO₂^{•–} from formate.^[72] We recognized that CO₂^{•–} is an appropriately matched reductant to reduce benzoate substrates ($E_{1/2}(\text{CO}_2/\text{CO}_2^{\bullet-}) = -2.2 \text{ V vs. SCE}$,^[73] $E_{1/2}(\text{MeOBz}/\text{MeOBz}^{\bullet-}) = -2.2 \text{ V vs. SCE}$).^[46] Furthermore, hydrogen atom transfer (HAT) from formate to an alkyl radical is thermodynamically favorable due to the low bond dissociation energy of the C–H bond of formate.^[74] The HAT event generates CO₂^{•–} as a co-product, propagating the putative chain process. We anticipated loss of CO₂ from the system as a gaseous byproduct would mitigate BET and promote reductive fragmentation.

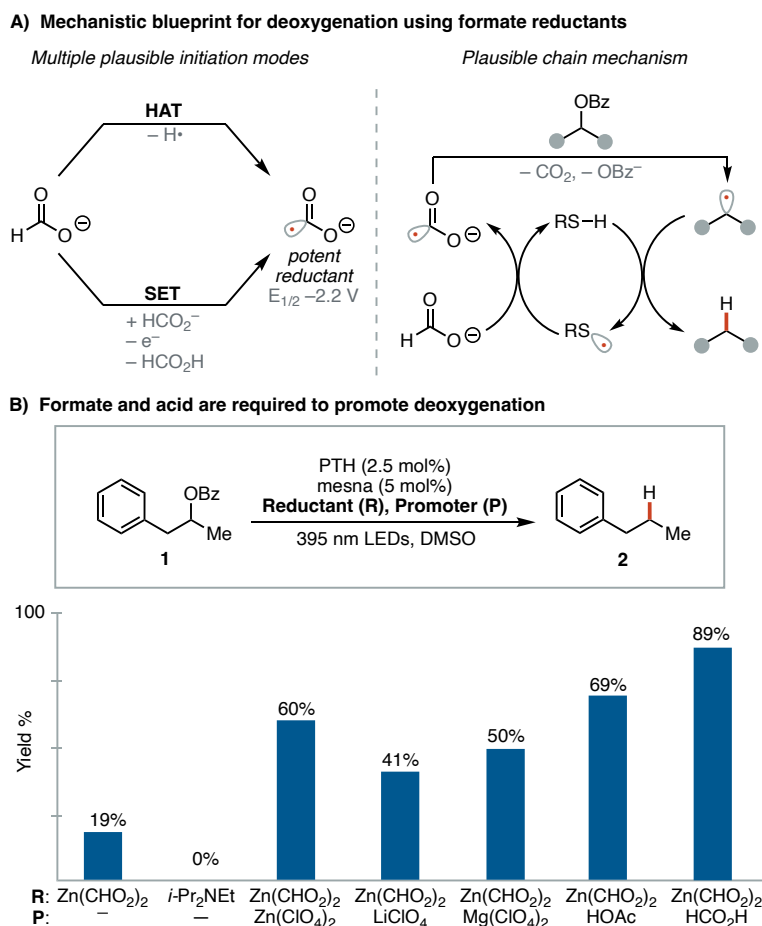


Figure 4.2 **A** Targeted system designed to promote deoxygenation via a $\text{CO}_2^{\bullet-}$ chain reaction. **B** Efficient deoxygenation enabled by formate and acid. PTH = *N*-phenylphenothiazine, mesna = sodium 2-mercaptoethanesulfonate. Reactions run on 0.1 mmol scale in DMSO (0.2 M) for 12 hours under 395 nm irradiation. Calibrated gas chromatography yields.

We commenced our investigation into deoxygenation using an unactivated secondary benzoate ester as the model substrate because such substrates remain difficult for the polar substitution processes that have become dominant Barton–McCombie alternatives. First, we examined a range of strategies to initiate the proposed formate-based $\text{CO}_2^{\bullet-}$ chain in combination with sodium 2-mercaptoethanesulfonate (mesna) as the HAT co-catalyst. We found that several photoinitiation approaches promoted $\text{C}(\text{sp}^3)\text{--O}$ bond cleavage, albeit in modest yields (see SI for details). Notably, our previously disclosed photoreductive system^[58] led to trace yield of the

deoxygenated product, despite the fact that far more thermodynamically difficult to reduce substrates were activated in these previous studies. These observations support our suspicion that this transformation requires not only a sufficiently strong reductant to generate the radical anion but also a means to promote its mesolytic cleavage.^[75] In our initial survey of reaction conditions, our highest yielding result (19%) was observed using the air-tolerant photocatalyst, N-phenylphenothiazine (PTH) alongside zinc formate as a terminal reductant. (Figure 4.2 B).^[76] Consistent with our hypothesis regarding the integral role of formate as a $\text{CO}_2^{\cdot-}$ source, several formate salts enabled reductive cleavage in modest yield whereas no conversion of **1** was observed with a more common terminal reductant for photoredox catalysis, diisopropylethylamine (*i*-Pr₂NEt).^[77] Given that zinc formate provided the highest conversion relative to other formate sources in our initial evaluation of conditions, we questioned whether the zinc cation might be playing a non-innocent role in the reaction.^[78] Specifically, we hypothesized that an acidic reaction component could engage the substrate following reduction and facilitate the C(sp³)–O bond fragmentation step. Following this line of inquiry, we uncovered that addition of either Lewis or Brønsted acids promoted deoxygenation of **1**. Among these, Brønsted acids were particularly effective and use of a buffered system comprised of zinc formate and formic acid furnished high yield of deoxygenated alkane product, **2**.

With robust and operationally simple deoxygenation conditions^[79] in hand, we next explored the scope of this process (Figure 4.3). First, we evaluated the generality of the reaction with respect to alcohol substructure. Simple unactivated secondary and tertiary alcohol derivatives underwent deoxygenation in good yields (**2**, **3**). A tertiary alkyl benzoate ester at a bridgehead position was also efficiently deoxygenated (**4**). Benzylic alcohol underwent rapid deoxygenation (**5**) as well when 4DPAIPN was employed as a photocatalyst.^[80] More challenging primary alcohol derivatives underwent deoxygenation with modest heating (60 °C), despite requisite generation of an unstabilized primary radical (**6**). This method tolerates several classes of saturated

heterocycles including morpholine (**7**), azapane (**8**), tetrahydrofuran (**9**), and lactone (**10**). Deoxygenation of electron deficient and hindered substrate giving product **10** highlights the unique utility of this method; this substructure is not amenable to alternative deoxygenation strategies based on carbocation formation, substitution, or elimination. A variety of unsaturated heterocycles are tolerated in this process, such as furan (**11**), pyrazole (**12**), triazole, (**13**), purine (**14**), and imidazole (**15**). Selective deoxygenation of a benzoate substrate bearing an aryl chloride yielding **15** is of particular note given that previous reports generating CO_2^- from formate have focused on aryl radical generation from aryl halides.^[58,59,70] Unprotected functional groups were found not to interfere with deoxygenation, such as anilides (**16**) and alcohols (**17–19**). A range of carbohydrates and related compounds were each selectively deoxygenated (**20, 21, 22**). Of note, the primary benzoate ester precursor of **22** can be selectively deoxygenated in the presence of acetyl-protected alcohols, even when an acetylated alcohol is present in the activated anomeric position. The deoxygenation of these naturally abundant and stereochemically-rich substrates highlights how this methodology can leverage established carbohydrate protecting group schemes^[81–84] for selective preparation of deoxy sugar analogs. Given that this new deoxygenation method employs a common benzoate protecting group, it can directly tap into well-developed conditions for selective benzylation of polyols^[81,83,85,86] and repurpose them for selective deoxygenation.

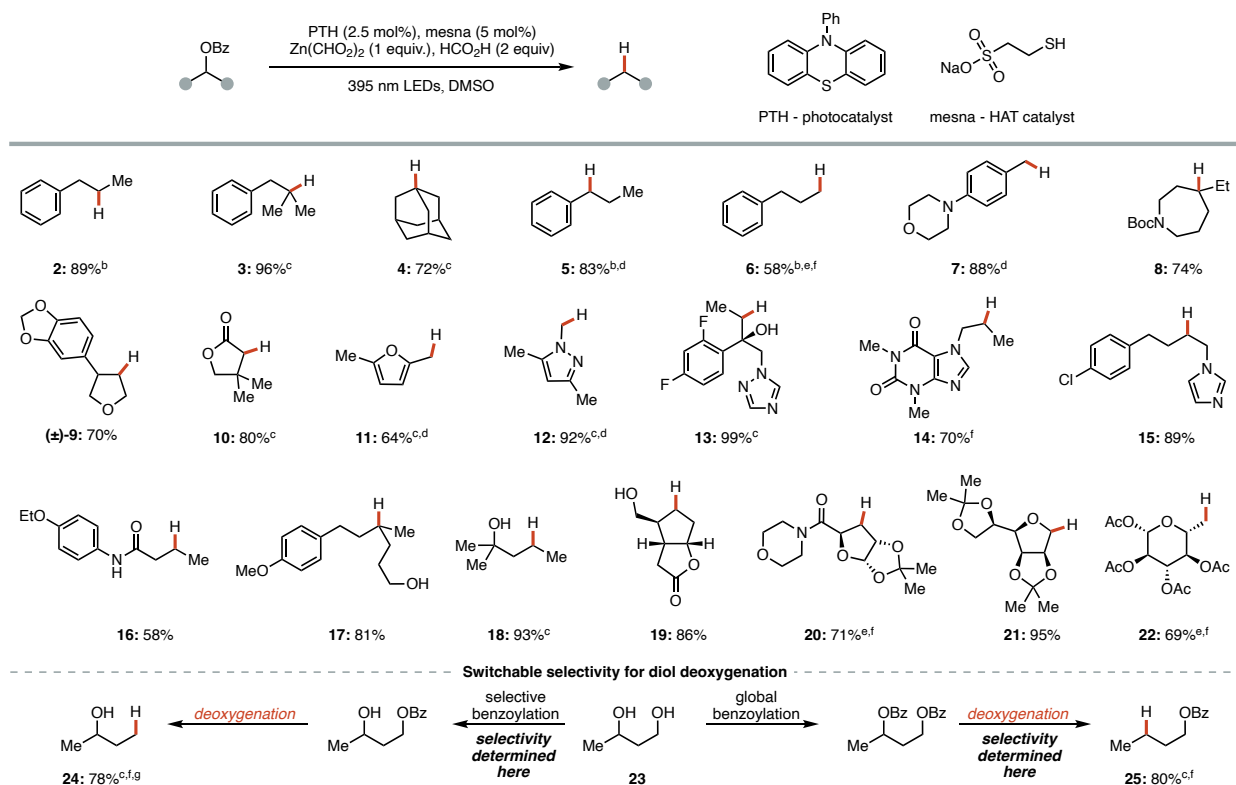


Figure 4.3 Deoxygenation scope and synthetic sequences. Reactions were conducted on 0.4 mmol scale in DMSO (0.2 M) for 24 hours under 395 nm irradiation. Isolated yields unless otherwise noted. ^b GC yield. ^c NMR yield. 4DPAIPN as photocatalyst. See SI for details. ^e 60 °C. ^f 48 hours. ^g 80 °C. Deoxygenation = standard conditions listed in top reaction scheme. See Supporting Information for details.

Since the deoxygenation rates in our initial studies are the inverse of intrinsic alcohol benzoylation rates, we questioned whether switchable site-selective deoxygenation of diols could be feasible. As an illustrative example, we examined site-selective deoxygenation of a model 1,3-diol (**23**). The less hindered primary alcohol can be selectively benzoylated and cleaved (**24**). However, if the 1,3-diol is instead perbenzoylated, the secondary alcohol can be selectively excised due to the faster fragmentation rate (**25**).

We next probed the efficacy of this new protocol to cleave C(sp³)–O bonds in a pair of specific cases that forced industrial process chemists to resort to stoichiometric trialkyl tin hydride on multigram scale.^[44,45] First, we benzoylated and deoxygenated carbohydrate **26** to furnish **27** in

69% overall yield (77% for the deoxygenation step, Figure 4.4). Next, we subjected **28** to trifluoromethyl addition followed by our benzoylation-deoxygenation protocol and obtained 76% overall yield of **29** (97% for the deoxygenation step). Both of these examples illustrate how this new formate-based protocol can circumvent use of toxic trialkyl tin hydrides in industrially relevant contexts. Of note, in their reported synthesis of **29** researchers at Merck explicitly described both challenges with installation of thiocarbonyl activating groups and poor performance of alternative tin-free protocols.

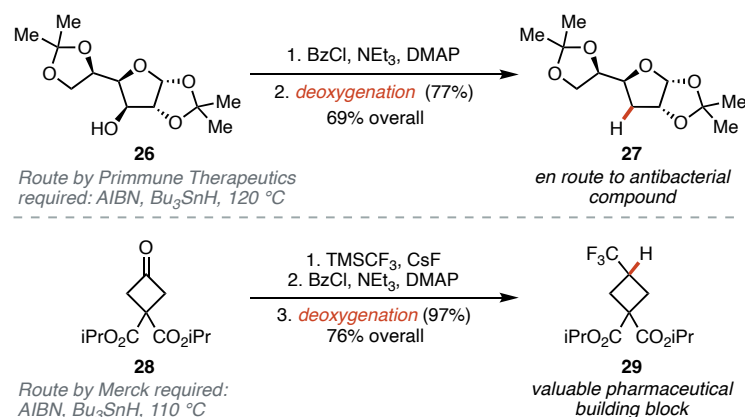


Figure 4.4 Industrially relevant examples. Deoxygenation reactions were conducted on 0.4 mmol scale in DMSO (0.2 M) for 24 hours under 395 nm irradiation. Isolated yields. See Supporting Information for details.

We envisioned that this new deoxygenation protocol would unlock powerful net transformations when combined with the robust and well-studied reactions enabled by oxygen-containing functional groups. First, we explored the feasibility of a Wolff–Kishner alternative that would circumvent the need for hydrazine, strong base, and forcing conditions. By following a simple sodium borohydride reduction with our alcohol deletion protocol, we achieved a mild complement to classic carbonyl deletion approaches in 60% yield over 3 steps converting **30** to **31** (71% yield in the key deoxygenation step, Figure 4.5). Next, we converted carbonyl **32** to the

homologous nitrile **33** via a cyanohydrin intermediate (47% yield over 3 steps). Inspired by Merck's synthesis of **29**,^[44] we suspected that this new deoxygenation protocol would enable efficient transformation of carbonyl groups to trifluoromethyl groups. To validate this synthetic sequence, aldehyde **34** was successfully transformed to trifluoromethylated **35** (92% yield over 3 steps). Strategically coupling this straightforward deoxygenation reaction to other carbonyl chemistry also introduces further unconventional functional group interconversions, such as ester **36** to cyclopropane **37** (67% yield over 3 steps).^[87,88]

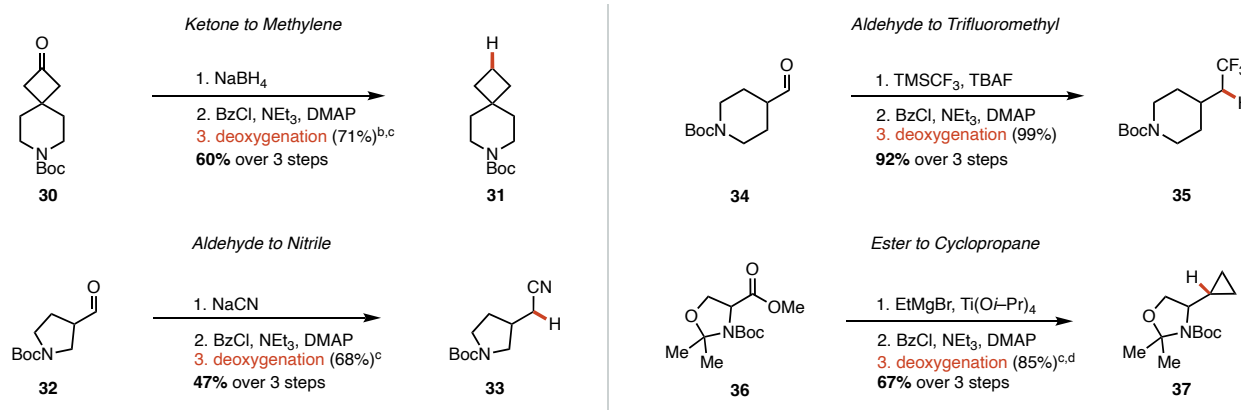


Figure 4.5 Net transformations enabled by deoxygenation Reactions were conducted on 0.4 mmol scale in DMSO (0.2 M) for 24 hours under 395 nm irradiation. Isolated yields unless otherwise noted. ^b 80 °C. ^c 48 hours. ^d 60 °C. Deoxygenation = standard conditions listed in Figure 4.3. See Supporting Information for details.

Next, we assessed the practicality of this new deoxygenation technology. First, we probed the scalability of this process using **38** as a model substrate because the product **29** previously required superstoichiometric tributyl tin hydride to synthesize. Our deoxygenation reaction was performed in batch on 37 mmol-scale with no other modification to the reaction procedure to deliver 9 grams of deoxygenated derivative **29** (Figure 4.6 A). Next, we investigated whether a formal alcohol deoxygenation was feasible by employing a one-pot protocol for benzylation and deoxygenation (Figure 4.6 B). We found that the one pot procedure had a minimal impact on yield

and validated its efficacy across a range of structurally diverse alcohols that we had previously studied from the benzoate (**10**, **12**, **21**, **13**). Of particular note, a representative 1,2 diol was selectively deoxygenated at the less hindered secondary alcohol using this one-pot protocol (**13**). Finally, we recognized that this reaction system employs non-volatile DMSO and is chemically inert in the absence of light. This allows for a solution of all reaction components (photocatalyst, thiol catalyst, zinc formate, and formic acid in DMSO) to be stored for extended periods of time without significant loss of activity (Figure 4.6 C). The pre-made deoxygenation solution can simply be added to substrate and irradiated, allowing for rapid reaction setup.

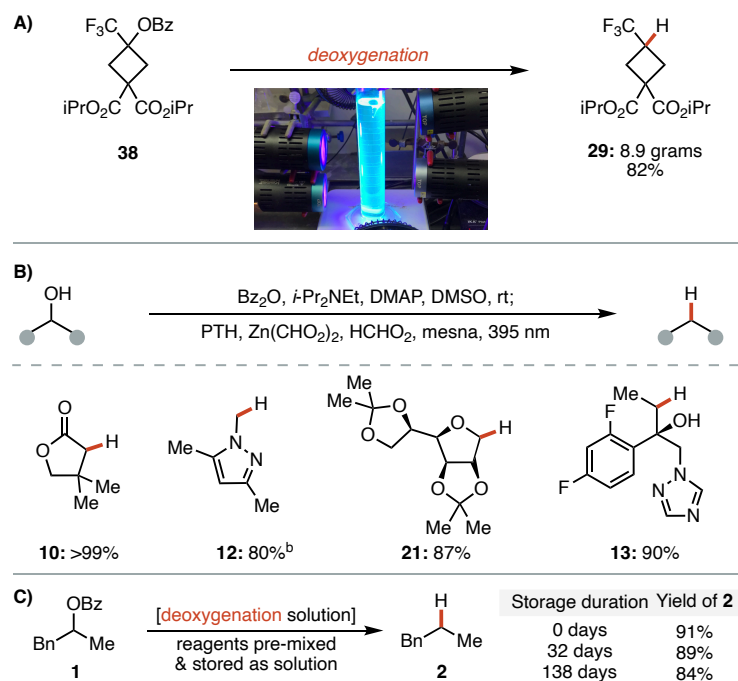


Figure 4.6 A Multi-gram scale deoxygenation. **B** One-pot deoxygenation of alcohols. **C** Reaction components without substrate can be pre-mixed and used after extended storage without activity loss (reaction components = PTH, mesna, formic acid, and zinc formate in DMSO). Deoxygenation = standard conditions from Figure 4.3. See Supporting Information for details.

We next aimed to elucidate the central mechanistic features of this new C(sp³)-O bond cleavage reaction. First, we probed the role of CO₂^{•-} as the SET reductant. If operative, carbon

dioxide would be generated throughout the reaction. By conducting the reaction in a sealed vessel equipped with a pressure transducer, we found that gas evolution occurred continuously throughout the reaction (Figure 4.7 A). The amount of gas produced was equal to the amount of substrate consumed and not to the total amount of formate added. Furthermore, gas chromatography analysis verified that the evolved gas was CO₂ (see SI for details). Next, we probed the intermediacy of an alkyl radical using a benzoate substrate bearing a pendant alkene, **39**. Upon subjecting **39** to deoxygenation conditions, cyclized product **40** was formed in high yield, consistent with the proposed alkyl radical intermediate (Figure 4.7 B). This experiment also validates that the radical species derived from alkyl benzoate substrates can be engaged in C–C bond formation under these conditions and suggests that applications of this new C(sp³)–O bond cleavage strategy will transcend the specific alcohol deletion protocols described herein.

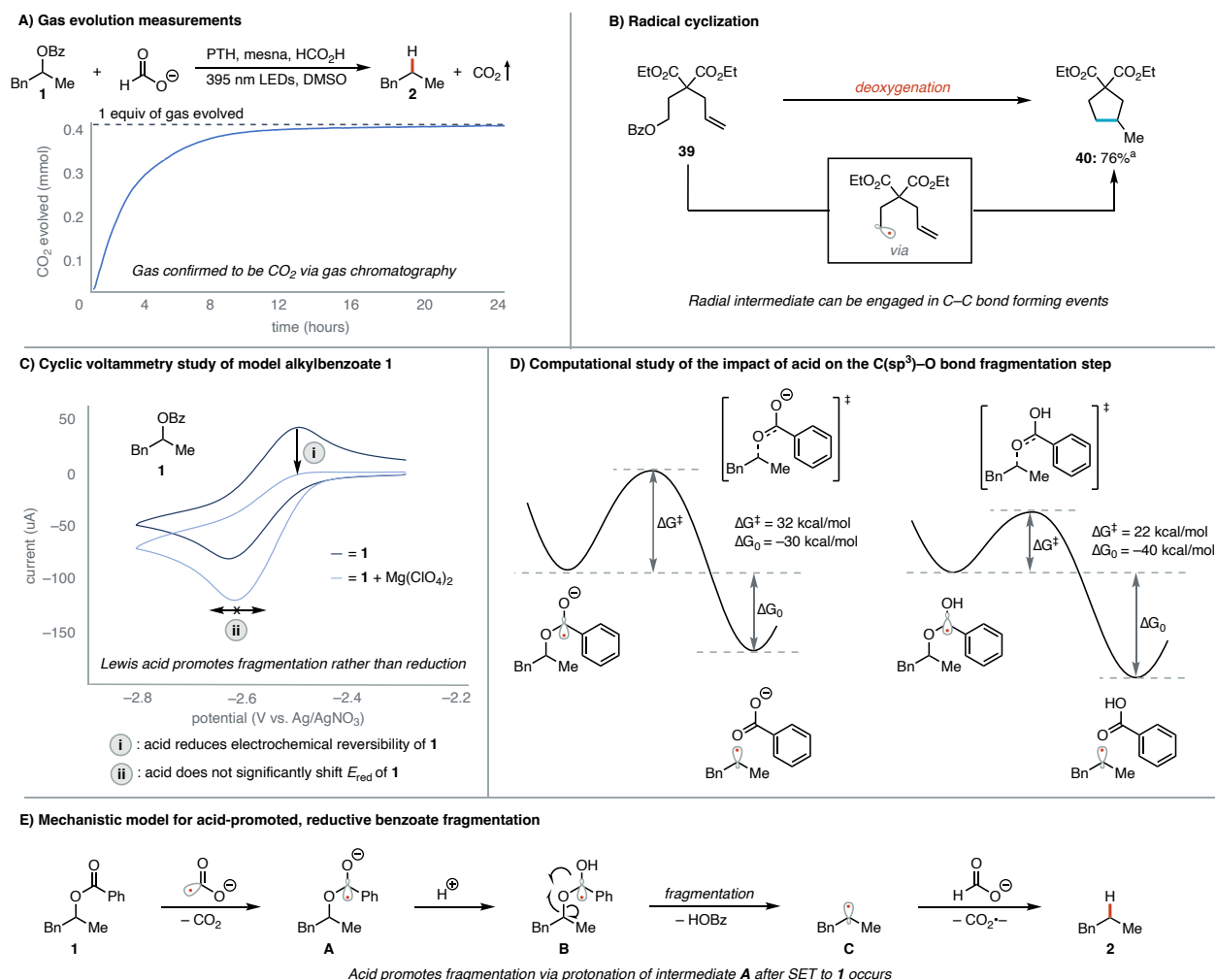


Figure 4.7 **A** Gas evolution measurements throughout standard deoxygenation reaction. **B** Cyclization under deoxygenation conditions consistent with generation of a radical intermediate. Deoxygenation = standard conditions from Figure 4.3. See Supporting Information for details. **C** Cyclic voltammograms of **1** with and without acid. **D** Computational study of the impact of acid on the C(sp³)–O bond fragmentation step. Ab initio calculations were carried out using Gaussian 16 at MP2/6-311+G(2d,p)/PCM(DMSO) level of theory. **E** Plausible mechanism for the acid-promoted, reductive C(sp³)–O bond fragmentation.

With data in hand supporting the proposed fundamental steps of the process, we next turned our attention to the role of acid in promoting deoxygenation. At the outset of our studies, we hypothesized that acid was promoting the C(sp³)–O bond fragmentation step that follows SET reduction of the substrate. However, we recognized that an alternative role of the acid could be facilitating SET reduction by adjusting benzoate ester **1** reduction potential. We probed these

distinct roles using cyclic voltammetry (CV, Figure 4.7 C). We found that addition of a Lewis acid to a solution of **1** resulted in a clear decrease in the electrochemical reversibility of benzoate ester **1** reduction, but did not significantly change the reduction potential.^[89] These data are consistent with acid facilitating fragmentation rather than single electron reduction and suggest that the benzoate radical anion intermediate engages with the acid, rather than the neutral benzoate substrate (see SI for details). While the analogous study using formic acid resulted in the same trend but with more complex behavior,^[90] we conducted a parallel computational analysis of the fragmentation step in the presence and absence of a proton.⁹¹ Consistent with the CV model study, we found the ΔG^\ddagger of fragmentation to be 10 kcal/mol lower for the protonated neutral radical compared to that of the unperturbed radical anion (Figure 4.7 D). Furthermore, the fragmentation elementary step itself was found to be 10 kcal/mol more thermodynamically favorable for the protonated pathway over the radical anion pathway.

These mechanistic data, taken together, are consistent with the following working mechanistic model for the elementary steps involved in the deoxygenation process following photochemical initiation (Figure 4.7 E). First, $\text{CO}_2^{\cdot-}$, derived from formate, reduces benzoate substrate **1** to generate radical anion intermediate **A** and CO_2 . Species **A** is then protonated by formic acid^[92] to form intermediate **B**. Subsequently, **B** then undergoes $\text{C}(\text{sp}^3)\text{--O}$ bond fragmentation to generate alkyl radical intermediate **C** and benzoic acid. This alkyl radical intermediate next formally abstracts a hydrogen atom from formate, a process we suspect is thiol-catalyzed,⁹³ to liberate the desired product **2** and an equivalent of $\text{CO}_2^{\cdot-}$ to propagate a chain reaction.

4. 4. Conclusions

Overall, we have developed an operationally simple deoxygenation protocol that proceeds under mild conditions, employs relatively non-toxic reagents, relies on commercially available catalysts, exhibits a broad scope, and is effective on decagram scale. This approach proceeds

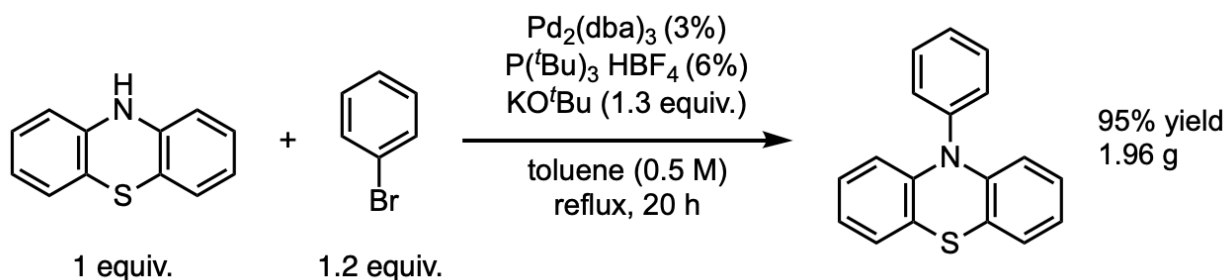
through reductive cleavage of readily accessible benzoate esters and produces only benzoic acid and CO₂ as easily purged byproducts. We illustrated several synthetic sequences that couple classic carbonyl chemistry with this new deoxygenation reaction to enable otherwise difficult net transformations of value in medicinal chemistry and beyond. Mechanistic studies are consistent with the proposal that this new photoinitiated process relies on CO₂^{•-} derived from formate salts to generate key radical intermediates. Electrochemical and computational studies support that the role of the acidic additive is to promote C(sp³)–O bond fragmentation. We anticipate this deoxygenation protocol will serve as a useful strategic tool for synthetic chemistry. More broadly, this study presents a roadmap to develop reductive bond cleavage reactions by coupling potent reductants to fragmentation promoters.

4. 5. Experimental

Unless otherwise noted, reactions were performed under air with anhydrous DMSO. Crude mixtures were evaluated by thin-layer chromatography using EMD/Merck silica gel 60 F254 pre-coated plates (0.25 mm) and were visualized by UV, CAM, p- anisaldehyde, or KMnO₄ staining. Flash chromatography was performed with a Biotage Isolera One automated chromatography system with re-packed silica columns (technical grade silica, pore size 60 Å, 230-400 mesh particle size, 40-63 particle size). Purified materials were dried *in vacuo* (0.050 Torr) to remove trace solvent. ¹H, ¹³C, ¹⁹F spectra were taken using a Bruker Avance-400 with a BBFO Probe or a Bruker Avance-500 with a DCH Cryoprobe. NMR data are reported relative to residual CHCl₃ (¹H, δ = 7.26 ppm), CDCl₃ (¹³C, δ = 77.16 ppm). Data for ¹H NMR spectra are reported as follows: chemical shift (δ ppm) (multiplicity, coupling constant (Hz), integration). Multiplicity and qualifier abbreviations are as follows: s = singlet, d = doublet, t = triplet, q = quartet, m = multiplet, br = broad. GC traces were taken on an Agilent 7890A GC with dual DB-5 columns (20 m × 180 μm × 0.18 μm), dual FID detectors, and hydrogen as the carrier gas.

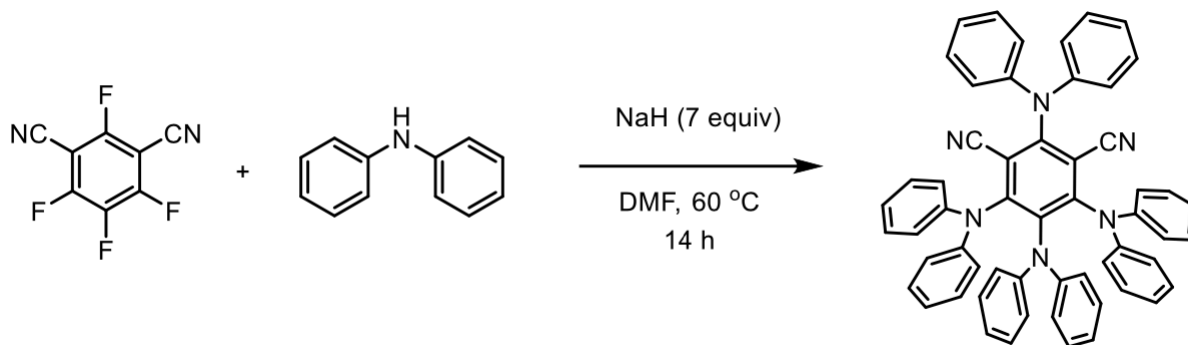
4. 5. 2. Preparation of Catalysts and Starting Materials

10-phenyl-10H-phenothiazine (**PTH**)

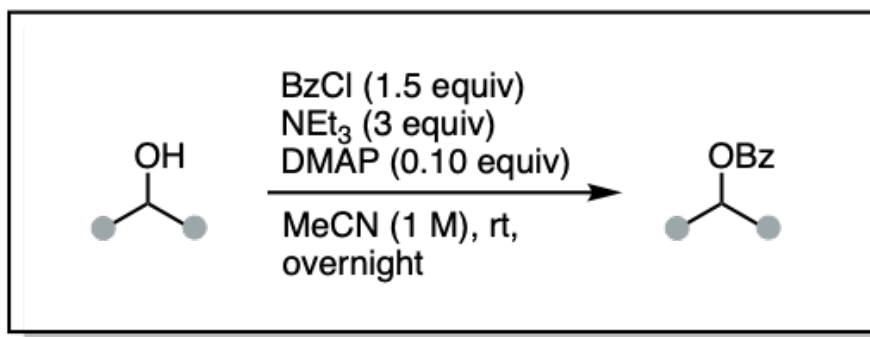


10H-phenothiazine (1.49 g, 1 Eq, 7.50 mmol) was dissolved in anhydrous toluene (14 mL). Bromobenzene (1.44 g, 964 μL , 1.22 Eq, 9.15 mmol), potassium tert-butoxide (1.09 g, 1.29 Eq, 9.67 mmol) and tri-tert-butylphosphonium tetrafluoroborate (131 mg, 0.06 Eq, 450 μmol) were added, followed by bis(dibenzylideneacetone)palladium (129 mg, 0.03 Eq, 225 μmol). The reaction mixture was degassed using three freeze-pump-thaw cycles and finally stirred under reflux for 20 h. After cooling to room temperature, the reaction mixture was filtered. 200 mL EtOAc and 100 mL water were added to the reaction mixture. After phase separation, the aqueous phase was extracted additionally with 3 \times 200 mL EtOAc. The combined organic phase was washed with sodium chloride (sat. aq.). The combined organic phases were dried over sodium sulfate. The solvent was evaporated and the crude product purified by column chromatography to provide a white solid (1.96 g, 95% yield). $^1\text{H NMR}$ (400 MHz, CDCl_3) δ 7.31 – 7.23 (m, 4H), 7.14 – 6.97 (m, 14H), 6.95 – 6.83 (m, 8H), 6.73 – 6.65 (m, 10H), 6.59 – 6.51 (m, 4H), consistent with reported spectrum (Beilstein J. Org. Chem. 2019, 15, 52–59).

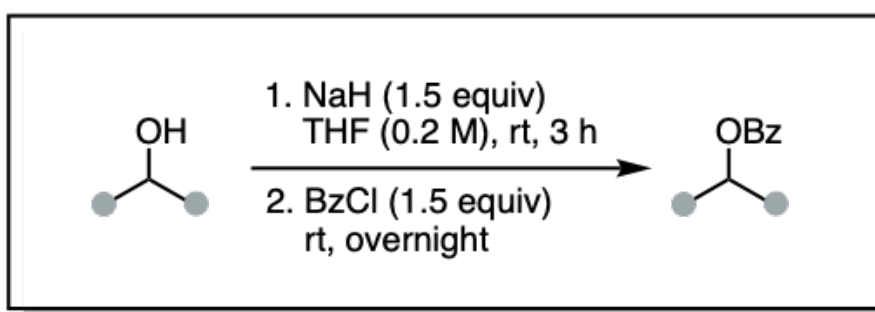
2,4,5,6-tetrakis(diphenylamino)isophthalonitrile (**4DPAIPN**)



To a flame-dried flask under N₂, NaH (60% dispersion, 3.0 g, 75 mmol, 7 equiv) was added and evacuated then backfilled with N₂ three times. THF (100 mL) was added to the flask followed by diphenylamine (8.5 g, 50 mmol, 5 equiv) in THF (25 mL). The diphenylamine solution was slowly added to the flask then heated to 60 °C and stirred for 1 hour. 2,4,5,6-tetrafluoroisophthalonitrile (2.0 g, 10 mmol, 1 equiv) in THF (25 mL) was slowly added to the reaction mixture. The solution was then cooled and stirred at 40 °C overnight. After cooling the reaction to room temperature, excess NaH was quenched with isopropanol. Water (200 mL) was then added to precipitate the crude product. The precipitate was filtered then washed with excess water and dried in vacuo. The crude product dissolved in DCM then filtered through a silica plug and recrystallized from DCM hexanes to provide pure product as a yellow solid (5.0 g, 6.2 mmol, 62%). ¹H NMR (400 MHz, CDCl₃) δ 7.31 – 7.23 (m, 4H), 7.14 – 6.97 (m, 14H), 6.95 – 6.83 (m, 8H), 6.73 – 6.65 (m, 10H), 6.59 – 6.51 (m, 4H), consistent with reported spectrum (Angew. Chem. Int. Ed. 2019, 131, 8266-8270).

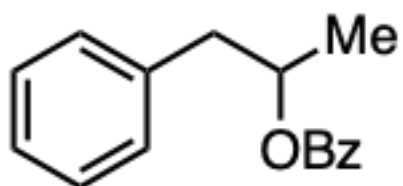


General Procedure A for benzoylation: Alcohol substrate was dissolved in acetonitrile (1 M). Triethylamine (3 equiv) and 4-dimethylaminopyridine (10 mol %) were added to the reaction mixture. Finally, benzoyl chloride (1.5 equiv) was added to the reaction dropwise. Reactions were run overnight at room temperature. After reaction completion, reactions were quenched with sodium bicarbonate (sat. aq.) then extracted with ethyl acetate or diethyl ether. The organic layer was washed with sodium chloride (sat. aq.) then dried over sodium sulfate, filtered, and concentrated in vacuo. The crude mixtures were purified via flash chromatography.

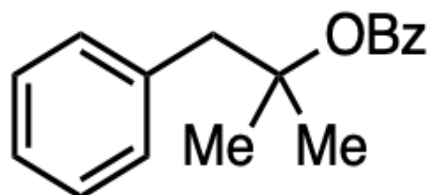


General Procedure B for benzoylation: To a flame-dried flask under nitrogen atmosphere, sodium hydride (1.5 equiv) was added then flushed with argon. Sodium hydride was rinsed with hexanes three times then flushed with nitrogen until dry. Sodium hydride was suspended in THF (0.2 M). Then the alcohol substrate was added dropwise and stirred at room temperature for 3 hours. Then benzoyl chloride (1.5 equiv) was added to the reaction mixture. The reactions were

run overnight at room temperature. After reaction completion, reactions were quenched with sodium bicarbonate (sat. aq.) then extracted with ethyl acetate or diethyl ether. The organic layer was washed with sodium chloride (sat. aq.) then dried over sodium sulfate, filtered, and concentrated in vacuo. The crude mixtures were purified via flash chromatography.

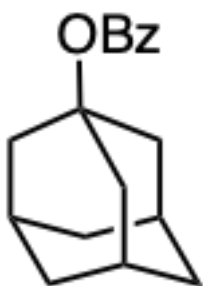


1-phenylpropan-2-yl benzoate (1): Compound was synthesized from 1-phenyl-2-propanol according to General Procedure A on 13.00 mmol scale. 3.03 g and 97% yield was obtained as a colorless oil. ¹H NMR (400 MHz, CDCl₃) δ 8.06 – 7.99 (m, 2H), 7.59 – 7.50 (m, 1H), 7.43 (dd, J = 8.4, 7.0 Hz, 2H), 7.34 – 7.17 (m, 5H), 5.37 (h, J = 6.3 Hz, 1H), 3.09 (dd, J = 13.6, 6.5 Hz, 1H), 2.91 (dd, J = 13.7, 6.5 Hz, 1H), 1.35 (d, J = 6.2 Hz, 3H). Spectrum in accordance with literature: Org. Biomol. Chem., **2018**, 16, 8467-8471.

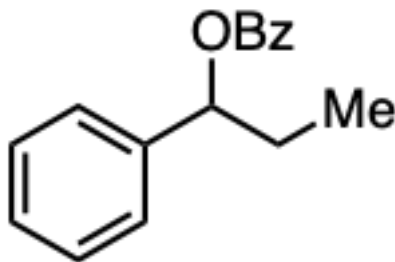


2-methyl-1-phenylpropan-2-yl benzoate: Compound was synthesized from 2-methyl-1-phenyl-2-propanol on a 2.00 mmol scale. To a flame-dried flask under nitrogen atmosphere, alcohol was dissolved in THF (0.2 M) and cooled to 0 °C. n-Butyllithium (2 M in hexanes) was added slowly. Then benzoyl chloride (1.1 equiv) was added to the reaction mixture slowly. After completion, the

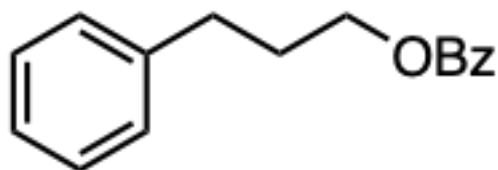
reaction was quenched with ammonium chloride (sat. aq.) then extracted with ethyl acetate. The organic layer was washed with sodium chloride (sat. aq.) then dried over sodium sulfate, filtered, and concentrated in vacuo. The crude mixtures were purified via flash chromatography. The reaction was let come to room temperature overnight. 414 mg and 81% yield was obtained as an oil. **¹H NMR** (500 MHz, CDCl₃) δ 8.01 – 7.95 (m, 2H), 7.57 – 7.50 (m, 1H), 7.42 (t, J = 7.7 Hz, 2H), 7.31 – 7.20 (m, 5H), 3.23 (s, 2H), 1.61 (s, 6H). Spectrum in accordance with literature: J. Chem. Soc., Perkin Trans. 1, **1993**, 2999-3005



adamantan-1-yl benzoate: Compound was synthesized from adamantane-1-ol according to General Procedure B on 0.80 mmol scale. 186 mg, 89% yield was obtained as a white solid. **¹H NMR** (400 MHz, CDCl₃) δ 8.28 – 7.89 (m, 2H), 7.69 – 7.45 (m, 1H), 7.41 (dd, J = 8.4, 7.0 Hz, 2H), 2.47 – 2.14 (m, 9H), 1.84 – 1.63 (m, 6H). Spectrum in accordance with literature: Synlett **2020**; 31(07): 730-736.

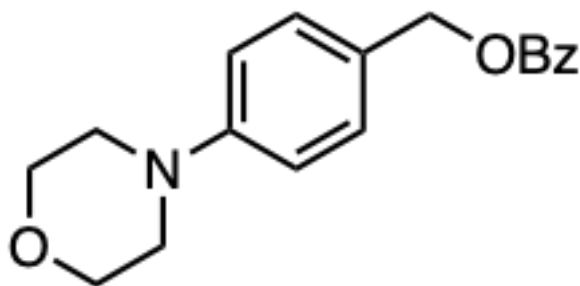


1-phenylpropyl benzoate: Compound was synthesized according to General Procedure A on a 4.00 mmol scale. 951 mg (99% yield) was obtained as an oil. $^1\text{H NMR}$ (400 MHz, CDCl_3) δ 8.13 – 8.06 (m, 2H), 7.61 – 7.52 (m, 1H), 7.49 – 7.39 (m, 4H), 7.39 – 7.32 (m, 2H), 7.32 – 7.26 (m, 1H), 5.93 (dd, J = 7.4, 6.2 Hz, 1H), 2.08 (dt, J = 13.8, 7.3 Hz, 1H), 2.02 – 1.89 (m, 1H), 0.97 (t, J = 7.4 Hz, 3H).. Spectrum in accordance with literature: Chem. Commun., **2020**, 56, 8143-8146.



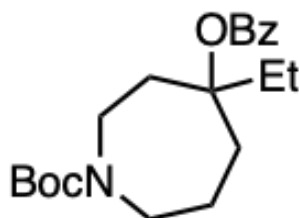
3-phenylpropyl benzoate: Compound was synthesized from 3-phenyl-1-propanol according to General Procedure A on a 4.00 mmol scale. 945 mg, 98% yield was obtained as a colorless oil.

$^1\text{H NMR}$ (400 MHz, CDCl_3) δ 8.08 – 8.01 (m, 2H), 7.61 – 7.52 (m, 1H), 7.45 (dd, J = 8.4, 7.0 Hz, 2H), 7.35 – 7.26 (m, 2H), 7.25 – 7.16 (m, 3H), 4.35 (t, J = 6.5 Hz, 2H), 2.80 (dd, J = 8.5, 6.8 Hz, 2H), 2.17 – 2.06 (m, 2H). Spectrum in accordance with literature: Org. Lett. **2015**, 17, 21, 5172–5175.

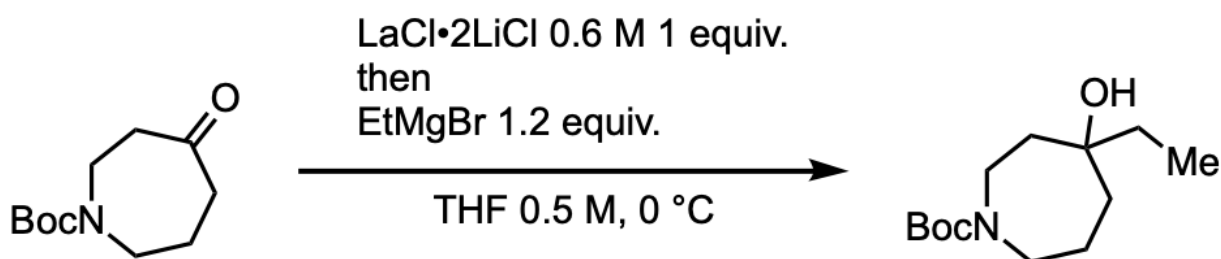


4-morpholinobenzyl benzoate: Compound was synthesized according to General Procedure A on a 3.00 mmol scale. 844 mg (95% yield) was obtained as an off-white crystalline solid. $^1\text{H NMR}$

(500 MHz, CDCl₃) δ 8.12 – 7.86 (m, 2H), 7.65 – 7.49 (m, 1H), 7.49 – 7.32 (m, 4H), 6.98 – 6.86 (m, 2H), 5.29 (s, 2H), 4.09 – 3.75 (m, 4H), 3.38 – 2.95 (m, 4H). ¹³C NMR (126 MHz, CDCl₃) δ 166.57, 151.32, 132.91, 130.36, 129.86, 129.68, 128.32, 127.22, 115.46, 66.87, 66.66, 49.11. **HRMS** (ESI⁺) Calc: [M+H]⁺ for C₁₈H₁₉NO₃ = 298.1438; measured 298.1434 = 1.3 ppm difference.

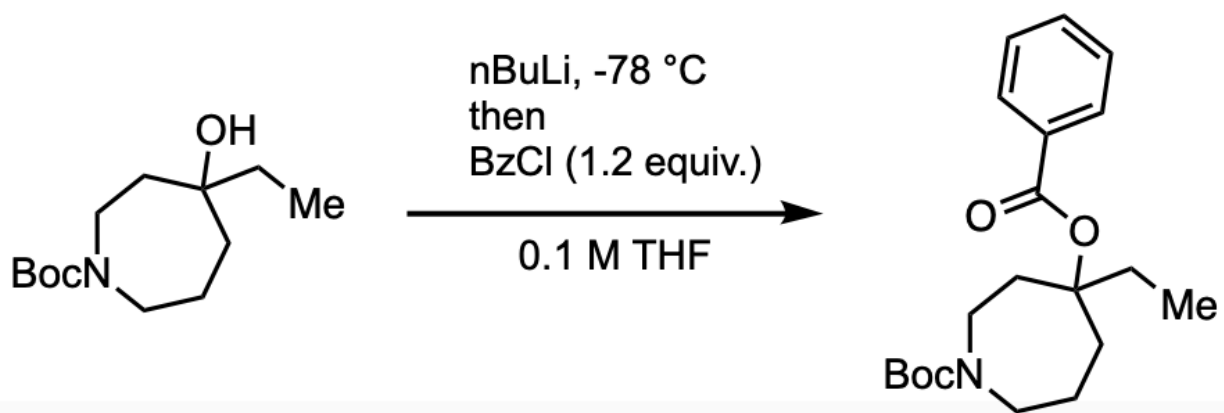


tert-butyl 4-(benzyloxy)-4-ethylazepane-1-carboxylate: Compound was synthesized via Grignard addition (method reported by Knochel, ACIE, **2006**, 45, 497–500) into a ketone followed by benzoylation.

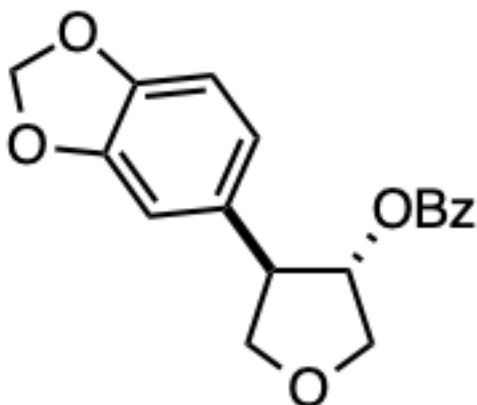


In a flame-dried, nitrogen-flushed flask equipped with a septum and a magnetic stirring bar was added LaCl₃·2LiCl in THF (0.6 M; 2.4 mL, 4 mmol, 1.00 equiv.). Tert-butyl 4-oxoazepane-1-carboxylate, (853 mg; 4.00 mmol, 1.00 equiv.) was added, and the resulting mixture was stirred for 1 h at room temperature. The reaction mixture was cooled to 0°C, EtMgBr (4.8 mL of a 1 M solution in THF, 4.80 mmol, 1.2 equiv.) was added dropwise, and the reaction mixture was allowed to stir, warming to room temperature overnight. Saturated aqueous NH₄Cl and water were added.

The aqueous layer was extracted with diethyl ether, and the combined extracts were dried (Na_2SO_4) and concentrated to dryness. The crude residue was purified by flash column chromatography to give a colorless oil, which was carried on to the next step.

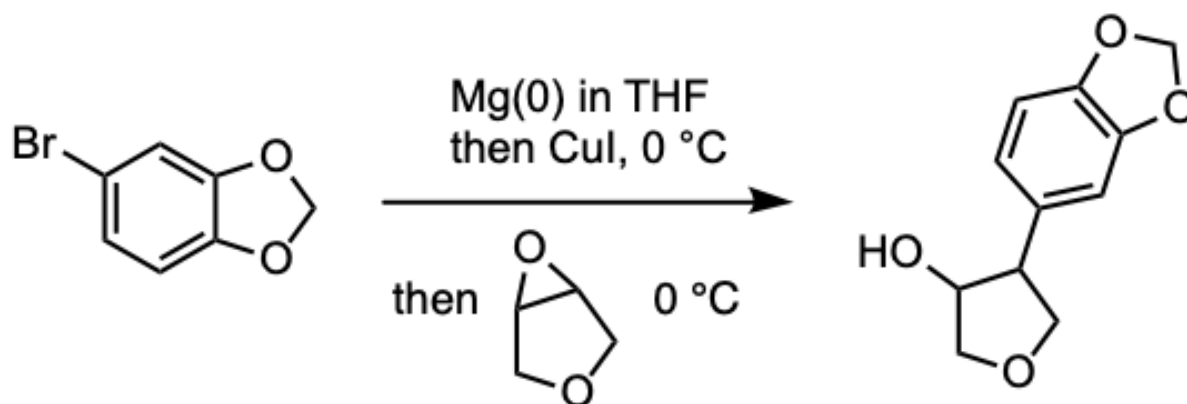


The tertiary alcohol product was transferred to a flask, azeotropically dried with benzene, then dissolved in THF (40 mL). The flask was cooled to $-78\text{ }^\circ\text{C}$ and $n\text{BuLi}$ (2 mL, 2 M in hexanes, mmol, 1 equiv.) was added dropwise. Benzoyl chloride (0.511 mL, 4.40 mmol 1.1 equiv.) was then added dropwise and the reaction mixture was allowed to stir, warming to room temperature overnight. 815 mg and 59% yield was obtained as a clear oil. **$^1\text{H NMR}$** (500 MHz, CDCl_3) δ 8.03 – 7.97 (m, 2H), 7.59 – 7.51 (m, 1H), 7.47 – 7.40 (m, 2H), 3.90 – 3.47 (m, 2H), 3.34 – 3.19 (m, 2H), 2.74 – 2.51 (m, 1H), 2.49 – 2.33 (m, 1H), 2.30 – 1.89 (m, 2H), 1.77 (ddt, $J = 15.0, 11.1, 4.1$ Hz, 3H), 1.66 – 1.59 (m, 1H), 1.43 (d, $J = 6.9$ Hz, 9H), 0.89 (td, $J = 7.4, 2.5$ Hz, 3H). **$^{13}\text{C NMR}$** (126 MHz, CDCl_3) δ 165.54, 155.75, 155.66, 132.86, 131.60, 129.55, 128.51, 86.81, 86.75, 79.43, 46.61, 45.67, 41.50, 41.12, 38.43, 38.32, 35.15, 31.72, 28.63, 22.18, 21.92, 8.13. **HRMS** (ESI^+) Calc: $[\text{M}+\text{Na}]^+$ for $\text{C}_{20}\text{H}_{29}\text{NO}_4 = 370.1989$; measured 370.1980 = 2.4 ppm difference.



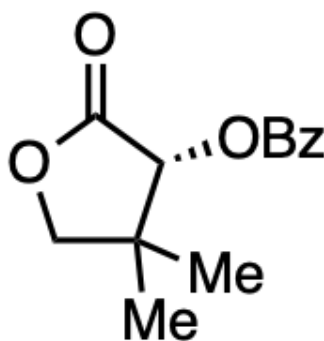
trans-4-(benzo[d][1,3]dioxol-5-yl)tetrahydrofuran-3-yl benzoate: Compound was synthesized via an organocuprate addition into an epoxide followed by benzylation.

Washing Magnesium Turnings: The turnings were rinsed with hexanes and decanted three times. 1 M HCl was added to the turnings and swirled vigorously then decanted. The turnings were washed and filtered with DI water two times, followed by two ethanol rinses, and lastly, two diethyl ether rinses. The magnesium turnings were transferred to a flask then dried under vacuum overnight and stored under nitrogen in a desiccator.



trans-4-(benzo[d][1,3]dioxol-5-yl)tetrahydrofuran-3-ol: Magnesium turnings were (182 mg, 1.5 equiv., 7.50 mmol) activated with an I₂ crystal and dissolved in 2.5 mL THF. 5-bromobenzo[d][1,3]dioxole (1.51 g, 1.5 equiv., 7.50 mmol) in 3.75 mL THF (2 M) was slowly added. The solution was cooled to 0 °C and copper(I) iodide (190 mg, 0.2 equiv., 1.00 mmol) added. The solution was stirred for 15 min. 3,6-dioxabicyclo[3.1.0]hexane (430 mg, 1 equiv., 5.00 mmol) in 1.25 mL of THF (4 M) was added dropwise at 0 °C. The solution was stirred for 30 min. The reaction was quenched with ammonium chloride (sat. aq.). The organic materials were diluted with diethyl ether then extracted twice with diethyl ether. The combined organic extracts were washed with sodium chloride (sat. aq.) and dried over sodium sulfate, filtered, and concentrated in vacuo. The resulting crude residue was purified by flash column chromatography on silica gel to furnish the alcohol product. 771 mg and 74% yield was obtained as a colorless oil. **¹H NMR** (400 MHz, CDCl₃) δ 6.80 – 6.68 (m, 3H), 5.94 (s, 2H), 4.41 – 4.32 (m, 1H), 4.30 (dd, J = 9.0, 7.2 Hz, 1H), 4.18 – 4.02 (m, 1H), 3.87 (dd, J = 9.0, 5.8 Hz, 1H), 3.78 (dd, J = 9.8, 3.4 Hz, 1H), 3.23 (ddd, J = 7.2, 5.8, 3.6 Hz, 1H), 1.94 (d, J = 4.8 Hz, 1H). Spectrum in accordance with literature: JACS, **2015**, 137, 9, 3327-3240.

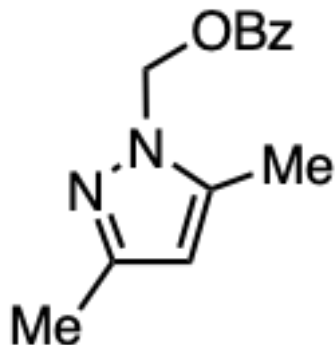
Benzoylation was performed according to General Procedure A on a 3.70 mmol scale. 1.07 g and 92% yield was obtained as a white crystalline solid. **¹H NMR** (500 MHz, CDCl₃) δ 8.09 – 8.04 (m, 2H), 7.62 – 7.54 (m, 1H), 7.50 – 7.42 (m, 2H), 6.87 – 6.76 (m, 3H), 5.95 (s, 2H), 5.39 (dt, J = 5.0, 2.4 Hz, 1H), 4.32 (dd, J = 9.0, 6.8 Hz, 1H), 4.27 (dd, J = 10.7, 5.2 Hz, 1H), 4.06 – 3.97 (m, 2H), 3.55 (ddd, J = 7.1, 4.6, 2.7 Hz, 1H). **¹³C NMR** (126 MHz, CDCl₃) δ 166.36, 148.22, 146.78, 133.72, 133.41, 129.97, 129.83, 128.60, 120.72, 108.64, 108.00, 101.21, 82.11, 73.19, 72.69, 51.34. **HRMS** (ESI⁺) Calc: [M+H]⁺ for C₁₈H₁₆O₅ = 313.1070; measured 313.1060 = 3.2 ppm difference.



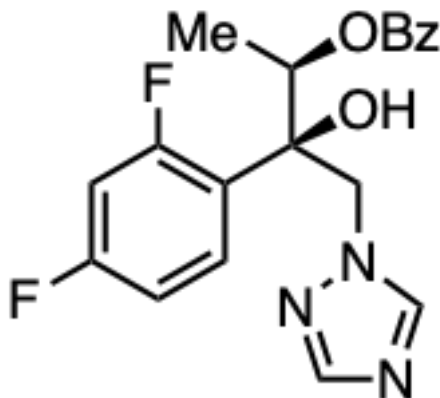
(2R)-2-benzoyloxy-3,3-dimethyl-4-butanolide: Compound was synthesized from (2R)-2-hydroxy-3,3-dimethyl-4-butanolide according to General Procedure A on 2.00 mmol scale. 442 mg, 94% yield was obtained as a white solid. $^1\text{H NMR}$ (400 MHz, CDCl_3) δ 8.14 – 8.07 (m, 2H), 7.66 – 7.57 (m, 1H), 7.52 – 7.42 (m, 2H), 5.62 (s, 1H), 4.13 (d, J = 9.0 Hz, 1H), 4.10 (d, J = 9.1 Hz, 1H), 1.28 (s, 3H), 1.23 (s, 3H). Spectrum in accordance with literature: Org. Lett. **2013**, 15, 24, 6132–6135.



(5-methylfuran-2-yl)methyl benzoate: Compound was synthesized according to General Procedure A on a 3.00 mmol scale. 592 mg (91% yield) was obtained as a colorless oil. $^1\text{H NMR}$ (400 MHz, CDCl_3) δ 8.24 – 7.92 (m, 2H), 7.55 (t, J = 7.4 Hz, 1H), 7.42 (t, J = 7.7 Hz, 2H), 6.37 (d, J = 3.0 Hz, 1H), 6.11 – 5.83 (m, 1H), 5.25 (s, 2H), 2.31 (s, 3H). Spectrum in accordance with literature: Tetrahedron, 53, 50, **1997**, 17115-17126.

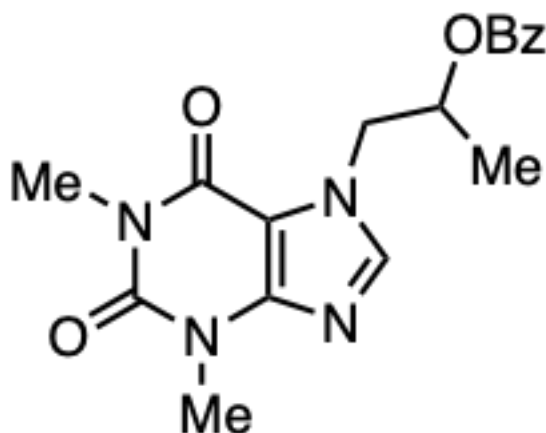


(3,5-dimethyl-pyrazol-1-yl)methyl benzoate: Compound was synthesized according to General Procedure A on a 3.00 mmol scale. 479 mg (69% yield) was obtained as an off-white crystalline solid. $^1\text{H NMR}$ (500 MHz, CDCl_3) δ 8.05 (dd, $J = 8.3, 1.4$ Hz, 2H), 7.69 – 7.50 (m, 1H), 7.42 (dd, $J = 8.2, 7.4$ Hz, 2H), 6.17 (s, 2H), 5.88 (s, 1H), 2.37 (d, $J = 0.8$ Hz, 3H), 2.24 (s, 3H). Spectrum in accordance with literature: Adv. Synth. Catal. **2022**, 364, 2922– 2925.



(2R,3R)-3-(2,4-difluorophenyl)-3-hydroxy-4-(1,2,4-triazol-1-yl)butan-2-yl benzoate: Alcohol substrate (4.0 mmol, 1.0 equiv) was dissolved in DCM (0.5 M). Triethylamine (3 equiv) was added to the reaction mixture and the contents cooled to 0 °C. Benzoyl chloride (1.0 equiv) was added to the reaction dropwise. Reaction was run overnight at room temperature. After reaction completion, reaction was quenched with sodium bicarbonate (sat. aq.) then extracted with DCM. The organic layer was washed with sodium chloride (sat. aq.) then dried over sodium sulfate,

filtered, and concentrated in vacuo. The crude mixture was purified via flash chromatography. 717 mg (71% yield) was obtained as an off-white crystalline solid. **¹H NMR** (500 MHz, CDCl₃) δ 8.27 – 8.04 (m, 2H), 7.84 (s, 1H), 7.77 (s, 1H), 7.65 – 7.58 (m, 1H), 7.54 (td, J = 9.0, 6.4 Hz, 1H), 7.49 (t, J = 7.8 Hz, 2H), 6.85 – 6.73 (m, 2H), 5.73 (q, J = 6.5 Hz, 1H), 4.99 (dd, J = 14.2, 1.4 Hz, 1H), 4.87 (s, 1H), 4.62 (d, J = 14.1 Hz, 1H), 1.23 (d, J = 6.4 Hz, 3H). **¹³C NMR** (126 MHz, CDCl₃) δ 165.90, 152.05, 144.02, 133.47, 130.65 (dd, J = 9.6, 5.7 Hz), 129.80, 129.71, 128.57, 111.98 (dd, J = 20.8, 3.2 Hz), 104.44, 104.24, 104.22, 104.02, 77.88 (d, J = 5.4 Hz), 73.04 (d, J = 3.8 Hz), 54.74 (d, J = 6.5 Hz), 14.53. **HRMS** (ESI⁺) Calc: [M+H]⁺ for C₁₉H₁₇N₃O₃F₂ = 374.1311; measured 374.1302 = 2.4 ppm difference.

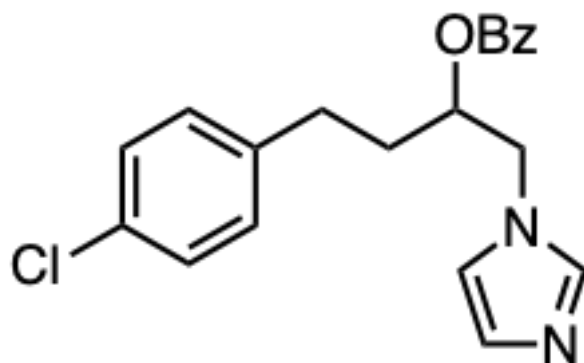


1-(1,3-dimethyl-2,6-dioxo-1,2,3,6-tetrahydro-7H-purin-7-yl)propan-2-yl

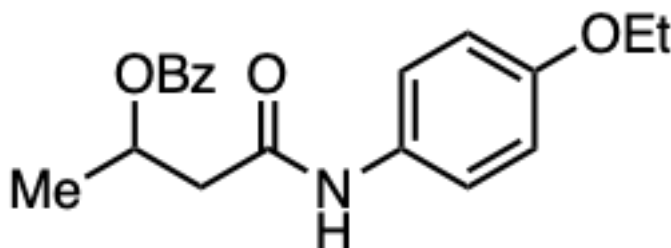
benzoate:

Compound was synthesized from 7-(2-hydroxypropyl)-1,3-dimethyl-3,7-dihydro- 1H-purine-2,6-dione according to General Procedure A on a 4.00 mmol scale. 1.36 g and 99% yield was obtained as a white solid. **¹H NMR** (500 MHz, CDCl₃) δ 7.97 – 7.91 (m, 2H), 7.59 – 7.52 (m, 2H), 7.46 – 7.38 (m, 2H), 5.52 (ddp, J = 12.8, 6.4, 3.2 Hz, 1H), 4.68 (dd, J = 14.3, 3.0 Hz, 1H), 4.49 (dd, J = 14.4, 7.8 Hz, 1H), 3.54 (s, 3H), 3.37 (s, 3H), 1.43 (d, J = 6.4 Hz, 3H). **¹³C NMR** (126 MHz, CDCl₃) δ 165.55, 155.42, 151.72, 148.82, 141.64, 133.46, 129.71, 129.59, 128.63, 107.26, 69.98, 50.83,

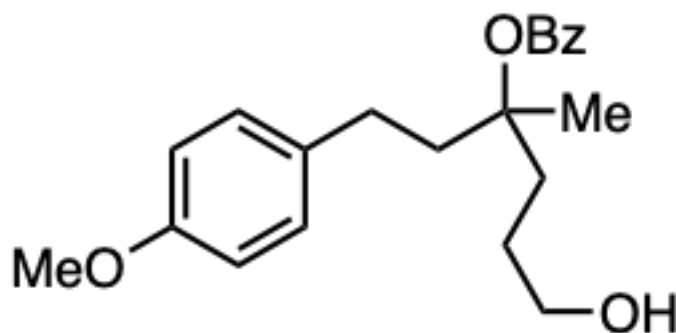
29.88, 28.05, 17.39. **HRMS** (ESI⁺) Calc: [M+H]⁺ for C₁₇H₁₈N₄O₄ = 343.1401; measured 343.1395 = 1.7 ppm difference.



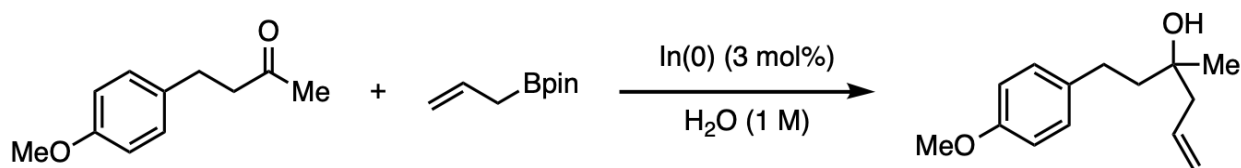
4-(4-chlorophenyl)-1-(imidazol-1-yl)butan-2-yl benzoate: Compound was synthesized from 4-(4-chlorophenyl)-1-(1H-imidazol-1-yl)butan-2-ol according to General Procedure A and obtained as a white solid. ¹H NMR (400 MHz, CDCl₃) δ 8.25 – 7.86 (m, 2H), 7.69 – 7.55 (m, 1H), 7.51 – 7.35 (m, 3H), 7.22 (d, J = 8.2 Hz, 2H), 7.05 (d, J = 7.8 Hz, 3H), 6.91 (d, J = 1.3 Hz, 1H), 5.34 (dq, J = 9.1, 4.7 Hz, 1H), 4.33 – 4.10 (m, 2H), 2.91 – 2.50 (m, 2H), 2.26 – 1.72 (m, 2H). ¹³C NMR (101 MHz, CDCl₃) δ 165.75, 138.82, 137.81, 133.59, 132.13, 129.67, 129.65, 129.31, 128.74, 128.65, 119.80, 72.17, 49.85, 32.95, 31.01. **HRMS** (ESI⁺) Calc: [M+H]⁺ for C₂₀H₁₉ClN₂O₂ = 355.1208; measured 355.1204 = 1.1 ppm difference.



4-((4-ethoxyphenyl)amino)-4-oxobutan-2-yl benzoate: Compound was synthesized from 4-((4-ethoxyphenyl)amino)-4-oxobutan-2-ol according to General Procedure A on a 2.00 mmol scale. 403 mg and 62% yield was obtained as a white crystalline solid. $^1\text{H NMR}$ (600 MHz, CDCl_3) δ 8.03 (dd, $J = 8.2, 1.4$ Hz, 2H), 7.62 – 7.54 (m, 1H), 7.44 (t, $J = 7.7$ Hz, 2H), 7.35 (d, $J = 8.9$ Hz, 2H), 6.82 (d, $J = 8.9$ Hz, 2H), 5.56 (q, $J = 6.2$ Hz, 1H), 3.99 (q, $J = 7.0$ Hz, 2H), 2.82 (dd, $J = 14.6, 6.5$ Hz, 1H), 2.69 (dd, $J = 14.6, 5.7$ Hz, 1H), 1.52 (d, $J = 6.3$ Hz, 3H), 1.39 (t, $J = 7.0$ Hz, 3H). $^{13}\text{C NMR}$ (151 MHz, CDCl_3) δ 167.40, 166.07, 155.90, 133.18, 130.60, 130.16, 129.58, 128.47, 121.80, 114.79, 69.06, 63.70, 44.36, 20.18, 14.83. **HRMS** (ESI^+) Calc: $[\text{M}-\text{H}]^-$ for $\text{C}_{19}\text{H}_{21}\text{NO}_4 = 326.1398$; measured 326.1398 = <0.1 ppm difference.



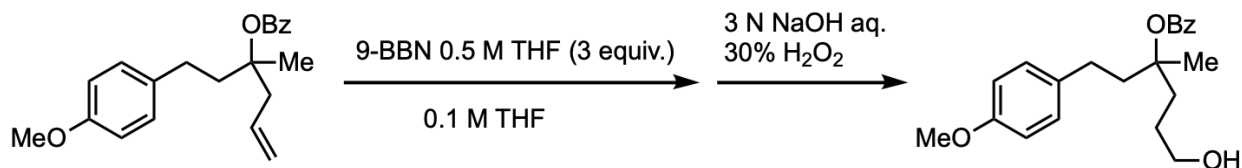
6-hydroxy-1-(4-methoxyphenyl)-3-methylhexan-3-yl benzoate: Compound was synthesized via a ketone allylation reaction followed by benzoylation, then a hydroboration/oxidation sequence.



Allylation was performed according to a procedure from JACS, **2008**, 130, 42, 13824–13825.

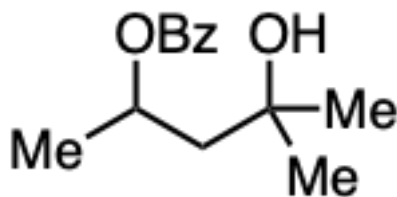
To a flask under a nitrogen atmosphere with a magnetic stirring bar was added indium(0) powder (14.1 mg; 3 mol%). After addition of water (4.0 mL; 1 M), 4-(4-methoxyphenyl)-2-butanone (713 mg, 4.00 mmol), then 2-allyl-4,4,5,5-tetramethyl-1,3,2-dioxaborolane (6.0 mmol; 1.5 equiv) were added. The reaction mixture was vigorously stirred at room temperature for 24 h, before addition of dichloromethane. After phase separation, the aqueous phase was extracted with dichloromethane (three times). The combined organic layers were dried (Na₂SO₄), filtered and concentrated in vacuo. The residues were purified by column chromatography to give 654 mg and 74% yield as a colorless oil. **¹H NMR** (400 MHz, CDCl₃) δ 7.15 – 7.08 (m, 2H), 6.87 – 6.80 (m, 2H), 5.89 (ddt, J = 17.6, 10.4, 7.5 Hz, 1H), 5.21 – 5.10 (m, 2H), 3.79 (s, 3H), 2.65 (ddd, J = 11.3, 6.2, 1.6 Hz, 2H), 2.29 (d, J = 7.5 Hz, 2H), 1.79 – 1.70 (m, 2H), 1.48 (s, 1H), 1.25 (s, 3H). Spectrum in accordance with literature: JACS, **2008**, 130, 42, 13824–13825.

Benzoylation was performed according to General Procedure B on a 2.96 mmol scale. 410 mg and 43% yield was obtained as a colorless oil. **¹H NMR** (500 MHz, CDCl₃) δ 8.02 – 7.96 (m, 2H), 7.57 – 7.50 (m, 1H), 7.46 – 7.39 (m, 2H), 7.15 – 7.08 (m, 2H), 6.85 – 6.78 (m, 2H), 5.86 (ddt, J = 17.4, 10.2, 7.3 Hz, 1H), 5.22 – 5.05 (m, 2H), 3.77 (s, 3H), 2.85 (ddt, J = 14.1, 7.3, 1.3 Hz, 1H), 2.80 – 2.70 (m, 1H), 2.66 (ddd, J = 9.8, 6.2, 2.7 Hz, 2H), 2.30 (ddd, J = 14.0, 10.3, 6.8 Hz, 1H), 2.14 (ddd, J = 14.0, 10.6, 6.7 Hz, 1H), 1.63 (s, 3H). **¹³C NMR** (126 MHz, CDCl₃) δ 165.68, 157.97, 134.17, 133.26, 132.70, 131.88, 129.57, 129.40, 128.40, 118.77, 114.00, 84.51, 55.42, 43.20, 40.86, 29.34, 24.01.

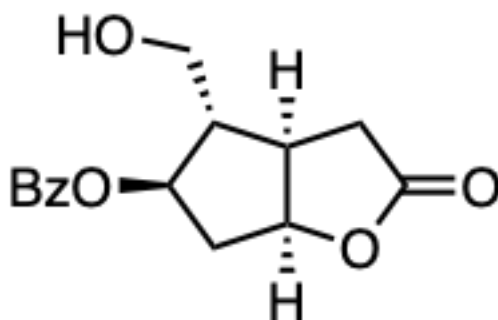


Hydroboration/oxidation was performed according to a procedure from ACIE, **2011**, 50, 9452 – 9455.

To a stirred solution of the homoallylic alcohol (410 mg, 1.26 mmol) in THF (12.6 mL, 0.1 M) was added a solution of 9-BBN in THF (7.56 mL, 0.5 M, 3.78 mmol, 3.0 equiv.) dropwise at 0 °C, and the resultant solution was stirred at room temperature. After the starting material disappeared, 3N NaOH aqueous solution (10 mL) and 30 % H₂O₂ solution (10 mL) were added to the reaction mixture and the resultant mixture was stirred at room temperature. After the reaction was completed, H₂O (5 mL) was added to the reaction mixture, and the aqueous layer was extracted with Et₂O (10 mL × 2). The combined organic layers were washed with brine (5 mL), dried (Na₂SO₄), filtered, and concentrated under reduced pressure. The residue was purified by flash chromatography. 396 mg and 91% yield was obtained as a colorless oil. ¹H NMR (500 MHz, CDCl₃) δ 8.03 – 7.96 (m, 2H), 7.57 – 7.50 (m, 1H), 7.42 (dd, J = 8.4, 7.1 Hz, 2H), 7.15 – 7.08 (m, 2H), 6.85 – 6.78 (m, 2H), 3.77 (s, 3H), 3.68 (t, J = 6.6 Hz, 2H), 2.71 – 2.61 (m, 2H), 2.37 – 2.27 (m, 1H), 2.22 – 2.09 (m, 2H), 2.06 – 1.96 (m, 1H), 1.72 – 1.65 (m, 2H), 1.64 (s, 3H). ¹³C NMR (126 MHz, CDCl₃) δ 165.74, 157.97, 134.11, 132.74, 131.80, 129.56, 129.37, 128.41, 114.01, 85.02, 63.19, 55.41, 41.01, 34.92, 29.44, 27.26, 24.08.

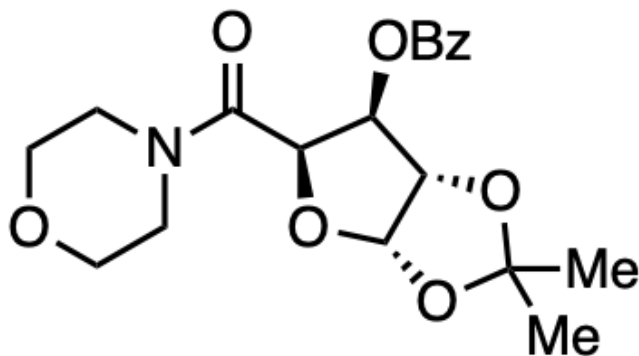


4-Benzoyloxy-2-methyl-2-pentanol: Compound was synthesized from 2-methyl-2,4-pentanediol according to General Procedure A on a 4.00 mmol scale. 678 mg and 76% yield was obtained as a colorless oil. $^1\text{H NMR}$ (400 MHz, CDCl_3) δ 8.07 – 8.00 (m, 2H), 7.60 – 7.51 (m, 1H), 7.48 – 7.39 (m, 2H), 5.42 (ddp, J = 12.4, 6.2, 3.1 Hz, 1H), 2.07 (dd, J = 14.9, 8.8 Hz, 1H), 1.99 (s, 1H), 1.77 (dd, J = 14.9, 3.3 Hz, 1H), 1.40 (d, J = 6.2 Hz, 3H), 1.26 (d, J = 7.2 Hz, 6H). Spectrum in accordance with literature: Tetrahedron 66 (2010) 7939–7945.

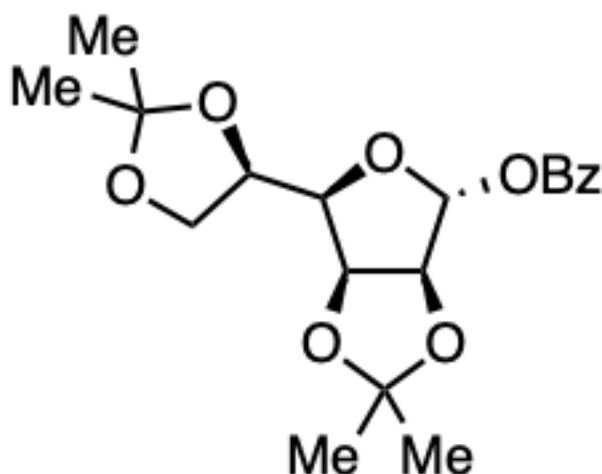


(3aR,4S,5R,6aS)-4-(hydroxymethyl)-2-oxohexahydro-2H-cyclopenta[b]furan-5-yl

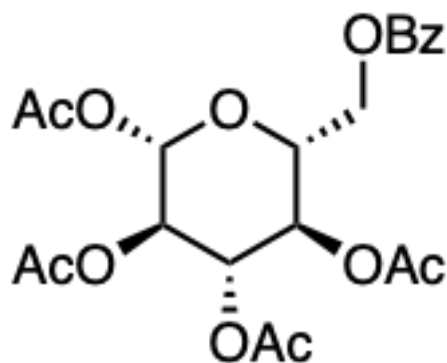
benzoate: Compound was commercial and purchased from BLDpharm, CAS 39746-00-4.



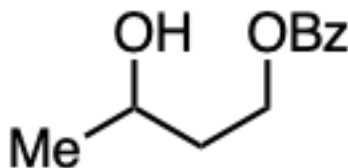
(3a*S*,5*R*,6*S*,6a*S*)-2,2-dimethyl-5-(morpholine-4-carbonyl)tetrahydrofuro[2,3-*d*][1,3]dioxol-6-yl benzoate: Compound was synthesized according to General Procedure A on a 2.00 mmol scale. 666 mg (88% yield) was obtained as an off-white crystalline solid. ^1H NMR (500 MHz, CDCl_3) δ 8.02 – 7.96 (m, 2H), 7.61 – 7.54 (m, 1H), 7.43 (t, J = 7.8 Hz, 2H), 6.22 (d, J = 3.7 Hz, 1H), 5.72 (d, J = 3.5 Hz, 1H), 5.19 (d, J = 3.6 Hz, 1H), 4.73 (d, J = 3.7 Hz, 1H), 3.85 – 3.25 (m, 8H), 1.56 (s, 3H), 1.36 (s, 3H). ^{13}C NMR (126 MHz, CDCl_3) δ 165.28, 164.45, 133.72, 129.91, 128.88, 128.58, 112.75, 105.14, 83.28, 66.66, 66.35, 45.70, 42.48, 26.94, 26.32. **HRMS** (ESI^+) Calc: $[\text{M}+\text{H}]^+$ for $\text{C}_{19}\text{H}_{24}\text{NO}_7$ = 378.1547; measured 378.1542 = 1.3 ppm difference.



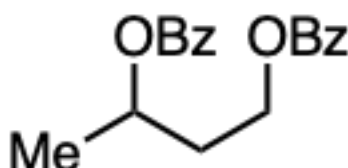
2,3:5,6-Di-O-isopropylidene- α -mannofuranosyl benzoate: Compound was synthesized from 2,3:5,6-di-O-isopropylidene-D-mannofuranose according to General Procedure A on a 2.00 mmol scale. 615 mg, 84% yield was obtained as a white solid. $^1\text{H NMR}$ (500 MHz, CDCl_3) δ 8.05 – 7.99 (m, 2H), 7.63 – 7.56 (m, 1H), 7.50 – 7.42 (m, 2H), 6.37 (s, 1H), 4.95 (dd, J = 5.9, 3.5 Hz, 1H), 4.88 (d, J = 5.8 Hz, 1H), 4.45 (ddd, J = 8.1, 6.1, 4.1 Hz, 1H), 4.15 – 4.09 (m, 2H), 4.06 (dd, J = 9.0, 4.1 Hz, 1H), 1.53 (s, 3H), 1.46 (s, 3H), 1.38 (s, 3H), 1.38 (s, 3H). Spectrum in accordance with literature: J. Chem. Soc., Perkin Trans. 2, **2000**, 737-747.



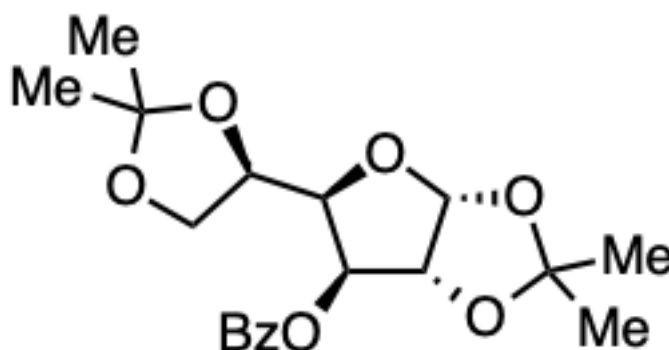
(2S,3R,4S,5R,6R)-6-((benzyloxy)methyl)tetrahydro-2H-pyran-2,3,4,5-tetraol tetraacetate: Compound was synthesized according to General Procedure A and 91% yield (1.18 grams) was obtained as a white solid. $^1\text{H NMR}$ (600 MHz, CDCl_3) δ 8.22 – 7.92 (m, 2H), 7.64 – 7.52 (m, 1H), 7.45 (t, J = 7.8 Hz, 2H), 5.76 (d, J = 8.2 Hz, 1H), 5.32 – 5.21 (m, 2H), 5.16 (dd, J = 9.3, 8.3 Hz, 1H), 4.49 (dd, J = 12.4, 2.4 Hz, 1H), 4.38 (dd, J = 12.4, 4.5 Hz, 1H), 3.98 (ddd, J = 9.8, 4.6, 2.5 Hz, 1H), 2.10 (s, 3H), 2.04 (s, 3H), 2.02 (s, 3H), 2.01 (s, 3H). $^{13}\text{C NMR}$ (151 MHz, CDCl_3) δ 181.27, 170.12, 169.33, 169.29, 168.94, 166.11, 133.28, 129.82, 129.51, 128.46, 91.74, 72.87, 72.73, 70.28, 68.11, 62.16, 20.82, 20.59. **HRMS** (ESI^+) Calc: $[\text{M}+\text{NH}_4]^+$ for $\text{C}_{21}\text{H}_{24}\text{O}_{11}$ = 470.1657; measured 470.1655 = 0.4 ppm difference.



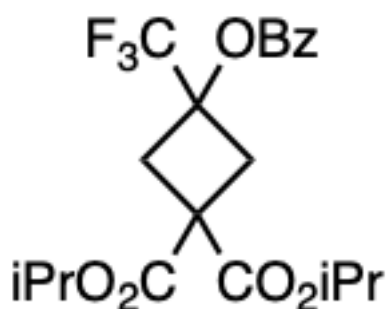
3-hydroxybutyl benzoate: Alcohol substrate (3.50 mmol, 1.0 equiv) was dissolved in DCM (0.5 M). Triethylamine (3 equiv) was added to the reaction mixture and the contents cooled to 0 °C. Benzoyl chloride (1.0 equiv) was added to the reaction dropwise. Reaction was run overnight at room temperature. After reaction completion, reaction was quenched with sodium bicarbonate (sat. aq.) then extracted with DCM. The organic layer was washed with sodium chloride (sat. aq.) then dried over sodium sulfate, filtered, and concentrated in vacuo. The crude mixture was purified via flash chromatography. 547 mg (81% yield) was obtained as an oil. $^1\text{H NMR}$ (400 MHz, CDCl_3) δ 8.07 – 8.00 (m, 2H), 7.61 – 7.52 (m, 1H), 7.44 (t, J = 7.8 Hz, 2H), 4.61 (ddd, J = 11.4, 8.6, 5.0 Hz, 1H), 4.38 (dt, J = 11.2, 5.5 Hz, 1H), 3.98 (ddt, J = 14.6, 9.9, 5.9 Hz, 1H), 2.07 (s, 1H), 2.00 – 1.77 (m, 2H), 1.27 (d, J = 6.3 Hz, 3H). Spectrum in accordance with literature: Org. Lett. **2012**, 14, 18, 4910–4913.



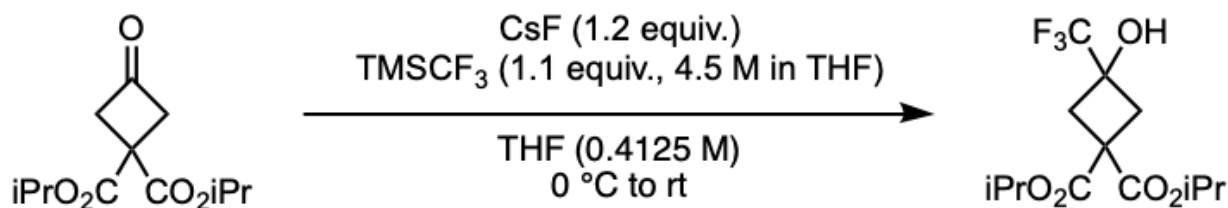
butane-1,3-diyl dibenzoate: Compound was synthesized according to General Procedure A, but with 2.0 equiv. BzCl and 4 equiv. NEt_3 , on a 3.50 mmol scale. 932 mg (89% yield) was obtained as an oil. $^1\text{H NMR}$ (400 MHz, CDCl_3) δ 8.02 (ddd, J = 9.6, 8.2, 1.4 Hz, 4H), 7.59 – 7.49 (m, 2H), 7.41 (td, J = 7.7, 5.6 Hz, 4H), 5.46 – 5.33 (m, 1H), 4.50 (dt, J = 11.9, 6.1 Hz, 1H), 4.42 (ddd, J = 11.4, 7.5, 5.8 Hz, 1H), 2.30 – 2.08 (m, 2H), 1.45 (d, J = 6.3 Hz, 3H). Spectrum in accordance with literature: Bulletin of the Chemical Society of Japan, **1976**, 49, 510 - 513



1,2:5,6-Di-O-isopropylidene- α -D-glucufuranosyl benzoate: Compound was synthesized according to General Procedure A on a 2.00 mmol scale. 657 mg and 90% yield was obtained as a white solid. $^1\text{H NMR}$ (500 MHz, CDCl_3) δ 8.06 – 8.00 (m, 2H), 7.63 – 7.56 (m, 1H), 7.50 – 7.43 (m, 2H), 5.95 (d, J = 3.7 Hz, 1H), 5.50 (d, J = 2.9 Hz, 1H), 4.64 (d, J = 3.7 Hz, 1H), 4.41 – 4.30 (m, 2H), 4.11 (qd, J = 8.6, 5.3 Hz, 2H), 1.56 (s, 3H), 1.42 (s, 3H), 1.32 (s, 3H), 1.27 (s, 3H). Spectrum in accordance with literature: Org. Lett. **2019**, 21, 6888–6892

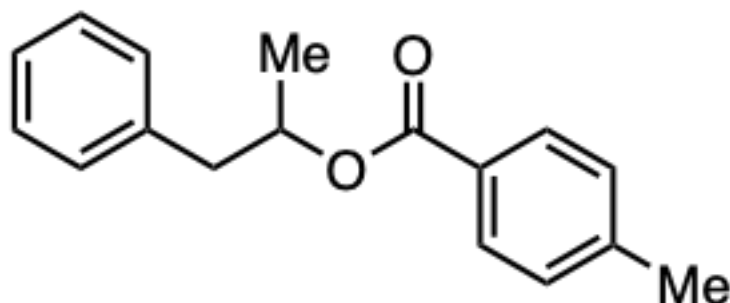


diisopropyl 3-(benzoyloxy)-3-(trifluoromethyl)cyclobutane-1,1-dicarboxylate: Compound was synthesized via trifluoromethyl anion addition into a ketone followed by benzoylation.

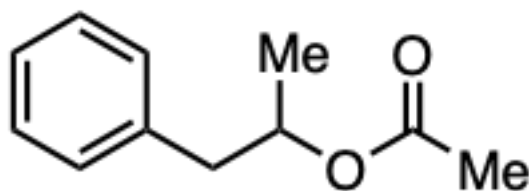


diisopropyl 3-hydroxy-3-(trifluoromethyl)cyclobutane-1,1-dicarboxylate: Procedure from Org. Process Res. Dev. **2021**, 25, 1, 82–88. Diisopropyl 3-oxocyclobutane-1,1-dicarboxylate (1.60 g, 6.60 mmol) was charged into a round-bottom flask followed by THF (16 mL) and CsF (1.20 g, 7.92 mmol). The system was purged with N₂ three times, and was cooled to 0 °C. The above flask was charged dropwise with a solution of TMSCF₃ (1.03 g, 7.26 mmol) in THF (1.60 mL), and the reaction was stirred at room temperature overnight. TLC indicated that the starting material was consumed completely. The reaction mixture was filtered through a pad Celite. The filtrate was concentrated in vacuum, and the residue was redissolved in 20 mL of ethyl acetate. The organic phase was washed with brine (5 mL × 2) and separated. It was dried with anhydrous MgSO₄, filtered, and concentrated in vacuum. The crude product was carried forward without further purification.

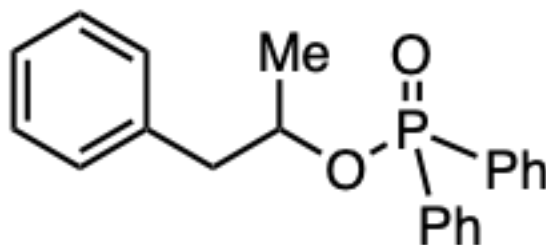
Benzoylation was performed according to General Procedure A on a 6.6 mmol scale. 2.15 g (85% yield) was obtained as white solid. ¹H NMR (500 MHz, CDCl₃) δ 8.05 – 7.99 (m, 2H), 7.63 – 7.56 (m, 1H), 7.49 – 7.42 (m, 2H), 5.08 (dhept, J = 21.1, 6.3 Hz, 2H), 3.41 – 3.34 (m, 2H), 3.33 – 3.25 (m, 2H), 1.27 (d, J = 6.3 Hz, 6H), 1.22 (d, J = 6.3 Hz, 6H). ¹³C NMR (126 MHz, CDCl₃) δ 169.95, 169.11, 164.18, 133.83, 130.10, 129.42, 128.66, 124.23 (q, J = 282.1 Hz), 75.20 (q, J = 33.8 Hz), 70.01, 69.82, 46.68, 35.79 (q, J = 1.9 Hz), 21.60, 21.60. ¹⁹F NMR (377 MHz, CDCl₃) δ -80.70. **HRMS** (ESI⁺) Calc: [M+H]⁺ (C₂₀H₂₄F₃O₆) 417.1519; measured 417.1513 = 1.4 ppm difference.



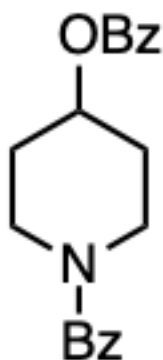
1-phenylpropan-2-yl 4-methylbenzoate: Compound was synthesized according to General Procedure A except with 4-methyl benzoyl chloride on a 2.14 mmol scale. 409 mg (75% yield) was obtained as a colorless oil. **¹H NMR** (500 MHz, CDCl₃) δ 8.03 – 7.70 (m, 2H), 7.33 – 7.15 (m, 7H), 5.36 (h, J = 6.4 Hz, 1H), 3.08 (dd, J = 13.6, 6.4 Hz, 1H), 2.90 (dd, J = 13.7, 6.5 Hz, 1H), 2.41 (s, 3H), 1.34 (d, J = 6.2 Hz, 3H). **¹³C NMR** (126 MHz, CDCl₃) δ 166.12, 143.40, 137.64, 129.56, 129.55, 129.02, 128.36, 128.02, 126.48, 71.90, 42.36, 21.65, 19.51. **HRMS** (ESI⁺) Calc: [M+Na]⁺ for C₁₇H₁₈O₂ = 277.1199; measured 277.1193 = 2.2 ppm difference.



1-phenylpropan-2-yl acetate: Compound was synthesized according to General Procedure A except with 1.1 equiv. acetyl chloride and 1.1 equiv. NEt₃ on a 4.00 mmol scale. 291 mg (41% yield) was obtained as an oil. **¹H NMR** (400 MHz, CDCl₃) δ 7.37 – 7.22 (m, 5H), 5.17 (h, J = 6.4 Hz, 1H), 2.99 (dd, J = 13.6, 6.7 Hz, 1H), 2.81 (dd, J = 13.6, 6.5 Hz, 1H), 2.05 (s, 3H), 1.28 (d, J = 6.3 Hz, 3H). Spectrum in accordance with literature: Tetrahedron, **2017**, 73, 20, 2984-2989.



1-phenylpropan-2-yl diphenylphosphinate: Compound was synthesized according to General Procedure A except with diphenylphosphorous oxychloride on a 2.14 mmol scale. 640 mg (89% yield) was obtained as a colorless oil. $^1\text{H NMR}$ (500 MHz, CDCl_3) δ 7.95 – 7.71 (m, 2H), 7.57 (ddd, J = 12.2, 8.2, 1.4 Hz, 2H), 7.51 (dddd, J = 8.4, 7.0, 5.3, 1.4 Hz, 1H), 7.45 (dddd, J = 8.2, 6.5, 4.2, 1.3 Hz, 3H), 7.35 (td, J = 7.7, 3.5 Hz, 2H), 7.31 – 7.23 (m, 3H), 7.19 – 7.13 (m, 2H), 4.71 (dh, J = 8.0, 6.3 Hz, 1H), 3.05 (dd, J = 13.6, 6.6 Hz, 1H), 2.90 (ddd, J = 13.7, 6.3, 1.1 Hz, 1H), 1.39 (d, J = 6.2 Hz, 3H). $^{13}\text{C NMR}$ (126 MHz, CDCl_3) δ 137.47, 133.05, 132.33, 131.96 (d, J = 2.8 Hz), 131.82 (d, J = 2.8 Hz), 131.69 (d, J = 10.2 Hz), 131.58 (d, J = 10.1 Hz), 131.25, 129.74, 128.42 (d, J = 5.3 Hz), 128.38, 128.32 (d, J = 5.1 Hz), 126.58, 74.38 (d, J = 6.3 Hz), 44.53 (d, J = 5.7 Hz), 22.03 (d, J = 2.5 Hz). **HRMS** (ESI^+) Calc: $[\text{M}+\text{H}]^+$ for $\text{C}_{21}\text{H}_{21}\text{O}_2\text{P}$ = 337.1352; measured 337.1345 = 2.1 ppm difference.



1-benzoylpiperidin-4-yl benzoate: benzoyl chloride (2.90 ml, 25.00 mmol) was dissolved in dichloromethane (0.6 M) and the resulting mixture was cooled to 0 °C. Piperidin-4-ol (1.011 g, 10

mmol) was then added dropwise followed by a slow addition of triethylamine (4.18 ml, 30.0 mmol). After completion of addition, the ice bath was removed and the reaction was stirred for 24 hours at room temperature. The solution was transferred into a separatory funnel and sequentially washed with H₂O, 1.0 M NaOH, 1.0 M HCl, and then brine. The organic phase was dried over anhydrous Na₂SO₄ and the filtrate was concentrated under vacuo. Desired product 1-benzoylpiperidin-4-yl benzoate (2.517 g, 8.14 mmol, 81 % yield) was obtained as off-white solids after flash chromatography. **¹H NMR** (600 MHz, MeOD) δ 8.05 (d, J = 7.4 Hz, 1H), 7.61 (t, J = 7.4 Hz, 1H), 7.54 – 7.40 (m, 4H), 5.29 (sep, J = 3.65 Hz, 1H), 4.04 (br, 1H), 3.72 (d, J = 49.0 Hz, 2H), 3.46 (br, 1H), 1.95 (dd, J = 74.1, 45.7 Hz, 4H). **¹³C NMR** (151 MHz, MeOD) δ 172.60, 167.08, 136.98, 134.34, 131.58, 131.09, 130.53, 129.76, 129.62, 127.84, 71.12, 46.03, 40.42, 32.14, 31.38.

4. 5. 3. General Experimental Procedures for Photoredox Reductions

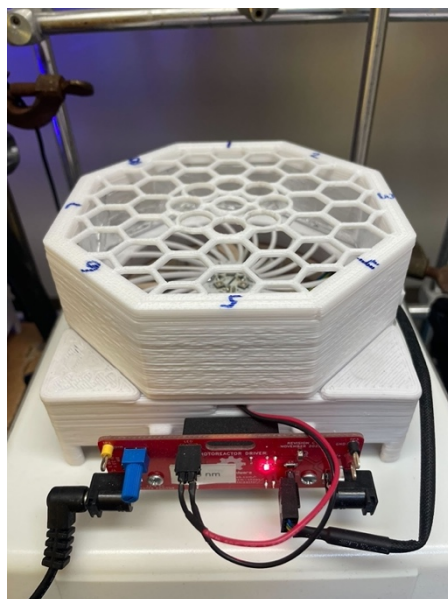
General Procedure C for Deoxygenation: To a vial with a stir bar under air, add substrate (0.1 or 0.4 mmol), PTH (2.5 mol %), Zn(CHO₂)₂ (1 equiv), and mesna (5 mol %). Reaction components were suspended in DMSO (0.2 M). Lastly, formic acid (2 equiv) was added to the reaction. The vial was sealed under air and stirred for ~5 minutes until homogenous. Once homogeneous, the reaction was irradiated for 12–24 hours (0.1 mmol scale = 12 hours, 0.4 mmol scale = 24 hours). Reactions were either analyzed by NMR, GC, or were isolated via flash chromatography. See below for workup procedures.

Aliquot Workups for NMR Analysis: Dibromomethane was added to the crude reaction mixture as an internal standard. The reaction was shaken vigorously before an aliquot was removed and

quenched with sodium chloride (sat. aq., 1 mL). CDCl_3 (1 mL) was added to the aliquot and separated from the aqueous layer. The separated CDCl_3 layer was used for NMR analysis.

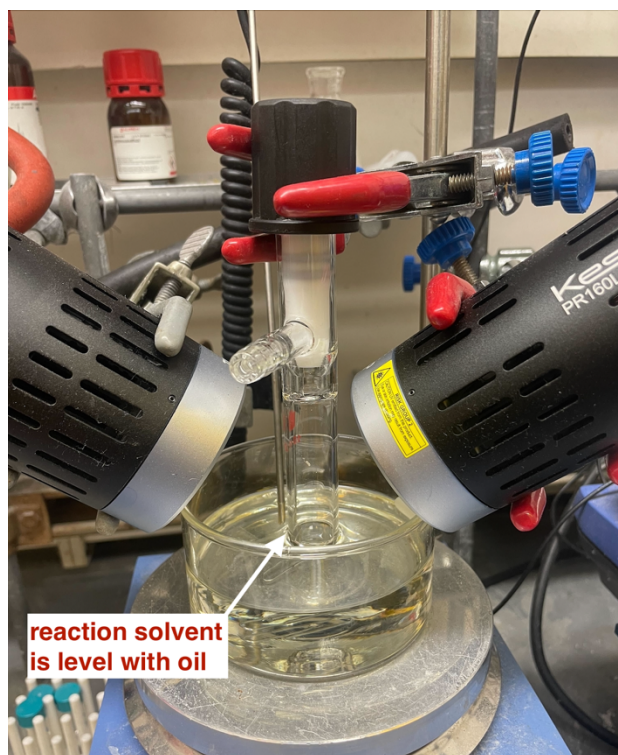
Aliquot Workups for Gas Chromatography Analysis: Dibenzylether was added to the crude reaction mixture as an internal standard. The reaction was shaken vigorously before an aliquot was removed and quenched with sodium chloride (sat. aq., 1 mL). Diethyl ether (1 mL) was added to the aliquot and separated from the aqueous layer. The separated ether layer was used for GC analysis.

Workup for Chromatography: Reactions were diluted with ethyl acetate then quenched with sodium bicarbonate (sat. aq.). The ethyl acetate layer was separated and extracted twice with ethyl acetate. The ethyl acetate layer was washed with sodium chloride (sat. aq.), then dried over sodium sulfate, filtered, and concentrated *in vacuo*. The crude material was purified via flash chromatography to afford pure deoxygenated material.



Reaction setup for General Procedure C. Reactor holds 8 half-dram vials in the central ring. This is an open source 3D printed photoreactor with 395 nm LEDs. For more details, see: *Org. Lett.* 2021, 23, 13, 5277–5281.

General Procedure D for Deoxygenation: To a 10 mL schlenk tube under air, was added PTH (2.5 mol %), mesna (5 mol %), zinc formate (1 equiv), and substrate (1 equiv). The reaction components were dissolved in DMSO (0.2 M). Then, formic acid (2 equiv) was added to the reaction mixture. The reaction vessel was sealed under air and stirred until homogenous (about 5 minutes). The reaction was placed in an oil bath and irradiated with two 390 nm Kessil lamps at 60 °C for 48 hours. Reactions were either analyzed via gas chromatography (see GC procedure above) or purified via flash chromatography.



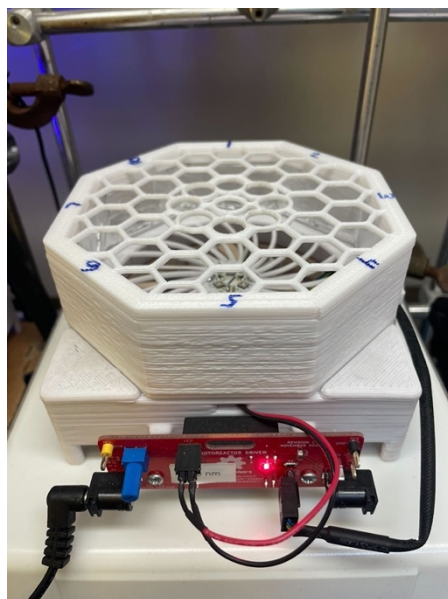
Reaction setup for General Procedure D with two 390 nm Kessil lamps (KSPR160L-390).

General Procedure E for Benzylic Deoxygenation: To a schlenk tube equipped with stir bar under air, benzoylated substrate (0.4 mmol, 1 equiv) was added, followed by 4DPAIPN (2.5 mol %) and sodium formate (3 equiv). The reaction contents were dissolved in DMSO (0.2 M) then CySH (5 mol %) was added. The reaction was then freeze-pump-thawed three times. The reaction was sealed under nitrogen, stirred, and irradiated (405 nm with fan) for 24 hours.

General Procedure F for One-Pot Deoxygenation: To a one-dram vial equipped with stir bar under air, alcohol substrate (0.4 mmol, 1 equiv) was added, followed by benzoic anhydride (1.1 equiv) and DMAP (10 mol %). Reagents were dissolved in DMSO (0.2 M) then DIPEA (1.1 equiv) was added. The reaction stirred at room temperature overnight (14 hours). Next, deoxygenation

reagents were added to the reaction mixture. This included PTH (2.5 mol %), mesna (5 mol %), zinc formate (1 equiv), and finally, formic acid (2 equiv). The mixture was stirred and irradiated (395 nm with fan) for 24 hours.

Aliquot Workups for NMR Analysis: Dibromomethane was added to the crude reaction mixture as an internal standard. The reaction was shaken vigorously before an aliquot was removed and quenched with sodium bicarbonate (sat. aq., 1 mL). CDCl_3 (1 mL) was added to the aliquot and separated from the aqueous layer. The separated CDCl_3 layer was used for NMR analysis



Reaction setup for General Procedure E. This is an open source 3D printed photoreactor with 395 nm LEDs. For more details, see: *Org. Lett.* 2021, 23, 13, 5277–5281.

General Procedure G for One-Pot Benzylic Deoxygenation: To a one-dram vial equipped with stir bar under air, alcohol substrate (0.4 mmol, 1 equiv) was added, followed by benzoic anhydride

(1.1 equiv) and DMAP (10 mol %). Reagents were dissolved in DMSO (0.2 M) then DIPEA (1.1 equiv) was added. The reaction stirred at room temperature overnight (14 hours). Next, deoxygenation reagents were added to the reaction mixture. This included 4DPAIPN (2.5 mol %), CySH (5 mol %), and sodium formate (3 equiv). The reaction was then freeze-pump-thawed three times. The reaction was sealed under nitrogen, stirred, and irradiated (405 nm with fan) for 24 hours.

4. 5. 4. Recent examples of Barton-McCombie in synthesis

Alcohol deoxygenation is commonly used as an enabling strategy in the synthesis of complex molecules. The following recent examples illustrate that modern methods for deoxygenation, despite their more appealing reaction conditions, have failed to supplant the classic tin-based Barton-McCombie deoxygenation.

Polar-type deoxygenation reactions are often attempted first due to their more practical reaction conditions. However, they often lead to undesired elimination products or low reactivity. As a result, chemists resort to using the tin-based Barton-McCombie protocol.

Sarpong, *J. Am. Chem. Soc.* **2022**, 144, 21398–21407. Attempted C17 deoxygenation of keto-alcohol form: no conversion observed using Myers' deoxygenation protocol and Barton–McCombie is used instead.

Sarpong, *J. Am. Chem. Soc.*, **2021**, 143, 2710–2715 and *J. Am. Chem. Soc.*, **2022**, 144, 19173–19185. Ionic deoxygenation of a tertiary benzylic alcohol fails and Barton–McCombie is used instead.

Merck, *Org. Process Res. Dev.* **2021**, 25, 82–88. Numerous deoxygenation methods were attempted but tributyltin hydride-mediated deoxygenation was required. Alternative attempts at deoxygenation included elimination of the corresponding mesylate and triflate, which did not undergo elimination and only decomposition was observed. Additionally, palladium-catalyzed hydrogenation of the mesylate gave no reaction, and thiocarbonyl radical precursors could not be synthesized efficiently. Due to concerns about the tin-mediated approach, particularly with regards to scaling the reaction in order to access significant quantities of the desired building block, “additional efforts were made to improve process practicality, safety, and greenness by eliminating the expensive and toxic reagent Bu_3SnH ”. However, replacement of tributyltin hydride with phenylsilane, or Hantzsch ester under photochemical conditions failed to cleanly provide deoxygenated material. Thus, the authors were forced to use highly undesirable tributyltin hydride on 223 g scale. (540 mmol; 8.88 g = 54.1 mmol AIBN, 205 g = 703 mmol tin).

Maimone, *J. Am. Chem. Soc.* **2020**, 142, 1206–1210. 50 mg scale Barton–McCombie deoxygenation. Of note, this process was found not to be scalable and the route needed to be redesigned as part of future work to avoid the Barton–McCombie step (*Angew. Chem. Int. Ed.* **2022**, 61, e2022094).

Carreira, *J. Am. Chem. Soc.* **2022**, 144, 15475–15479. Aldol addition coupled to secondary alcohol deoxygenation using Barton-McCombie protocol.

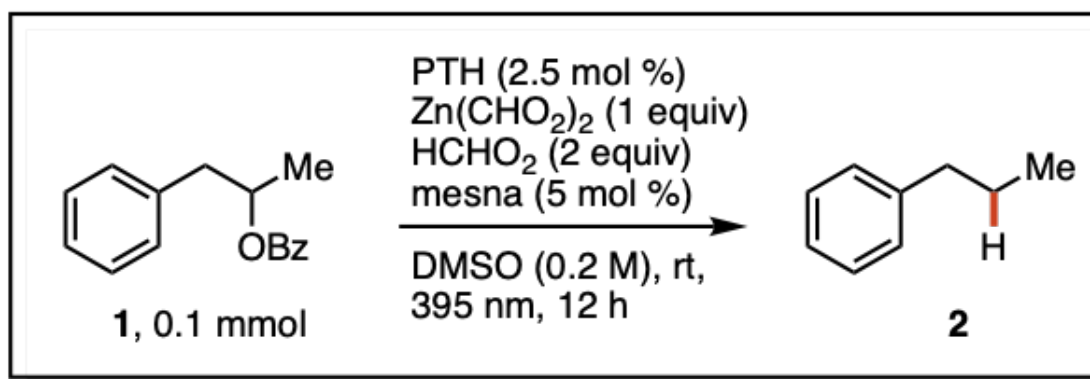
Snyder, *Chem. Sci.*, **2020**, 11, 10939–10944. Secondary alcohol deoxygenation using Barton-McCombie protocol.

Sarpong, *J. Am. Chem. Soc.* **2022**, 144, 19253–19257. Secondary alcohol deoxygenation using Barton-McCombie protocol.

4. 5. 5. Additional experiments

Following General Procedure C on 0.1 mmol scale (unless otherwise noted), the following parameters were evaluated during optimization of this reaction. Reactions were analyzed via gas chromatography.

Control Reactions



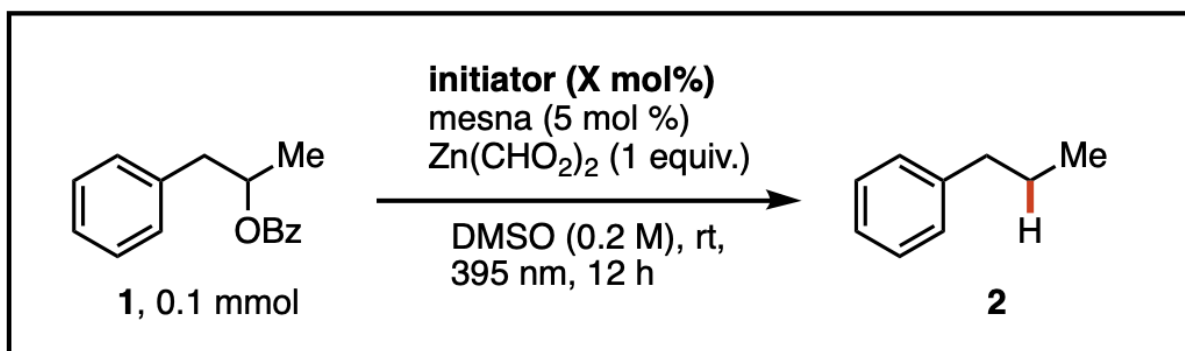
Entry	Modification	Yield
1	none	89
2	no mesna	11
3	no $\text{Zn(CHO}_2)_2$	< 1
4	no HCHO_2	19
5	no PTH	< 1
6 ^a	no light	< 1
7 ^b	no HCHO_2 , DIPEA instead of $\text{Zn(CHO}_2)_2$	0
8 ^b	no HCHO_2 , DIPEA instead of $\text{Zn(CHO}_2)_2$, with $\text{Zn(ClO}_4)_2$	7

^ano light control was run in an amber vial under the standard reaction setup (irradiated at 395 nm in the Wisconsin Photoreactor) to account for heat from the lights. ^b $\text{Zn(ClO}_4)_2$ was added to probe if Zn^{2+} is responsible for deoxygenation rather than formate.

Alternative Initiation Methods

Photochemical: To a vial with a stir bar, a homogeneous solution of substrate (0.1 mmol), $\text{Zn(CHO}_2)_2$ (1 equiv), and mesna (5 mol %) in DMSO (0.2 M) was added. Then the initiator was

added. The vial was sparged with argon and sealed. The reactions were irradiated at 395 nm for 12 hours and analyzed by gas chromatography.



Entry	Initiator	Yield	Conversion
1	MeSSMe (20 mol%)	0	9
2	PhSSPh (5 mol%)	34	83
3	PhSSPh (20 mol%)	46	91
4	benzophenone (100 mol%)	0	9
5	4DPAIPN (10 mol%)	0	13
6	4CzIPN (5 mol%)	8	23
7	acridinium (5 mol%)	0	13

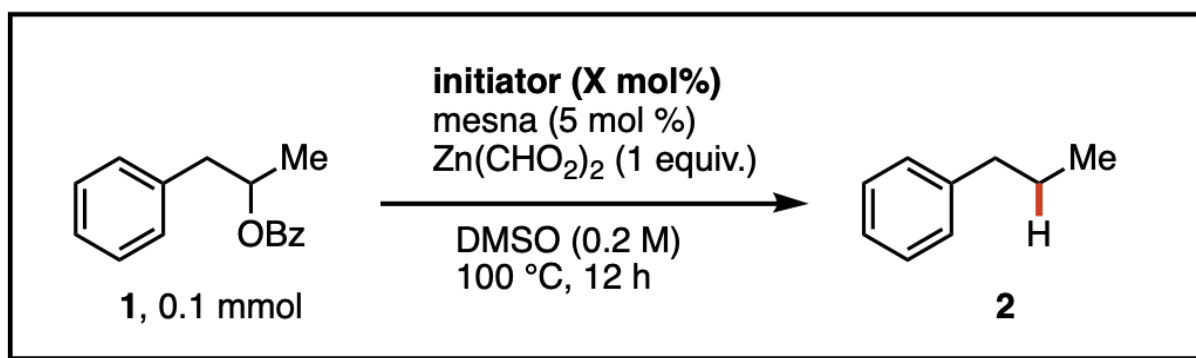
4CzIPN = 1,2,3,5-Tetrakis(carbazol-9-yl)-4,6-dicyanobenzene CAS 1416881-52-1

acridinium = 9-Mesityl-10-phenylacridinium tetrafluoroborate CAS 1621019-96-2

PhSSPh was observed to be an effective promoter of deoxygenation presumably via in situ generated PhSH acting as a Brønsted acidic fragmentation promoter. However, the catalytic reactions demonstrated poor mass balance (52 and 55%, entries 2 and 3 respectively).

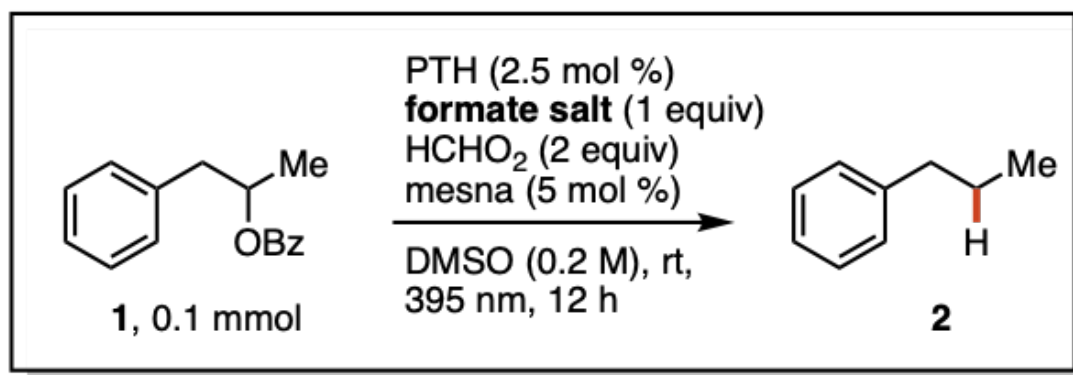
Plating of zinc(0) was observed in entries 6 and 7. Use of cesium formate instead of zinc formate led to 1% yield for both 4DPAIPN and 4CzIPN.

Thermal: To a Schlenk tube with a stir bar, a homogeneous solution of substrate (0.1 mmol), $\text{Zn}(\text{CHO}_2)_2$ (1 equiv), and mesna (5 mol %) in DMSO (0.2 M) was added. Then the initiator was added. The Schlenk tube was placed under a nitrogen atmosphere and sealed. The reactions were heated to 100 °C for 12 hours and analyzed by gas chromatography.



Entry	Initiator	Yield	Conversion
1	ammonium persulfate (20 mol%)	0	11
2	AIBN (20 mol%)	0	8

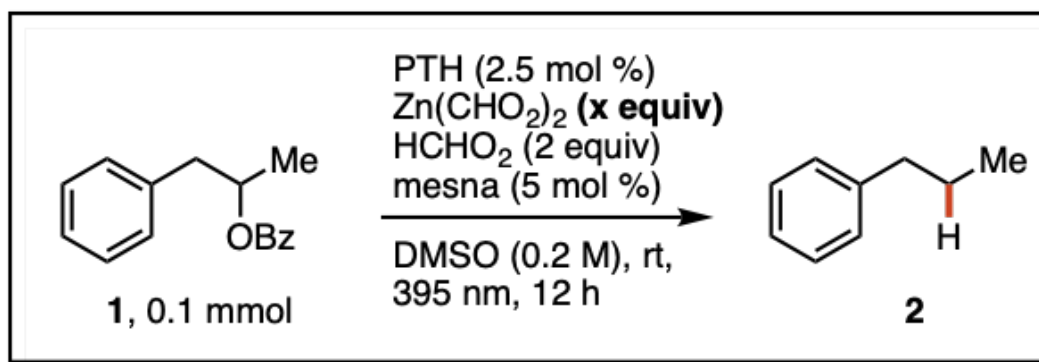
Formate Salt Screen



Entry	Formate Counterion	Yield
1	Zn	89
2	Na	43
3	K	35
4	Cs	45
5	Mg (dihydrate)	25
6	Ca	14
7	NH ₄	50

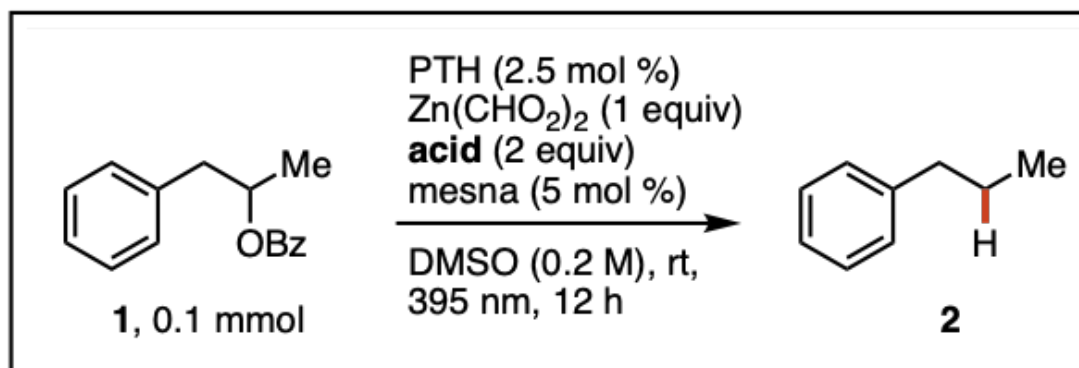
Note: Given the beneficial yields observed with the zinc counterion, we were interested in probing if DIPEA could replace zinc formate in the presence of a zinc Lewis acid. When the reaction was conducted with DIPEA and Zn(ClO₄)₂ (rather than zinc formate and formic acid), only 7% yield was observed. This is consistent with formate/CO₂^{•−} being necessary for promoting an efficient deoxygenation. We hypothesize that the zinc counterion is beneficial in part because of its Lewis acidity, but mostly due to its solubility in DMSO (homogenous at room temperature after stirring for ~5 minutes).

Zinc Formate Loading



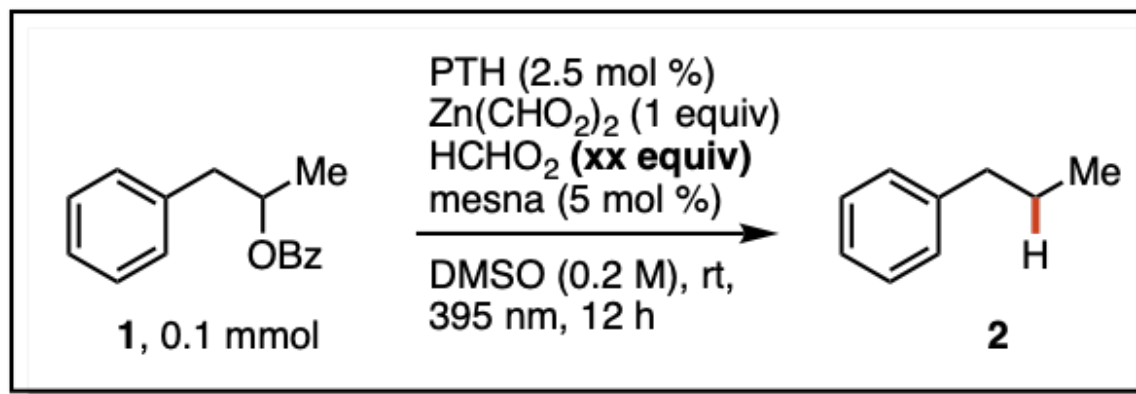
Entry	$\text{Zn}(\text{CHO}_2)_2$ Equiv	Yield
1	0	< 1
2	0.5	55
3	1.0	89
4	1.5	77

Acid Screening



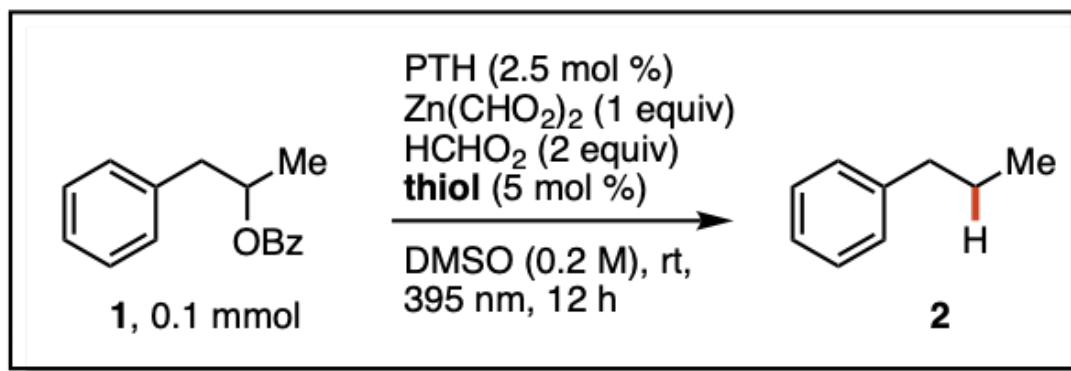
Entry	Acid	Yield
1	HCHO_2	89
2	LiClO_4	41
3	$\text{Mg}(\text{ClO}_4)_2$	50
4	$\text{Zn}(\text{ClO}_4)_2$	60
5	AcOH	69

Formic Acid Loading

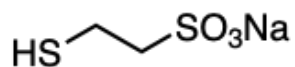


Entry	HCHO ₂ Equiv	Yield
1	0	19
2	0.5	63
3	1.0	71
4	1.5	79
5	2	89
6	4	81
7	8	73

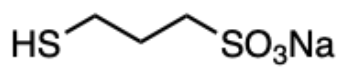
Thiol Screening



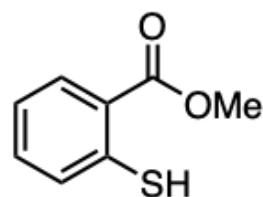
Entry	Thiol	Yield
1	mesna	89
2	CySH	62
3	methyl thiosalicylate	52
4	PhSSPh	57
5	mpsna	70



mesna

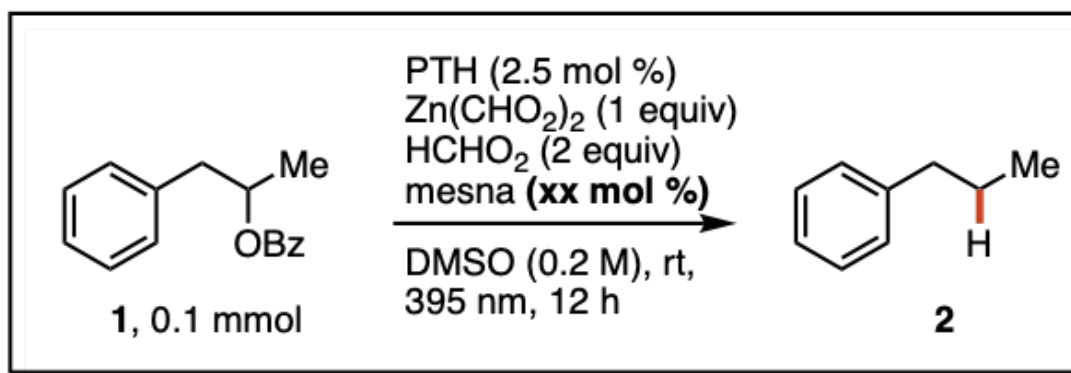


mpsna



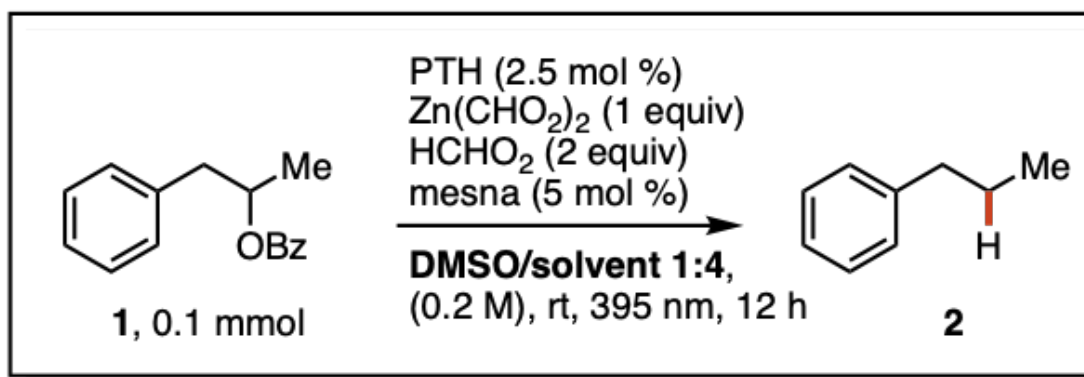
methyl thiosalicylate

Thiol Loading



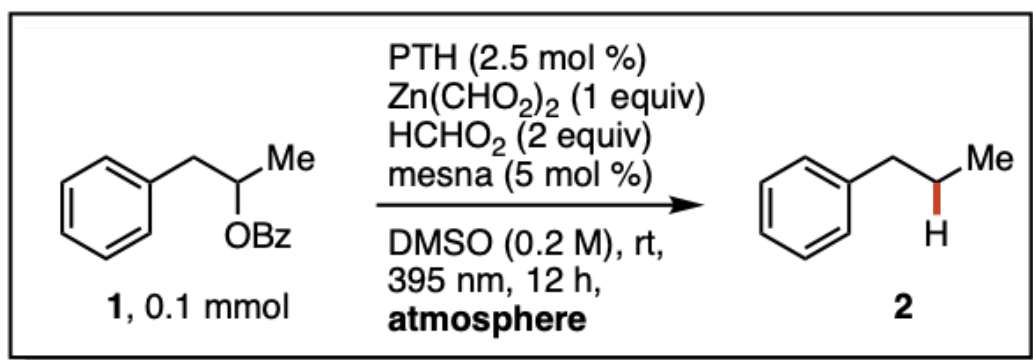
Entry	Thiol Loading	Yield
1	1	72
2	2.5	73
3	5	89
4	10	65
5	20	64

Co-Solvent Screening



Entry	Co-Solvent	Yield
1	none (DMSO)	89
2	MeCN	0
3	DMF	22
4	HFIP	1
5	PhMe	19
6	THF	22
7	tBuOH	14
8	MeOH	17
9	H ₂ O	1

Atmosphere Screening

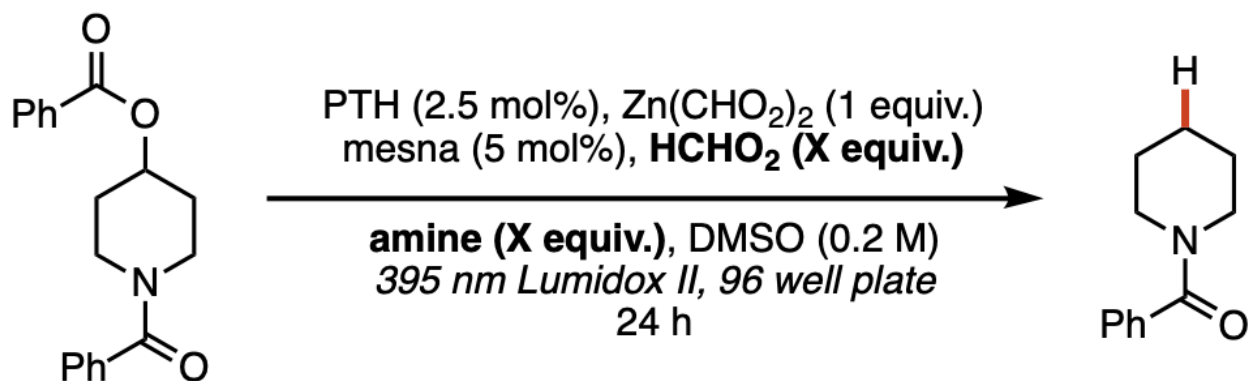


Entry	Atmosphere	Yield
1	air	83
2	N ₂	73
3	O ₂	61
4	CO ₂	69

High-throughput experimentation (HTE) screen for combination of amine type, amine loading, and formic acid loading:

We hypothesized that the solubility of zinc formate contributed to its high performance. To test if other soluble formate salts would be successful, formic acid and substoichiometric amine bases were tested. We found that they were also effective reductants.

1-benzoylpiperidin-4-yl benzoate was chosen as an adequate substrate for LCMS analysis.



A stock solution of 1-benzoylpiperidin-4-yl benzoate (356.38 mg; 1.15 mmol), mesna (9.5 mg; 57.6 μmol), PTH (7.93 mg; 28.8 μmol), and DMSO (3.84 mL) was stirred until homogeneous. This mixture was distributed into a 96 well plate. To each vial, the appropriate amount of formic acid in DMSO, and amine in DMSO were added as indicated in the results table below. Each well had 10.0 μmol of 1-benzoylpiperidin-4-yl benzoate (0.1 M in DMSO). The photo-HTE plate was sealed and irradiated with 395 nm using LumidoxII lights at stage 2 intensity for 24 hours (see below). For analysis, an aliquot was taken from each vial and analyzed by LCMS using UV peak area ratio of starting material and desired product.

Note: during the photo-HTE screening, the plate overheated (up to 70 $^{\circ}\text{C}$) causing the LEDs to turn off, resulting in non-continuous irradiation for the 24 hour reaction.

<i>formic acid (equiv.)</i>	2	2	2	2	2	1	1.5	2.5	4	1	4	8
<i>amine (equiv.)</i>	0.15	0.3	0.6	1	1.2	0.3	0.3	0.3	0.3	0.15	0.6	1.2
DIPEA												
NnBu3												
Quinuclidine												
DIPA												
Benzylamine												
pyridine												
DBU												
Hhpp												

0%

100%

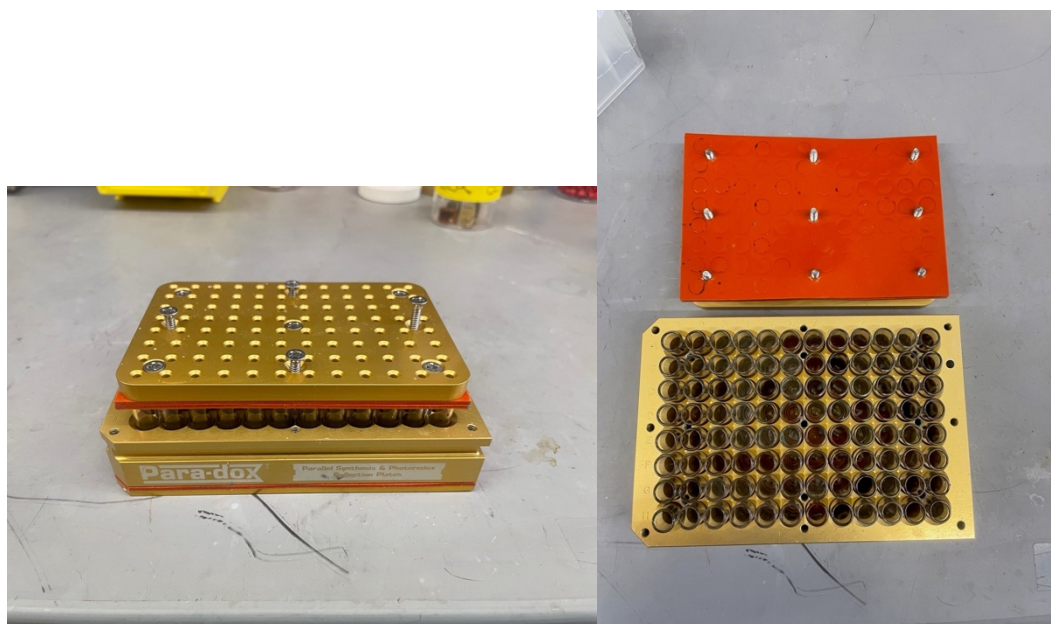
HTE plate conversion key: LCMS peak ratio of desired product/starting material

DIPEA = *N,N*-diisopropylethylamine, DIPA = diisopropylamine, DBU = diazabicycloundecene,

Hhpp = triazabicyclodecene or 1,3,4,6,7,8-Hexahydro-2*H*-pyrimido[1,2-*a*]pyrimidine.

HTE setup:

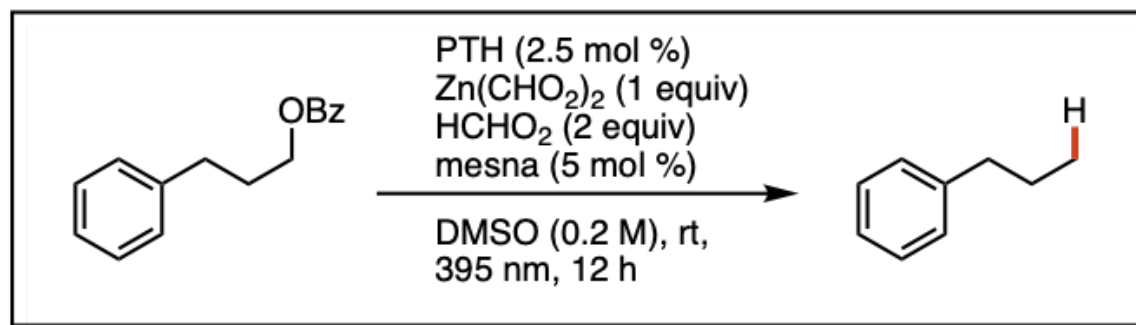
96 well plate



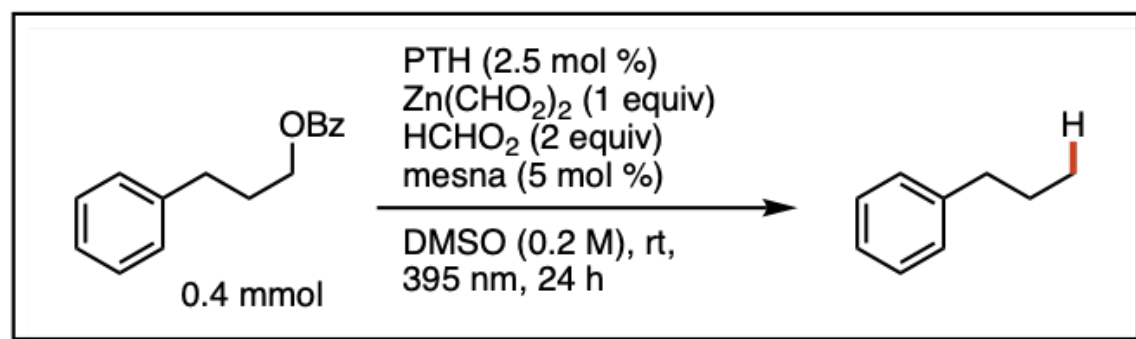
Lumidox Gen II 24-Position LED Array (LUM296DA395) used for plate irradiation



Primary Benzoate Screening



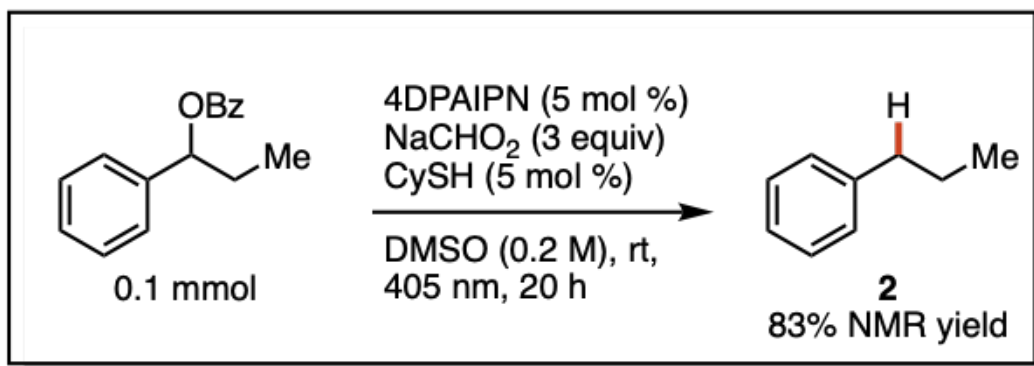
Entry	Modification	Prdt
1	none	30
2	4 eq HCHO ₂	24
3	2 eq Zn(CHO ₂) ₂	35
4	4 eq HCHO ₂ , 2 eq Zn(CHO ₂) ₂	29
5	0.5 M	22



Entry	Temp °C	Prdt	Modification
1	rt	27	—
2	60	48	—
3	80	52	—
4	110	45	—
5	60	58	48 hours

Note: For entry 5 (60 °C, 48 hours) 20% returned starting material was observed. The reaction was run for an additional 4 hours and no further conversion was observed.

Conditions for Benzylic Deoxygenation

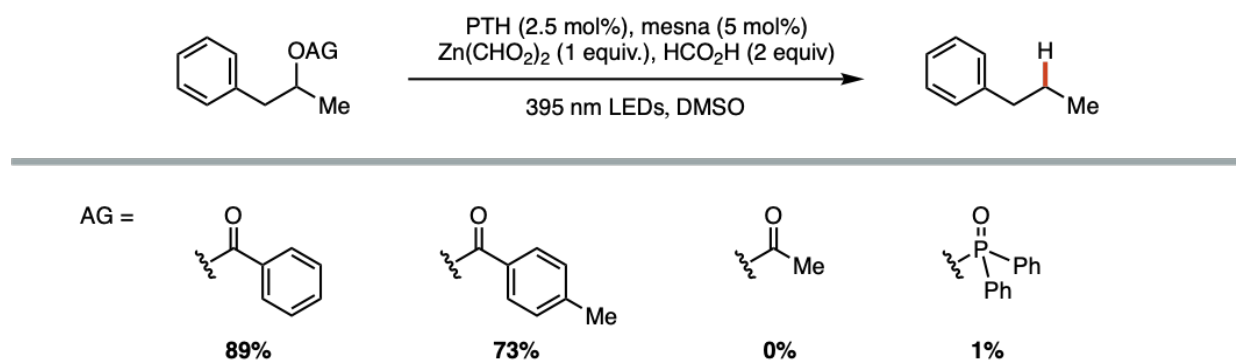


To an oven-dried 10 mL schlenk tube with flea stir bar, added 4DPAIPN (2.5 mol %) and sodium formate (3 equiv). Evacuated and backfilled the vessel with nitrogen three times. While under active nitrogen, cyclohexanethiol (5 mol %) and benzoate substrate (0.1 mmol, 1 equiv) were added to the vial, followed by degassed DMSO. The tube was sealed under nitrogen. The reaction was stirred and irradiated with a 405 nm lamp (3.5 cm from reaction vessel with fan cooling) for 20 hours total. At the 6 hour mark, an additional 2.5 mol % of 4DPAIPN was added (for 5 mol % total) as a stock solution (2.5 mol % in 100 uL degassed DMSO) while under active nitrogen. The tube was resealed under nitrogen and the reaction stirred under irradiation for the remaining 14 hours. Upon reaction completion, dibromomethane was added to the reaction as an internal standard. An aliquot was removed and transferred into a 1-dram vial with 1 mL sodium chloride (sat. aq.) and extracted with 1 mL CDCl₃. The CDCl₃ layer was separated and used for NMR analysis.

When General Procedure C was employed on the benzylic substrate above, full conversion was observed, however, yield of compound **2** was < 5 %. We hypothesize that the benzylic radical following deoxygenation undergoes undesired dimerization. Optimization attempts included lower loadings for PTH, zinc formate, formic acid, and thiol, as well as decreasing overall reaction concentration. All attempts led to nearly full conversion of the substrate with < 5 % yield of desired product **2**.

Conversely, the 4DPAIPN conditions above work efficiently for the benzylic substrate. However, unactivated substrates such as compound **1** only lead to < 5 % deoxygenation under 4DPAIPN conditions.

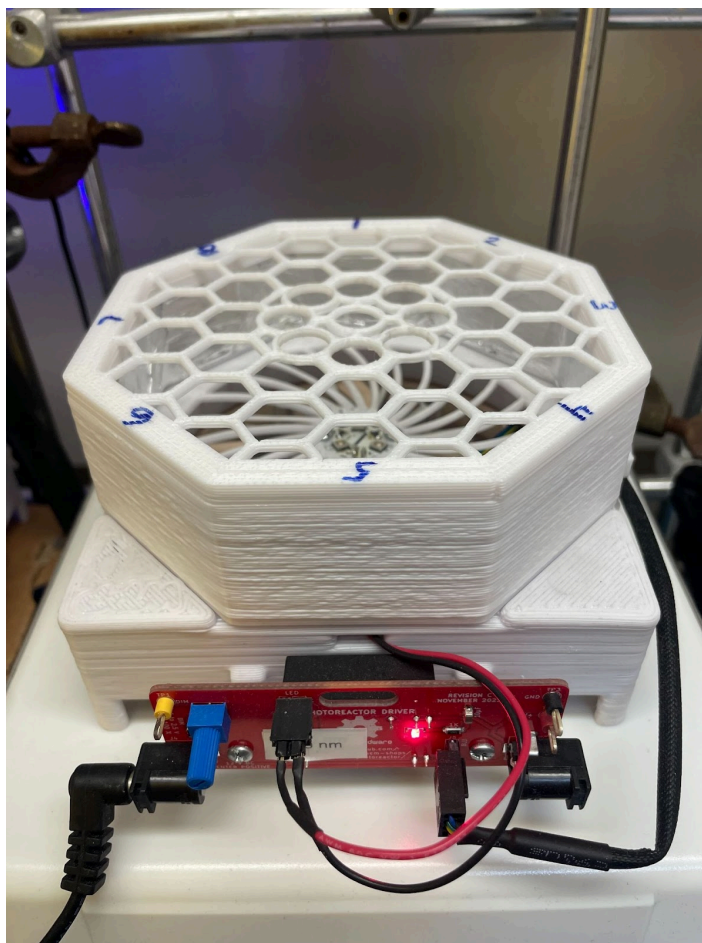
Alternative Activating Groups



Remaining mass balance was returned starting material.

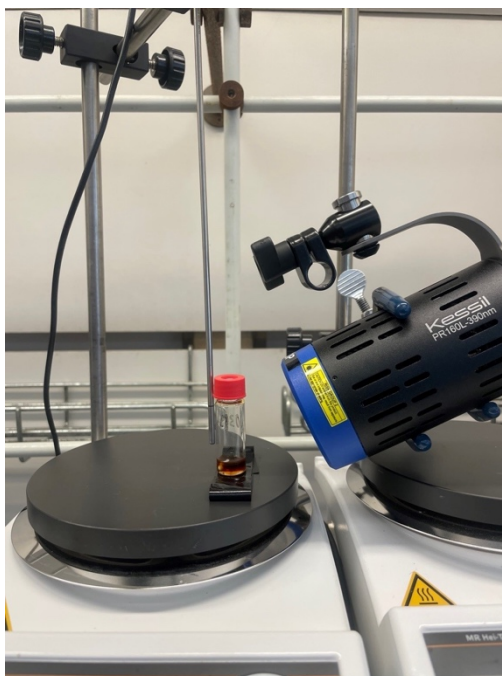
4. 5. 6. Alternative Reaction Setups

Standard Photoreactor Setup



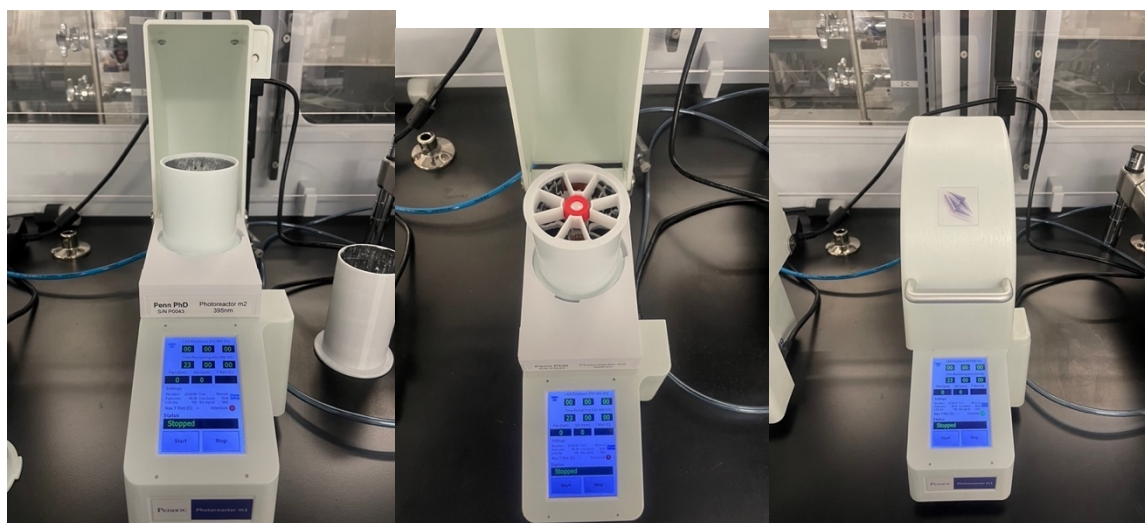
General procedure C was followed using secondary benzoate **1** (0.1 mmol scale) in the standard photoreactor with 395 nm LEDs to give 89% yield of the desired product **2**. Yield was determined by GC using tert-butyl benzene as an internal standard.

Kessil Lamp Setup



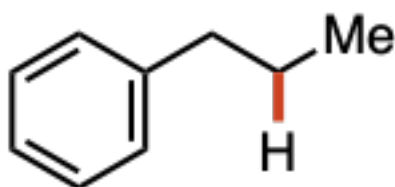
General procedure C was followed using secondary benzoate **1** (0.2 mmol scale) and a 390 nm Kessil lamp with fan cooling to give 80% yield of the desired product **2**. Yield was determined by NMR using CH_2Br_2 as an internal standard.

Pennoc Reactor Setup

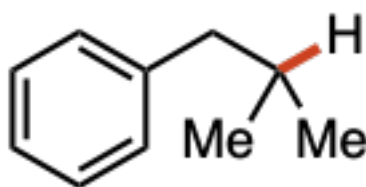


General procedure C was followed from secondary benzoate **1** (0.2 mmol scale) using a Pennoc reactor (Penn PhD Photoreactor M2, Sigma-Aldrich Z744035) to give 80% yield of the desired product **2**. Yield was determined by NMR using CH₂Br₂ as an internal standard.

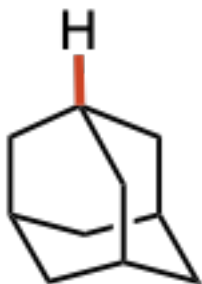
4. 5. 7. Product Characterization



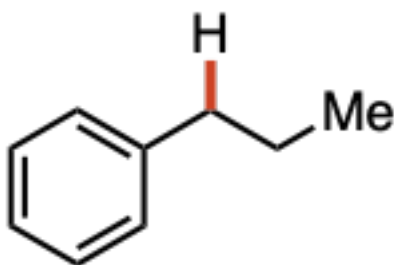
propylbenzene (2): Compound was synthesized from 1-phenylpropan-2-yl benzoate according to General Procedure C on 0.4 mmol scale. 89% yield was observed via gas chromatography.



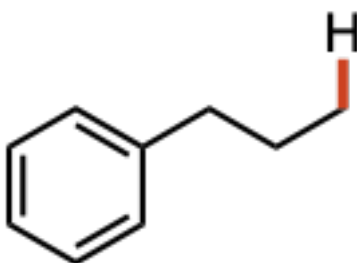
Isobutylbenzene (3): Compound was synthesized from 2-methyl-1-phenylpropan-2-yl benzoate according to General Procedure C on 0.1 mmol scale in DMSO-d₆. 96% yield was observed via ¹H NMR. NMR spectrum in accordance with literature: *JACS*, **2015**, 137, 35, 11340–11348



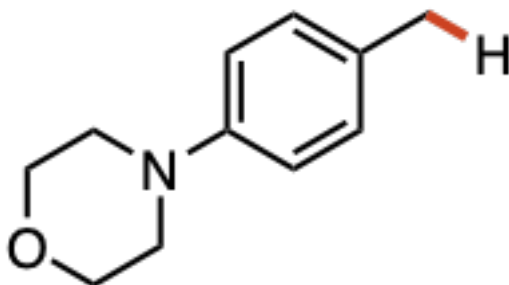
Adamantane (4): Compound was synthesized from adamantan-1-yl benzoate according to General Procedure C on 0.4 mmol scale. 72% yield was observed via ^1H NMR. NMR spectrum in accordance with literature: *Org. Lett.* **2022**, 24, 2, 686–691.



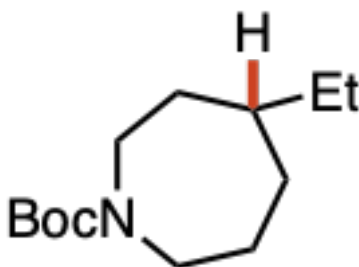
propylbenzene (5): Compound was synthesized from 1-phenylpropyl benzoate according to General Procedure E on 0.4 mmol scale. 83% yield was observed via gas chromatography.



propylbenzene (6): Compound was synthesized from 3-phenylpropyl benzoate according to General Procedure D on 0.4 mmol scale. 58% yield was observed via gas chromatography.

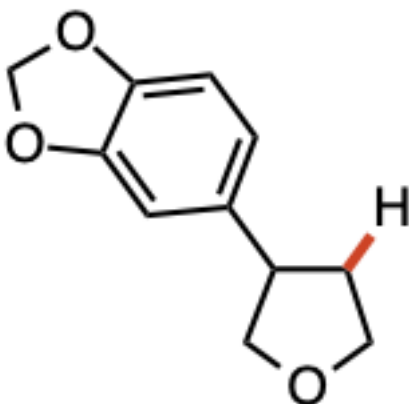


4-(p-tolyl)morpholine (7): Compound was synthesized from 4-morpholinobenzyl benzoate according to General Procedure E on a 0.4 mmol scale. 63 mg (89% yield) was obtained as a white crystalline solid. $^1\text{H NMR}$ (400 MHz, CDCl_3) δ 7.12 (d, J = 8.3 Hz, 2H), 6.86 (d, J = 8.6 Hz, 2H), 3.99 – 3.73 (m, 4H), 3.43 – 2.96 (m, 4H), 2.30 (s, 3H). Spectrum in accordance with literature: *J. Am. Chem. Soc.* **2018**, 140, 24, 7667–7673.

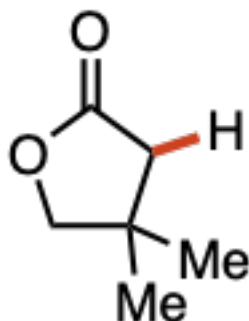


tert-butyl 4-ethylazepane-1-carboxylate (8): Compound was synthesized from tert-butyl 4-(benzyloxy)-4-ethylazepane-1-carboxylate according to General Procedure C on 0.4 mmol scale. 74% yield was obtained as a colorless oil. $^1\text{H NMR}$ (500 MHz, CDCl_3) δ 3.65 – 3.06 (m, 4H), 1.80 (s, 2H), 1.71 (d, J = 13.2 Hz, 1H), 1.60 – 1.49 (m, 1H), 1.46 (s, 9H), 1.36 – 1.20 (m, 4H), 1.14 (s, 1H), 0.88 (td, J = 7.1, 2.2 Hz, 3H). $^{13}\text{C NMR}$ (126 MHz, CDCl_3) δ 155.83, 79.03, 46.94, 46.45, 45.61, 45.22, 41.07, 40.52, 34.67, 34.50, 33.45, 32.80, 30.20, 28.70, 27.38, 27.14, 11.86

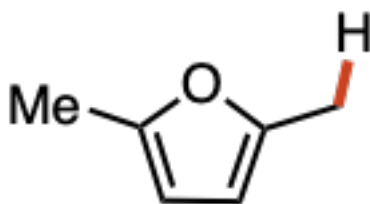
(rotamers observed). **HRMS** (ESI⁺) Calc: [M+Na]⁺ for C₁₃H₂₅NO₂ = 250.1778; measured 250.1774 = 1.6 ppm difference.



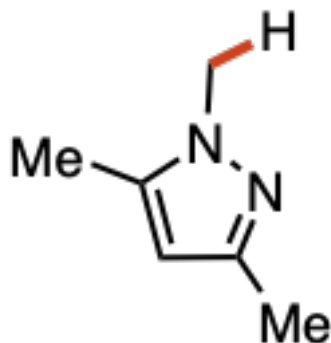
5-(tetrahydrofuran-3-yl)benzo[d][1,3]dioxole (9): Compound was synthesized from *trans*-4-(benzo[d][1,3]dioxol-5-yl)tetrahydrofuran-3-yl benzoate according to General Procedure C on 0.4 mmol scale. 70% yield was obtained as a colorless oil. **¹H NMR** (500 MHz, CDCl₃) δ 6.77 – 6.72 (m, 2H), 6.69 (dd, *J* = 8.0, 1.8 Hz, 1H), 5.92 (s, 2H), 4.09 (t, *J* = 8.0 Hz, 1H), 4.04 (td, *J* = 8.4, 4.5 Hz, 1H), 3.89 (q, *J* = 7.9 Hz, 1H), 3.66 (dd, *J* = 8.4, 7.5 Hz, 1H), 3.33 (p, *J* = 7.8 Hz, 1H), 2.32 (dtd, *J* = 12.3, 7.7, 4.5 Hz, 1H), 1.94 (dq, *J* = 12.4, 8.1 Hz, 1H). **¹³C NMR** (126 MHz, CDCl₃) δ 147.96, 146.21, 136.66, 120.32, 108.31, 107.63, 101.02, 74.81, 68.54, 44.87, 34.85. **HRMS** (ESI⁺) Calc: [M+H]⁺ for C₁₁H₁₂O₃ = 193.0859; measured 193.0859 = <0.1 ppm difference.



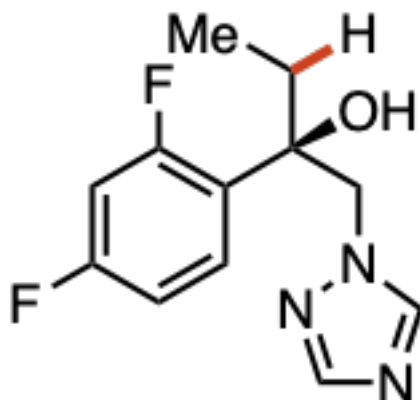
4,4-dimethyldihydrofuran-2(3H)-one (10): Compound was synthesized from (2R)-2-benzoyloxy-3,3-dimethyl-4-butanolide according to General Procedure C on 0.4 mmol scale. 80% yield was observed via ^1H NMR. NMR spectrum in accordance with literature: *Org. Lett.* 2016, 18, 24, 6472–6475.



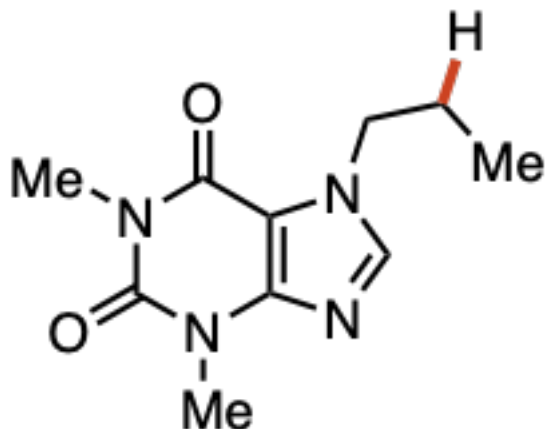
2,5-dimethylfuran (11): Compound was synthesized from (5-methylfuran-2-yl)methyl benzoate according to General Procedure E except without CySH on a 0.4 mmol scale. 64% yield was observed via ^1H NMR. Product was also confirmed via GC by comparing with an authentic sample of product. Spectrum in accordance with literature: *Org. Process Res. Dev.* **2021**, 25, 4, 892–899.



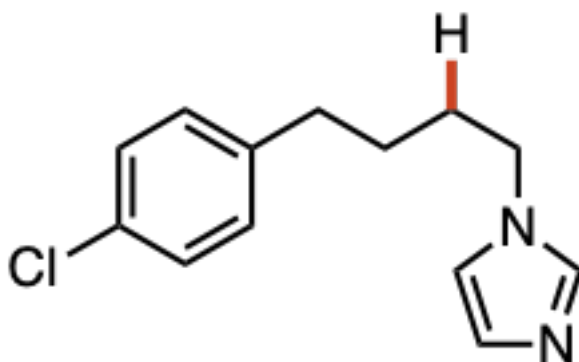
1,3,5-trimethyl-pyrazole (12): Compound was synthesized from (3,5-dimethyl- pyrazol-1-yl)methyl benzoate according to General Procedure E on a 0.4 mmol scale. 92% yield was observed via ^1H NMR. Spectrum in accordance with literature: *J. Org. Chem.* 791, **2015** 303-310.



(R)-2-(2,4-difluorophenyl)-1-(1H-1,2,4-triazol-1-yl)butan-2-ol (13): Compound was synthesized from (2R,3R)-3-(2,4-difluorophenyl)-3-hydroxy-4-(1,2,4-triazol-1-yl)butan-2-yl benzoate according to General Procedure C on a 0.4 mmol scale. >99% yield was observed via ^1H NMR. Spectrum in accordance with literature: *Euro. J. Med. Chem.* 133 (**2017**) 309-318.

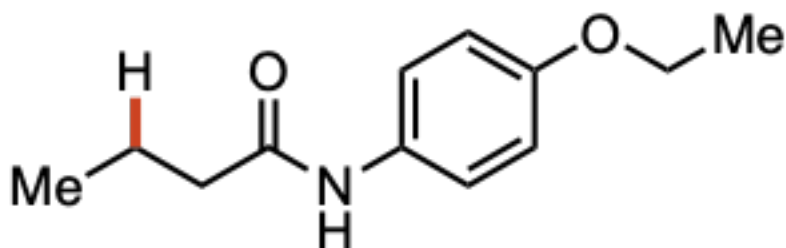


1,3-dimethyl-7-propyl-3,7-dihydro-1H-purine-2,6-dione (14): Compound was synthesized from 1-(1,3-dimethyl-2,6-dioxo-1,2,3,6-tetrahydro-7H-purin-7-yl)propan-2-yl benzoate according to General Procedure C on 0.4 mmol scale with the modification of running for 48 hours. 70% yield was obtained as a white solid. **¹H NMR** (400 MHz, CDCl₃) δ 7.53 (s, 1H), 4.25 (t, J = 7.1 Hz, 2H), 3.59 (s, 3H), 3.41 (s, 3H), 1.91 (h, J = 7.4 Hz, 2H), 0.95 (t, J = 7.4 Hz, 3H). Spectrum in accordance with literature: *Org. Lett.* **2011**, 13, 6, 1378–1381.

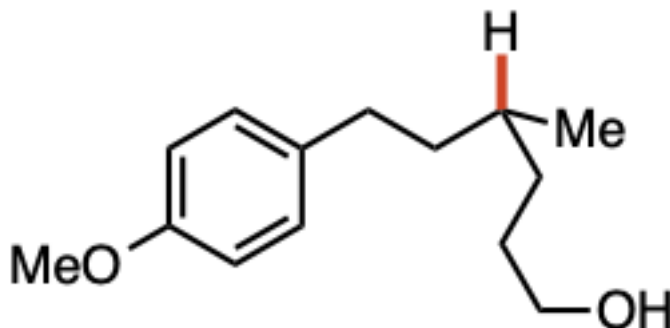


1-(4-(4-chlorophenyl)butyl)-imidazole (15): Compound was synthesized from 4-(4-chlorophenyl)-1-(imidazol-1-yl)butan-2-yl benzoate according to General Procedure C on 0.4 mmol scale. 89% yield was obtained as a pale yellow oil. **¹H NMR** (400 MHz, CDCl₃) δ 7.39 (s, 1H), 7.25 – 7.09 (m, 2H), 7.06 – 6.93 (m, 3H), 6.80 (s, 1H), 3.86 (t, J = 7.0 Hz, 2H), 2.52 (t, J =

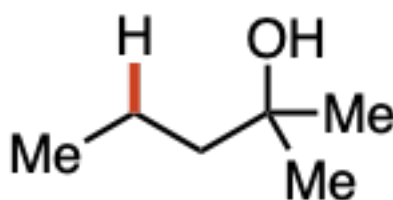
7.6 Hz, 2H), 1.72 (p, $J = 7.1$ Hz, 2H), 1.52 (p, $J = 7.7$ Hz, 2H). **^{13}C NMR** (101 MHz, CDCl_3) δ 139.87, 137.05, 131.79, 129.68, 129.47, 128.56, 118.74, 46.86, 34.63, 30.49, 28.18. **HRMS** (ESI^+) Calc: $[\text{M}+\text{H}]^+$ for $\text{C}_{13}\text{H}_{15}\text{ClN}_2 = 235.0997$; measured 235.0994 = 1.3 ppm difference.



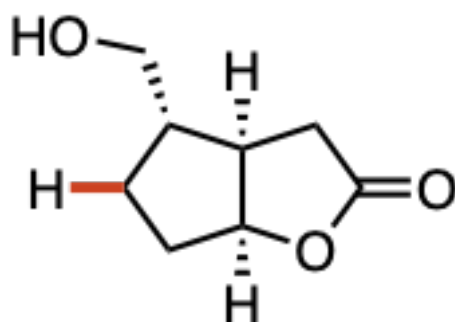
N-(4-ethoxyphenyl)butyramide (16): Compound was synthesized from 4-((4-ethoxyphenyl)amino)-4-oxobutan-2-yl benzoate according to General Procedure C on 0.4 mmol scale. 58% was obtained as a white solid. **^1H NMR** (600 MHz, CDCl_3) δ 7.39 (d, $J = 8.9$ Hz, 2H), 7.04 (s, 1H), 6.84 (d, $J = 8.9$ Hz, 2H), 4.01 (q, $J = 7.0$ Hz, 2H), 2.31 (t, $J = 7.5$ Hz, 2H), 1.75 (p, $J = 7.4$ Hz, 2H), 1.40 (t, $J = 7.0$ Hz, 3H), 1.01 (t, $J = 7.4$ Hz, 3H). **^{13}C NMR** (151 MHz, CDCl_3) δ 171.00, 155.72, 130.92, 121.69, 114.78, 63.71, 39.57, 19.15, 14.85, 13.79. **HRMS** (ESI^+) Calc: $[\text{M}+\text{H}]^+$ for $\text{C}_{12}\text{H}_{17}\text{NO}_2 = 208.1332$; measured 208.1331 = 0.5 ppm difference.



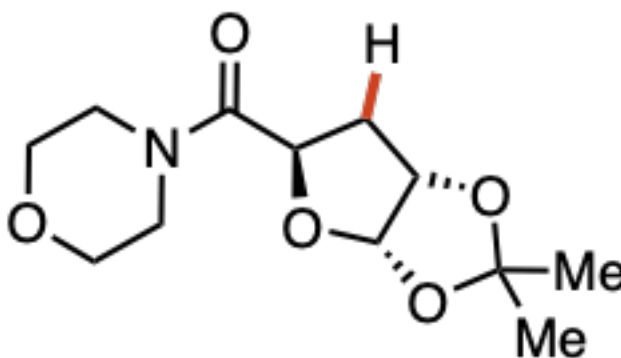
6-(4-methoxyphenyl)-4-methylhexan-1-ol (17): Compound was synthesized from 6-hydroxy-1-(4-methoxyphenyl)-3-methylhexan-3-yl benzoate according to General Procedure C on 0.4 mmol scale. 81% yield was obtained as a colorless oil. **¹H NMR** (500 MHz, CDCl₃) δ 7.09 (d, J = 8.6 Hz, 2H), 6.82 (d, J = 8.6 Hz, 2H), 3.79 (s, 3H), 3.63 (t, J = 6.6 Hz, 2H), 2.60 (ddd, J = 13.5, 10.2, 5.3 Hz, 1H), 2.52 (ddd, J = 13.7, 9.8, 6.1 Hz, 1H), 1.67 – 1.36 (m, 6H), 1.36 – 1.15 (m, 2H), 0.94 (d, J = 6.3 Hz, 3H). **¹³C NMR** (126 MHz, CDCl₃) δ 157.77, 135.18, 129.32, 113.87, 63.54, 55.41, 39.22, 32.96, 32.61, 32.37, 30.40, 19.68. **HRMS** (ESI⁺) Calc: [M+NH₄]⁺ for C₁₄H₂₂O₂ = 240.1958; measured 240.1955 = 1.2 ppm difference.



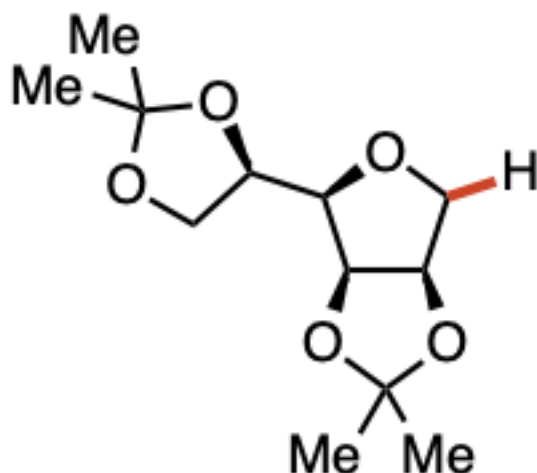
2-methylpentan-2-ol (18): Compound was synthesized from 4-Benzoyloxy-2-methyl-2-pentanol according to General Procedure C on 0.4 mmol scale. 93% yield was observed via ¹H NMR. **¹H NMR** (600 MHz, CDCl₃) δ 1.44 – 1.40 (m, 2H), 1.39 – 1.30 (m, 2H), 1.18 (s, 6H), 0.91 (t, J = 7.2 Hz, 3H). **¹³C NMR** (151 MHz, CDCl₃) δ 71.01, 46.35, 29.18, 17.58, 14.62. **HRMS** (ESI⁺) Calc: [M+H]⁺ for C₁₅H₂₂ClNO₂ = 120.1383; measured 120.1382 = 0.8 ppm difference.



(3aR,4S,6aS)-4-(hydroxymethyl)hexahydro-2H-cyclopenta[b]furan-2-one (19): Compound was synthesized from (3aR,4S,5R,6aS)-4-(hydroxymethyl)-2-oxohexahydro-2H-cyclopenta[b]furan-5-yl benzoate according to General Procedure C on 0.4 mmol scale. Reaction was run for 48 hours using the *Kessil Lamp Setup* (see section 5. **Alternative Reaction Setups**). 86% yield was obtained as colorless oil. ¹H NMR (600 MHz, CDCl₃) δ 4.98 (td, *J* = 6.4, 2.2 Hz, 1H), 3.62 (dd, *J* = 10.5, 6.1 Hz, 1H), 3.55 (dd, *J* = 10.5, 6.7 Hz, 1H), 2.82 (dd, *J* = 18.2, 9.7 Hz, 1H), 2.64 – 2.59 (m, 1H), 2.44 (dd, *J* = 18.3, 2.1 Hz, 1H), 2.08 – 2.02 (m, 1H), 2.01 – 1.90 (m, 3H), 1.56 – 1.47 (m, 1H). Spectra in accordance with literature: *J. Org. Chem.* **1995**, 60, 5319-5323.

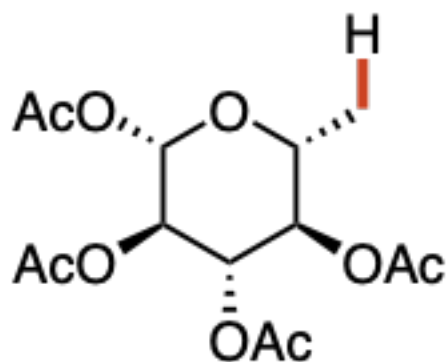


((3aS,5R,6aS)-2,2-dimethyltetrahydrofuro[2,3-d][1,3]dioxol-5-yl)(morpholino) methanone (20): Compound was synthesized from (3aS,5R,6S,6aS)-2,2-dimethyl-5- (morpholine-4-carbonyl)tetrahydrofuro[2,3-d][1,3]dioxol-6-yl benzoate according to General Procedure D on a 0.4 mmol scale. 73 mg (71% yield) was obtained as a colorless oil. ¹H NMR (500 MHz, CDCl₃) δ 5.86 (d, *J* = 3.6 Hz, 1H), 4.90 – 4.66 (m, 2H), 3.92 – 3.59 (m, 6H), 3.50 (dddd, *J* = 16.8, 13.1, 7.5, 3.3 Hz, 2H), 2.33 (ddd, *J* = 13.9, 10.4, 4.7 Hz, 1H), 2.22 (dd, *J* = 13.9, 5.0 Hz, 1H), 1.51 (s, 3H), 1.33 (s, 3H). ¹³C NMR (126 MHz, CDCl₃) δ 167.25, 111.35, 105.84, 79.79, 74.92, 66.97, 66.76, 46.09, 42.54, 35.45, 26.94, 26.02. **HRMS** (ESI⁺) Calc: [M+H]⁺ for C₁₂H₁₉NO₅ = 258.1336; measured 258.1332 = 0.8 ppm difference.

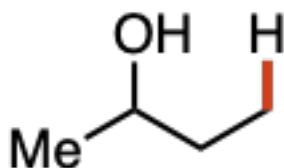


(3aR,4R,6aS)-4-((S)-2,2-dimethyl-1,3-dioxolan-4-yl)-2,2-dimethyltetrahydrofuro[3,4-

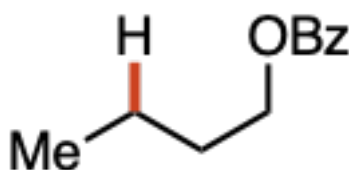
d][1,3]dioxole (21): Compound was synthesized from 2,3:5,6-Di-O-isopropylidene- α -mannofuranosyl benzoate according to General Procedure C on 0.4 mmol scale. 95% yield was obtained as a white solid without need for flash chromatography. $^1\text{H NMR}$ (400 MHz, CDCl_3) δ 4.69 (ddd, $J = 22.0, 6.2, 3.6$ Hz, 2H), 4.34 (ddd, $J = 7.2, 6.1, 4.9$ Hz, 1H), 4.10 – 3.94 (m, 3H), 3.42 (ddd, $J = 10.0, 9.0, 3.6$ Hz, 2H), 1.42 (s, 3H), 1.38 (s, 3H), 1.31 (s, 3H), 1.27 (s, 3H). Spectrum in accordance with literature: *Chem. Eur. J.* **2010**, 16, 8545 – 8556.



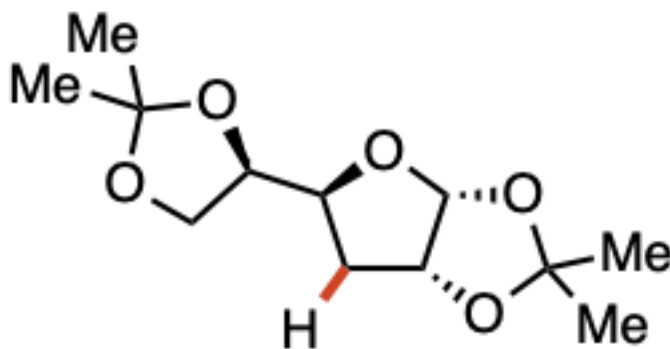
(2S,3R,4S,5R,6R)-6-methyltetrahydro-2H-pyran-2,3,4,5-tetraol tetraacetate (22): Compound was synthesized from (2S,3R,4S,5R,6R)-6-((benzoyloxy)methyl)tetrahydro-2H-pyran-2,3,4,5-tetraol tetraacetate according to General Procedure D on 0.4 mmol scale. 69% yield was obtained as a colorless oil. $^1\text{H NMR}$ (400 MHz, CDCl_3) δ 5.69 (d, $J = 8.2$ Hz, 1H), 5.21 (t, $J = 9.5$ Hz, 1H), 5.10 (dd, $J = 9.6, 8.2$ Hz, 1H), 4.86 (t, $J = 9.6$ Hz, 1H), 3.71 (dq, $J = 9.7, 6.1$ Hz, 1H), 2.11 (s, 3H), 2.05 (s, 3H), 2.03 (s, 3H), 2.01 (s, 3H), 1.24 (d, $J = 3.0$ Hz, 3H). Spectrum in accordance with literature: *Org. Process Res. Dev.* **2014**, 18, 12, 1728–1739.



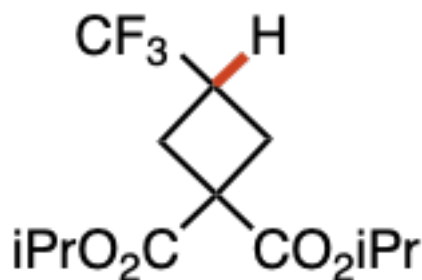
butan-2-ol (24): Compound was synthesized from 3-hydroxybutyl benzoate according to General Procedure D except in DMSO-d_6 at 80°C on a 0.4 mmol scale. 78% yield was observed via $^1\text{H NMR}$. Spectrum in accordance with literature: *Green Chem.*, **2021**, 23, 8428-8433.



butyl benzoate (25): Compound was synthesized from butane-1,3-diyl dibenzoate according to General Procedure C except in DMSO-d_6 for 48 h on a 0.4 mmol scale. 80% yield was observed via $^1\text{H NMR}$. Spectrum in accordance with literature: *Chem. Asian J.* **2019**, 14, 2639.



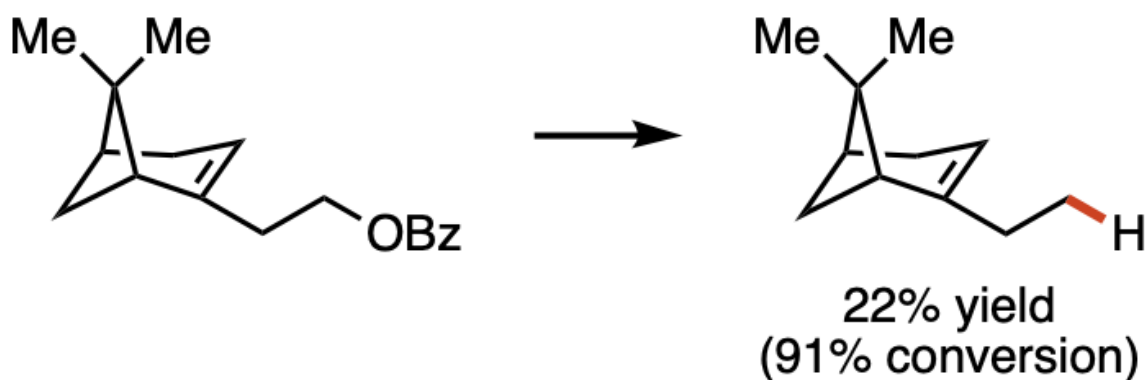
(3aR,5S,6aR)-5-((S)-2,2-dimethyl-1,3-dioxolan-4-yl)-2,2-dimethyltetrahydrofuro[2,3-d][1,3]dioxole (27): Compound was synthesized from 1,2:5,6-Di-O-isopropylidene- α -D-glucofuranosyl benzoate according to General Procedure C on 0.4 mmol scale with the modification of running for 48 hours. 77% yield was obtained as a white solid. Note: 54% isolated yield when ran for the standard 24 hours. $^1\text{H NMR}$ (400 MHz, CDCl_3) δ 5.81 (d, $J = 3.6$ Hz, 1H), 4.75 (dd, $J = 4.8, 3.7$ Hz, 1H), 4.36 – 4.00 (m, 3H), 3.93 – 3.68 (m, 1H), 2.18 (dd, $J = 13.4, 4.1$ Hz, 1H), 1.76 (ddd, $J = 13.5, 10.0, 4.8$ Hz, 1H), 1.51 (s, 3H), 1.42 (s, 3H), 1.35 (s, 3H), 1.31 (s, 3H). Spectrum in accordance with literature: *Eur. J. Org. Chem.* **2019**, 2224–2233.



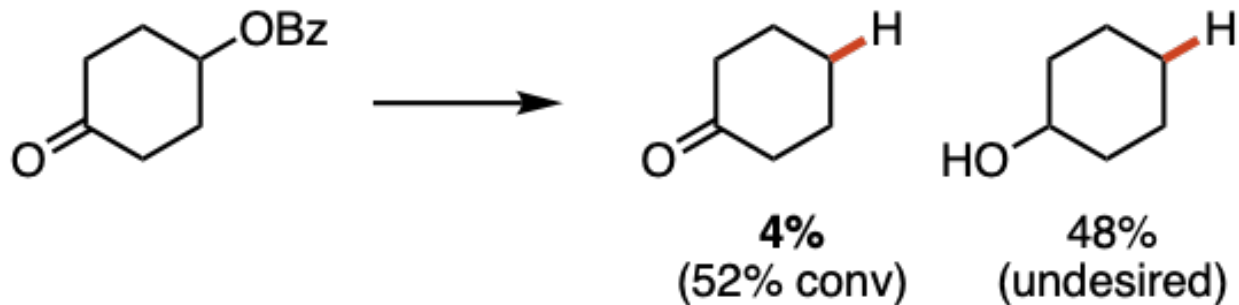
diisopropyl 3-(trifluoromethyl)cyclobutane-1,1-dicarboxylate (29): Compound was synthesized from diisopropyl 3-(benzoyloxy)-3-(trifluoromethyl)cyclobutane-1,1-dicarboxylate according to General Procedure C on a 0.4 mmol scale. 115 mg (97% yield) was obtained as pale

yellow oil. $^1\text{H NMR}$ (500 MHz, CDCl_3) δ 5.16 – 4.94 (m, J = 6.2 Hz, 2H), 3.02 (dq, J = 17.6, 8.8 Hz, 1H), 2.79 – 2.33 (m, 4H), 1.24 (dd, J = 6.3, 4.3 Hz, 12H). Spectrum in accordance with literature: *Org. Process Res. Dev.* **2021**, 25, 1, 82–88.

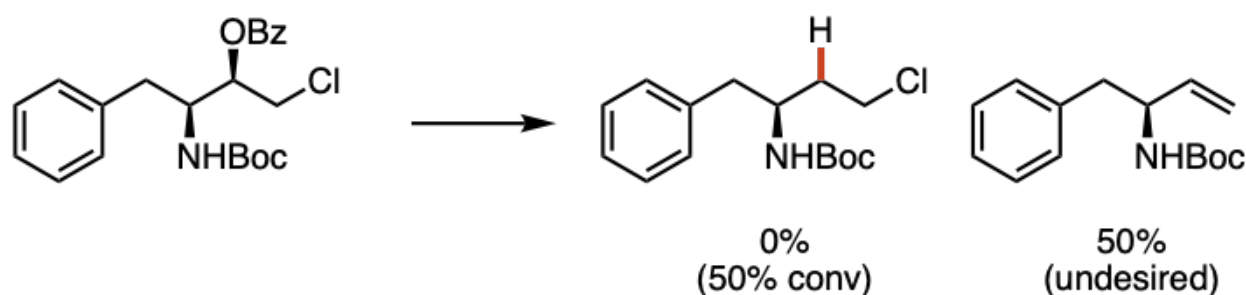
4. 5. 8. Failed Scope Entries



Compound was subjected to General Procedure D. Low mass balance possibly due to alkene hydrocarboxylation. For examples of alkene hydrocarboxylation using formate, see: *JACS*, **2021**, 143, 33, 13022-13028.

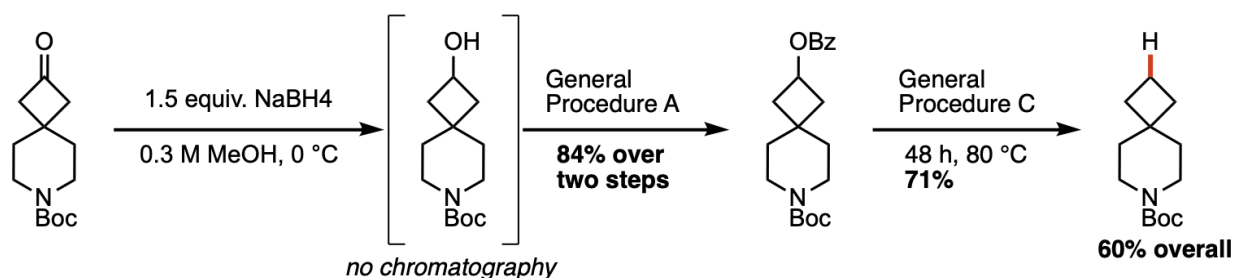


Compound was subjected to General Procedure C. Ketone reduction was observed in addition to deoxygenation. For examples of carbonyl reduction using formate, see: *JACS*, **2021**, 143, 24, 8987-8992.



Compound was subjected to General Procedure C. Elimination product was observed possibly via alkyl chloride reduction followed by reduction of alkyl radical to an anion. For examples of alkyl chloride reduction using potent reductants, see: *Nature Catalysis*, **2020**, 3, 872-886.

4. 5. 9. Synthetic Sequences

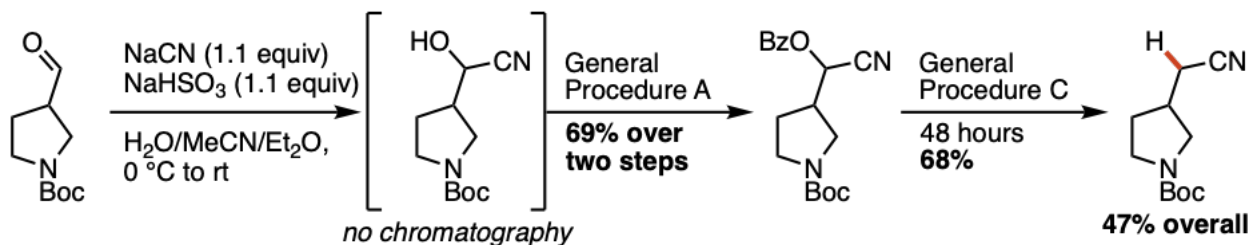


tert-butyl 2-hydroxy-7-azaspiro[3.5]nonane-7-carboxylate: To a round bottom flask equipped with a stir bar, the ketone (479 mg, 2.00 mmol) was dissolved in MeOH (0.3 M, 7 mL). The flask was cooled to 0 °C. Sodium borohydride (113 mg, 3 mmol, 1.5 equiv) was added portionwise. After reaction completion, MeOH was removed under reduced pressure and then the reaction

contents were taken up in EtOAc. The organic layer was washed once with 1 M HCl (aq.), twice with saturated NaCl (aq.), then dried over sodium sulfate, filtered, and concentrated *in vacuo*. The crude material was carried forward to the benzylation conditions without further purification as a colorless oil.

tert-butyl 2-(benzyloxy)-7-azaspiro[3.5]nonane-7-carboxylate: Benzylation of tert-butyl 2-hydroxy-7-azaspiro[3.5]nonane-7-carboxylate was performed according to General Procedure A on a 2.00 mmol scale and was purified via flash chromatography. 582 mg and 84% yield was obtained as a white solid. **¹H NMR** (500 MHz, CDCl₃) δ 8.07 – 8.01 (m, 2H), 7.59 – 7.52 (m, 1H), 7.44 (dd, *J* = 8.5, 7.1 Hz, 2H), 5.30 – 5.20 (m, 1H), 3.41 – 3.35 (m, 2H), 3.35 – 3.30 (m, 2H), 2.49 – 2.41 (m, 2H), 2.02 – 1.94 (m, 2H), 1.59 (q, *J* = 4.4, 3.2 Hz, 4H), 1.45 (s, 9H). **¹³C NMR** (126 MHz, CDCl₃) δ 166.26, 155.06, 133.09, 130.41, 129.70, 128.49, 79.53, 66.30, 39.82, 39.27, 36.55, 32.37, 28.61. **HRMS** (ESI⁺) Calc: [M+Na]⁺ for C₂₀H₂₇NO₄ = 368.1832; measured 368.1828 = 1.1 ppm difference.

tert-butyl 7-azaspiro[3.5]nonane-7-carboxylate (31): Compound was synthesized from tert-butyl 2-(benzyloxy)-7-azaspiro[3.5]nonane-7-carboxylate according to General Procedure C on 0.4 mmol scale with the modification of running for 48 hours at 80 °C. 71% yield deoxygenation (60% overall yield from ketone) was obtained as a pale yellow oil. **¹H NMR** (500 MHz, CDCl₃) δ 3.33 – 3.27 (m, 4H), 1.94 – 1.84 (m, 2H), 1.79 – 1.72 (m, 4H), 1.52 (t, *J* = 5.7 Hz, 4H), 1.45 (s, 9H). **¹³C NMR** (126 MHz, CDCl₃) δ 155.18, 79.28, 37.97, 37.51, 31.68, 28.63, 15.25. **HRMS** (ESI⁺) Calc: [M+H]⁺ for C₁₃H₂₃NO₂ = 226.1802; measured 226.1799 = 1.3 ppm difference.

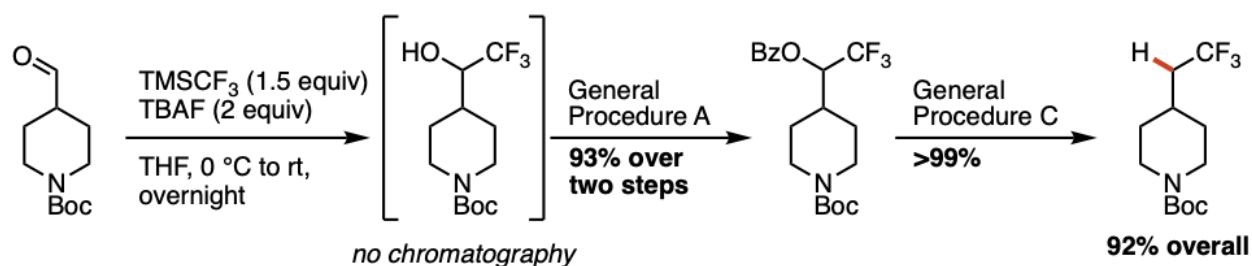


tert-butyl 3-(cyano(hydroxy)methyl)pyrrolidine-1-carboxylate: To a flame-dried 100 mL round bottom flask equipped with stir bar under nitrogen, sodium bisulfite (2.8 mmol, 1.1 equiv) was added and dissolved in 25 mL water then cooled to $0\text{ }^\circ\text{C}$. The aldehyde starting material (500 mg, 2.5 mmol) was dissolved in 2:1 water:MeCN (3 mL) then added dropwise to the bisulfite solution and stirred at $0\text{ }^\circ\text{C}$ for 40 minutes. Sodium cyanide (2.8 mmol, 1.1 equiv) was then dissolved in 2 mL water and added dropwise to the reaction mixture and stirred at $0\text{ }^\circ\text{C}$ for 1 hour. Finally, 15 mL diethyl ether was added and stirred at room temperature for 20 minutes. The organic layer was separated and extracted twice with 5 mL diethyl ether. The ether layer was washed with sodium chloride (sat. aq.), then dried over sodium sulfate, filtered, and concentrated *in vacuo*. The crude material was carried forward to the benzylation conditions without further purification as a colorless oil.

tert-butyl 3-((benzyloxy)(cyano)methyl)pyrrolidine-1-carboxylate: Starting with tert-butyl 3-(cyano(hydroxy)methyl)pyrrolidine-1-carboxylate, this compound was synthesized according to General Procedure A for benzylation and was purified via flash chromatography. This gave 69% yield (572 mg) of two diastereomers (1:1) over the first two steps as a colorless oil. **^1H NMR** (500 MHz, DMSO, $80\text{ }^\circ\text{C}$) δ 8.01 (ddd, $J = 8.4, 3.1, 1.4\text{ Hz}$, 1H), 7.83 – 7.68 (m, 1H), 7.58 (tt, $J = 7.4, 1.1\text{ Hz}$, 1H), 5.82 (diastereomer A: d, $J = 6.1\text{ Hz}$, 0.5H), 5.77 (diastereomer B: d, $J = 6.9\text{ Hz}$, 0.5H), 3.58 (ddd, $J = 11.2, 7.9, 1.5\text{ Hz}$, 1H), 3.48 (ddt, $J = 10.7, 8.4, 4.2\text{ Hz}$, 1H), 3.36 – 3.21 (m, 1H), 3.03 – 2.91 (m, 1H), 2.32 – 2.06 (m, 1H), 2.03 – 1.78 (m, 1H), 1.41 (diastereomer A: s, 4.4H), 1.40 (diastereomer B: s, 4.6H). **^{13}C NMR** (126 MHz, DMSO) δ 164.81, 153.85, 134.81, 130.03,

129.51, 128.36, 117.10, 79.06, 64.64, 63.91, 47.66, 47.43, 45.51, 28.64. Distinct peaks of other diastereomer: ^{13}C NMR (126 MHz, DMSO) δ 164.88, 134.84, 129.51, 117.07, 79.04, 28.65. **HRMS** (ESI⁺) Calc: $[\text{M}+\text{Na}]^+$ for $\text{C}_{18}\text{H}_{22}\text{N}_2\text{O}_4$ = 353.1472; measured 353.1468 = 1.1 ppm difference.

tert-butyl 3-(cyanomethyl)pyrrolidine-1-carboxylate (33): Compound was synthesized from tert-butyl 3-((benzoyloxy)(cyano)methyl)pyrrolidine-1-carboxylate according to General Procedure C on 0.4 mmol scale with the modification of running for 48 hours. 68% yield deoxygenation (47% overall yield from aldehyde) was obtained as a pale yellow oil. ^1H NMR (500 MHz, CDCl_3) δ 3.60 (dd, J = 10.8, 7.1 Hz, 1H), 3.48 (s, 1H), 3.41 – 3.22 (m, 1H), 3.09 (dd, J = 11.0, 7.1 Hz, 1H), 2.53 (p, J = 7.1 Hz, 1H), 2.45 (d, J = 9.8 Hz, 2H), 2.23 – 2.03 (m, 1H), 1.74 (s, 1H), 1.46 (s, 9H). Spectrum in accordance with literature: *Euro. J. Med. Chem.* 225 (2021) 113724.

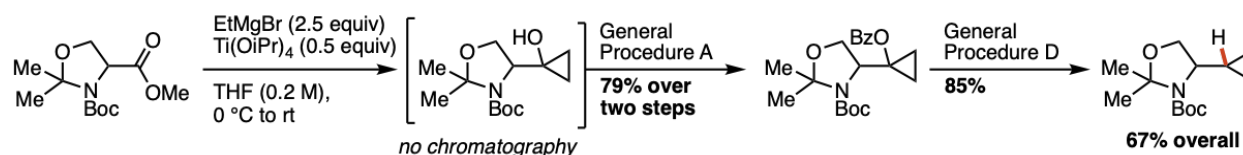


tert-butyl 4-(2,2,2-trifluoro-1-hydroxyethyl)piperidine-1-carboxylate: To a flame dried 100 mL round bottom flask equipped with stir bar under nitrogen, was added the aldehyde substrate (2.13 grams, 10 mmol), which was then dissolved in THF (35 ml). TMSCF_3 (1.5 equiv) was added and the solution was then cooled to 0 °C. TBAF (1 equiv, 1 M in THF) was added dropwise to the reaction mixture. The flask was gradually warmed to room temperature and stirred for 6 hours. Then an additional 1 equiv TBAF (1 M in THF) was added and the mixture was stirred overnight.

The reaction was quenched with 1 M HCl, then neutralized with bicarbonate (sat. aq.). Note: this was done cautiously, as many bubbles formed during neutralization. The reaction was diluted with ethyl acetate then extracted three times. The ethyl acetate layer was washed with sodium chloride (sat. aq.) then dried over sodium sulfate, filtered, and concentrated *in vacuo*. The crude material was carried forward to the benzylation conditions without further purification as a colorless oil.

tert-butyl 4-(1-(benzoyloxy)-2,2,2-trifluoroethyl)piperidine-1-carboxylate: Compound was synthesized from tert-butyl 4-(2,2,2-trifluoro-1-hydroxyethyl)piperidine-1-carboxylate according to General Procedure A. 93% yield over two steps was obtained as a pale yellow oil via flash chromatography. $^1\text{H NMR}$ (400 MHz, CDCl_3) δ 8.29 – 7.94 (m, 2H), 7.62 (d, J = 7.5 Hz, 1H), 7.49 (dd, J = 8.4, 7.1 Hz, 2H), 5.46 (qd, J = 7.3, 5.7 Hz, 1H), 4.34 – 3.97 (m, 2H), 2.98 – 2.44 (m, 2H), 2.24 – 2.09 (m, 1H), 1.80 (t, J = 15.1 Hz, 2H), 1.43 (s, 11H). $^{13}\text{C NMR}$ (101 MHz, CDCl_3) δ 164.92, 154.61, 133.93, 130.06, 128.67, 128.47, 125.26, 79.68, 72.61, 72.30, 71.99, 45.98, 35.98, 28.40, 26.04. $^{19}\text{F NMR}$ (376 MHz, CDCl_3) δ -73.12. **HRMS** (ESI $^+$) Calc: $[\text{M}+\text{Na}]^+$ for $\text{C}_{19}\text{H}_{24}\text{F}_3\text{NO}_4$ = 410.1550; measured 410.1543 = 1.7 ppm difference.

tert-butyl 4-(2,2,2-trifluoroethyl)piperidine-1-carboxylate (35): Compound was synthesized from tert-butyl 4-(1-(benzoyloxy)-2,2,2-trifluoroethyl)piperidine-1-carboxylate according to General Procedure C on 0.4 mmol scale. The crude material was rinsed with hexanes through a pipette column to remove PTH then eluted with 30% ethyl acetate in hexanes to give 99% yield deoxygenation (92% overall yield from aldehyde) as a pale yellow oil. $^1\text{H NMR}$ (400 MHz, CDCl_3) δ 4.09 (d, J = 13.8 Hz, 2H), 2.79 – 2.60 (m, 2H), 2.03 (qd, J = 11.3, 6.5 Hz, 2H), 1.83 (dtd, J = 10.4, 6.8, 3.5 Hz, 1H), 1.76 (dd, J = 14.5, 3.5 Hz, 2H), 1.45 (s, 9H), 1.21 (qd, J = 12.5, 4.4 Hz, 2H). Spectrum in accordance with literature: *J. Am. Chem. Soc.* **2013**, 135, 7, 2505–2508.

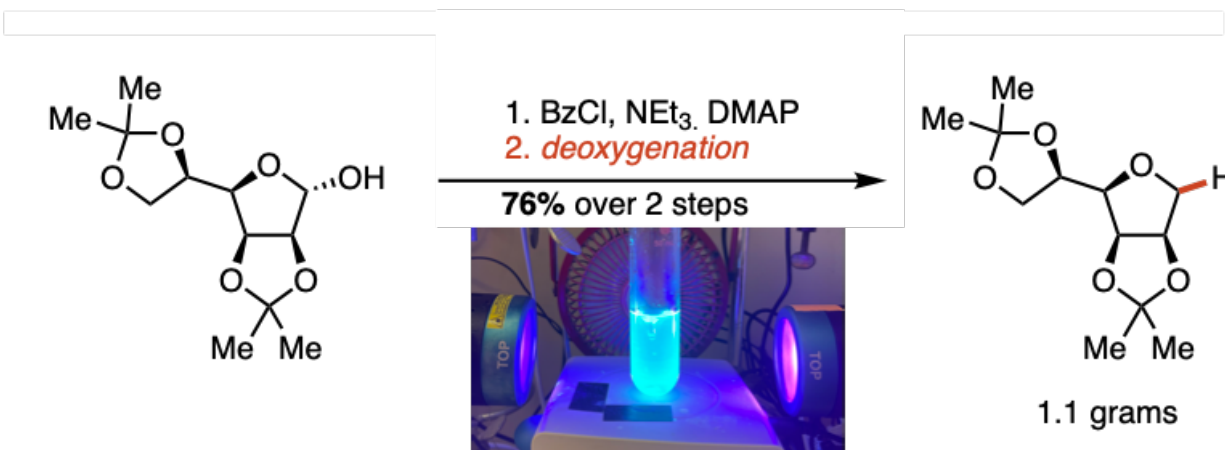


tert-butyl 4-(1-hydroxycyclopropyl)-2,2-dimethyloxazolidine-3-carboxylate: To a flame dried 100 mL round bottom flask equipped with stir bar under nitrogen, added substrate (1 gram, 3.9 mmol) then added 1 mL THF and stirred under nitrogen with vent line for ~5 min until solvent evaporated (to dry the substrate). Added remaining THF (19 mL) then cooled to 0 °C. Once cooled, added Ti(OiPr)₄ (0.5 equiv) dropwise. Then slowly added EtMgBr (2.5 equiv) dropwise. The reaction turned yellow then black. The mixture was gradually warmed to room temperature and stirred overnight. The reaction was quenched with ammonium chloride (sat. aq.) then extracted with ethyl acetate three times. The ethyl acetate layer was washed with brine (sat. aq.), then dried over sodium sulfate, filtered, and concentrated *in vacuo* to obtain colorless oil. The crude mixture was carried forward to the benzoylation step without further purification.

tert-butyl 4-(1-(benzoyloxy)cyclopropyl)-2,2-dimethyloxazolidine-3-carboxylate: Compound was synthesized from tert-butyl 4-(1-hydroxycyclopropyl)-2,2-dimethyloxazolidine-3-carboxylate according to General Procedure A for benzoylation and purified via flash chromatography. 79% yield (1.1 grams) was obtained as a pale yellow oil. **¹H NMR** (500 MHz, DMSO) δ 7.90 (d, J = 7.6 Hz, 2H), 7.63 (t, J = 7.4 Hz, 1H), 7.50 (t, J = 7.6 Hz, 2H), 4.66 – 3.82 (m, 3H), 1.41 (m, J = 6.4 Hz, 15H), 1.30 – 0.74 (m, 4H). **¹³C NMR** (126 MHz, DMSO) δ 166.02, 152.52, 133.58, 130.77, 129.66, 128.97, 93.93, 80.39, 79.81, 60.14, 59.69, 28.46, 28.41, 11.90. **HRMS** (ESI⁺) Calc: [M+H]⁺ for C₂₀H₂₇NO₅ = 362.1962; measured 362.1956 = 1.7 ppm difference.

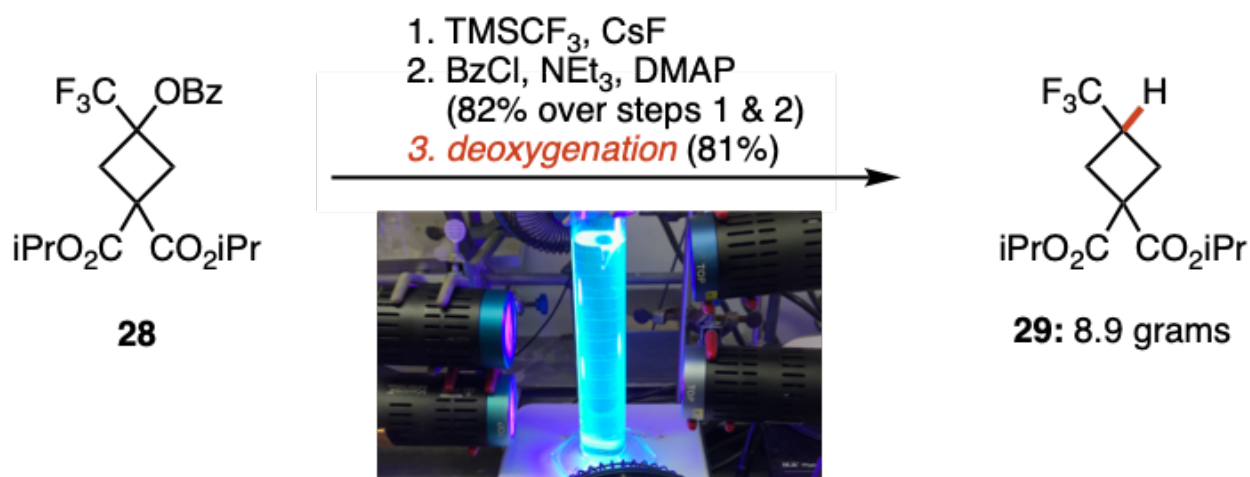
tert-butyl 4-cyclopropyl-2,2-dimethyloxazolidine-3-carboxylate (37): Compound was synthesized from tert-butyl 4-(1-(benzyloxy)cyclopropyl)-2,2-dimethyloxazolidine-3-carboxylate according to General Procedure D. 85% yield deoxygenation (67% overall yield from ester) was obtained as a colorless oil. $^1\text{H NMR}$ (500 MHz, DMSO, 60 °C) δ 3.87 (dd, J = 8.8, 5.8 Hz, 1H), 3.66 (dd, J = 8.8, 1.4 Hz, 1H), 3.43 (s, 1H), 1.52 (s, 3H), 1.43 (s, 9H), 1.41 (s, 3H), 1.02 (dtd, J = 13.2, 8.0, 5.1 Hz, 1H), 0.50 (q, J = 7.3 Hz, 2H), 0.36 (ddt, J = 12.3, 8.1, 4.4 Hz, 1H), 0.23 – 0.01 (m, 1H). $^{13}\text{C NMR}$ (126 MHz, DMSO) δ 149.83, 91.13, 77.05, 65.19, 58.20, 26.32, 13.11, 2.25, -0.50. **HRMS** (ESI $^+$) Calc: $[\text{M}+\text{H}]^+$ for $\text{C}_{13}\text{H}_{23}\text{NO}_3$ = 242.1751; measured 242.1746 = 2.1 ppm difference.

4. 5. 10 Utility in Synthesis



Gram Scale Batch Benzoylation and Deoxygenation: Following General Procedure A, alcohol 2,3:5,6-Di-O-isopropylidene- α -mannofuranose was benzoylated and purified via flash chromatography to give 1.6 grams (77% yield) of benzoylated sugar **21** as a white solid. The benzoylated sugar was subjected to deoxygenation conditions General Procedure C with the modification that a 50 mL storage flask was used as the reaction vessel and the reaction was stirred for 45 minutes before irradiation to ensure homogeneity. After 24 hours of irradiation, this

gave 1.1 grams (>99% deoxygenation) of compound **21**. Spectrum in accordance with characterization data gathered in the **Product Characterization** section.



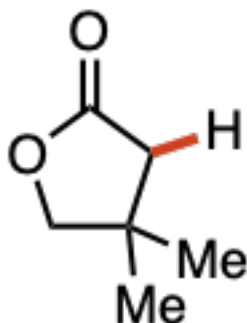
Decagram scale batch alcohol synthesis, benzylation, and deoxygenation: Procedure from *Org. Process Res. Dev.* **2021**, 25, 1, 82–88. Diisopropyl 3-oxocyclobutane-1,1-dicarboxylate (12.11 g, 50.00 mmol) was charged into a round-bottom flask followed by THF (121 mL) and CsF (9.114 g, 60.00 mmol). The system was purged with N₂ three times, and was cooled to 0 °C. The above flask was charged dropwise with a solution of TMSCF₃ (8.25 mL, 55.00 mmol) in THF (12 mL), and the reaction was stirred at room temperature overnight. TLC indicated that the starting material was consumed completely. The reaction mixture was filtered through a pad Celite. The filtrate was concentrated in vacuum, and the residue was redissolved in 150 mL of ethyl acetate. The organic phase was washed with brine (40 mL × 2) and separated. It was dried with anhydrous MgSO₄, filtered, and concentrated in vacuum. The NMR spectrum of the crude material revealed a 55:45 ratio of free alcohol to trimethylsilyl ether. The crude material was dissolved in THF (25 mL), cooled to 0 °C, and treated with TBAF (1.5 equiv., 34 mL, 1 M in THF). TLC indicated that the trimethylsilyl ether was consumed completely. The reaction mixture was concentrated in vacuum, and the residue was redissolved in 100 mL of ethyl acetate. The organic phase was

washed with 100 mL of water. The aqueous layer was extracted with ethyl acetate (100 mL × 2). The organic phases were combined and washed with 100 mL brine. The organic phase was dried with anhydrous MgSO₄, filtered, and concentrated in vacuum. The crude product was carried forward without further purification.

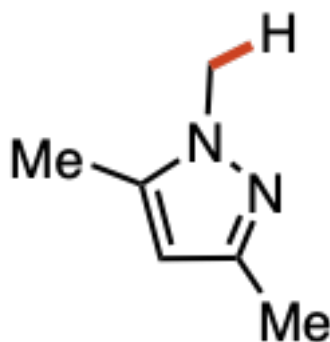
Benzoylation was performed according to General Procedure A on a 50 mmol scale. 17.00 g (82% yield from the ketone) was obtained as white solid. Spectrum in accordance with characterization data gathered in the **Product Characterization** section.

Deoxygenation was performed according to General Procedure C on a 37 mmol scale in a mL graduated cylinder using four 390 nm Kessil lamps and two cooling fans (30 °C measured at end of reaction). Full conversion as detected by TLC and confirmed by NMR aliquot was observed at 18 h. Reaction mixture was diluted with 200 mL of ethyl acetate and quenched with 250 mL sodium bicarbonate (sat. aq.) and 250 mL of water. The aqueous layer was extracted twice more, ethyl acetate 200 mL x 2. The organic layers were combined and washed with 200 mL saturated sodium chloride (sat. aq.). Then dried over sodium sulfate, filtered, and concentrated *in vacuo*. The crude material was purified via a silica plug (hexanes/ethyl acetate). 8.9 g (81% yield) was obtained as an oil. Spectrum in accordance with characterization data gathered in the **Product Characterization** section.

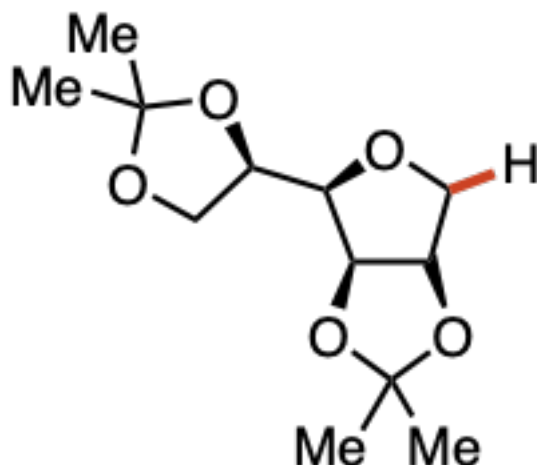
One-pot scope



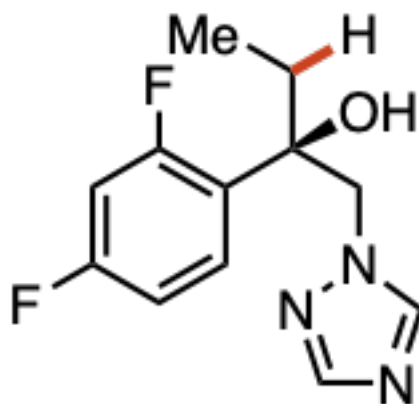
4,4-dimethyldihydrofuran-2(3H)-one (10): Compound was synthesized from (2R)-2-benzoyloxy-3,3-dimethyl-4-butanolide according to General Procedure F on 0.4 mmol scale. >99% yield was observed via ^1H NMR. NMR spectrum in accordance with literature: *Org. Lett.* 2016, 18, 24, 6472–6475.



1,3,5-trimethylpyrazole (12): Compound was synthesized from (3,5-dimethylpyrazol-1-yl)methyl benzoate according to General Procedure G on 0.4 mmol scale. 80% yield was observed via ^1H NMR. NMR spectrum in accordance with literature: *J. Org. Chem.* 791, **2015** 303–310.

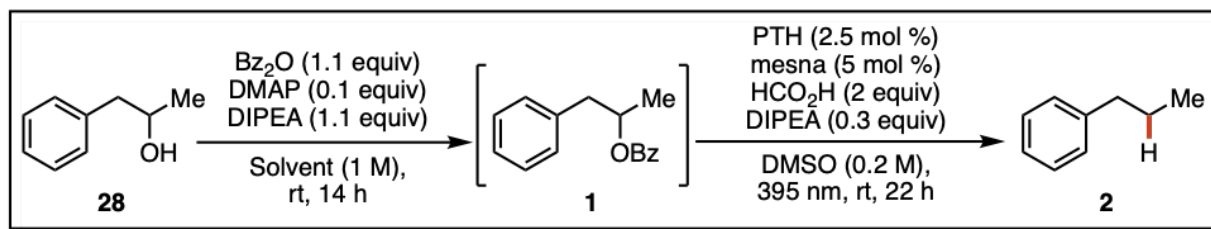


(3aR,4R,6aS)-4-((S)-2,2-dimethyl-1,3-dioxolan-4-yl)-2,2-dimethyltetrahydrofuro[3,4-d][1,3]dioxole (21): Compound was synthesized from 2,3:5,6-Di-O-isopropylidene- α -mannofuranose according to General Procedure F on 0.4 mmol scale. 87% yield was observed via ^1H NMR. Spectrum in accordance with literature: *Chem. Eur. J.* **2010**, 16, 8545 – 8556.



(R)-2-(2,4-difluorophenyl)-1-(1H-1,2,4-triazol-1-yl)butan-2-ol (13): Compound was synthesized from (2R,3R)-3-(2,4-difluorophenyl)-3-hydroxy-4-(1,2,4-triazol-1-yl)butan-2-yl benzoate according to General Procedure F on 0.4 mmol scale. 90% yield was observed via ^1H NMR. NMR spectrum in accordance with literature: *Euro. J. Med. Chem.* 133 (**2017**) 309-318.

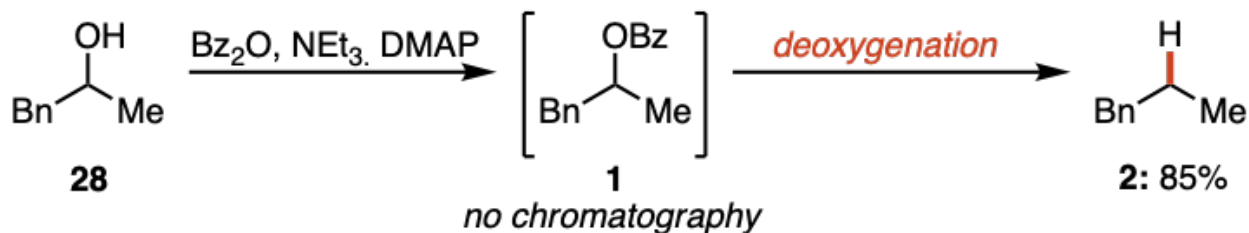
Telescope Screening



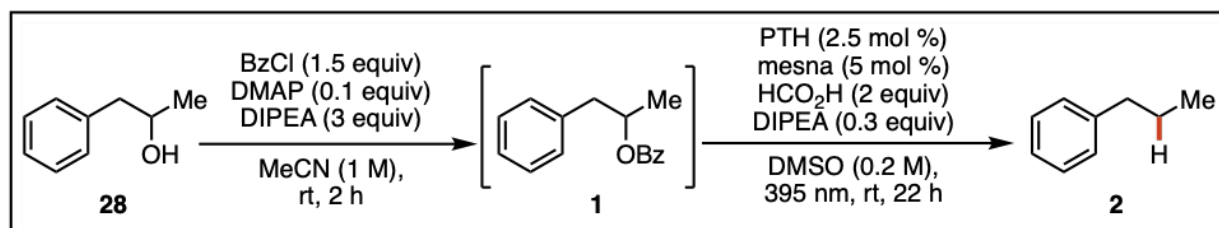
Entry	Solvent	Yield % 2	Yield % 1	Yield % 28	Modification
1	MeCN	9	91	0	—
2	MeCN	6	91	0	5 equiv formic acid
3	DCM	13	87	0	—
4	DMSO	8	92	0	—
5	DCM	26	72	0	aq. workup ^a
6	DCM	2	93	0	silica plug ^b
7	DCM	12	80	0	aq. workup ^a & silica plug ^b
8	DMSO	52	22	9	aq. workup ^a

^aAq. workup = reaction was diluted with diethyl ether and quenched with bicarbonate (sat. aq.), then extracted with ether three times. The combined ether layer was washed with sodium chloride (sat. aq.), dried over sodium sulfate, filtered, and concentrated *in vacuo*. ^bSilica plug = reaction mixture was diluted with 1 mL 1:1 ethyl acetate/hexanes and filtered through a pipette pad of silica. The solvent was then concentrated *in vacuo*.

One-pot and telescope screening was performed under our sub-optimal conditions (using DIPEA as the reductant rather than zinc formate), however, we learned that the deoxygenation protocol is sensitive to DCM and the benzoate anion. When 30% DCM was added to the deoxygenation conditions listed above, only 4% yield of **2** was observed. Additionally, when 1 equiv. lithium benzoate was added to the deoxygenation conditions above, only 15% yield of **2** was observed. To circumvent these issues, the benzoylation was performed in DMSO, followed by an aqueous workup (entry 8), leading to the best results. These conditions (entry 8) translated well when coupled to our optimized deoxygenation conditions (General Procedure C) and led to 85% yield of compound **2** from the starting alcohol (see below).



Telescoping Conditions: Compound **28** was added to a 1-dram vial under air and dissolved in DMSO (1 M). Benzoic anhydride (1.1 equiv), DMAP (0.1 equiv), and DIPEA (1.1 equiv) were added to the vial. The reaction was sealed under air and stirred for 14 hours at room temperature. Once complete, the reaction was diluted with diethyl ether and quenched with bicarbonate (sat. aq.), then extracted with ether three times. The combined ether layer was washed with sodium chloride (sat. aq.), dried over sodium sulfate, filtered, and concentrated *in vacuo*. Following workup, the crude mixture was subjected to General Procedure C to obtain compound **2** in 85% GC yield.



Entry	Amine	Workup	Reductant	Yield % 2	Yield % 1	Yield % 28
1	DIPEA	aq. workup ^a	DIPEA	4	17	76
2	NEt ₃	aq. workup ^a	DIPEA	13	70	0
3	NEt ₃	silica plug ^b	Zn(CHO ₂) ₂	74	5	0

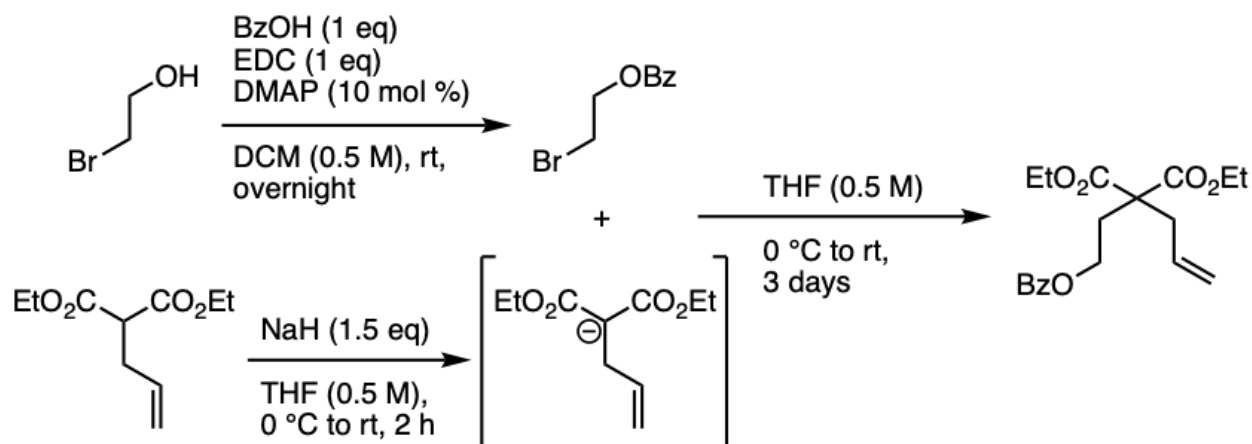
^aAq. workup = reaction was diluted with diethyl ether and quenched with bicarbonate (sat. aq.), then extracted with ether three times. The combined ether layer was washed with sodium chloride (sat. aq.), dried over sodium sulfate, filtered, and concentrated *in vacuo*. ^bSilica plug = reaction mixture was diluted with 1 mL 1:1 ethyl acetate/hexanes and filtered through a pipette pad of silica. The solvent was then concentrated *in vacuo*.

Alternative Telescoping Conditions: General Procedure A can be employed as the benzoylation conditions if an alternative workup is used. Rather than the aqueous workup mentioned above for “Telescoping Conditions” the crude material after General Procedure A was diluted with 1 mL 1:1 ethyl acetate/hexanes and filtered through a pipette pad of silica. The solvent was then concentrated *in vacuo* and subjected to deoxygenation conditions General Procedure C to yield 74% GC yield of compound **2**.

Pre-mixed and storable deoxygenation solution: PTH (0.025 equiv.), mesna (0.05 equiv.), zinc formate (1 equiv.) and formic acid (2 equiv.) were added to an amber vial and dissolved in DMSO (0.2 M). The contents were stirred until homogeneous. The headspace was flushed with nitrogen gas and the vial was sealed with a Teflon lined cap for storage at room temperature. To perform a deoxygenation reaction the desired amount of benzoate ester substrate was added to a clear reaction vessel equipped with a magnetic stir bar, then 0.5 mL of this solution per 0.1 mmol of benzoate ester substrate was added. The solution was then irradiated to initiate the deoxygenation reaction. This solution was effective for promoting deoxygenation up to at least 138 days of storage, evaluated via gas chromatography using substrate **1** on a 0.1 mmol scale.

4. 5. 11. Mechanistic Experiments

Synthesis of radical cyclization substrate

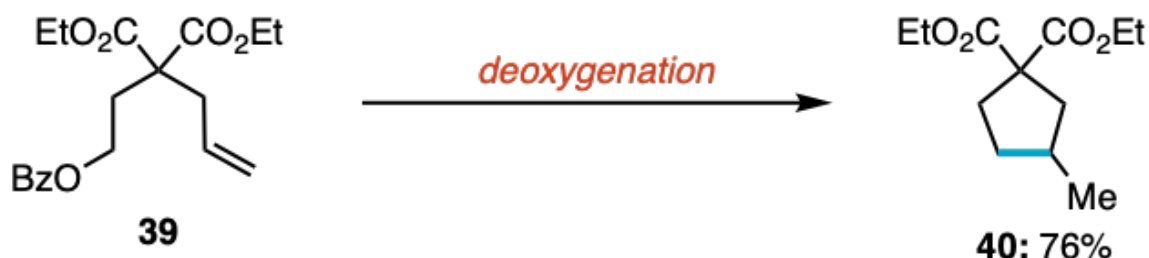


2-bromoethyl benzoate: To a 50 mL round bottom flask equipped with a stir bar under nitrogen, added 2-bromoethanol (1g, 8 mmol) then anhydrous DCM (16 mL, 0.5 M). Next, added benzoic acid (1 equiv) followed by EDC solution (1 equiv EDC dissolved in 2 mL DCM) and DMAP (0.10 equiv). Reaction was stirred at room temperature overnight. Reaction was diluted with 15 mL DCM and washed with bicarbonate solution (20 mL, sat. aq.), then sodium chloride (sat. aq., 15 mL) and dried over sodium sulfate. The solids were filtered off and the solution was concentrated in vacuo. The crude material was purified by flash chromatography to yield 71% product (1.3 grams) as a colorless oil.

diethyl 2-allyl-2-(2-(benzoyloxy)ethyl)malonate (39): A solution of diethyl allylmalonate (400 mg, 2 mmol) in THF (4 mL) was added dropwise to a suspension of NaH (60% dispersion, 1.5 equiv) in THF (10 mL) at 0 °C. The ice bath was removed and the mixture was stirred for 2 h at room temperature (reaction was slightly yellow and heterogenous). 2-bromoethyl benzoate in THF (1 mL) was added slowly over 5 min and the resulting mixture was stirred for 3 days at room temperature. The reaction was quenched with sat. aq. ammonium chloride then extracted with DCM (2 × 15 mL). The combined DCM layer was washed with sodium chloride (sat. aq.), then dried over sodium sulfate, filtered, and concentrated in vacuo. The crude material was purified by flash chromatography and 83% yield (575 mg) was obtained as a colorless oil. ¹H NMR (600 MHz,

CDCl₃) δ 8.00 (dd, J = 8.1, 1.5 Hz, 2H), 7.60 – 7.51 (m, 1H), 7.43 (t, J = 7.8 Hz, 2H), 5.69 (ddt, J = 17.3, 10.1, 7.3 Hz, 1H), 5.28 – 5.03 (m, 2H), 4.40 (t, J = 6.7 Hz, 2H), 4.25 – 4.03 (m, 4H), 2.85 – 2.68 (m, 2H), 2.40 (t, J = 6.7 Hz, 2H), 1.22 (t, J = 7.1 Hz, 6H). ¹³C NMR (151 MHz, CDCl₃) δ 170.74, 166.32, 133.01, 132.07, 130.04, 129.62, 128.34, 119.54, 61.50, 61.00, 55.69, 37.47, 31.38, 14.02. **HRMS** (ASAP-MS) Calc: $[M+H]^+$ for C₁₉H₂₄O₆ = 349.1646; measured 349.1641 = 1.4 ppm difference.

Radical Cyclization



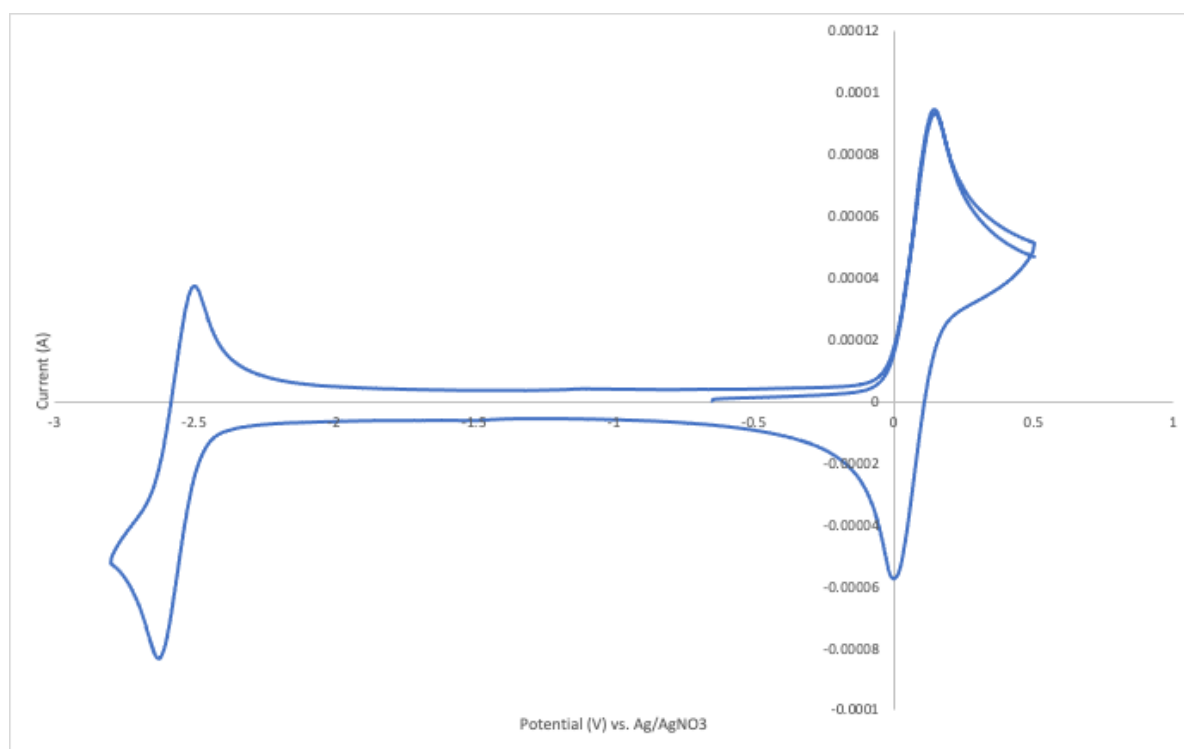
diethyl 3-methylcyclopentane-1,1-dicarboxylate (40): Compound was synthesized from diethyl 2-allyl-2-(2-(benzoyloxy)ethyl)malonate according to General Procedure D. 72% NMR yield was observed. Spectrum in accordance with literature: Angew. Chem. Int. Ed. **2019**, 58, 4869–4874.

Cyclic voltammetry studies

All cyclic voltametric (CV) experiments were carried out using a Pine WaveNowXV. CV experiments were carried out in a three-electrode cell configuration with a glassy carbon (GC)

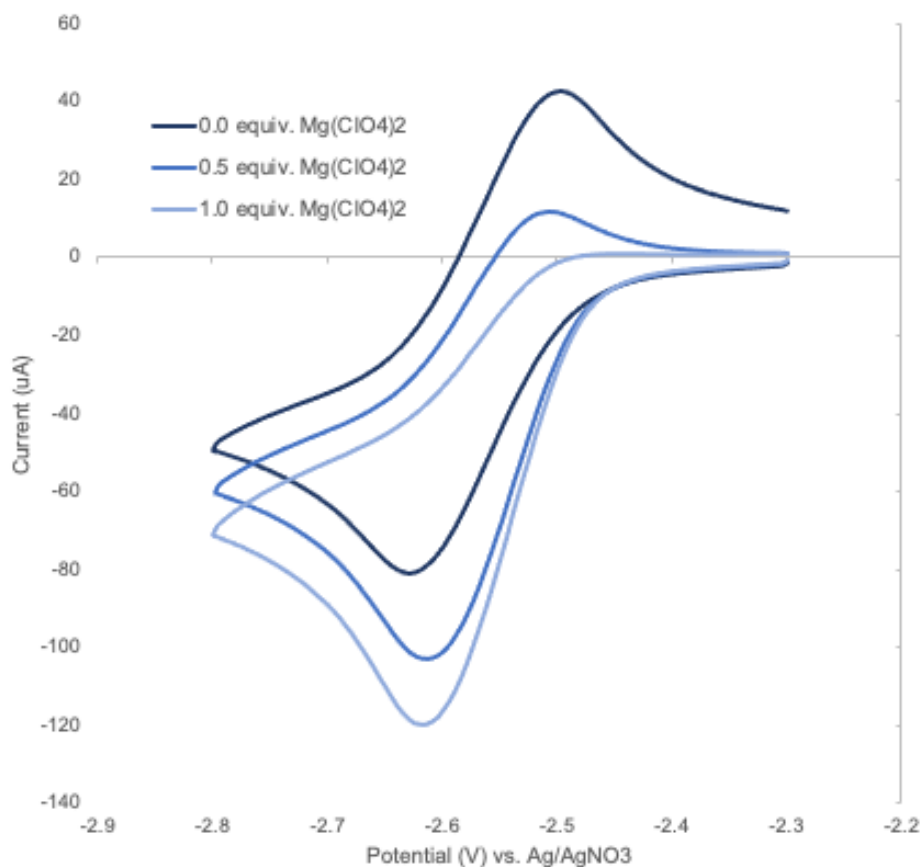
working electrode (3 mm diameter) and a platinum wire counter electrode. The working electrode potentials were measured against a Ag/AgNO₃ reference electrode (internal solution, 0.1 M Bu₄N•PF₆ and 0.01 M AgNO₃ in MeCN). The GC working electrode was polished with alumina powder before each experiment.

Benzoate ester **1** internally referenced to ferrocene



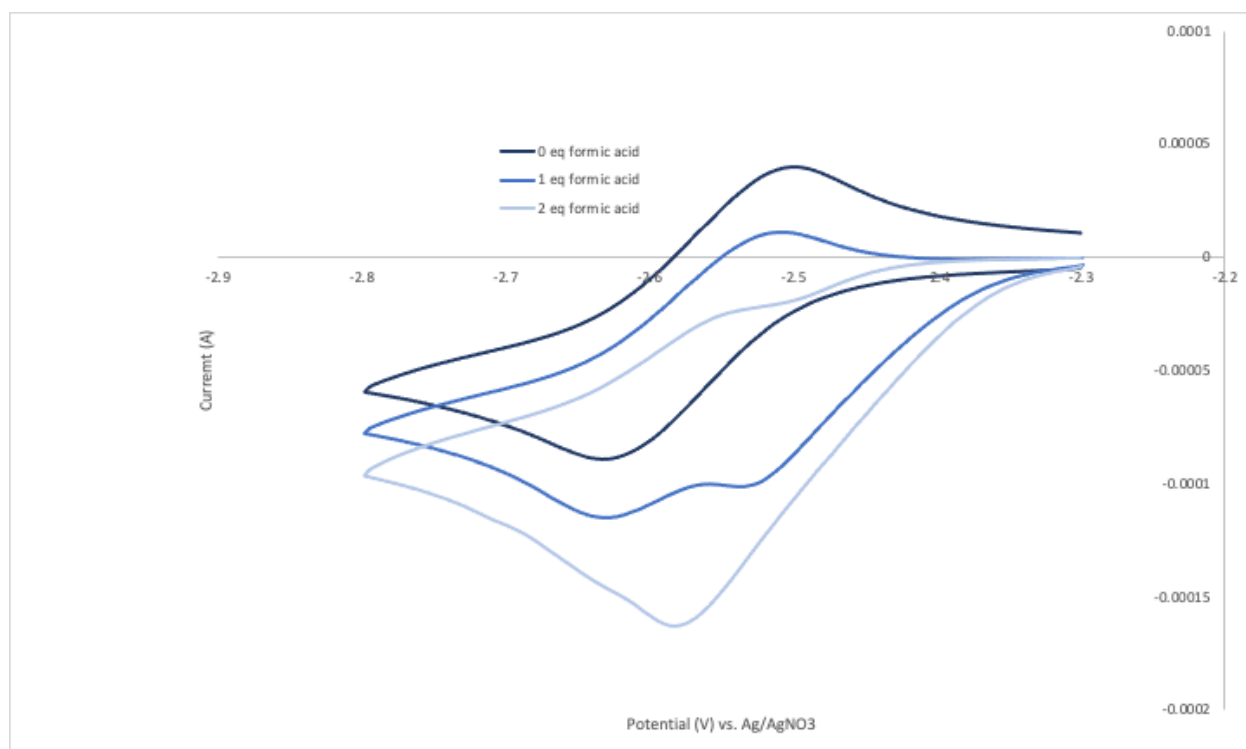
CV of **1** (5 mM) in DMSO in the presence of 0.25 M Bu₄N•PF₆ as an electrolyte with a scan rate of 200 mV/s. The redox potential of ferrocenium/ferrocene (Fc⁺/Fc) was measured under the same experimental conditions and used to provide an internal reference. The E_{1/2} of **1** was determined to be -2.6 V vs. Fc⁺/Fc.

Benzoate ester **1** with increasing amounts of Mg(ClO₄)₂



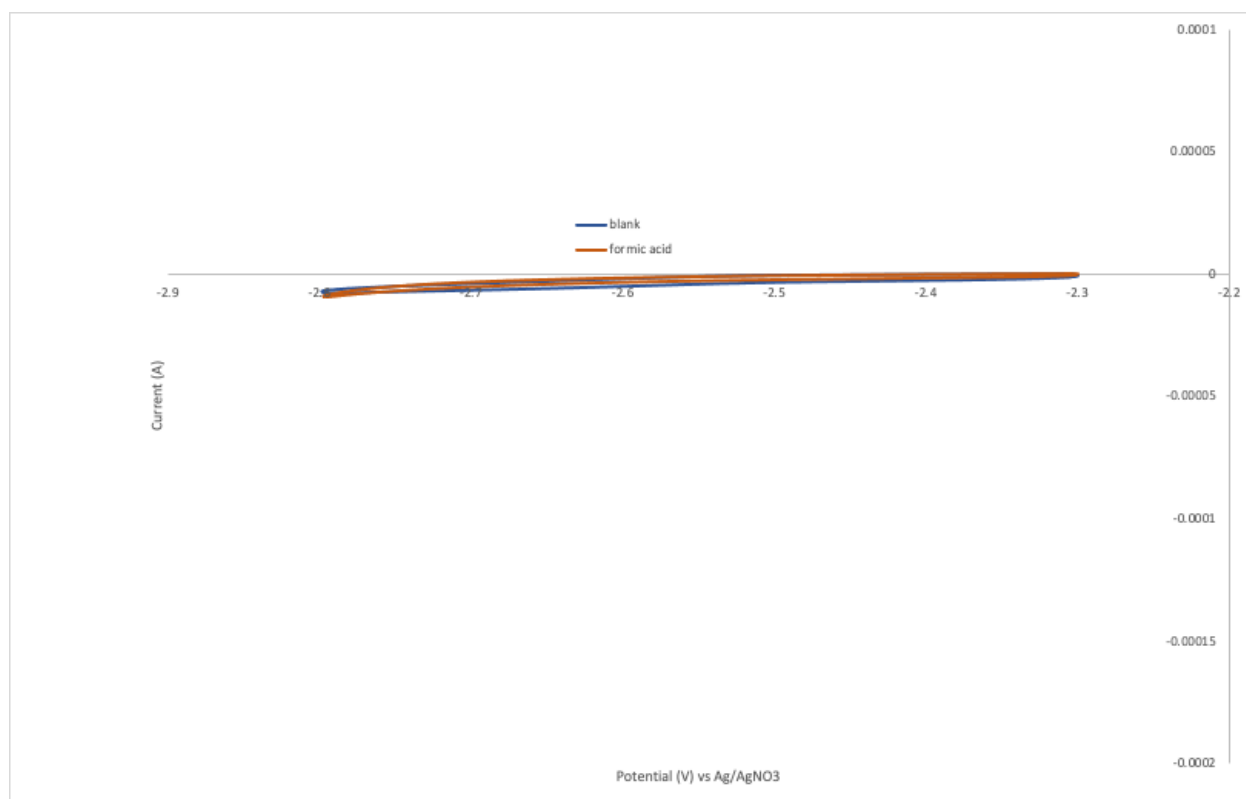
CV of **1** (5 mM) in DMSO in the presence of 0.25 M $\text{Bu}_4\text{N}^+\text{PF}_6^-$ as an electrolyte with a scan rate of 200 mV/s. $\text{Mg}(\text{ClO}_4)_2$ was iteratively added to the same solution with stirring between data collection. Voltammograms were collected with 0, 0.5, and 1 equivalents of $\text{Mg}(\text{ClO}_4)_2$.

Benzoate ester **1** with increasing amounts of formic acid



CV of **1** (5 mM) in DMSO in the presence of 0.25 M $\text{Bu}_4\text{N}^+\text{PF}_6^-$ as an electrolyte with a scan rate of 200 mV/s. Formic acid was iteratively added to the same solution with stirring between data collection. Voltammograms were collected with 0, 1, and 2 equivalents of formic acid. A new feature was observed upon the addition of formic acid. We hypothesize that this may be due to a proton-coupled electron transfer mechanism. The new feature is inconsistent with proton reduction, see below. While a decrease in electrochemical reversibility was still observed with this Brønsted acid additive, we chose to present the unconvoluted $\text{Mg}(\text{ClO}_4)_2$ Lewis acid data in the manuscript.

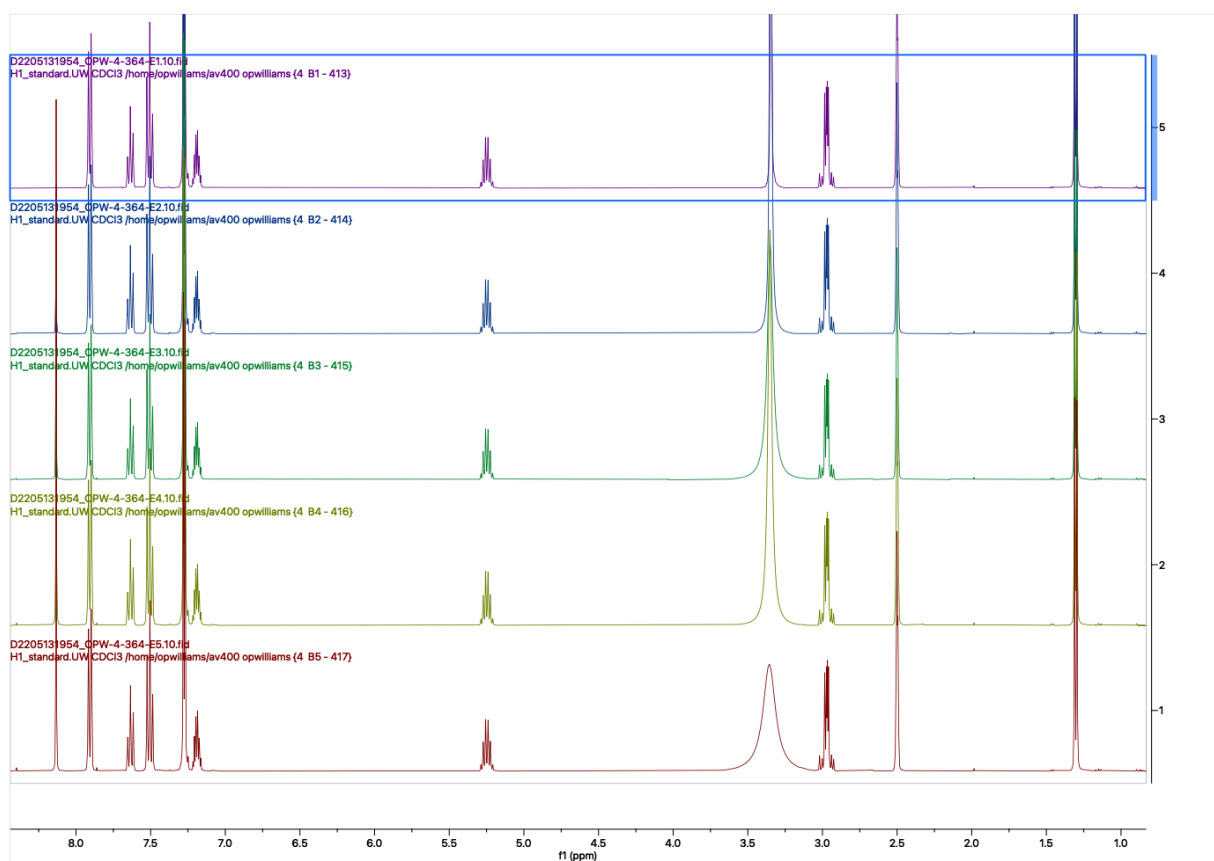
Formic acid



CV of formic acid (5 mM) in DMSO in the presence of 0.25 M Bu₄N•PF₆ as an electrolyte with a scan rate of 200 mV/s.

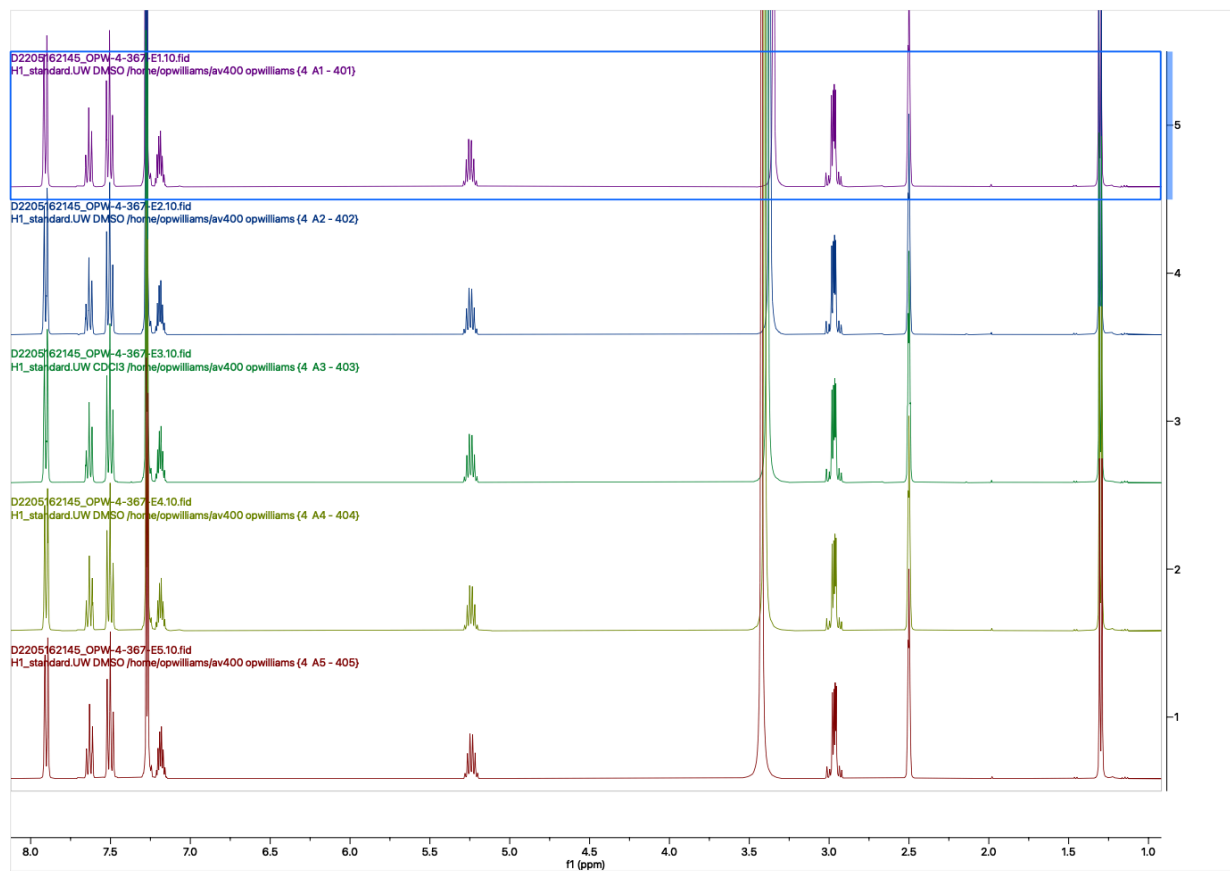
NMR titrations - formic acid, magnesium perchlorate, zinc formate

A stock solution of model benzoate ester substrate **2** in DMSO-d₆ (0.36 M) was prepared. 0.7 mL of this solution (0.025 mmol) was transferred to each of five NMR tubes. 0 microliters of formic acid were added to tube 1, 0.5 microliters added to tube 2, 1.0 microliters added to tube 3, 1.5 microliters added to tube 4, and 2.0 microliters added to tube 5.



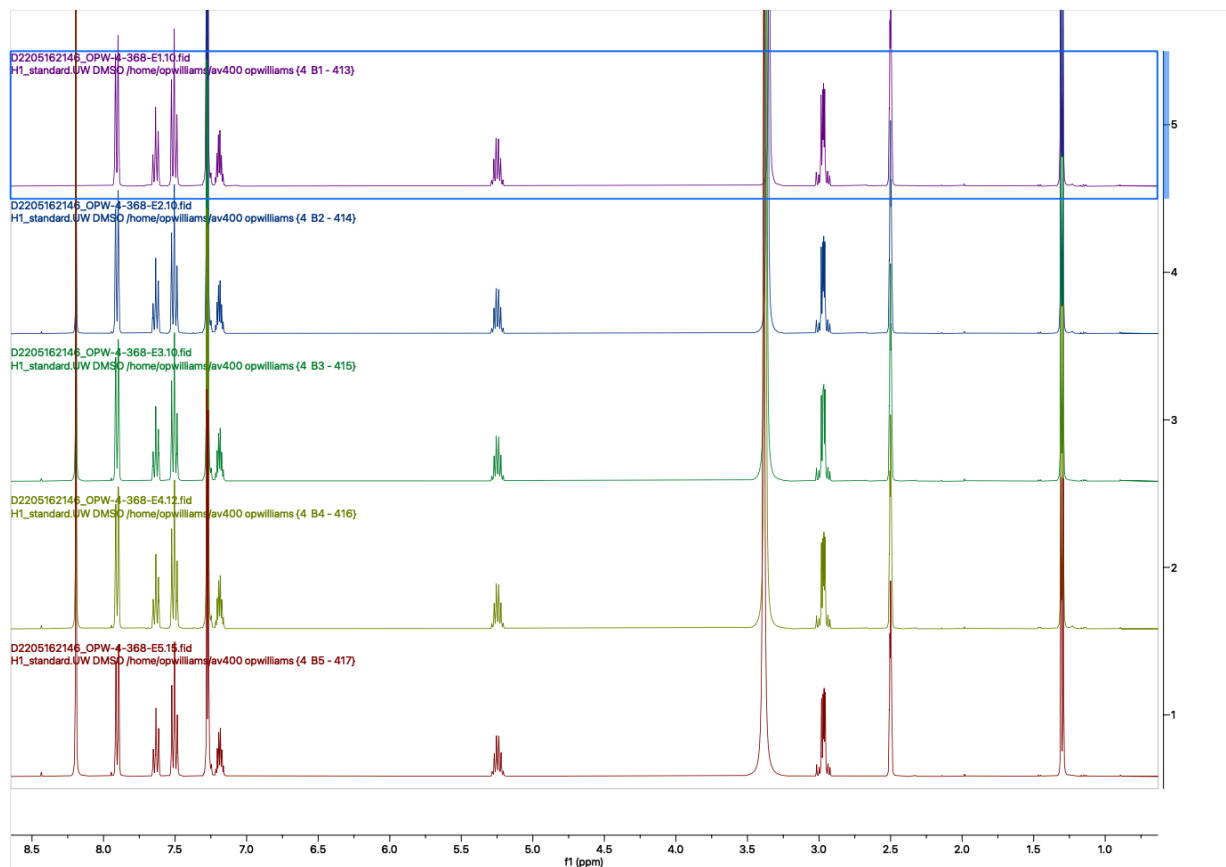
No significant shifts in the NMR spectra were observed (formic acid equivalents increasing from top to bottom).

A stock solution of model benzoate ester substrate **2** in DMSO-*d*₆ (0.36 M) was prepared. 0.7 mL of this solution (0.025 mmol) was transferred to each of five NMR tubes. 0 mg of magnesium perchlorate were added to tube 1 (0 equiv.), 2.79 mg added to tube 2 (0.5 equiv.), 5.58 mg added to tube 3 (1.0 equiv.), 8.37 mg added to tube 4 (1.5 equiv.), and 11.2 mg added to tube 5 (2.0 equiv.).



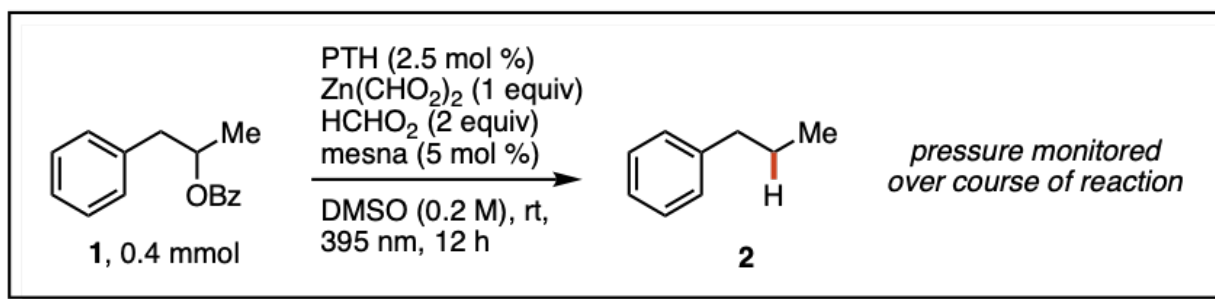
No significant shifts in the NMR spectra were observed (magnesium perchlorate equivalents increasing from top to bottom).

A stock solution of model benzoate ester substrate **2** in DMSO-d₆ (0.36 M) was prepared. 0.7 mL of this solution (0.025 mmol) was transferred to each of five NMR tubes. 0 mg of zinc formate were added to tube 1 (0 equiv.), 1.94 mg added to tube 2 (0.5 equiv.), 3.89 mg added to tube 3 (1.0 equiv.), 5.83 mg added to tube 4 (1.5 equiv.), and 7.77 mg added to tube 5 (2.0 equiv.).



No significant shifts in the NMR spectra were observed (zinc formate equivalents increasing from top to bottom).

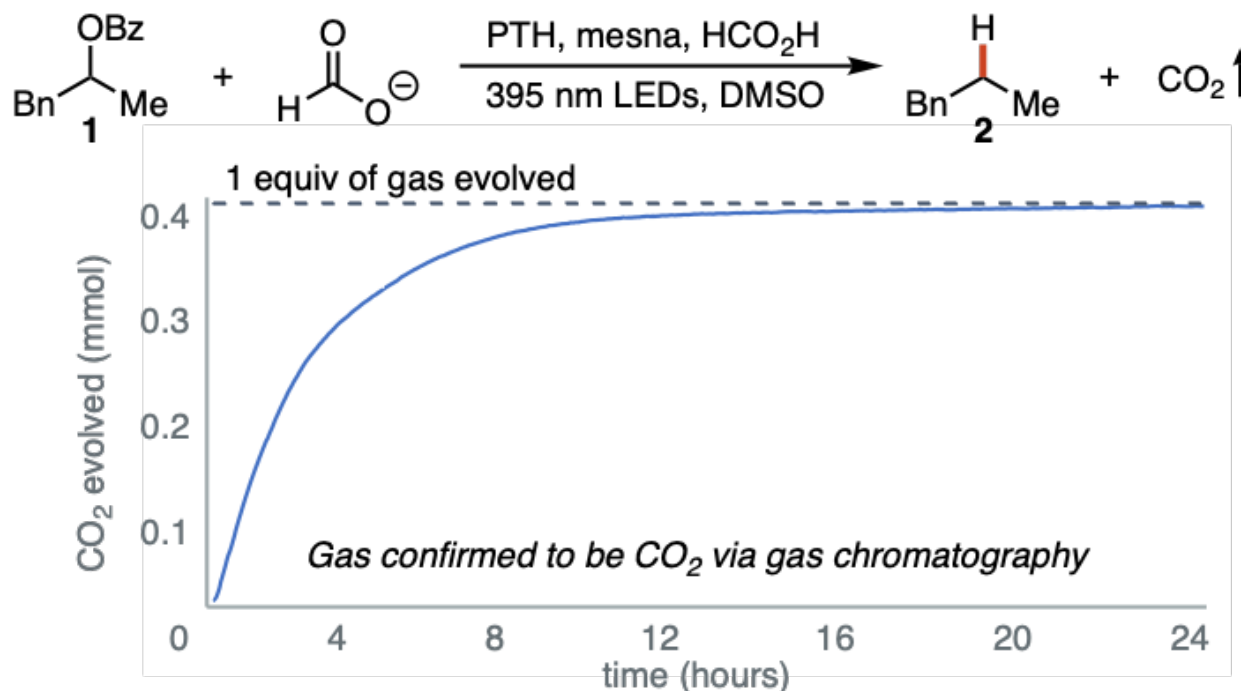
Gas Evolution Experiment



The gas evolution experiment was performed on an apparatus developed by the Stahl lab.

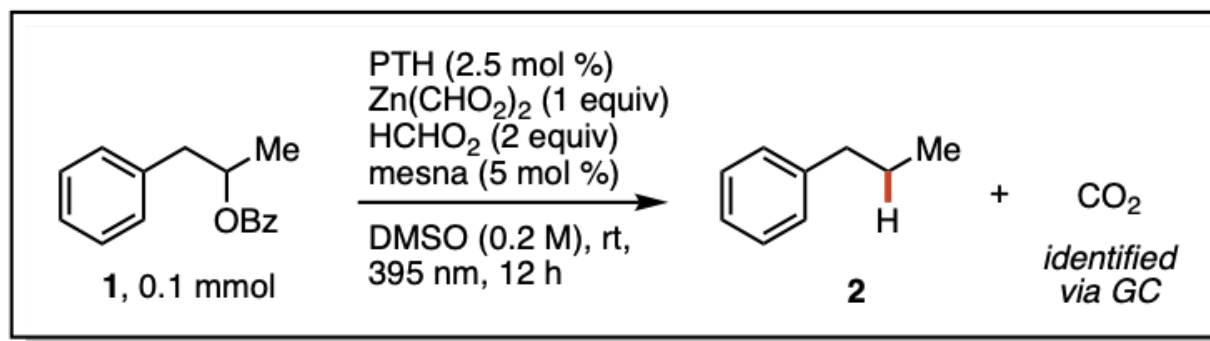
(Rev. Sci. Instrum. 92, 044103 (2021))

To the first heavy walled tube equipped with a stir bar of known volume was added 2 mL of DMSO and the benzoate ester substrate (0.400 mmol, 96.1 mg). This tube was used to account for the influence of heating in the photochemical reactions on pressure. To the second heavy walled tube equipped with a stir bar of known volume was added 2 mL of DMSO, the benzoate ester substrate (0.400 mmol, 96.1 mg), mesna (0.05 equiv., 3.28 mg), zinc formate (1 equiv., 62.2 mg), and formic acid (2 equiv., 30.2 microliters). Both tubes were equipped to pressure transducers, clamped above stir plates, and then irradiated with 390 nm Kessil lamps under fan cooling for 1 h to thermally equilibrate. Pressure monitoring was commenced and then 100 microliters of a 0.1 M PTH stock solution (10 micromoles, 0.025 equiv.) was injected into each tube through a thick rubber septum. To facilitate analysis, the uptake was normalized after the 0.1 mL catalyst injection. After 24 h of pressure monitoring, the final yield of the reaction was measured via gas chromatography using tert-butylbenzene as an internal standard. The data points were plotted over time to determine the amount of gas evolved during different phases of the reaction.

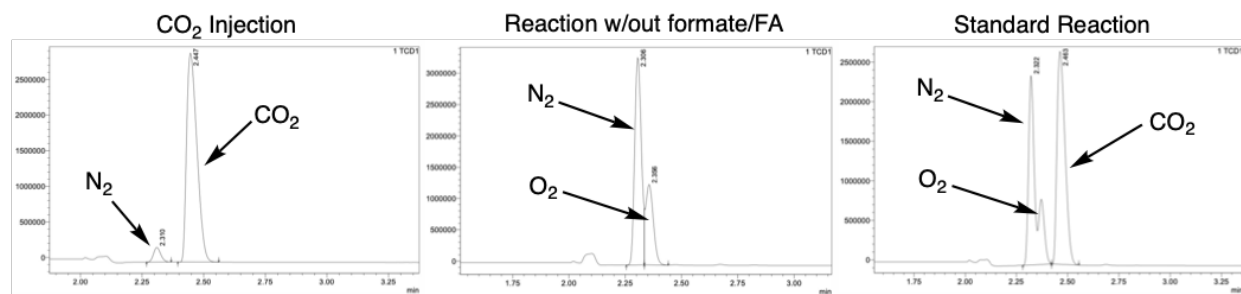


The reaction was run on a 0.400 mmol scale. 0.352 mmol of product was yielded and 0.400 mmol of substrate was consumed, as determined by gas chromatography. 0.397 mmol of gas were evolved during the course of the reaction, determined to be carbon dioxide (see next section of SI), despite the availability of 0.800 mmol of formate ions (0.400 mmol of divalent zinc formate). Collectively, this indicates that one equivalent of carbon dioxide is released per equivalent of substrate consumed. This is consistent with the substrate being necessary to generate carbon dioxide via accepting an electron from carbon dioxide radical anion.

Gas Chromatography to Identify Gas as Carbon Dioxide



Compound **1** was added to a 1.5 dram vial with septum cap and subjected to General Procedure C. Following reaction completion, a 1 mL gas-tight syringe was used to pierce the septum and remove 500 μL of the reaction headspace. The 500 μL of headspace was then injected into the GC. Three gasses were identified in the headspace: N_2 , O_2 , and CO_2 (see below, right). N_2 and O_2 originated from the ambient atmosphere (because the reaction was conducted under air, see below, middle). Whereas, CO_2 was generated throughout the reaction. An authentic sample of CO_2 was injected into the GC to confirm the gas generated was CO_2 (see below, left).




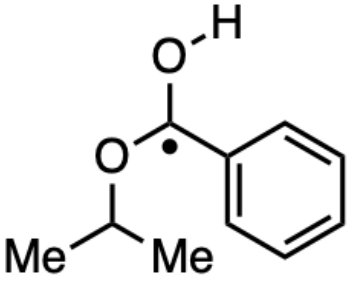
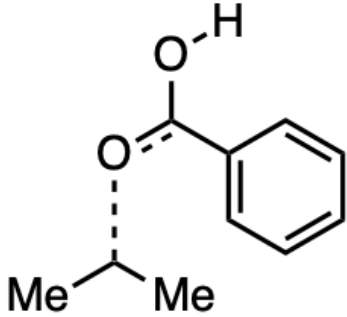
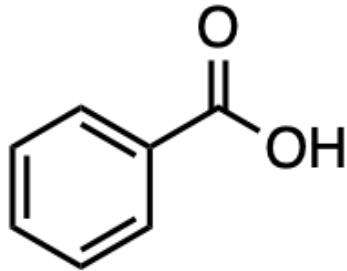
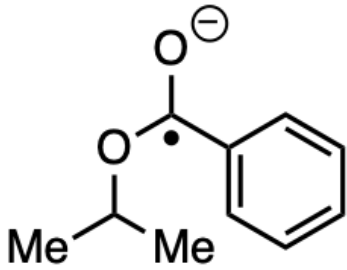
Computational Results

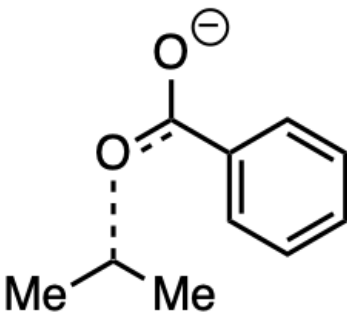
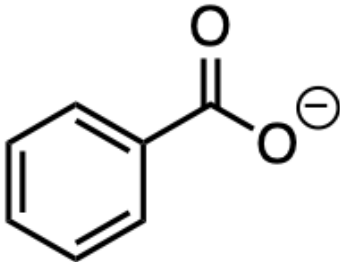
Calculations employed density functional theory using B3LYP functional and Møller–Plesset second order perturbation theory (MP2) in conjunction with 6-311+G(2d,p) basis set. Vibrational frequency calculations were performed to determine the nature of all structures. All calculations used the Polarizable Continuum Model (PCM) to model solvent. The solvent used was dimethyl sulfoxide. All calculations were performed using Gaussian 16. All optimized structures and energies are reported below.

Gaussian 16, Revision C.01, Frisch, M. J.; Trucks, G. W.; Schlegel, H. B.; Scuseria, G. E.; Robb, M. A.; Cheeseman, J. R.; Scalmani, G.; Barone, V.; Petersson, G. A.; Nakatsuji, H.; Li, X.; Caricato, M.; Marenich, A. V.; Bloino, J.; Janesko, B. G.; Gomperts, R.; Mennucci, B.; Hratchian, H. P.; Ortiz, J. V.; Izmaylov, A. F.; Sonnenberg, J. L.; Williams-Young, D.; Ding, F.; Lipparini, F.; Egidi, F.; Goings, J.; Peng, B.; Petrone, A.; Henderson, T.; Ranasinghe, D.; Zakrzewski, V. G.; Gao, J.; Rega, N.; Zheng, G.; Liang, W.; Hada, M.; Ehara, M.; Toyota, K.; Fukuda, R.; Hasegawa, J.; Ishida, M.; Nakajima, T.; Honda, Y.; Kitao, O.; Nakai, H.; Vreven, T.; Throssell, K.; Montgomery, J. A., Jr.; Peralta, J. E.; Ogliaro, F.; Bearpark, M. J.; Heyd, J. J.; Brothers, E. N.; Kudin, K. N.; Staroverov, V. N.; Keith, T. A.; Kobayashi, R.; Normand, J.; Raghavachari, K.; Rendell, A. P.; Burant, J. C.; Iyengar, S. S.; Tomasi, J.; Cossi, M.; Millam, J. M.; Klene, M.; Adamo, C.; Cammi, R.; Ochterski, J. W.; Martin, R. L.; Morokuma, K.; Farkas, O.; Foresman, J. B.; Fox, D. J. Gaussian, Inc., Wallingford CT, 2016.

Computed Energies

Molecule	MP2 free energy (Hartrees)	Structure
Isopropyl radical	-118.062947	

Protonated benzoate ester radical	-537.790832	
Protonated benzoate ester radical transition state	-537.75582	
Benzoic acid	-419.792413	
Benzoate ester radical anion	-537.358544	

Benzoate ester radical anion transition state	-537.307093	
Benzoate anion	-419.343693	

Standard orientations – MP2 optimized structures

Isopropyl radical

10

```

C      0.00000000  0.00000000  0.00000000
C      0.00000000  0.75007600 -1.28898600
C      0.00000000  0.00000000 -2.57797200
H     -0.17807600  0.65463800 -3.43273800
H      0.96317200 -0.50390000 -2.74607900
H     -0.76467500 -0.78278800 -2.57699900
H      0.33745900  1.78014600 -1.28898600
H     -0.17807600  0.65463800  0.85476600
H     -0.76467500 -0.78278800 -0.00097300
H      0.96317200 -0.50390000  0.16810700

```

Protonated benzoate ester radical

25

C	0.00000000	0.00000000	0.00000000
O	-1.25128600	-0.10782800	-0.76467400
C	-2.24470900	0.70319600	-0.38602700
C	-3.54622500	0.22858400	-0.24388300
C	-4.64918500	1.09601300	-0.06624400
C	-5.90813200	0.59474400	0.08897300
C	-6.14561800	-0.77113700	0.07010900
C	-5.07079600	-1.63501700	-0.11830600
C	-3.80501700	-1.16364100	-0.27425500
H	-2.97625700	-1.84708200	-0.41632000
H	-5.24228600	-2.70677500	-0.14029300
H	-7.15008900	-1.15824100	0.19361600
H	-6.73715200	1.28276800	0.22161200
H	-4.51436600	2.17314800	-0.07357300
O	-1.87744200	2.00213100	-0.26956700
H	-2.54548600	2.48719000	0.23810100
C	-0.26627700	-0.33435300	1.45281800
H	-0.99396700	0.35253400	1.89046600
H	-0.64661900	-1.35479700	1.54046500
H	0.66187400	-0.25556600	2.02312700
C	0.95230100	-0.96162600	-0.67066100
H	1.08188300	-0.70503100	-1.72309400
H	1.92594700	-0.91699800	-0.17915000
H	0.57110200	-1.98262800	-0.59857200
H	0.36107300	1.02538600	-0.09859500

Protonated benzoate ester radical transition state

25

C	0.00000000	0.00000000	0.00000000
O	-1.35098200	0.63456700	-1.22185400
C	-2.34013000	1.18923400	-0.74737300
C	-3.62875300	0.50901900	-0.52099000
C	-4.79488700	1.17679300	-0.21106300
C	-5.96428000	0.48623800	-0.03856900
C	-5.99138000	-0.87605900	-0.17577500
C	-4.83193400	-1.54810800	-0.49830000
C	-3.66805100	-0.86535700	-0.67358600
H	-2.75454100	-1.38875600	-0.93228600
H	-4.84563700	-2.62676500	-0.61510100
H	-6.91857100	-1.42126800	-0.03788600
H	-6.87332300	1.02684800	0.20286900
H	-4.82086600	2.25817700	-0.11581000
O	-2.22490400	2.50824200	-0.41827300
H	-2.98649400	2.79613700	0.10694900
C	-0.77133000	-0.22031900	1.24136800
H	-1.68125400	0.40881400	1.23604200
H	-1.08983100	-1.25879400	1.34815700
H	-0.20106300	0.07629700	2.12646700
C	0.49554700	-1.14113300	-0.81122000
H	0.76554900	-0.81636400	-1.81794400
H	1.39070700	-1.57567900	-0.34856700
H	-0.25972500	-1.92701400	-0.87925800
H	0.59567100	0.90499500	-0.03406600

Benzoic acid

15

C	0.00000000	0.00000000	0.00000000
---	------------	------------	------------

C	-1.12329300	-0.83165800	0.00000000
C	-2.40420900	-0.27405800	0.00000000
C	-2.56789300	1.11070600	0.00000000
C	-1.43987700	1.94032900	0.00000000
C	-0.15553200	1.38437700	0.00000000
H	0.70679500	2.04244000	0.00000000
C	-1.56013600	3.42088900	0.00000000
O	-2.84382600	3.84409100	0.00000000
H	-2.81751600	4.81750200	0.00000000
O	-0.61778600	4.19110700	0.00000000
H	-3.56080300	1.54522400	0.00000000
H	-3.27719800	-0.91867600	0.00000000
H	-1.00065400	-1.91012000	0.00000000
H	0.99578000	-0.43128400	0.00000000

Benzoate ester radical anion

24

C	0.00000000	0.00000000	0.00000000
C	0.45270900	0.41820800	1.38667100
H	-0.12433300	1.27427500	1.73790700
H	0.32255200	-0.41087800	2.08688000
H	1.50991200	0.69476500	1.36868600
C	0.73036300	-1.22555600	-0.50732100
H	0.37474200	-1.50384300	-1.50073600
H	1.80176700	-1.02183400	-0.56512400
H	0.57447700	-2.06810100	0.17065000
O	-1.40340300	-0.36475200	0.03697600
C	-2.30337900	0.66362200	-0.01543400
C	-3.66906400	0.21688100	0.10880500
C	-4.73287900	1.16937000	0.02398200

C	-6.02351500	0.77702200	0.12504700
C	-6.38955700	-0.57356000	0.31974800
C	-5.33583800	-1.51038400	0.40695300
C	-4.03439600	-1.15277000	0.30797600
H	-3.25667900	-1.90640500	0.38036700
H	-5.57206200	-2.56264600	0.55958700
H	-7.42708500	-0.87565100	0.40019200
H	-6.80294300	1.53447700	0.05355900
H	-4.48581900	2.21647400	-0.12585700
O	-1.94028000	1.82781400	-0.16481100
H	0.11640200	0.83050000	-0.69848600

Benzoate ester radical anion transition state

24

C	0.00000000	0.00000000	0.00000000
C	0.76425200	0.24087100	-1.24762300
C	1.36144600	-0.90777000	-1.98623600
H	1.65790700	-0.60907100	-2.99526900
H	2.25308000	-1.29892100	-1.47926900
H	0.63819900	-1.72414200	-2.06579700
H	1.34116000	1.15964600	-1.26890200
H	-0.99354700	0.48955300	-0.07188500
H	-0.18098100	-1.06509400	0.16711100
H	0.49174200	0.42117600	0.88264900
O	-0.53619100	0.70930000	-2.47259600
C	-1.50707800	1.41180100	-1.99922700
C	-2.79632100	0.69106900	-1.76596000
C	-3.93985800	1.38092700	-1.40424500
C	-5.12987400	0.72520000	-1.23399400
C	-5.21985700	-0.63120000	-1.41941600

```

C    -4.08310600 -1.32481400 -1.78658000
C    -2.89761000 -0.67826200 -1.96244700
H    -2.00659100 -1.22464600 -2.25303600
H    -4.13321600 -2.39960600 -1.93990900
H    -6.16375900 -1.14847700 -1.28335200
H    -6.01319400  1.29033400 -0.94808100
H    -3.87257900  2.45280400 -1.25215600
O    -1.43428900  2.63760900 -1.72078100

```

Benzoate anion

14

```

C    0.00000000  0.00000000  0.00000000
C    0.00184200 -1.20739500  0.70421500
C    0.00368400 -2.41479000  0.00000000
C    0.00184200 -2.41257600 -1.39628800
C    0.00184200 -1.20739500 -2.10949200
C    0.00184200 -0.00221400 -1.39628800
H    0.00259600  0.92978200 -1.95127200
C    0.00184200 -1.20739500 -3.63850900
O    0.08106700 -0.08034700 -4.20529300
O    -0.07738300 -2.33444300 -4.20529300
H    0.00108800 -3.34457200 -1.95127200
H    0.00606400 -3.35728000  0.54021900
H    0.00184200 -1.20739500  1.79018000
H    -0.00238000  0.94249000  0.54021900

```

Molecule	MP2 energy calculated from MP2 optimized structures (Hartrees)	MP2 energy calculated from B3LYP optimized structures (Hartrees)
----------	--	--

Isopropyl radical	-118.1254332	-118.1252718
Protonated benzoate ester radical	-537.9637552	-537.9616205
Protonated benzoate ester radical transition state	-537.9265549	-537.9195132
Benzoic acid	-419.8743746	-419.8741594
Benzoate ester radical anion	-537.5178738	-537.513898
Benzoate ester radical anion transition state	-537.4657477	-537.4584046
Benzoate anion	-419.4138126	-419.4136141

Standard orientations – B3LYP optimized structures

Isopropyl radical

10

```

C    0.00000000  0.00000000  0.00000000
C    0.00000000  0.73388100 -1.29498900
C    0.00000000  0.00000000 -2.58997800
H   -0.18436500  0.66319700 -3.43767100
H    0.96435100 -0.50090600 -2.77688700
H   -0.75776300 -0.79240500 -2.60349900
H    0.23238800  1.79298800 -1.29498900
H   -0.18436500  0.66319700  0.84769300
H   -0.75776300 -0.79240500  0.01352100
H    0.96435100 -0.50090600  0.18690900

```

Protonated benzoate ester radical

25

C	0.00000000	0.00000000	0.00000000
O	-1.30361500	-0.13869900	-0.66758600
C	-2.29919900	0.68154300	-0.30535400
C	-3.62077000	0.21864100	-0.20269000
C	-4.72580600	1.11035000	-0.06219400
C	-6.01520600	0.62668600	0.06098900
C	-6.27446700	-0.74754400	0.04264900
C	-5.20290900	-1.63807800	-0.10972600
C	-3.90694400	-1.17934400	-0.23143000
H	-3.08973700	-1.87879500	-0.34395700
H	-5.39057500	-2.70579500	-0.13119400
H	-7.28768500	-1.11688400	0.13856000
H	-6.83494800	1.32849300	0.16492700
H	-4.57339000	2.18353900	-0.07242000
O	-1.93512100	1.98992200	-0.21276700
H	-2.59618700	2.48747800	0.28588300
C	-0.11125200	-0.44440400	1.44926300
H	-0.85361800	0.14725700	1.98860200
H	-0.39203900	-1.49822400	1.51061400
H	0.85087400	-0.31339500	1.94924900
C	0.96648100	-0.83403100	-0.81760800
H	0.99983800	-0.48759000	-1.85181900
H	1.97017200	-0.75400400	-0.39613400
H	0.67325900	-1.88638400	-0.80977200
H	0.28200800	1.05198000	-0.04966800

Protonated benzoate ester radical transition state

25

C	0.00000000	0.00000000	0.00000000
O	-1.46098900	0.48079500	-1.22476600
C	-2.46505200	1.06693000	-0.74343300
C	-3.75310900	0.43339800	-0.54086700
C	-4.91154400	1.15019400	-0.16936700
C	-6.12824100	0.50160800	-0.01172200
C	-6.23202700	-0.87219900	-0.22139400
C	-5.09640400	-1.59337800	-0.60153300
C	-3.87930200	-0.95594200	-0.76363700
H	-3.00372300	-1.51707000	-1.06076900
H	-5.16670700	-2.66133400	-0.77219700
H	-7.18350600	-1.37411800	-0.09659000
H	-7.00293500	1.07442600	0.27272600
H	-4.88297200	2.22354400	-0.01948700
O	-2.27797900	2.38083700	-0.39582400
H	-3.02236300	2.71148800	0.12348300
C	-0.67173300	-0.58031900	1.19201400
H	-1.50586700	0.04437600	1.52648000
H	-1.04148600	-1.58917500	1.00039700
H	0.03343200	-0.63288300	2.03220900
C	0.79641800	-0.86904600	-0.90619100
H	1.03917200	-0.35452300	-1.83778100
H	1.74569500	-1.14479600	-0.42718900
H	0.26582100	-1.79525700	-1.13880500
H	0.36484800	1.01412300	0.11919200

Benzoic acid

15

C	0.00000000	0.00000000	0.00000000
C	-1.11999200	-0.82935900	0.00000000

C	-2.39863600	-0.27735600	-0.00000000
C	-2.56171500	1.10249100	-0.00000000
C	-1.43991400	1.93775400	-0.00000000
C	-0.15837500	1.37881900	0.00000000
H	0.70240600	2.03443100	0.00000000
C	-1.56360500	3.41652200	-0.00000000
O	-2.84255700	3.84831000	-0.00000000
H	-2.82333700	4.81888600	-0.00000000
O	-0.62693500	4.18859700	-0.00000000
H	-3.55386300	1.53221300	-0.00000000
H	-3.26864200	-0.92224900	-0.00000000
H	-0.99584500	-1.90560300	0.00000000
H	0.99413900	-0.42949600	0.00000000

Benzoate ester radical anion

24

C	0.00000000	0.00000000	0.00000000
C	0.43407000	0.19272500	1.45019500
H	-0.15850100	0.97332400	1.92967400
H	0.30968000	-0.73552700	2.01482000
H	1.48661700	0.48459100	1.49894300
C	0.77619200	-1.10745400	-0.69829500
H	0.45177200	-1.21354900	-1.73548600
H	1.84507600	-0.88106500	-0.69494300
H	0.62971200	-2.06522100	-0.19154000
O	-1.39055800	-0.36452000	-0.05774300
C	-2.33776500	0.67037700	-0.06901700
C	-3.67638800	0.21049300	0.04713100
C	-4.76483700	1.14935400	-0.00733700
C	-6.07622200	0.73619700	0.09320300

C	-6.40842000	-0.62537400	0.25487100
C	-5.35495500	-1.56210200	0.31157700
C	-4.03543700	-1.17282300	0.21185600
H	-3.25231500	-1.91842300	0.25940000
H	-5.58452400	-2.61652600	0.43643500
H	-7.44123300	-0.94209200	0.33337200
H	-6.86858700	1.47790200	0.04670200
H	-4.53424400	2.20035900	-0.13185800
O	-1.96739300	1.86378500	-0.19989900
H	0.12824000	0.93925500	-0.54008300

Benzoate ester radical anion transition state

24

C	0.00000000	0.00000000	0.00000000
C	0.63302700	0.68455100	-1.16355300
C	1.53805200	-0.09435000	-2.05740000
H	1.80219600	0.47702900	-2.95058100
H	2.47583500	-0.35753500	-1.54763600
H	1.06843300	-1.03073500	-2.37331100
H	0.93812900	1.70885200	-0.97730600
H	-0.91008000	0.52239900	0.31464700
H	-0.26537200	-1.03289500	-0.23896500
H	0.67294500	-0.02024400	0.86884800
O	-0.80456500	1.06526300	-2.36693300
C	-1.78276100	1.77590900	-1.86520100
C	-3.07424000	1.09056100	-1.67874200
C	-4.22200400	1.81661300	-1.27997600
C	-5.45774500	1.19717100	-1.14959900
C	-5.60361900	-0.16824700	-1.40677700
C	-4.47775500	-0.90300400	-1.80450100

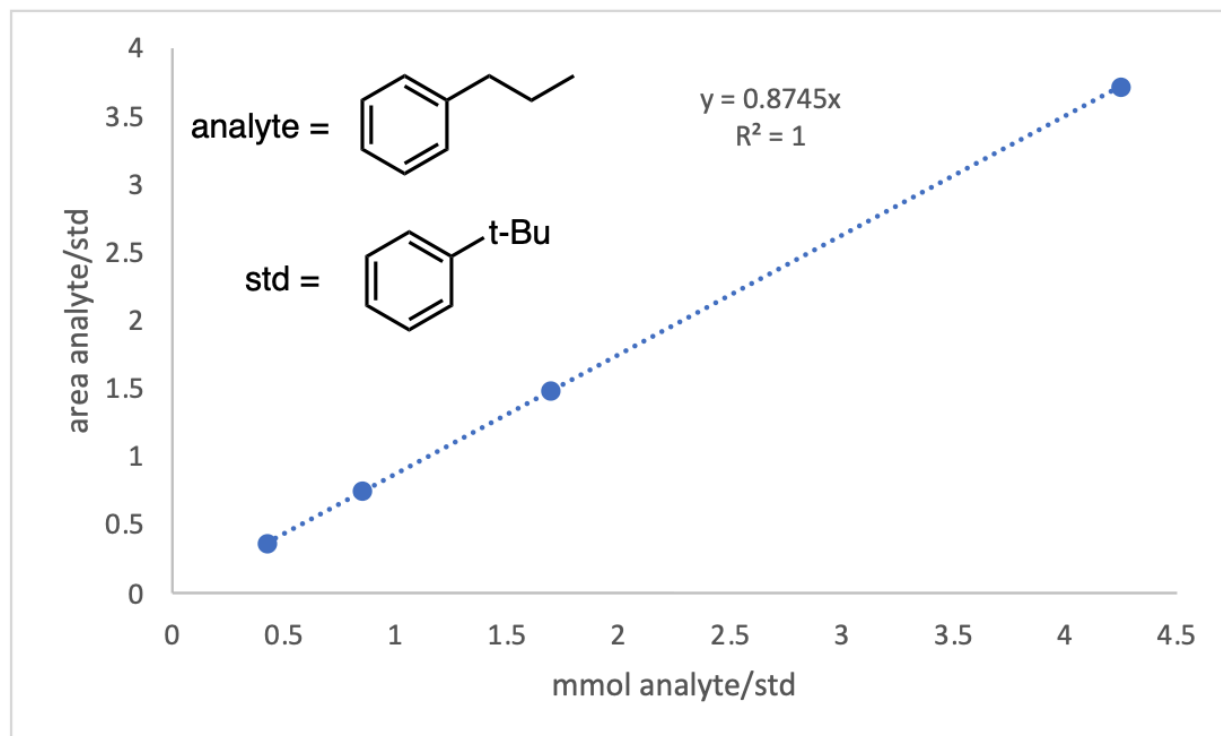
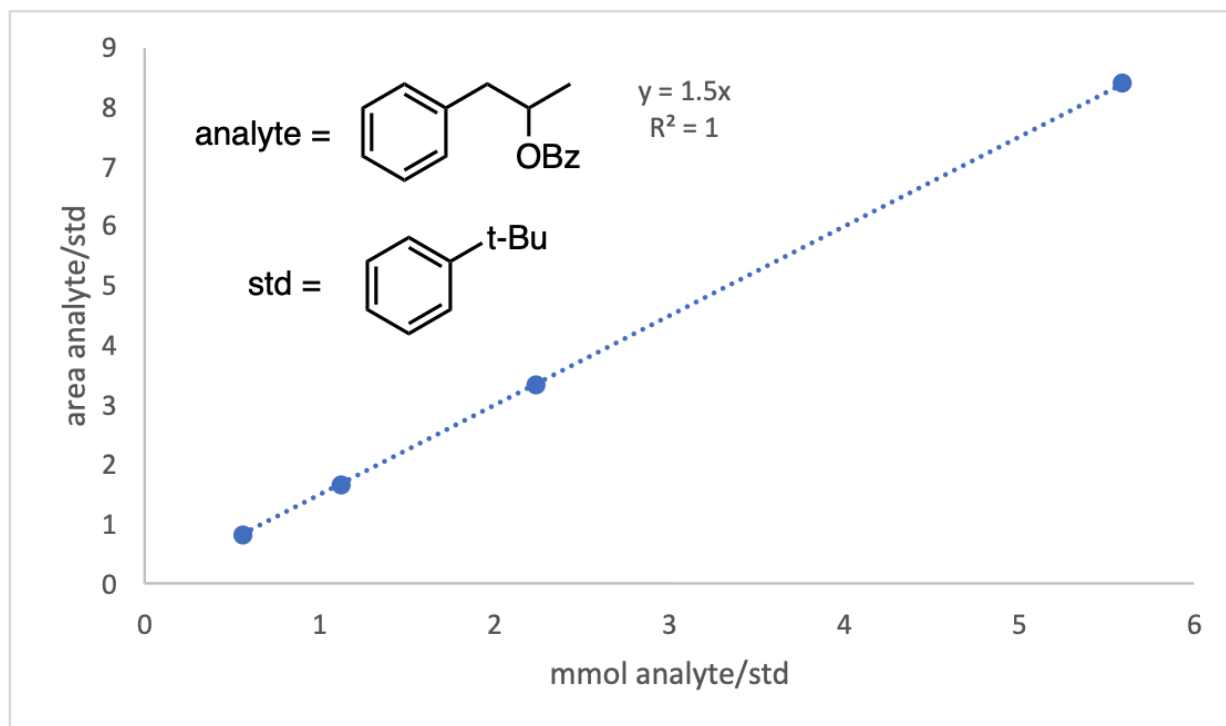
C	-3.24369600	-0.28885400	-1.94213800
H	-2.38278400	-0.86512100	-2.25482600
H	-4.57221900	-1.96469400	-2.00836600
H	-6.56871500	-0.65004900	-1.30354700
H	-6.31868100	1.78179200	-0.84131900
H	-4.11604700	2.87422900	-1.07529200
O	-1.64626900	2.99856600	-1.53792300

Benzoate anion

14

C	0.00000000	0.00000000	0.00000000
C	-0.00180400	1.20395200	0.70099800
C	-0.00360800	2.40790400	0.00000000
C	-0.00180400	2.40464600	-1.39195000
C	-0.00180400	1.20395200	-2.10660700
C	-0.00180400	0.00325800	-1.39195000
H	-0.00240700	-0.92750600	-1.94436200
C	-0.00180400	1.20395200	-3.63825600
O	-0.05571300	0.08190900	-4.20760900
O	0.05210500	2.32599500	-4.20760900
H	-0.00120100	3.33541000	-1.94436200
H	-0.00590300	3.34865900	0.53899400
H	-0.00180400	1.20395200	1.78494600
H	0.00229500	-0.94075500	0.53899400

4. 5. 12. Gas Chromatography Calibration Curves



4. 6. References

- (1) Shieh, P.; Hill, M. R.; Zhang, W.; Kristufek, S. L.; Johnson, J. A. Clip Chemistry: Diverse (Bio)(Macro)Molecular and Material Function through Breaking Covalent Bonds. *Chem. Rev.* **2021**, *121* (12), 7059–7121.
- (2) Jurczyk, J.; Woo, J.; Kim, S. F.; Dherange, B. D.; Sarpong, R.; Levin, M. D. Single-Atom Logic for Heterocycle Editing. *Nat. Synth* **2022**, *1* (5), 352–364.
- (3) Kennedy, S. H.; Dherange, B. D.; Berger, K. J.; Levin, M. D. Skeletal Editing through Direct Nitrogen Deletion of Secondary Amines. *Nature* **2021**, *593* (7858), 223–227.
- (4) Berger, K. J.; Driscoll, J. L.; Yuan, M.; Dherange, B. D.; Gutierrez, O.; Levin, M. D. Direct Deamination of Primary Amines via Isodiazene Intermediates. *J. Am. Chem. Soc.* **2021**, *143* (42), 17366–17373.
- (5) Smaligo, A. J.; Swain, M.; Quintana, J. C.; Tan, M. F.; Kim, D. A.; Kwon, O. Hydrodealkenylative C(Sp³)–C(Sp²) Bond Fragmentation. *Science* **2019**, *364* (6441), 681–685.
- (6) Roque, J. B.; Kuroda, Y.; Göttemann, L. T.; Sarpong, R. Deconstructive Fluorination of Cyclic Amines by Carbon-Carbon Cleavage. *Science* **2018**, *361* (6398), 171–174.
- (7) Murphy, S. K.; Park, J.-W.; Cruz, F. A.; Dong, V. M. Rh-Catalyzed C–C Bond Cleavage by Transfer Hydroformylation. *Science* **2015**, *347* (6217), 56–60.
- (8) Majid, M. H.; Atefe, B.; Zeinab, F. Applications of Barton-McCombie Reaction in Total Syntheses. *Current Organic Synthesis* **2014**, *11* (6), 787–823.
- (9) For selected recent examples strategically employing deoxygenation after bond forming reactions in complex molecule synthesis, see refs 10–12.
- (10) Wang, J.; Hong, B.; Hu, D.; Kadonaga, Y.; Tang, R.; Lei, X. Protecting-Group-Free Syntheses of Ent-Kaurane Diterpenoids: [3+2+1] Cycloaddition/Cycloalkenylation Approach. *J. Am. Chem. Soc.* **2020**, *142* (5), 2238–2243.
- (11) Hung, K.; Hu, X.; Maimone, T. J. Total Synthesis of Complex Terpenoids Employing Radical Cascade Processes. *Nat. Prod. Rep.* **2018**, *35* (2), 174–202.
- (12) Jasperse, C. P.; Curran, D. P.; Fevig, T. L. Radical Reactions in Natural Product Synthesis. *Chem. Rev.* **1991**, *91* (6), 1237–1286.
- (13) For selected recent examples removing oxygen atoms to access enantioenriched building blocks from carbohydrates, see refs 14 and 15.
- (14) Luo, M.; Wu, S.; Kalkeri, R.; Ptak, R. G.; Zhou, T.; Mellaert, L. V.; Wang, C.; Dumbre, S. G.; Block, T.; Groaz, E.; Jonghe, S. D.; Li, Y.; Herdewijn, P. Scalable Synthesis, In Vitro CccDNA Reduction, and In Vivo Antihepatitis B Virus Activity of a Phosphonomethoxydeoxythreosyl Adenine Prodrug. *Journal of Medicinal Chemistry* **2020**.
- (15) Bender, T. A.; Dabrowski, J. A.; Gagné, M. R. Homogeneous Catalysis for the Production of Low-Volume, High-Value Chemicals from Biomass. *Nat Rev Chem* **2018**, *2* (5), 35–46.
- (16) Barton, D. H. R.; McCombie, S. W. A New Method for the Deoxygenation of Secondary Alcohols. *J. Chem. Soc., Perkin Trans. 1* **1975**, No. 16, 1574–1585.

- (17) Chenneberg, L.; Ollivier, C. Tin-Free Alternatives to the Barton-McCombie Deoxygenation of Alcohols to Alkanes Involving Reductive Electron Transfer. *CHIMIA International Journal for Chemistry* **2016**, *70* (1), 67–76.
- (18) Chatgililoglu, C.; Ferreri, C. Progress of the Barton-McCombie Methodology: From Tin Hydrides to Silanes. *Res. Chem. Intermed.* **1993**, *19* (8), 755–775.
- (19) Chatgililoglu, C.; Ferreri, C.; Landais, Y.; Timokhin, V. I. Thirty Years of (TMS)₃SiH: A Milestone in Radical-Based Synthetic Chemistry. *Chem. Rev.* **2018**, *118* (14), 6516–6572.
- (20) Chenneberg, L.; Baralle, A.; Daniel, M.; Fensterbank, L.; Goddard, J.-P.; Ollivier, C. Visible Light Photocatalytic Reduction of O-Thiocarbamates: Development of a Tin-Free Barton–McCombie Deoxygenation Reaction. *Advanced Synthesis & Catalysis* **2014**, *356* (13), 2756–2762.
- (21) Herrmann, J. M.; König, B. Reductive Deoxygenation of Alcohols: Catalytic Methods Beyond Barton–McCombie Deoxygenation. *European Journal of Organic Chemistry* **2013**, *2013* (31), 7017–7027.
- (22) Carder, H. M.; Suh, C. E.; Wendlandt, A. E. A Unified Strategy to Access 2- and 4-Deoxygenated Sugars Enabled by Manganese-Promoted 1,2-Radical Migration. *J. Am. Chem. Soc.* **2021**, *120*, 9790–9833.
- (23) Turner, J. A.; Rosano, N.; Gorelik, D. J.; Taylor, M. S. Synthesis of Ketodeoxysugars from Acylated Pyranosides Using Photoredox Catalysis and Hydrogen Atom Transfer. *ACS Catal.* **2021**, 11171–11179.
- (24) Dai, X.-J.; Li, C.-J. En Route to a Practical Primary Alcohol Deoxygenation. *J. Am. Chem. Soc.* **2016**, *138* (16), 5433–5440.
- (25) Park, H. S.; Lee, H. Y.; Kim, Y. H. Facile Barton–McCombie Deoxygenation of Alcohols with Tetrabutylammonium Peroxydisulfate and Formate Ion. *Org. Lett.* **2005**, *7* (15), 3187–3190.
- (26) Cook, A.; MacLean, H.; St. Onge, P.; Newman, S. G. Nickel-Catalyzed Reductive Deoxygenation of Diverse C–O Bond-Bearing Functional Groups. *ACS Catal.* **2021**, *11* (21), 13337–13347.
- (27) For recent progress developing deoxygenative coupling reactions, see refs 28–35.
- (28) Anwar, K.; Merkens, K.; Aguilar Troyano, F. J.; Gómez-Suárez, A. Radical Deoxyfunctionalisation Strategies**. *European Journal of Organic Chemistry* **2022**, *2022* (26), e202200330.
- (29) Dong, Z.; MacMillan, D. W. C. Metallaphotoredox-Enabled Deoxygenative Arylation of Alcohols. *Nature* **2021**, *598* (7881), 451–456.
- (30) Guo, H.-M.; Wu, X. Selective Deoxygenative Alkylation of Alcohols via Photocatalytic Domino Radical Fragmentations. *Nat Commun* **2021**, *12* (1), 5365.
- (31) Lackner, G. L.; Quasdorf, K. W.; Overman, L. E. Direct Construction of Quaternary Carbons from Tertiary Alcohols via Photoredox-Catalyzed Fragmentation of Tert-Alkyl N-Phthalimidoyl Oxalates. *J. Am. Chem. Soc.* **2013**, *135* (41), 15342–15345.
- (32) Ye, Y.; Chen, H.; Sessler, J. L.; Gong, H. Zn-Mediated Fragmentation of Tertiary Alkyl Oxalates Enabling Formation of Alkylated and Arylated Quaternary Carbon Centers. *J. Am. Chem. Soc.* **2019**, *141* (2), 820–824.

- (33) Chi, B. K.; Widness, J. K.; Gilbert, M. M.; Salgueiro, D. C.; Garcia, K. J.; Weix, D. J. In-Situ Bromination Enables Formal Cross-Electrophile Coupling of Alcohols with Aryl and Alkenyl Halides. *ACS Catal.* **2022**, 12 (1), 580–586.
- (34) Li, Z.; Sun, W.; Wang, X.; Li, L.; Zhang, Y.; Li, C. Electrochemically Enabled, Nickel-Catalyzed Dehydroxylative Cross-Coupling of Alcohols with Aryl Halides. *J. Am. Chem. Soc.* **2021**, 143 (9), 3536–3543.
- (35) Stache, E. E.; Ertel, A. B.; Rovis, T.; Doyle, A. G. Generation of Phosphoranyl Radicals via Photoredox Catalysis Enables Voltage-Independent Activation of Strong C–O Bonds. *ACS Catal.* **2018**, 8 (12), 11134–11139.
- (36) Drosos, N.; Ozkal, E.; Morandi, B. Catalytic Selective Deoxygenation of Polyols Using the B(C₆F₅)₃/Silane System. *Synlett* **2016**, 27 (12), 1760–1764.
- (37) Jang, D. O.; Kim, J.; Cho, D. H.; Chung, C.-M. Radical Deoxygenation of Alcohols via Their Trifluoroacetate Derivatives with Diphenylsilane. *Tetrahedron Letters* **2001**, 42 (6), 1073–1075.
- (38) Yasuda, M.; Onishi, Y.; Ueba, M.; Miyai, T.; Baba, A. Direct Reduction of Alcohols: Highly Chemoselective Reducing System for Secondary or Tertiary Alcohols Using Chlorodiphenylsilane with a Catalytic Amount of Indium Trichloride. *J. Org. Chem.* **2001**, 66 (23), 7741–7744.
- (39) Perea, M. A.; Wang, B.; Wyler, B. C.; Ham, J. S.; O'Connor, N. R.; Nagasawa, S.; Kimura, Y.; Manske, C.; Scherübl, M.; Nguyen, J. M.; Sarpong, R. General Synthetic Approach to Diverse Taxane Cores. *J. Am. Chem. Soc.* **2022**, 144 (46), 21398–21407.
- (40) Sennari, G.; Gardner, K. E.; Wiesler, S.; Haider, M.; Eggert, A.; Sarpong, R. Unified Total Syntheses of Benzenoid Cephalotane-Type Norditerpenoids: Cephanolides and Ceforalides. *J. Am. Chem. Soc.* **2022**, 144 (41), 19173–19185.
- (41) Haelsig, K. T.; Xuan, J.; Maimone, T. J. Total Synthesis of (–)-Curvulamine. *J. Am. Chem. Soc.* **2020**, 142 (3), 1206–1210.
- (42) Amberg, W. M.; Carreira, E. M. Enantioselective Total Synthesis of (+)-Aberrarone. *J. Am. Chem. Soc.* **2022**, 144 (34), 15475–15479.
- (43) Na, C. G.; Kang, S. H.; Sarpong, R. Development of a C–C Bond Cleavage/Vinylation/Mizoroki–Heck Cascade Reaction: Application to the Total Synthesis of 14- and 15-Hydroxypatchoulol. *J. Am. Chem. Soc.* **2022**, 144 (42), 19253–19257.
- (44) Song, Z. J.; Qi, J.; Emmert, M. H.; Wang, J.; Yang, X.; Xiao, D. Two Scalable Syntheses of 3-(Trifluoromethyl)Cyclobutane-1-Carboxylic Acid. *Org. Process Res. Dev.* **2021**, 25 (1), 82–88.
- (45) Primmune Therapeutics, US2021/155652, **2021**, A1. *Primmune Therapeutics, US2021/155652, 2021, A1.*
- (46) Masnovi, J. Radical Anions of Esters of Carboxylic Acids. Effects of Structure and Solvent on Unimolecular Fragmentations. *J. Am. Chem. Soc.* **1989**, 111 (25), 9081–9089.
- (47) Lam, K.; Markó, I. E. Using Toluates as Simple and Versatile Radical Precursors. *Org. Lett.* **2008**, 10 (13), 2773–2776.
- (48) Paquette, L. A.; Geng, F. A Highly Abbreviated Synthesis of Pentalenene by Means of the Squarate Ester Cascade. *Org. Lett.* **2002**, 4 (25), 4547–4549.

- (49) Saito, Isao.; Ikehira, Hideyuki.; Kasatani, Ryuichiro.; Watanabe, Masakazu.; Matsuura, Teruo. Photoinduced Reactions. 167. Selective Deoxygenation of Secondary Alcohols by Photosensitized Electron-Transfer Reaction. A General Procedure for Deoxygenation of Ribonucleosides. *J. Am. Chem. Soc.* **1986**, *108* (11), 3115–3117.
- (50) Lam, K.; Markó, I. E. Organic Electrosynthesis Using Toluates as Simple and Versatile Radical Precursors. *Chem. Commun.* **2008**, No. 1, 95–97.
- (51) Romero, N. A.; Nicewicz, D. A. Organic Photoredox Catalysis. *Chem. Rev.* **2016**, *116* (17), 10075–10166.
- (52) Ruccolo, S.; Qin, Y.; Schnedermann, C.; Nocera, D. G. General Strategy for Improving the Quantum Efficiency of Photoredox Hydroamidation Catalysis. *J. Am. Chem. Soc.* **2018**, *140* (44), 14926–14937.
- (53) Rackl, D.; Kais, V.; Kreitmeier, P.; Reiser, O. Visible Light Photoredox-Catalyzed Deoxygenation of Alcohols. *Beilstein J. Org. Chem.* **2014**, *10*, 2157–2165.
- (54) Kolusu, S. R. N.; Nappi, M. Metal-Free Deoxygenative Coupling of Alcohol-Derived Benzoates and Pyridines for Small Molecules and DNA-Encoded Libraries Synthesis. *Chem. Sci.* **2022**, *13* (23), 6982–6989.
- (55) Conversely, electron-rich activating groups have been employed because they undergo rapid fragmentation. However, these analogs are more challenging to reduce. See: K. Lam, I. E. Markó, *Org. Lett.* **2011**, *13*, 406–409.
- (56) Cowper, N. G. W.; Chernowsky, C. P.; Williams, O. P.; Wickens, Z. K. Potent Reductants via Electron-Primed Photoredox Catalysis: Unlocking Aryl Chlorides for Radical Coupling. *J. Am. Chem. Soc.* **2020**, *142* (5), 2093–2099.
- (57) Chernowsky, C.; Chmiel, A.; Wickens, Z. Photocatalytic Activity of Diverse Organic Radical Anions: Catalyst Discovery Enables Cleavage of Strong C(Sp²)-N and C(Sp²)-O Bonds. *Angew. Chem. Int. Ed.* **2021**, *60*, 21418–21425.
- (58) Chmiel, A. F.; Williams, O. P.; Chernowsky, C. P.; Yeung, C. S.; Wickens, Z. K. Non-Innocent Radical Ion Intermediates in Photoredox Catalysis: Parallel Reduction Modes Enable Coupling of Diverse Aryl Chlorides. *J. Am. Chem. Soc.* **2021**.
- (59) Hendy, C. M.; Smith, G. C.; Xu, Z.; Lian, T.; Jui, N. T. Radical Chain Reduction via Carbon Dioxide Radical Anion (CO₂^{•-}). *J. Am. Chem. Soc.* **2021**, *143* (24), 8987–8992.
- (60) MacKenzie, I. A.; Wang, L.; Onuska, N. P. R.; Williams, O. F.; Begam, K.; Moran, A. M.; Dunietz, B. D.; Nicewicz, D. A. Discovery and Characterization of an Acridine Radical Photoreductant. *Nature* **2020**, *580* (7801), 76–80.
- (61) Ghosh, I.; Ghosh, T.; Bardagi, J. I.; König, B. Reduction of Aryl Halides by Consecutive Visible Light-Induced Electron Transfer Processes. *Science* **2014**, *346* (6210), 725–728.
- (62) Cole, J. P.; Chen, D.-F.; Kudisch, M.; Pearson, R. M.; Lim, C.-H.; Miyake, G. M. Organocatalyzed Birch Reduction Driven by Visible Light. *J. Am. Chem. Soc.* **2020**, *142* (31), 13573–13581.
- (63) Kim, H.; Kim, H.; Lambert, T. H.; Lin, S. Reductive Electrophotocatalysis: Merging Electricity and Light To Achieve Extreme Reduction Potentials. *J. Am. Chem. Soc.* **2020**, *142* (5), 2087–2092.

- (64) Connell, T. U.; Fraser, C. L.; Czyz, M. L.; Smith, Z. M.; Hayne, D. J.; Doeven, E. H.; Agugiaro, J.; Wilson, D. J. D.; Adcock, J. L.; Scully, A. D.; Gómez, D. E.; Barnett, N. W.; Polyzos, A.; Francis, P. S. The Tandem Photoredox Catalysis Mechanism of $[\text{Ir}(\text{Ppy})_2 (\text{Dtb-Bpy})]^+$ Enabling Access to Energy Demanding Organic Substrates. *J. Am. Chem. Soc.* **2019**, *141* (44), 17646–17658.
- (65) Peters, B. K.; Rodriguez, K. X.; Reisberg, S. H.; Beil, S. B.; Hickey, D. P.; Kawamata, Y.; Collins, M.; Starr, J.; Chen, L.; Udyavara, S.; Klunder, K.; Gorey, T. J.; Anderson, S. L.; Neurock, M.; Minter, S. D.; Baran, P. S. Scalable and Safe Synthetic Organic Electroreduction Inspired by Li-Ion Battery Chemistry. *Science* **2019**, *363* (6429), 838–845.
- (66) Hayashi, K.; Griffin, J.; Harper, K. C.; Kawamata, Y.; Baran, P. S. Chemoselective (Hetero)Arene Electroreduction Enabled by Rapid Alternating Polarity. *J. Am. Chem. Soc.* **2022**, *144* (13), 5762–5768.
- (67) Constantin, T.; Zanini, M.; Regni, A.; Sheikh, N. S.; Juliá, F.; Leonori, D. Aminoalkyl Radicals as Halogen-Atom Transfer Agents for Activation of Alkyl and Aryl Halides. *Science* **2020**, *367* (6481), 1021–1026.
- (68) Widness, J. K.; Enny, D. G.; McFarlane-Connelly, K. S.; Miedenbauer, M. T.; Krauss, T. D.; Weix, D. J. CdS Quantum Dots as Potent Photoreductants for Organic Chemistry Enabled by Auger Processes. *J. Am. Chem. Soc.* **2022**, *144* (27), 12229–12246.
- (69) Tian, X.; Karl, T. A.; Reiter, S.; Yakubov, S.; de Vivie-Riedle, R.; König, B.; Barham, J. P. Electro-Mediated PhotoRedox Catalysis for Selective C(Sp³)-O Cleavages of Phosphinated Alcohols to Carbanions. *Angewandte Chemie International Edition* **2021**, *60* (38), 20817–20825.
- (70) Wang, H.; Gao, Y.; Zhou, C.; Li, G. Visible-Light-Driven Reductive Carboarylation of Styrenes with CO₂ and Aryl Halides. *J. Am. Chem. Soc.* **2020**, *142* (18), 8122–8129.
- (71) Alektiar, S. N.; Wickens, Z. K. Photoinduced Hydrocarboxylation via Thiol-Catalyzed Delivery of Formate Across Activated Alkenes. *J. Am. Chem. Soc.* **2021**, *143* (33), 13022–13028.
- (72) Electrochemical Oxidation of Formate in Dimethylsulfoxide at Gold and Platinum Electrodes. *Journal of Electroanalytical Chemistry and Interfacial Electrochemistry* **1968**, *16* (3), 351–360.
- (73) Koppenol, W. H.; Rush, J. D. Reduction Potential of the Carbon Dioxide/Carbon Dioxide Radical Anion: A Comparison with Other C1 Radicals. *J. Phys. Chem.* **1987**, *91* (16), 4429–4430.
- (74) Grills, D. C.; Lyman, S. V. Radiolytic Formation of the Carbon Dioxide Radical Anion in Acetonitrile Revealed by Transient IR Spectroscopy. *Phys. Chem. Chem. Phys.* **2018**, *20* (15), 10011–10017.
- (75) Vogt, D. B.; Seath, C. P.; Wang, H.; Jui, N. T. Selective C–F Functionalization of Unactivated Trifluoromethylarenes. *J. Am. Chem. Soc.* **2019**, *141* (33), 13203–13211.
- (76) Discekici, E. H.; Treat, N. J.; Poelma, S. O.; Mattson, K. M.; Hudson, Z. M.; Luo, Y.; Hawker, C. J.; Alaniz, J. R. de. A Highly Reducing Metal-Free Photoredox Catalyst: Design and Application in Radical Dehalogenations. *Chem. Commun.* **2015**, *51* (58), 11705–11708.

- (77) To probe whether zinc formate was required in the reaction as a result of the Lewis-acidic zinc counterion, we conducted an experiment in which *i*-Pr₂NEt was employed with Zn(ClO₄)₂. This experiment only led to 7% deoxygenation. See SI for details.
- (78) Ischay, M. A.; Anzovino, M. E.; Du, J.; Yoon, T. P. Efficient Visible Light Photocatalysis of [2+2] Enone Cycloadditions. *J. Am. Chem. Soc.* **2008**, *130* (39), 12886–12887.
- (79) This reaction is run under air, water tolerant (up to 5 equivalents without diminished yields and up to 50 equivalents with yields still above 50%), and fully homogeneous.
- (80) These modified conditions were found to be less active for C(sp³)–O bond cleavage and reduced byproduct formation, which was tentatively assigned as homodimerization. See SI for details.
- (81) Wang, T.; Demchenko, A. V. Synthesis of Carbohydrate Building Blocks via Regioselective Uniform Protection/Deprotection Strategies. *Org. Biomol. Chem.* **2019**, *17* (20), 4934–4950.
- (82) Sakonsinsiri, C.; Turnbull, W. B. Protecting Groups at the Anomeric Position of Carbohydrates. In *Protecting Groups*; John Wiley & Sons, Ltd, 2019; pp 145–168.
- (83) Codée, J. D. C.; Ali, A.; Overkleeft, H. S.; van der Marel, G. A. Novel Protecting Groups in Carbohydrate Chemistry. *Comptes Rendus Chimie* **2011**, *14* (2), 178–193.
- (84) Guo, J.; Ye, X.-S. Protecting Groups in Carbohydrate Chemistry: Influence on Stereoselectivity of Glycosylations. *Molecules* **2010**, *15* (10), 7235–7265.
- (85) Lv, J.; Luo, T.; Zhang, Y.; Pei, Z.; Dong, H. Regio/Site-Selective Benzoylation of Carbohydrates by Catalytic Amounts of FeCl₃. *ACS Omega* **2018**, *3* (12), 17717–17723.
- (86) Yanagi, M.; Ueda, Y.; Ninomiya, R.; Imayoshi, A.; Furuta, T.; Mishi, K.; Kawabata, T. Synthesis of 4-Deoxy Pyranosides via Catalyst-Controlled Site-Selective Toluoylation of Abundant Sugars. *Org. Lett.* **2019**, *21* (13), 5006–5009.
- (87) A recent report for the titanium-catalyzed diastereoselective synthesis of cyclopropanols also expands the scope of this reaction, see ref 88.
- (88) Ni, J.; Xia, X.; Zheng, W.-F.; Wang, Z. Ti-Catalyzed Diastereoselective Cyclopropanation of Carboxylic Derivatives with Terminal Olefins. *J. Am. Chem. Soc.* **2022**, *144* (17), 7889–7900.
- (89) The minor shift in peak reduction potential upon addition of Lewis acid can be predicted using the Nernst equation and is likely a consequence of introducing a rapid chemical step following electrochemical reduction, which changes the concentration of the species in electrochemical equilibrium. See: R. D. Little, *J. Org. Chem.* **2020**, *85*, 13375–13390.
- (90) When the CV experiments of substrate **1** were conducted in the presence of formic acid, significant broadening and a minor new peak was observed in the voltammogram. See SI for details.
- (91) Gaussian 16, Revision C.01, Frisch, M. J.; Trucks, G. W.; Schlegel, H. B.; Scuseria, G. E.; Robb, M. A.; Cheeseman, J. R.; Scalmani, G.; Barone, V.; Petersson, G. A.; Nakatsuji, H.; Li, X.; Caricato, M.; Marenich, A. V.; Bloino, J.; Janesko, B. G.; Gomperts, R.; Mennucci, B.; Hratchian, H. P.; Ortiz, J. V.; Izmaylov, A. F.; Sonnenberg, J. L.; Williams-Young, D.; Ding, F.; Lipparini, F.; Egidi, F.; Goings, J.; Peng, B.; Petrone, A.; Henderson, T.; Ranasinghe, D.; Zakrzewski, V. G.; Gao, J.; Rega, N.; Zheng, G.; Liang, W.; Hada, M.; Ehara, M.; Toyota, K.; Fukuda, R.; Hasegawa, J.; Ishida, M.; Nakajima, T.; Honda, Y.; Kitao, O.; Nakai, H.; Vreven, T.; Throssell, K.; Montgomery, J. A., Jr.; Peralta, J. E.; Ogliaro, F.; Bearpark, M. J.; Heyd, J. J.; Brothers, E. N.; Kudin, K. N.; Staroverov, V. N.; Keith, T. A.; Kobayashi, R.;

Normand, J.; Raghavachari, K.; Rendell, A. P.; Burant, J. C.; Iyengar, S. S.; Tomasi, J.; Cossi, M.; Millam, J. M.; Klene, M.; Adamo, C.; Cammi, R.; Ochterski, J. W.; Martin, R. L.; Morokuma, K.; Farkas, O.; Foresman, J. B.; Fox, D. J. Gaussian, Inc., Wallingford CT, 2016. *Gaussian 16, Revision C.01*, Frisch, M. J.; Trucks, G. W.; Schlegel, H. B.; Scuseria, G. E.; Robb, M. A.; Cheeseman, J. R.; Scalmani, G.; Barone, V.; Petersson, G. A.; Nakatsuji, H.; Li, X.; Caricato, M.; Marenich, A. V.; Bloino, J.; Janesko, B. G.; Gomperts, R.; Mennucci, B.; Hratchian, H. P.; Ortiz, J. V.; Izmaylov, A. F.; Sonnenberg, J. L.; Williams-Young, D.; Ding, F.; Lipparini, F.; Egidi, F.; Goings, J.; Peng, B.; Petrone, A.; Henderson, T.; Ranasinghe, D.; Zakrzewski, V. G.; Gao, J.; Rega, N.; Zheng, G.; Liang, W.; Hada, M.; Ehara, M.; Toyota, K.; Fukuda, R.; Hasegawa, J.; Ishida, M.; Nakajima, T.; Honda, Y.; Kitao, O.; Nakai, H.; Vreven, T.; Throssell, K.; Montgomery, J. A., Jr.; Peralta, J. E.; Ogliaro, F.; Bearpark, M. J.; Heyd, J. J.; Brothers, E. N.; Kudin, K. N.; Staroverov, V. N.; Keith, T. A.; Kobayashi, R.; Normand, J.; Raghavachari, K.; Rendell, A. P.; Burant, J. C.; Iyengar, S. S.; Tomasi, J.; Cossi, M.; Millam, J. M.; Klene, M.; Adamo, C.; Cammi, R.; Ochterski, J. W.; Martin, R. L.; Morokuma, K.; Farkas, O.; Foresman, J. B.; Fox, D. J. Gaussian, Inc., Wallingford CT, 2016.

- (92) Proton-coupled electron transfer (PCET) cannot be excluded based on the data collected and should also be considered as a plausible mechanism. For a recent review focused on applications of PCET in synthetic chemistry, see: Murray, P. R. D.; Cox, J. H.; Chiappini, N. D.; Roos, C. B.; McLoughlin, E. A.; Hejna, B. G.; Nguyen, S. T.; Ripberger, H. H.; Ganley, J. M.; Tsui, E.; Shin, N. Y.; Koronkiewicz, B.; Qiu, G.; Knowles, R. R. Photochemical and Electrochemical Applications of Proton-Coupled Electron Transfer in Organic Synthesis. *Chem. Rev.* **2022**, 122 (2), 2017–2291.
- (93) Roberts, B. P. Polarity-Reversal Catalysis of Hydrogen-Atom Abstraction Reactions: Concepts and Applications in Organic Chemistry. *Chem. Soc. Rev.* **1999**, 28 (1), 25–35.